Behavioral Characteristics of Partially Reinforced Loadbearing Masonry Wall Structures

A Thesis

Submitted for the Partial Fulfillment of
the Requirements for the Degree
of
Doctor of Philosophy
in
Structural Engineering

by

Gouda Mohamed Mohamed Ghanem
B. Sc. and M. Sc.

Supervisors

Dr. Ahmad A. Hamid
Prof. of Structural Engineering
Drexel University, USA

Dr . Sherif A. El-Maged
Prof. of Structural Analysis
Helwan University

Dr. Amr E. Salama
Prof. of Properties and
Strength of Materials
Helwan University

Dr. Ahmed S. Essawy
Lecturer Structural Engineering
Ain Shams University

Helwan University
Faculty of Engineering and Technology, Mataryia
Department of Civil Engineering
1992

To Sally and Ahmed

ACKNOWLEDGEMENT

The author wishes to express his devout appreciation and gratitude to Dr. Ahmad A. Hamid for his professional guidance, helpful suggestions, encouragement and supervision during this research. The valuable comments offered by Dr. Hamid during the experimental program and the effort he expended in the manuscript are greatly appreciated.

The author would like to thanks his supervisors Dr. Sherif Abu-Elmagd, Dr. Amr E. Salama and Dr. Ahmed Sherif for their continued guidance, encouragement and sincere supervision through the courses and the research. Also acknowledgement is due to them for their reviewing the manuscript and their valuable comments.

Appreciation is extended to Dr. Hassan Hosny, the vice Dean at faculty of Eng. and Technology Helwan University and Dr. Sherif Helmy, the Department Head of Civil Eng. for their assistance.

Special thanks are due to Drexel University for the use of its facilities and equipments and MTS System at the Structural Testing Laboratory. The help provided by the Department of Civil and Arch. Eng. for the use of its computers, library and all the facilities is appreciated.

The financial support provided by the Egyptian Ministry of Higher Education and Helwan University is gratefully acknowledged.

Finally, I would like to extend my gratitude and deep appreciation to my mother and my wife for their continued support and encouragement.

Above all, I thank Allah for his blessings, and pray to him that this dissertation would be a contribution to knowledge.

TABLE OF CONTENTS

LIST OF TABLES

LIST OF ILLUSTRATIONS

ABSTRACT

Behavioral Characteristics of Partially Reinforced Loadbearing Masonry Wall Structures

by

Gouda Mohamed Mohamed Ghanem

Partially reinforced masonry structures as an alternative to fully reinforced masonry structures in areas of low wind or seismic forces offers an attractive cost-efficient building system. The in-plane behavior of partially reinforced masonry shear walls have not yet been addressed and no information is available on the design of such a system. Design equations in current masonry codes are developed based on fully grouted reinforced masonry wall construction. There is a need for research on the behavior and design of partially reinforced masonry shear walls. The available knowledge on the behavior of reinforced masonry walls are utilized and modified for application to partially reinforced masonry walls. Due to the prohibitative cost of full-scale testing of masonry structures, potential problems of workmanship and capacity limitation of loading equipment a more economical method utilizing the direct modeling technique is proposed as a replacement to full-scale testing. The technique and methodology used in modeling the masonry component materials at 1/3-scale are presented and discussed. The geometrical, physical and mechanical properties of all model masonry component materials (concrete block units, mortar, grout and steel reinforcement) are investigated. Correlation are made with the available prototype data. For the importance of determination of compressive strength and tensile strength of masonry in different orientations, the behavioral characteristics of 1/3-scale direct models of small assemblages under axial compression, bed joint shear and splitting tension at different orientations from the bed joints are investigated experimentally.

The effects of grouting, mortar bedding and block strength on the behavior of small assemblages are examined. The present study focuses on the behavior of partially reinforced masonry shear walls subjected to in-plane monotonically increasing and reversed cyclic loading representing wind or earthquake actions. The gravity loads transmitted from the above floors are represented by a constant axial load acting at the top of the shear walls. A total of fourteen (not including a pilot wall) 1/3-scale model of partially reinforced concrete block masonry shear walls were constructed and tested under in-plane lateral loads, with axial precompression. Eleven shear walls were tested under monotonically increasing loads and two shear walls were tested under fully reversed cyclically loading. Later, one infilled frame was chosen to be tested under monotonic loading for comparison purpose. Five parameters were investigated, namely: axial stress, block strength, type of lateral load (monotonic and cyclic), amount and distribution of vertical and horizontal reinforcement.

The main objective of the test program is to evaluate the in-plane behavior of partially reinforced concrete block masonry shear walls under in-plane monotonically increasing and reversed cyclic loading using small-scale direct modeling techniques. This would provide to have a better understanding of the behavioral characteristics of partially reinforced concrete block masonry shear walls under combined in-plane vertical and lateral loads.

Analytical study of the behavioral characteristics of partially reinforced masonry shear walls using finite element method is presented. Correlation with the experimental results are included. The main objective of the analytical study is to provide a means of covering a wide range of parameters which can not be investigated experimentally due to budget and time constraints. To allow a meaningful analysis of analytical data and to provide a better understanding on full-scale of a partially reinforced masonry shear wall response, a parametric studies were chosen to cover a number of design variables, such as distribution and amount of vertical and horizontal reinforcement, axial compressive stress, masonry strength, extent of grouting, and aspect ratio of the wall panel.

The results show that the distribution (spacing) of vertical and horizontal steel has a significant effect on failure mode, load-deflection curve and strength of partially reinforced

masonry shear walls. The axial stress has a significant effect on failure mode, ductility and cracking load. Whereas block strength has a significant effect only on cracking load and propagation of cracks. Grouting of the unreinforced parts of the wall panel has no effect on the wall behavior, but slightly increases the load carrying capacity. The aspect ratio of the wall panel has a very significant effect on the wall behavior, load-deflection curve and load carrying capacity (shear resistance of the wall).

Expressions for determining the geometric properties (effective area and effective moment of inertia) of partially reinforced walls are developed. Based on the experimental data an empirical formula is proposed to determine the shear strength of partially reinforced masonry shear walls. Analytical expressions are developed to determine the flexure strength of such a wall. Design charts for determining the residual strength of partially reinforced masonry shear walls, and interaction curves for determining the flexural strength are proposed as a design aid.

The application of the proposed formula on full-scale shear walls analyzed analytically, illustrates acceptable accuracy of the formula for predicting the shear strength of partially reinforced masonry shear walls.

The analytical analysis on full-scale shear walls indicates that 1/3-scale modeling techniques can be successfully used to investigate the behavioral characteristics of partially reinforced masonry shear walls.

The ability of partially reinforced masonry shear walls to develop a large deformation capacity under cyclic load is limited. Therefore, it is not recommended for use in a moderate or high seismic areas.

The experimental and analytical work presented in this study clearly demonstrates the adequacy of partially reinforced loadbearing masonry as an alternative building system to conventional infilled reinforced concrete frame construction in areas of low wind or seismic forces.

خصائص السلوك للمنشآت ذات
حوائط الطوب الحاملة المسلحة جزئيا

رسالة
مقدمة للحصول علي الدكتوراه
في
الهندسة الإنشائية

إعداد
جودة محمد محمد غانم
بكالوريوس هندسة مدنية ١٩٨٢
ماجستير هندسة إنشائية ١٩٨٧

إشراف

أ.د./ أحمد عبد الحميد
أستاذ الهندسة الإنشائية
جامعة دركسل - أمريكا

أ.د./ شريف على أبو المجد
أستاذ تحليل الإنشاءات
كلية الهندسة - جامعة حلوان

أ.د./ عمرو عزت سلامة
أستاذ خواص ومقاومة المواد
كلية الهندسة - جامعة حلوان

د. / أحمد شريف
مدرس بقسم الهندسة الإنشائية
جامعة عين شمس

جامعة حلوان
كلية الهندسة والتكنولوجيا- المطرية
قسم الهندسة المدنية
١٩٩٢م

ملخص

"خصائص السلوك للمنشآت ذات حوائط الطوب الحاملة المسلحة جزئيا"

مقدمة :

إن البناء بنظام الحوائط الحاملة فى مصر له مميزات عديدة عند مقارنته بالبناء بنظام الهيكل الخرسانى ، ولكى تكون الحوائط الحاملة أكثر فاعلية فى مقاومة القوى الجانبية فإنه يلزم تسليحها بأسياخ من الحديد لمقاومة قوى القص والإنحناء ، ولما كانت مصر من البلاد الآمنة من الزلازل وأحمال الرياح بها غير عالية فإن استخدام الحوائط الحاملة المسلحة جزئيا (تسليح خفيف) يكون اكثر اقتصاديا من استخدام الحوائط الحاملة المسلحة كليا والتى تستخدم فى اوربا وامريكا.

وسواء بمصر او بالخارج فإن تصرف الحوائط الحاملة من الطوب المسلح جزئيا لم تلق العناية الكافية من البحاث تحت الأحمال التى تقع فى نفس المستوى ، ولذا فقد عنى هذاالبحث بدراسة طريقة تصرف الحوائط من الطوب المسلح جزئيا تحت تأثير أحمال أفقية ورأسية فى نفس مستوى الحائط ، وقد تمت دراسة العوامل الآتية على تصرف الحوائط معمليا :

أ - توزيع صلب التسليح الأفقى والرأسى فى الحائط

ب - كمية صلب التسليح الأفقى والرأسى.

ج - درجة الضغط الرأسى الواقع على الحائط.

د - مقاومة بلوكات الطوب للضغط .

ه - نوع الحمل الأفقى (أستاتيكى أو متكرر فى اتجاهين متصادين) .

كما تمت دراسة نظرية بأستخدام الحاسب الآلى لدراسة تأثير كل العوامل السابقة بالاضافة الى تأثير نسبة الاستطالة للحائط (الأرتفاع : الطول) وتأثير امتداد حقن الحوائط بالخرسانة خارج نطاق أماكن اسياخ التسليح .

ولما كانت تكلفة أختبار الحوائط بالمقياس الحقيقى عالية لان دراسة تأثير العوامل السابقة تتطلب أختبار الحائط كله وليس جزء منه فقد تم عمل الأختبارات المعملية باستخدام نماذج الطوب (٣/١ البعد أى ٢٧/١ من الحجم) وتم عمل دراسة لخواص المونة والخرسانة المستخدمة فى الحقن وصلب التسليح والطوب نفسه لتتوائم مع حجم النموذج المستخدم ، وشملت هذه الدراسة تجارب على المواد المختلفة

كل على حده وكذلك تجارب على اجزاء من الحائط لدراسة سلوك الحائط تحت تأثير أحمال الضغط والقص والشد فى ثلاث اتجاهات بالنسبة للمونة الأفقية ، هذه الاجزاء صممت من مجموعات من الطوب (من ٤ الى ٨) كل مجموعة تناسب نوع الحمل المؤثر عليها .

وقامت الدراسة النظرية على اساس استخدام طريقة العناصر المحددة فى تمثيل الحوائط ، حيث مثلت الطوبة والخرسانة الحاقنة والمونة بعنصر واحد حددت خواصه معمليا ومثل صلب التسليح بطبقة مستوية فى منتصف سمك الحائط ، فتكون نموذج الحائط من عناصر ليس بها تسليح وعناصر بها طبقة التسليح فى الاماكن التى وضع فيها التسليح الجزئى للحائط .

وقد أظهرت الدراسة المعملية والنظرية تطابقا فى سلوك الحوائط سواء السلوك الإنحنائى أو السلوك القصى عند أخذ العومل السابقة فى الإعتبار، وكانت أهم نتائج الدراسة المعملية مايلى:

١ - توزيع صلب التسليح الأفقى يؤثر على سلوك الحوائط تأثيراً ملحوظا ، فكلما تحسن توزيعه (كلما قلت المسافة بين الأسياخ) كلما أدى ذلك الى تصرف سلوك الحائط بطريقة انحنائية بعيدا عن السوك القصى الغير مرغب فيه والذى يؤدى الى انهيار مفاجىء ، أما السلوك الإنحنائى فتظهر فيه نذر الإنهيار مبكرا ويكون التشكل كبيرا قبل الإنهيار.

٢ - زيادة كمية صلب التسليح الرأسى تؤدى أيضا الى سلوك الحوائط سلوكا إنحنائيا تحت تأثير الأحمال الأفقية ، ولما كانت الحوائط المدروسة مسلحة جزئيا وليس كليا فيمكن تركيز الحديد الرأسى فى الأطراف للحصول على هذا السلوك المرغوب.

٣ - زيادة الأحمال الرأسية على الحائط تؤدى الى سلوكه سلوكا قصيا وهو سلوك غير مرغوب فيه وعلى ذلك فالمبانى قليلة الإرتفاع تصلح لها الحوائط الحاملة والمسلحة جزئيا أكثرمن المبانى المرتفعة التى يناسبها أكثر التسليح الكلى خصوصاا لأدوار السفلى.

٤ - تمت الدراسة باستخدام نوعين من البلوكات ، الأول بلوك يتناسب مع الأنواع الموجودة فى مصر ، والثانى يقارب النوع المستخدم فى الولايات المتحدة وله ضعف مقاومة النوع الأول للضغط . ، وقد ظهر من الدراسة أن إختلاف مقاومة الضغط للبلوك لا يؤثرعلى سلوك الحائط ولكن يؤثر على حمل الشرخ وشكل وتوزيع الشروخ قبيل الكسر ، والحوائط من البلوكات الأقوى تتحمل أحمالا أعلى وتسرى الشروخ فيها فى المونة الأفقية والرأسية أما الحوائط من البلوكات الأضعف فيصعب تحديد مسار الشروخ فيها لانه قد يسرى فى البلوك نفسه وليس فى المونة فقط .

٥ - تغيير نوع الحمل من استاتيكى الى متكرر ، أظهر أن التسليح الجزئى لا يصلح للحوائط المعرضة لأحمال متكررة تغير اتجاهها (وهى تمثل احمال الزلازل) ولابد فى المناطق المعرضة للزلازل من تسليح الحائط كليا حسب المواصفات ، ومن نعم الله أن من علينا ببلد ليس معرضا لمثل هذه الأحمال.

كما أضافت الدراسة النظرية النتيجتين التاليتين :

٦ - تأثير نسبة الأستطالة للحائط (الارتفاع : الطول) أظهر انه كلما زادت نسبة أرتفاع الحائط الى طوله كلما كان تصرفه انحنائيا اكثر ولكنها تقلل بدرجة كبيرة قدره الحائط على مقاومة الأحمال الأفقية.

٧ - حقن الخلايا التى ليس بها أسياخ تسليح لم تؤثر تأثير ملحوظا على زيادة قدرة الحائط على مقاومة الأحمال الأفقية ، ولذا فإن المطلوب فقط حقن الخلايا التى تحتوى على أسياخ تسليح .

كما تمت محاولة للوصول الى طريقة مثلى لتصميم الحوائط المسلحة جزئيا بناءا على التجارب المعملية ، والدراسة النظرية وقد تم التوصل الى معادلة لحساب قوى القص فى الحوائط ذات السلوك القصى أخذت فى اعتبارها:

توزيع الحديد الأفقى ، كمية الحديد الرأسى ، درجة اجهاد الضغط الرأسى ، ومقاومة البلوكات للضغط ، وبتطبيق هذه المعادلة على حالات مختلفة ظهر التطابق بينها وبين نتائج الحاسب الآلى باستخدام طريقة العناصرالمحددة ، وتم عمل منحنيات تساعد المصمم على حساب قوى القص التى يستطيع تحميلها الحائط . وباستخدام دراسة نظرية تم التوصل الى معادلة لحساب أقصى عزم انحناء يستطيع الحائط مقاومته أخذا فى الإعتبار :

كمية صلب التسليح الرأسى وتوزيعه ، درجة إجهاد الضغط الرأسى ومقاومة البلوك للضغط وتم عمل منحنيات تساعد المصمم على حساب عزوم الإنحناء التى يستطيع الحائط تحملها .

محتويات الرسالة

تتكون الرسالة من ثمانية أبواب :

الباب الأول

يحتوى على مقدمة لأهمية البحث وأهدافه ومجاله ويشمل أيضا مكونات الرسالة.

الباب الثانى

يحتوى على ملخص لأهمية ومميزات طريقة النماذج (المقياس المصغر) المستخدمة للمبانى وكذلك العوامل المختلفة المؤثرة على دقة هذه النماذج ومتطلبات التشابه. ويتضمن هذا الباب أيضا طريقة انتاج نماذج البلوكات المستخدمة فى هذا البحث بالمعمل وكذا عمل نتؤات بصلب التسليح والإختبارات المعملية لدراسة خواص البلوكات والمونة والخرسانة المستخدمة فى الحقن وكذا صلب التسليح.

الباب الثالث

فى هذا الباب تم اختبار عدد ٣٦ حائط صغير (أجزاء من الحائط ، كل جزء يتكون من مجموعات من البلوكات من ٤ – ٨ بلوك كل مجموعة تناسب الحمل المؤثر) لدراسة سلوك الحائط تحت تأثيرأحمال الضغط ، القص ، والشد فى ثلاث اتجاهات بالنسبة للمونة الأفقية أخذا فى الإعتبار تأثير مقاومة البلوك للضغط والحقن بالخرسانة وتم مقارنة هذه النتائج بالنتائج المتاحة باستخدام المقياس الحقيقى.

الباب الرابع

يحتوى هذا الباب على ملخص موجز لاهم الدراسات السابقة للحوائط الغير مسلحة والمسلحة كليا والمعرضة لاحمال فى اتجاه المستوى حيث لا توجد ابحاث للحوائط المسلحة جزئيا . فى هذا الباب تم شرح الخطوات المختلفة لانشاء عدد ١٤ نموذج حائط بابعاد ٠ر١ مترx ٠ر١ متر (مقياس حقيقى ٠ر٣ مترx٠ر٣متر) ويتضمن ايضا نظام التحميل الذى تم تصميمه ليناسب امكانيات المعمل وظروف الاختبار ، وفيه تم ايضا عرض لاجهزة القياسات المختلفة وتوصيلها بجهاز التحميل الاليكترونى الميكانيكى حيث يتم تجميع المعلومات بواسطة جهاز خاص بذلك متصل بالحاسب الآلى ومنه يمكن عمل رسومات بيانية اثناء وبعد التحميل مباشرة .

الباب الخامس

يعرض هذا الباب النتائج المعملية وتحليلها ودراسة العوامل الآتية: توزيع صلب التسليح الرأسى والأفقى ، كمية صلب التسليح الرأسى والأفقى ، درجة اجهاد الضغط الرأسى ، مقاومة البلوكات للضغط ونوع الحمل الأفقى على تصرف سلوك الحوائط وأيضا تمت دراسة قابلية الحوائط للتشكل و الجساءة القصية ، وتم عمل مقارنة للحوائط التى اختبرت تحت تأثير حمل استاتيكى وحمل متكرر فى اتجاهين ويشمل أيضا ملخص موجز لأهم النتائج المعملية التى تم الوصول اليها.

الباب السادس

يشمل هذا الباب الدراسة النظرية باستخدام طريقة العناصر المحددة وفيه تم دراسة النماذج التى سبق اختبارها معمليا ، وقد أظهرت النتائج تطابق تام فى سلوك الحوائط تحت تأثير العوامل السابقة.

وأيضا تم دراسة سلوك الحوائط ذات المقياس الحقيقى تحت تأثير العوامل السابقة بالإضافة الى هذين العاملين : تأثير نسبة ارتفاع طول الحائط وتأثير امتداد الحقن بالخرسانة خارج نطاق أماكن أسياخ التسليح . وتضمن أيضا ملخص موجز لأهم النتائج التى تم الوصول اليها نظريا .

الباب السابع

فى هذا الباب تم اعداد معادلات لحساب مساحة تقطع وعزم القصور الذاتى للحائط المحقن بالخرسانة جزئيا بدلالة طول الحائط وعدد الخلايا المحقونة .

بناءا على التجارب المعملية والدراسة النظرية ، تم التوصل الى معادلات لحساب قوى القص فى الحوائط ذات السلوك القصى آخذا فى الأعتبار : توزيع صلب التسليح الأفقى ، كمية صلب التسليح الرأسى ، درجة اجهاد الضغط الرأسى ، ومقاومة البلوكات للضغط . بتطبيق هذه المعادلات على الحوائط ذات السلوك القصى ومقارنتها بمعادلات اخرى وايضا مقارنتها بنتائج الحاسب الالى ، أظهرت تطابقا . وتم عمل منحنيات مساعدة للتصميم يمكن بواسطتها حساب قوى القص التى يمكن للحائط تحملها .

وباستخدام دراسة نظرية تم التوصل الى معادلة لحساب أقصى عزم انحناء يستطيع الحائط مقاومته آخذا فى الإعتبار : كمية صلب التسليح الرأسى وتوزيعه ، درجة إجهاد الضغط الرأسى ومقاومة البلوك للضغط . وبتطبيق هذه المعادلات على الحوائط ذات السلوك الإنحنائى ومقارنتها بمعادلات أخرى وأيضا بنتائج الحاسب الآلى أظهرت تطابقا . وتم عمل رسومات بيانية مساعدة للتصميم يمكن بواسطتها حساب عزوم الإنحناء التى يمكن للحائط تحملها.

الباب الثامن

يشمل هذا الباب على ملخص موجز لأهم النتائج التى تم التوصل إليها فى هذه الدراسة المعملية والنظرية وأهم التوصيات للدراسات المستقبلية فى هذا المجال.

CHAPTER 1
INTRODUCTION

1.1 GENERAL

Although masonry is one of man's oldest building materials, it has probably remained the least understood of major construction materials at least as far as its structural behavior is concerned .

The strength of plain (unreinforced) masonry walls depends upon the mortar and the masonry units with their high degree of compressive strength. These components in turn must act as an integral combination in order to resist both vertical compressive and shear forces.

The achievement of lateral stability by gravity places a practical economic limit on the size of the structure. This has led designers and engineers to seek ways in which these massive bearing walls could be decreased in thickness without losing their stability in the process. Perhaps[150] the dilemma that was faced by the designers of another era is most dramatically portrayed by the 16-story Manadnock Building, a brick bearingwall structure built in Chicago in 1889-1891. Its 6 ft (1.8 m) thick unreinforced masonry walls at the base of the building provided the required stability against wind loads. Such structures made it rather apparent at the turn of the century that a size limit had been reached on masonry structures using empirical design methods then currently employed. If modern design techniques and construction methods had been available at that time, the designers of the Manadnock might have used instead masonry walls 1 ft (0.3 m) or less thickness. Comparing this massive building with the modern Hanalei Hotel in San Diego, California, with its 8 in. thick walls at the bottom story clearly indicates the progress and current trend in masonry construction.

As the building height increases, a main factor began to be recognized as a formidable limitation on height. This is the lateral force imposed upon the face of the

structure by the wind pressures or seismic motion that occur in many parts of the world. This led to the evolvement of plain loadbearing masonry into reinforced loadbearing masonry. Such concept utilizes floors and roofs as diaphragms to distribute the lateral forces to walls which in turn provide the horizontal shear resistances needed in addition to carrying the normal vertical live and dead loads. These types of structures may be defined as a box system or a shear wall system. Such walls if constructed of plain masonry may or may not be capable of resisting the magnitude of horizontal shear and bending forces imposed upon them depending upon the level of lateral loads and the level of precompression from gravity loads. Modern reinforced masonry walls contain reinforcing steel to resist shear and developed tensile stresses . When these walls are subjected to lateral in-plane or out-of-plane forces, they would exhibit either a shear type of failure or a flexural type of failure. Therefore, reinforcing steel must be provided to resist both shear and tensile stresses .

The combination of masonry and reinforcement is a very compatible one. Masonry brings to the system a high degree of compressive resistance, weathering, durability, fire protection and stability. Its stiffness minimizes flexural and shear deflections, and its composite heterogeneous nature tends to maximize the damping response to dynamic vibratory forces. Although, principally reinforcing steel develops the flexural tensile resistance, so necessary to resist lateral loads, it also imparts to the composite material the resilience and ductility needed in high-rise construction .

In Egypt, the infilled reinforced concrete frame structures are dominant in residential building construction. This system is becoming more expensive due to the high cost of framework, reinforcement and plastering. There is an urgent need to introduce new building systems that are cost-effecient. Loadbearing masonry offers an attractive building system with multifunctional characteristics. This system can save formwork, reduce the amount of reinforcement needed and eliminate expensive exterior plastering with the added advantages of speed of construction, simple erection techniques and dimensional

tolerances. Loadbearing walls act as structural elements and exterior and interior partitions with excellent thermal, fire and acoustical insulations.

In order to implement loadbearing masonry as a cost-effecient building system in Egypt, national design code and standard specifications should be developed based on local materials, level of quality control and common construction practics. This requires long-term research effort to provide adequate data base for the development of design procedure for loadbearing masonry.

Today's multistory loadbearing structures with modern slender reinforced walls offer a competitive and an economical system. This is due to the multi-functional characteristics of masonry systems; namely: structural framework, define geometric space, great variety of architectural finishes, water proof enclosure, thermal, fire and acoustical insulations, flexibility and simplicity of erection and construction techniques.

Reinforced masonry building are built mainly in regions of high seismicity. Such structures are usually resist the gravity loads as well as the vertical and lateral in-plane loads induced by wind and earthquake. Failure characteristics and load carrying capacity of reinforced walls depend mainly upon the amount and distribution of vertical and horizontal reinforcement. For this reason most codes specify the minimum amount of steel as 0.002 times the gross cross-sectional area of wall and the maximum spacing of vertical and horizontal steel as 4 ft (1.2 m). In addition to this requirement, there are other design requirements for earthquake zones (zones 3 & 4 in the U.S.A.).

In areas where seismic or wind forces are not considered to be critical the use of reinforced masonry becomes uneconomical. The most cost-efficient system in such cases is masonry walls with partial (light) reinforcement to resist tensile and shear forces.

Masonry walls constructed of hollow concrete blocks the walls having reinforced cores widely spaced, greater than 4 ft (1.2 m) or the amount of steel in the cores less than 0.002 times the gross cross-sectional area of the wall are referred to as partially (lightly) reinforced masonry. Masonry is considered partially reinforced when either any of the two

requirements of reinforced masonry (amount and distribution of vertical and horizontal steel) is violated.

Chandrakeerthy and Hamid[29] presented an overview of the potential for use of partially reinforced masonry specifically in third world countries. Their major conclusion is that: partially reinforced concrete masonry has many advantages, its shortcomings can be overcomed, and hence it has potential for wider usage. Knowledge on the behavior of this material is insufficient for inclusion in masonry codes and a considerable scope exists for research on the lines serving the codes as well as research directed towards the needs of the developing countries. Further efforts are needed for increased utilization of this material .

The partially reinforced concrete masonry shear walls has the following advantages[29] :

1) It has great potential in non-seismic areas to replace reinforced concrete infilled-frame wall system by loadbearing walls.

2) Partially reinforced masonry allows an increase in compression, shear and flexural tensile strength compared to hollow masonry without any increase in wall thickness.

3) It can accommodate larger openings in loadbearing walls, as piers on either side of the opening can be reinforced, thus giving greater flexibility to the architect.

4) Grouting enables utilization of higher stresses specified by the codes.

5) It increases shear strength perpendicular to the bed joints significantly thus allowing economics in shear wall design.

6) It provides greater protection against accidental damage or concentrated impulsive forces by the ability to confine failure or damage to localized areas and by load redistribution.

7) It can minimize the incidence of cracking due to shrinkage, foundation settlement, thermal movement, or structural action by placing steel reinforcement in the wall.

8) Its judicious application results in cost reductions such as in replacement of reinforced concrete frames and in using lower strength blocks or narrower blocks.

9) For construction workers experienced in hollow concrete masonry and reinforced concrete, new craft skills required to carry out grouting can be easily attained.

10) It enables easy installation of services in hollow cells which can not be accommodated in fully grouted concrete masonry walls.

11) It can be used for strengthening old hollow concrete masonry walls .

For the less demanding Egyptian environment from the standpoint of wind/earthquake lateral loads, the partially reinforced system, as compared to the fully reinforced system, is more suitable and more cost efficient to the Egyptian market .

Partially reinforced masonry shear wall is a concrete masonry wall where some of the cavities are reinforced and grouted. The upper limit of steel reinforcement is governed by either the minimum steel reinforcement required for reinforced masonry walls and the minimum spacing is taken equal to the maximum spacing required in reinforced concrete masonry wall (i.e. contains reinforcement at larger spacing) . The construction of full-scale partially reinforced walls for testing is unpractical difficult because this new system requires larger and higher walls to represent reinforcement at larger spacing. Due to space limitation in the Structural Testing Laboratory of Drexel University, full-scale testing of partially reinforced walls is not feasible.

The use of small-scale modeling in this case offers a feasible and cost- efficient experimental technique. The present experimental study was undertaken in the Structural Testing Laboratory of Drexel University, Philadelphia USA to investigate the in-plane behavioral characteristics of partially reinforced concrete masonry shear walls by means of direct small-scale models techniques . A 1/3-scale was chosen for this experimental study .

In order to implement loadbearing masonry as a cost-efficient building system in Egypt, national design code and standard specifications should be developed based on local material, level of quality control and common construction practice . This will require long-term research effort to provide an adequate data base for the development of design procedures. The present study is a contribution to that effort.

A total of thirteen partially reinforced concrete block masonry shear walls and one infilled frame were constructed and tested under in-plane vertical and lateral loads.

Analytical study using the finite element technique is utilize to compliment the experimental work and to provide means of a better understanding of shear wall response and behavior. Analytical formulae are developed to predict key design parameters of partially reinforced masonry shear walls.

1.2 OBJECTIVE AND SCOPE OF STUDY

In this study the use of 1/3-scale direct modeling techniques was utilized to in predict the behavioral characteristics of partially reinforced masonry shear walls under the in-plane vertical and lateral loads. The model assemblages were built from scaled down concrete units, mortar, and grout. Five major objectives are considered in the present study:

1- Model and evaluate the components material of concrete block masonry (concrete block units, mortar, grout, and steel reinforcement) at 1/3-scale using the techniques and methodology of small-scale direct modeling.

2 - Study and evaluate the strength of small unreinforced concrete masonry assemblages under in-plane loading (axial compression, bed joint shear, and tension) taking into account the effects of block strength, mortar, and grouting by means of 1/3-scale direct model.

3 - Investigate the behavioral characteristics of partially reinforced masonry shear walls under combined in-plane vertical and lateral loads by using 1/3-scale model. The effects of block strength, level of axial load, lateral loads (monotonic and cyclic), horizontal and vertical steel reinforcement, crack patterns and failure modes, load-deflection relationship, and the ultimate load carrying capacity were studied.

4 - Examine and evaluate the applicability and feasibility of 1/3-scale direct modeling techniques in predicting the behavior of partially reinforced masonry shear walls. This is accomplished by comparing the model experimental results with analytical predictions.

5 - Propose potential design methodology for partially reinforced masonry shear walls.

To meet these objectives, experimental and analytical investigations were conducted and documented in this dissertation. For proper treatment each of the above objectives is studied separately. Therefore, the model masonry components materials, the model small masonry assemblages, and the model partially reinforced masonry shear walls are presented in different chapters. Each chapter contains an introduction, specific objectives, details of the experimental study and correlation between the model test results and available prototype test results on similar specimens and related conclusions The experimental study is followed by analytical investigation using the finite element method. This is followed by design methodology for partially reinforced masonry walls .

1.3 OUTLINE OF THE THESIS

To aid the researcher in following the material presented in this dissertation, the chapters are outlined as follow :

Chapter 2 Contains the techniques and methodology used in modeling the masonry component materials (concrete block units, mortar, grout, and steel reinforcement) at 1/3-scale with their physical and mechanical properties.

Chapter 3 Induces the strength of model small masonry assemblages under in-plane loading : axial compression, bed joint shear, and in-plane tension.

Chapter 4 Presents the experimental program for testing model partially reinforced masonry shear walls under in-plane combined vertical and lateral loads .

Chapter 5 Conducts discussions and analyses of the experimental results and design methodology of partially reinforced masonry shear walls.

Chapter 6 Contains analytical study of the behavioral characteristics of partially reinforced masonry shear walls using the finite element method.

Chapter 7 Presents the design methodology of partially reinforced masonry shear walls.

Chapter 8 Introduces general summary and conclusions.

CHAPTER 2
MODEL MATERIAL PROPERTIES

2.1 GENERAL

In order to predict the behavior and strength of masonry walls the material properties of the component materials should be clearly understood. The materials used for making the model concrete blocks and for the construction of the model assemblages and shear walls are all commercially available and are typical of those used in building construction in the Arab Repablic of Egypt and the United States. The partially reinforced masonry shear walls are constructed from four constituent materials with different properties: concrete block units, mortar, grout, and steel reinforcement.

In the area of small-scale testing of masonry materials one of the early attempts was carried out at Edinburgh University by Hendry[73]. Two conclusions of prime importance were found by the authors .

1) The structural behavior of masonry is a function of a variety of structural properties that might be grouped as follows :

a- Brick (block) properties; compressive strength, tensile strength, modulus of elasticity, and Poisson's ratio .

b- Mortar properties; compressive strength, tensile strength, modulus of elasticity, and Poisson's ratio .

c- Relative physical properties; relation between dimensions of bricks (blocks) and relative thicknesses between brick (block) and mortar .

d- Block (brick)/mortar interface properties.

2) Measured properties are greatly influenced by the method of testing as well as loading conditions .

The techniques and methodology used in modeling the masonry component materials at 1/3-scale are presented in this chapter. The geometrical, physical, and mechanical properties of all model masonry component materials are investigated and

reported. Correlations are made with the available prototype data. Similitude requirements and experimental behavior are the major consideration required to attain a replica model of the prototype[52&128].

2.2 SMALL SCALE MODELING

2.2.1 Historical Development

The use of small-scale models to assist building designers may be one of the oldest design tools ever employed. One does not have to stretch the imagination much to visualize ancient Egyptian, Greek, Persian, and Roman builders constructing small models to assist themselves in planning some of the marvelous structures built some hundreds or even thousands of years ago .

The designers of the past did not have available the knowledge of structural behavior, material properties, mathematics or the measurements methods that are known to us today. Thus, evaluation of structural features through model studies by these early builders was probably confined to very general observations regarding the interaction of assemblages of component parts and regarding methods of assembly .

The use of modeling techniques in structural research have been improved considerably in the past few decades due to the improvement in instrumentation and the use of more accurate loading devices. The direct small-scale modeling techniques, successfully applied to nonlinear problems of reinforced and prestressed concrete structures initially at MIT and Cornell University and later at the Structural Models Laboratory of Drexel University have proven to be a reliable techniques and is proposed as an economical alternative to full-scale testing for masonry structures[1&87] .

Small-scale structural models have played a much more scientific role as tools used to assist in the analysis of structural behavior in contemporary buildings. Probably the first truly scientific employment of small-scale models for experimental stress analysis came with the development of the photoelasticity technique .

An early attempt to model masonry structures was made in England by Vogt1 in the

mid-fifties. He modeled brickwork by using 1/4-scale and later used 1/10-scale. These attempts were some what exploratory in nature and did not intended to furnish design data. In the early sixties, research with model brickwork was started at Melbourne University[115,134&140]. Success was limited due to difficulties encountered in making the miniature bricks and manufacturing the brick wall specimens. Later greater success was achieved by Mohr[97] using commercially made 1/6-scale model bricks and a prefabrication method of manufacturing model brick wall specimens . Hendry and Murthy[74&101] established the modeling of brickwork in the mid-sixties at University of Edinburgh. They performed tests on full size, 1/3-scale, and 1/6-scale models of brickwork piers and walls, they concluded that the behavior of full size brickwork could be repeated by means of modeling.

An investigation for shear action of in-plane walls under lateral loads was carried out by Sinha[132&133] at University of Edinburgh. This study was conducted on a 1/6-scale model and full-scale test of a five story building. They concluded that, in general, despite some differences in stiffness between model and prototype, the model brickwork behaved in a manner similar to full-size brickwork and can closely predict behavior and strength. Tests on model masonry structures have also been successfully conducted in Australia in the early seventies by Baker[19]. He carried out tests on axially loaded and laterally loaded brick walls at 1/3-scale and 1/6-scale. Also, at the same time Fiorato[45] used 1/4-scale brickwork to study the interaction between infill and concrete frames. The results had considerable success in understanding the interaction mechanism between the brick infill and the boundary of the concrete frame .

The modeling of concrete masonry structures has not received as much attention as those of clay brick construction. The earliest attempt to model masonry structures was made in England by Voigt[143] in the late sixties using 1/4-scale brick and later 1/10-scale brick. The study, however, was not conclusive. In the mid-seventies, the methodology and techniques of 1/4-scale direct modeling of hollow concrete masonry were developed by

Harris and Becica[66&21] at Drexel University. Based on their limited preliminary tests, they concluded that direct modeling for ungrouted concrete masonry at 1/4-scale is feasible. Later in the early eighties, a more comprehensive study was conducted by Hamid and Abboud[60,61&64] using the same scale model used by Harris and Becica. Their results were correlated to available prototype results. These model results were very promising, and it was concluded that modeling of block masonry is feasible and capable of predicting the overall behavior. later, Harris and Larbi[87] carried out tests on shear walls subjected to in-plane loads using 1/3-scale direct models. Their results were correlated to full-scale tests conducted by Shing et al[126&129] at Colorado University. They concluded that model and full-scale results are in good agreement up to the ultimate state. Harris and Labrouki[86] also used the same scale [1/3-scale], the purpose of their study was to realize the possibility of the use of 1/3-scale in predicting the behavior of masonry structures. In all cases studied in this research, model test results had shown a very good correlation with prototype results .

In the present work 1/3-scale direct modeling approach has been used. At a physical scale of 1: 3, the detail in masonry construction can be performed by practicing qualified masons using the traditional materials employed in full-scale fabrication. Loading facilities can be much more manageable and less costly at 1/3-scale, since an order of magnitude of one-ninth reduction in failure load can be achieved by a threefold reduction in the geometric scale. The material characterization of the 1/3-scale direct modeling approach is described in this chapter .

2.2.2 Advantages and Limitations of Model Analysis

The main advantage of a physical model over an analytical model is that it portrays behavior of a complete structure loaded to the collapse stage. Although progress is continually made in computer-based procedure for analysis of structures, we still cannot predict accurately the failure capacity of a three-dimensional assemblage of reinforced concrete masonry elements. The prime motivation to conduct experiments on structures at

reduced scales is to reduce the cost. Cost reductions come about from two areas : reduction of loading equipment and associated restraint frames, etc. and a reduction in cost of test-structure fabrication, preparation and disposal after testing. The load-reduction factor is most dramatic since the concentrated load on a prototype is reduced in proportion to the square of the geometric scale factor of the model (a 100 ton prototype load is 11.1 ton on a 1/3 -scale model). This reduction is even more dramatic when a low-modulus material is used in the model .

The major limitations of using structural physical models in a design environment are those of time and expense. In comparing physical models with analytical models, we find that the latter are normally less expensive and faster. One cannot also expect physical models to supplant or replica to analytical modeling of structures when the latter procedure leads to acceptable definition of behavior of the prototype structures. Thus physical models are almost always confined to situations where the mathematical analysis is not adequate or not feasible. Another limiting factor is that changes in the prototype design resulting from the results of a model study may require a second model to check the design. Physical considerations therefore often dictate that the model will be used to verify a "nearly finalized" design .

2.2.3 Factors Affecting the Accuracy of Model Test

Once it has been decided that a model study should be made, the test engineer has the responsibility for planning the fabrication, loading ,and instrumentation of the model, for conducting the test and for interpreting the results in a manner that ensures accuracy commensurate with the project objectives, these factors which affect the accuracy of model tests are :

1) Model Material properties : For problems which are primarily concerned with the behavior at or below service load, the response of concrete masonry structure may often be satisfactorily approximated with a model which is linearly elastic. When considering the behavior of structures at or near to collapse other material properties such as tensile and

compressive strengths, ductility, and possible changes in the elastic constants become extremely significant.

2) Fabrication Accuracy : In small-scale models, there is always the question of how accurately the fabrication process can be controlled. If the model is to appropriately represent a physically larger specimens with the decrease of the geometric size the absolute fabrication tolerances have to be smaller. While it is obvious that there becomes a size below which it just becomes impractical to construct accurate models.

3) Loading Techniques : The success of many experimental studies depends upon how good the loads applied to the model represent the prototype design loads. For example, design loads are often assumed to be uniformly distributed. Reproduction of uniform loads in the laboratory is often not feasible and typically one resorts to a discretized approximation of the desired load. The required number of load points in the discretized system depends not only upon the type of structure but also upon the particular behavior which is being studied.

4) Measurements : The success or failure of any model studies depends directly upon the reliability of the measuring system which is used. The quantities which can be measured do not differ to great extent from those which can be measured in any other structural tests. It is almost always necessary to measure the load even if it consists only of a group of dead weights. Deformations are usually measured either by mechanical devices such as dial indicators or by electrical transducers. Some transducers are sensitive to 0.000001 in. (0.000025 mm) but more commonly least reading of 0.001 to 0.0001 in. (0.025 to 0.0025 mm) with dial indicators are taken. In certain cases with flexible models the reactive force of a dial indicator must not be overlooked. Such forces differ with indicator type and even among indicators of the same type. Forces from one quarter to two pounds (100 to 900 gm) are typical.

5) Interpretation of Results : The test engineer cannot relax his research for accurate, reliable results at the time of testing or during the interpretation of the results. One of the unfortunate aspects of most model study programs is that there is sufficient time and money for only one or a few tests. In order to guard against an erosion of accuracy due to some systematic errors in one or more of the techniques employed, there are no foolproof tactics, however, several "common sense" procedures can usually detect any potential error sources before the results are handed to the client. Examples of "common sense" procedure might include :

a) Calibration procedures prior to testing ,

b) Static checks during and after testing ,

c) Symmetry checks ,

d) Repeatability checks ,

e) Comparisons with analytical predictions ,

f) Observation of trends in the data, e.g., linearity ,

g) Gross behavior observations .

2.2.4 Similitude Requirements

Any structural model must be designed, loaded and interpreted according to a set of similitude requirements that relate the model to the prototype structure. These similitude requirements are based upon the theory of modeling, which can be derived from a dimensional analysis of physical phenomena involved in the behavior of the structure.The most general and useful modeling techniques used in the design and analysis of masonry structures subjected to static and dynamic loads are those which can predict elastic as well as inelastic behavior and have the ability to study with confidence the mode of failure of the structure .

A true or replica modeling (i.e. to produce models which obey all similitude requirements) has to be used. These modeling techniques are based on the choice of model materials and their methods of fabrication. Therefore, the small-scale direct model must

satisfy the similitude requirements of not only the masonry units but also the mortar joints, grout, and reinforcement. Using the theory of dimensional analysis[6&119] the set of necessary scaling model requirements can be derived for masonry. For replica modeling, the similitude requirements can be classified in five distinct categories: loading, geometry, material properties, prediction equation, and design. Based on the assumption of no significant time dependent effects which influence the structural behavior, the pertinent parameters that enter the modeling process in case of static loading are listed in Table 2-1, column (2). For complete similarity of the structural behavior including the inelastic effects of cracking and yielding, a dimensional analysis will give the scale factors shown in Table (2-1), column (4). If the stresses caused by the self-weight of the structure are neglected, as in most cases of load bearing masonry shear walls, the scale factors given in Table (2-1), column (5) will be adequate for modeling masonry structures. For this latter, practically true modeling approach, the stress-strain curves of both model and prototype masonry must be the same, presenting a very difficult challenge to the model analysis. The reason for this is that since masonry element is a composite material, one has to model all of its constituents: block, mortar, grout, and reinforcements. In addition, fabrication difficulties arise because of the small size of the individual units .

2.2.5 Geometric Scale Factor

The choice of a geometric scale factor for a specific type of model is governed by the physical capability of the test facility. In effect it dictates the limit of the model length factor. A very extended research in modeling concrete masonry structures, using a geometric scale factors of three and four have been successfully used at the Drexel University.

Table 2.1 Summary of Scale Factor for Masonry Structures Under Static Loading

Group (1)	Quantity (2)	True Dimensions (3)	Practically Model (4)	True Model (5)
Loading	Concentrated Load, Q	F	$S_\sigma S_l^2$	S_l^2
	Line Load, W	FL^{-1}	$S_\sigma S_l$	S_l
	Pressure, q	FL^{-2}	S_σ	1
	Moment, M	FL	$S_\sigma S_l^3$	S_l^3
Geometry	Linear Dimension, L	L	S_l	S_l
	Displacement, δ	L	S_l	S_l
	Angular Displacement, α	-	1	1
	Area, A	L^2	S^2	S^2
Material Properties	Block, Mortar and Grout Stress	FL^{-2}	S_σ	1
	Block, Mortar and Grout Strain	-	1	1
	Modulus of Elasticity of Block, Mortar and Grout	FL^{-2}	S_σ	1
	Poisson's Ratio, μ	-	1	1
	Specific Mass	FL^{-3}	S_σ/S_m	$1/S_l$
	Reinforcement Stress	FL^{-2}	S_σ	1
	Reinforcement Strain	-	1	1
	Modulus of Elasticity of Steel E_s	FL^{-2}	S_σ	1
Design	Assemblage Compressive Strength	FL^{-2}	S_σ	1
	Assemblage Strain	-	1	1
	Modulus of Elasticity of the Assemblages	FL^{-2}	S_σ	1
	Tensile Strength Normal to Bed Joint	FL^{-2}	S_σ	1
	Tensile Strength Parallel to Bed Joint	FL^{-2}	S_σ	1
	Tensile Strength Diagonal to Bed Joint	FL^{-2}	S_σ	1
	Shear Strength of Bed Joint	FL^{-2}	S_σ	1

S_l = Length Scale ; S_σ = Stress Scale

The choice of this scale factor was primarily based upon the fact that at Drexel University a block-making machine provides units having 1/4 the size of the prototype (8 in. unit) and that an earlier study[119] indicated that the use of scale factors smaller than 1/4 would cause difficulty in modeling the joint thickness and in incorporating representative construction details.

In this investigation, a scale factor of three was used to model the concrete block masonry components and shear walls. The introduction of the larger scale is principally motivated by a need to increase the facility's capabilities, to acquire wider knowledge in modeling masonry structures, and finally to minimize the scale effects and increase the accuracy of the detailing of the model .

2.3 MODEL UNITS

2.3.1 Configuration

The black-making machine shown in Fig. 2.1 was used to produce the 1/3-scale model units in this test program. The configuration of the units used throughout the experimental program resemble the autoclaved concrete masonry blocks and were particularly the standard 6 inch block having 2 cores. The nominal dimensions of these blocks are 6x8x16 inch (150x200x400 mm). The nominal dimensions of the 1/3-scale units 2x2.67x5.33 inch (50x66.67x133.33 mm).

2.3.2 Aggregate Gradation

The type of aggregate used in the block mixture is a river deposit concrete sand found in the local Delaware Valley area (USA). The maximum size to be used in the model concrete block was determined on the basis of similitude and the minimum thickness of the block shells .

Three types of aggregate grading were used throughout this experimental program. These types were chosen to be smaller than the minimum thickness of the face-shells and webs. The maximum particle sizes for the three types were those passing from U.S. sieves

#16, #8 & #4 (1.18, 2.23 &4.75 mm) respectively . The grading curves are presented in Fig. 2.3. These types were found to be satisfactory to use in the model block mixture and complies with the requirements of ASTM C-331[17] , except that passing from U.S. sieve #16 but it could be considered also complies with ASTM requirements after scaling down these limits. The last grading (pass sieve #16) was found to be the best grading for 1/3-scale and was used throughout the construction of the model masonry assemblages and also for model partially reinforced masonry shear walls .

2.3.3 Model Block Mix

The constituents used in the units consists of cementitious materials and aggregate combined with just enough water to achieve complete hydration. In the present study, commercially available type III (high early strength) portland cement ASTM C-150[8] was used in the block mixture as a cementitious material. The maximum size of aggregate used in the model unit was presented in section. 2.3.2 (see aggregate gradation curves in Fig. 2.3) .

Since there were no conventional rules to determine the material proportions for the block mix, different trial design mixes were tested to achieve the desired strength that is convenient and agree with the Egyptian (1100-2000 psi, 80-140 kg/cm^2) and American (2000-4000 psi, 140-280 kg/cm^2) specifications and requirements. A mixture consists of cement : aggregate : water in the ratio of 1: 4.85 : 0.5 respectively, by weight was selected for the model units .

2.3.4 Manufacturing

The 1/3-scale model concrete masonry units were fabricated using the block-making machine shown in Fig. 2.1 . This block-making machine is available at the

Structural Testing Laboratory of Drexel University . The mold was especially designed to fit in the block-making machine for the fabrication of the 1/3-scale model units, this mold can produce five separate block units as shown in Fig. 2.1 .

The production process of the model concrete block units was similar to that used in the production of the full scale units. The procedure of making-mold units is as follows :

Fill the mold with the correct mixture of material, and compact it manually using small rectangular trowel and then vibrate this mixture by a mechanical vibrator which is a part of the block-making machine for a controlled period of time (7 seconds) to ensure a good compaction, this procedure was repeated four times (method1). One more vibration was applied when the mold was turned over (method 2). This caused more compaction and consequently the height of the block decreased (close to 1/3-scale of prototype). A dry lubricant was used to ease the release of the units from the mold during the process. the model blocks were subsequently stripped from the mold box as shown in Fig. 2.4 and then placed in a steam room for curing. At an age of not less than 28 days, the concrete units were removed from the steam room and stored in the Structural Testing Laboratory under controlled temperature and humidity of 70 °F (21 °C) and 50 percent respectively until their use in constructing model masonry specimens .

2.3.5 Physical Properties

The physical properties of the model block units were obtained in accordance with ASTM C-140[22] for weight density, average net and gross areas, average net and gross volume, moisture content, and water absorption .

Three different types(type I, Type II, and Type III) of model units are considered according to the grading of aggregate; for type I all aggregate passing from U.S. sieve #16 were used, for Type II all aggregate passing from U.S. sieve #8 were used, and for Type III all aggregate passing from U.S. sieve #4 were used. For each grading type, the effect of method of vibration (degree of compaction) was taken into account (four and five times of vibrations during making the blocks as mentioned before) to study the effect of

aggregate size and compaction on Absorption and moisture content. Six units were used to determine the average physical properties for each type.

a. Dimensions: Dimensions of the units are obtained according to the ASTM C-140[9] Standard Specification. Six model units from each grading type (aggregate size) were chosen randomly from a sampling of 100 units. These units were measured with a caliper having 0.001 in. (0.025 mm) accuracy. Width, height, and length were measured at mid points and end points of adjoining sides and then averaged. Face-shell thickness was measured along the perimeter of the upper and lower bearing surface. An average measurement was taken for top end webs and also for bottom end webs . Typical cross-section. of the model and prototype units are shown in Fig. 2.5 . A summary of the geometric characteristics of the model and prototype units are presented in Table 2.2. It is worth noting that the width, length, and height were well scaled, but the height for method (1) (four vibration times) was oversized by 4.8 percent . Also central web thickness was oversized by 14.6 percent . All other dimensions were well scaled .

b. Absorption and Moisture Content: The tests for absorption and moisture content were carried out in accordance with the requirements of ASTM C-140[9] . The same six units for each aggregate size used for measurement were also used for absorption and moisture content determination. The average absorption and moisture content were calculated using the mean values of dimensions and weights .

Absorption represents the difference between the wet- weight density and the dry-weight density of the model units. Moisture content is the difference between the sampled-weight and the dry-weight density of the model units .

Procedure of evaluating absorption and moisture content are described below:The test Specimens are weighted first (sampled-weight) and then immerse them in water at room temperature at 60 to 80 °F for 24 hours, weigh the specimens while suspended by a rope and completely submerged in water (suspended immersed-weight). Then remove

Table 2.2 Geometric Characteristics of Model and Prototype Blocks

Description		ASTM Standards	Prototype[1]	1/3-Scale[2]	Model[3] 5 Vib.	Model[3] 4 Vib.
Width , in. (cm)		C-140	5.62 (14.2)	1.87 (4.75)	1.88 (4.77)	1.88 (4.77)
Height , in. (cm)		C-140	7.625 (19.36)	2.54 (6.45)	2.55 (6.47)	2.66 (6.75)
Length , in. (cm)		C-140	15.57 (39.54)	5.19 (13.18)	5.18 (13.15)	5.18 (13.15)
Minimum Face-shell Thickness		C-140				
in. (cm)	at Top		1.20 (3.05)	0.40 (1.02)	0.41 (1.04)	0.41 (1.04)
	at Bottom		1.01 (2.56)	0.33 (0.84)	0.34 (0.86)	0.34 (0.86)
Minimum Central Web Thickness		C-140				
in. (cm)	at Top		1.24 (3.15)	0.41 (1.04)	0.47 (1.19)	0.47 (1.19)
	at Bottom		1.01 (2.56)	0.33 (0.84)	0.34 (0.86)	0.34 (0.86)
Minimum End Web Thickness		C-140				
in. (cm)	at Top		1.30 (3.30)	0.43 (1.09)	0.41 (1.04)	0.41 (1.04)
	at Bottom		1.02 (2.59)	0.34 (0.86)	0.34 (0.86)	0.34 (0.86)
Gross Area , $in.^2$ (cm^2)		C-140	87.54 (565)	9.73 (62.8)	9.74 (62.8)	9.74 (62.8)
Net Area , $in.^2$ (cm^2)	at Top	C-140	49.87 (322)	5.54 (35.7)	5.56 (35.8)	5.56 (35.8)
	at Middle		46.71 (301)	5.19 (33.5)	5.15 (33.2)	5.15 (33.2)
	at Bottom		42.74 (275)	4.75 (30.6)	4.73 (30.5)	4.73 (30.5)
Percent Solid, %	at Top	C-140	56.97	56.97	57.00	57.00
	at Middle		53.36	53.36	52.85	58.85
	at Bottom		48.82	48.82	48.50	48.50

(1) Based on average of six specimens

(2) Scaling of column (1)

(3) Average of six model specimens for each type

specimens from the water and allow to drain for 1 min. by placing them on a 3/8 in. (9.5 mm) or coarser wire mesh, removing visible surface water with a damp cloth and immediately weigh the specimen (wet-weight) . Dry all specimens in a ventilated oven at 212 to 239°F (110 to 115 °C) for not less than 24 hours and until two successive weighings at intervals of 2 hours show an increment of loss not greater than 0.2 % of last previously determined weight of the specimens (dry-weight) .

The absorption and moisture content properties are calculated as follows:

Average Net Area (%) = (F / G) x 100

Net Volume F (ft^3) = B / I

Gross Volume G (ft^3) = (W x H x L) / 1728

Density I (pcf) = { B / (AC) } X 62.4

Absorption (lb/ft^3) = {(A-B) / (A-C)} x 62.4

Absorption (%) = {(AB) / B } x 100

Moisture Content (%) = {(DB) / (AB)} x 100

Where

A = Wet Weight of Unit (lb)

B = Dry Weight of Unit (lb)

C = Suspended Weight of Unit (lb)

D = Sampled Weight of Unit (lb)

H = Height of unit (in.)

L = Length of unit (in.)

W = Width of unit (in.)

The physical properties of the model and prototype concrete block units are listed in Table 2.3. It is worth noting in this Table that the unit weight values of the model units in method 1 (4 vibrations periods) for all types are close to the prototype, on the other hand

in method 2 (4 vibrations periods and one more vibration when the mold is turned upside down) for Type I, Type II, and Type III the density is obviously higher than that of the prototype by about 12, 17, and 22 percent, respectively.

Moisture content for all model units are in general higher than that of the prototype units as indicated in Table 2.3 . The absorption in percentage in method 2 of vibration for model units Type II and Type III is lower than that of the prototype by 3.8 and 9 percent, respectively but for Type I the absorption is approximately the same as the prototype. On the other hand in method 1 of vibration for model units Type I, Type II, and Type III the absorption is higher than that of the prototype by 24, 36, and 42 percent, respectively. The absorption in cubic feet per pound is close to the maximum UBC and ASTM limits listed below for absorption as a the function of the dry density

Dry density (pcf)	Absorption (pcf)
125	13
105 - 125	15
< 105	18

This indicates the feasibility of modeling techniques especially using method 2 of vibration in duplicating the physical properties of prototype units .

Effects of Compaction and Grading on the Water Absorption

As indicated in Table 2.3 for the same grading type, for method 2 of vibration (high compaction) resulted in smaller water absorption. In case of method 2 of vibration (high compaction) the absorption decreases with increasing the grain size. On the other hand, in the case of method 1 of vibration (low compaction) the absorption increases with increasing the grain size. This is attributed to the fact that the water content decreases as the maximum particle size increases and absorption increases as the maximum particle size increases.

When the absorption of the unit is very small no water may be removed from mortar to unit. On the other hand when the absorption of the unit is high, most of the water

would be removed after spreading the mortar on the block. The absorption of the units is very important issue in the behavior of masonry wall because the strength of the mortar depends upon the water to cement ratio after absorption by the blocks

2.3.6 Mechanical Characteristics

a. Compressive Strength

Compressive strength is the most important characteristic of masonry as a loadbearing material. Therefore, to establish the quality of the masonry unit its ultimate compressive strength must be determined. To comply with the requirements of the ASTM Method of Sampling and Testing of Concrete Masonry Units C-140[9], 36 selected units (6 from each aggregate size) were capped with hydrostone gypsum cement at top and bottom as shown in Fig. 2.6. The purpose of capping is to achieve uniform load on the bearing surface.

These model blocks were then tested under axial compression using the 120 Kips (55 ton) Universal testing machine. A steel bearing plate of 2/3 in. (17 mm) thickness, scaled down from the 2 in. (51 mm) thick plate required by ASTM C-140 was employed between 4 in. (102 mm) diameter spherically seated head machine and the top bearing surface of the units . A similar plate was also placed at the bottom of the unit. After centering the bearing surface of the unit with the spherically seated head of the testing machine, a loading rate was applied in a manner to cause failure in 2 to 3 minutes. A typical axial compression test set-up of the model unit is shown in Fig. 2.7a .

The axial compressive strengths of the model units were then calculated on the basis of the average net area (maximum load divided by the average net area). A summary of the axial compressive strengths for each type of model units and prototype are presented in Table 2.3 .

The mode of failure observed for all model units was in general a shear failure along the face-shell of the model units. Fig. 2.7b shows a typical failure mode of the model blocks. The same failure mode was observed by many researchers[21,30,32,52,93&125]

Table 2.3 Properties of Model and Prototype Masonry Concrete Blocks

Description	ASTM Standards	Prototype[1]	Model Type I[2] (5 Vib.)	Model Type I[2] (4 Vib.)	Model Type II[2] (5 Vib.)	Model Type II[2] (4 Vib.)	Model Type III[2] (5 Vib.)	Model Type III[2] (4 Vib.)
Physical Properties								
Net volume, ft^3 (cm^3)	C-140	0.21 (6060)	0.008 (226)	0.0081 (229)	0.008 (226)	0.0081 (229)	0.008 (226)	0.0081 (229)
Gross volume, ft^3 (cm^3)	C-140	0.39 (10930)	.0145 (410)	0.0153 (433)	0.0145 (410)	0.0153 (433)	0.0145 (410)	0.0153 (433)
Absorption,%	C-140	10.8	11.2	13.4	10.4	14.7	9.8	15.4
Absorption, pcf (gm/cm^3)	C-140	11.0 (.176)	12.6 (0.202)	15 (0.241)	11.5 (185)	14.3 (0.230)	10.6 (0.170)	16.0 (0.257)
Unit volume, pcf (gm/cm^3)	C-140	102 (1.64)	115 (1.85)	102 (1.64)	120 (1.93)	104 (1.67)	125 (2.0)	107 (1.72)
Moisture content, %	C-140	6.2	14.8	13.9	16.1	12.2	17.6	11.4
Mechanical Characteristics								
Axial Compressive Strength, psi (kg/cm^2)	C-140	2920 (204)	2800 (195)	1800 (125)	3300 (230)	1640 (115)	3800 (265)	1550 (108)
Splitting Tensile Strength, psi (kg/cm^2)	C-1006	280 (19.5)	282 (19.7)	200 (14)	335 (23.1)	175 (12.3)	380 (26.6)	158 (11)
Ratio of Tensile to Compressive Strength		0.096	0.100	0.111	0.102	0.107	0.100	0.102

(1) Results From Reference [128]

(2) Based on the Average of Six Specimens

for both model and full-scale masonry concrete units . As can be noted in Table 2.3, the compressive strength in method 2 of vibration of the model unit Type I is lower than that of the prototype by 4 percent while model units Type II and Type III showed higher values than that of the prototype by about 13 and 30 %,respectively. On the other hand, in case of method 1 of vibration the compressive strength of all model types is very low as compared to the prototype

The effect of compaction on the compressive strength of concrete blocks was studied.As expected more compaction result in higher compressive strength. It can be noticed from Table 2.3 that the compressive strength increases by about 80-150% with increasing the degree of compaction.

As mentioned earlier two degrees of compaction were considered in manufacturing the model units. For the same degree of compaction (high compaction) it, can be noted that the compressive strength of units Type III (pass sieve #4) is higher than that of both units type II (pass sieve #8) and type I (pass sieve #16) by about 15 and 35 percent, respectively. This agrees with the U.S. Bureau of Reclamation[87] in their specification of maximum particle size where they suggested that, in many cases it is desirable to use the largest maximum particle size of the aggregate permitted by the prevailing circumstances . This largest permissible particle size of the aggregate should not be larger, for instance than one-fifth of the narrowest dimension of the form (in making-blocks 1/5-thickness of the face-shell)

The water absorption is plotted versus the compressive strength of model concrete units in Fig. 2.8. From this figure it is evident that as the water absorption decreases the compressive strength increases for all grading types . This tendency is so remarkable that the water absorption can be considered as one of the estimating scales for the quality of the concrete masonry units .

b. Splitting Tensile Strength

The evaluation of the model splitting tensile strength is of prime importance since it is usually the governing parameter affecting the shear (diagonal tension) behavior of shear

walls. For evaluating the splitting tensile strength of masonry concrete units different testing techniques have been adopted by various researchers[26,32,38,52,93&125] .

The indirect splitting tensile method adopted by ASTM C-1006[32] for splitting masonry concrete units was used in this investigation to determine the splitting tensile strength of model units . Thirty six units (six units from each grading type) were tested under opposite compressive line loads, crossing the face-shells and between the center and end webs as indicated in Fig.9.a . The compressive loads applied to the unit were imposed by means of bearing rods of 1/4 in. (6.35 mm) diameter giving a lateral tensile stress distributed over almost the height of the unit for the split length of the unit. In order to avoid any stress concentration along the line of applied load, a strip of leather 1/4 in. wide by 1/8 in. thick was placed between the steel bar and the block .

The failure mode of the model units was splitting of the face-shells along the vertical plane between the two line loads. Fig. 2.9.b shows a typical mode of failure for units tested under line load. The calculation of the tensile stress at failure is obtained from the following equation

$$f_{bt} = 2P / (\pi A) \qquad (2.1)$$

where

f_{bt} = Splitting tensile strength of the model block

P = Splitting load at failure

A = Net sectional area of the splitting plane

Table 2.3 presents a summary of the splitting tensile strength results for each type of the model units. It is worth noting in this Table that method 2 of vibration the tensile splitting strength of the model units Type I is approximately the same as the prototype, but Type II and Type III have tensile splitting strength higher than the prototype by about 19 and 35 percent respectively. On the other hand in case of method 1 of vibration the tensile splitting strengths of all the model units are significantly lower than that of the prototype .

As apparently shown in Fig. 2.10 the model results appears to be within the variation of the prototype results. Moreover, the splitting tensile strength of model units is approximately five times the square root of its compressive strength ($f_{bt} = 5\ [f_{bc}]^{1/2}$), a fact which agrees with many findings[26,27,37,38] from full scale tests. This indicates that the modeling techniques in predicting the behavior of model blocks under splitting tension is found to be adequate .

The effect of compaction on the splitting tensile strength of concrete blocks was considered in this study. Table 2.3 indicates that for high compaction (method 2) the tensile splitting strength increases with increasing the grain size of the aggregate. On the other hand for low compaction (method 1) the tensile splitting strength decreases with increasing the grain size of the aggregate .

The effect of absorption on the splitting tensile strength of concrete blocks is shown in Fig. 2.11. From this figure it is clear that as the water absorption decreases the tensile splitting strength increases for all grading types . This tendency is so remarkable that the water absorption can be one of the estimating scales for the quality of the concrete masonry units .

2.4 MODEL MORTAR

The use of mortar was the first logical addition to the act of simply piling rock or cut stone one on top of others as was done in the early times. The original purpose of the mortar was to fill the irregularities between masonry units because they were unsightly . It further served to provide resistance to the penetration of light, wind, and water as well as to bond the units together, and possibly to add strength. Cement-lime mortar was used in the construction of the model specimens. The model masonry mortar materials used included portland cement Type III (high early strength) and lime (super limonid, air entertaining). The aggregate used was ordinary mortar sand, the Delaware valley concrete sand was modified by removing the coarser particles larger than sieve #16 (1.1 mm). The method used in scaling the size of the aggregate is to remove the undesired coarse parts of the same sand. This modified shape satisfied the similitude requirements as well as ASTM requirements C-144[12]. Also, these aggregate sizes is appropriate for model joint thickness of 1/8 in. (3 mm) scaled down from the 3/8 in. (10 mm) thickness commonly used in practice. This technique was followed by Harris et al[66] in testing model mortar. They indicated that the volume or the amount of the aggregate has the strongest influence on the model mortar behavior rather than the gradation .

In the present study one type of model masonry mortar was used for the construction of the model test specimens, it was basically a replica of type S mortar indicated by ASTM C-270[13]. Its proportions are listed by volume and representative weight in parentheses in Table 2.4. Proportioning by weight were used during construction instead of volume for better control. According to the requirements of ASTM C-270[13], the content of water should produce a workable mix with the initial flow ranging between 100 to 115 percent .

For quality control of model masonry mortar, two types of control specimens were cast in non-absorbent models. The first were two inch mortar cubes for compression test and the second were cylinders 2 in. diameter by 4 in. height for splitting tensile test.

During the construction of model masonry assemblages six mortar specimens were molded from each type. These control specimens were air cured in the laboratory under the same conditions as the assemblages. From each control specimen type three specimens were tested under compression and the remaining three specimens were tested under splitting tension at approximately the same age as the corresponding model test specimens. Figures 2.12 and 2.13 indicate typical test set-up of the model mortar and failure modes of specimens under axial compression and splitting tension. The compressive strength, the splitting strength, and flow of the model mortar specimens are illustrated in Table 2.5 .

Table 2.4 Proportions of Model Masonry Mortar

Proportions by volume (by weight)			
Cement	Lime	Sand	Water
1	0.5	4	0.993
(1)	(0.213)	(3.83)	(0.993)

Table 2.5 Strength and Flow of Model Masonry Mortar Specimens

Control Specimen Type	Compressive Strength Individual	Mean	Tensile Strength Individual	Mean	Flow
	psi (kg/cm^2)		psi (kg/cm^2)		
Cubes	2070 2310 2370	208 2250 (157)	205 232	215 (15)	116
Cylinders	2035 2140 2280	2150 (150)	255 212 239	235 (16)	116

2.5 MODEL GROUT

Grout is simply a high-slump concrete made with small-size aggregate such as sand and pea gravel. It derives its name from a Swedish term meaning "groot" or "porridge" which provide some indication of its pouring consistency. It must be fluid enough to fill all voids in the grouted space and to completely encase the reinforcement. It serves to: (1) bond the wythes together into a composite element of masonry construction, (2) bond the reinforcement to the masonry so that the two materials will act as something in the nature of a homogeneous material, (3) increase the masonry volume for bearing and fire resistance, and (4) develop continuity to the grouted walls. For reinforced masonry consideration the bonding function is absolutely essential if the desired flexural resistance as well as ductility is to be achieved, since the tensile forces can only be developed by the reinforcement.

The grout used in the construction of the model specimens represents the 1/3-scale replica of coarse grout specified in ASTM C-476[14]. The model masonry grout materials used included portland cement Type III (high early strength), lime, and aggregate. The aggregate used was ordinary sand, the Delaware valley concrete sand was modified by removing the coarser particles larger than sieve #4 (4.75 mm).

In this study one type of model grout was used, normal grout (GN) which satisfy ASTM C-476[14] specifications. Its proportions are listed in Table 2.6 by volume with equivalent weight in parentheses. Water content was used in a manner to provide a workable mix allowing the mixture to flow easily, without separation, into cores or cavities in the masonry assemblages with a minimum of required puddling. The controlling criteria for the fluidity of the grout was a slump of 10 inches (250 mm). The grouted cores were puddled with a steel rod and reconsolidated to provide good compaction of the grout and to ensure good bond between grout and the model units, and also the reinforcement steel (if present).

For quality control of model masonry grout, three types of control specimens were used, the first were block-molded grout prisms with dimensions of 1.25x1.25x2.5 inch

(32x32x64 mm) which gives nearly the same surface area-to-volume ratio as the cell in the block. The masonry surface that will be in contact with the grout was lined with paper towel to prevent bond to between the grout and the prisms. This type of control specimens shown in Fig. 2.14 is specified by ASTM C-1019[15] specification for grout. The second control specimens were prismatic grout cores which were cut from individually grouted model masonry units as shown in Fig. 2.14. It is argued[15] that this technique gives better results for the actual grout strength and water absorption. The grout core dimensions were 1x1x2 in. (25x25x50 mm) . The third control specimens were 2x4 in.(50x100 mm) non-absorbent cylinders for comparison between absorbent and non-absorbent control specimens, Fig. 2.14 shows the block modeling, cylinders, and cored cutted prisms of model grout .

During the construction of model masonry assemblages six grout specimens were molded from each type. All control specimens were air cured under the same conditions as the corresponding assemblages until the time of testing except the individually grouted model masonry units. They were similarly cured until 48 hours before testing, then the cores were cut and tested at the same age of the corresponding specimens. Three of the six specimens were tested under axial compression and the remaining three specimens were tested under splitting tension. Figures 2.15 and 2.16 shown typical test set-up of model grout and failure modes of axial compression and splitting tension, respectively .

In the current investigation, the grout strengths calculated from each type of control specimens were used to observe the difference among them. However, the grout strength calculated from the block-molded prisms is used in the present work as being representative of the grout strength in the blocks. It is used also for correlation purposes with the available prototype results, in which block modeling was used. A summary of the compressive strength , splitting tension and slump results of each type of control specimens are presented in Table 2.7 .

Table 2.6 Proportions of Model Masonry Grout

Proportions by Volume (by weight)			
Cement	Lime	Sand	Water
1	0.1	3.3	0.842
(1)	(0.043)	(2.809)	(0.842)

Table 2.7 Strength and Slump of Model Masonry Grout

Specimen Type	Compressive Strength		Tensile Strength		Slump
	Individual	Average	Individual	Average	inches
	psi (kg/cm^2)		psi (kg/cm^2)		(cm)
Block	4240		505		
Molded	4860	4500	548	515	8.2
Prisms	4400	(315)	492	(36)	(25)
Cut	4760		446		
Prisms	4100	4380	532	510	8.2
	4040	(305)	552	(35)	(25)
Non	3860		535		
Absorbent	4155	4100	578	545	8.2
Cylinders	4285	(287)	605	(38)	(25)

2.6 MODEL STEEL REINFORCEMENT

The technique of modeling small scale steel reinforcement represent probably one of the most difficult tasks in the modeling of reinforced concrete and masonry structures. This is because of the fact that the smallest bar size used is #3 which has a diameter of 0.375 in. (10 mm) and also the number of parameters that need to be scrutinized in order to produce an accurate model are geometry, yield, ultimate strengths, strains, yield plateau, strain hardening, modulus of elasticity and bond similitude. In order to produce protrusion ribs in the bars mechanical deformation technique was used. The mechanically deformed wire technique was initially developed by Harris et al[68] at Cornell University. A model constructed from knurled reinforcement showed a good simulation of the ultimate load. Harris et al[65] have shown through model pull-out tests that it is possible to develop average bond stresses comparable to those of prototype deformed bars. However, it has been shown by Clark[33] that the knurled wire used in flexural members indicates a lack of similitude for crack width, crack spacing, and post-cracking stiffness. This is because the knurled wires have deformations in the shape of internal valleys rather than external protrusions as in the prototype bars. This could result in different bond failure mechanisms in the model and prototype. Later, improvement was introduced at Drexel University by B. Abboud[1] . He produced external protrusions on plain steel wire by pulling it through a power driven knurling machine to which a predetermined clamping force is applied (see Fig. 2.17). The latter is equipped with a set of rollers having internal grooves reproducing the size and shape of the deformations of the prototype bar at the desired scale. Thus for each model size, a different set of rollers was used .

In the current investigation, the approach used in modeling deformed reinforcing bars was to produce bars at 1/3-scale with external protrusion ribs that were geometrically similar to those of prototype deformed bars. A special machine shown in Fig. 2.17 was used to produce model deformed bars. The model deformer machine basically consists of a pair of semi-circular gears driven by a constant speed motor through a gear train with a

load cell attached to the top gear to control the depth of the protrusion ribs. The model steel reinforcement was produced by rolling a smooth wire between the grooves which resulted in the formation of the ribs by the grooved gears. The wire is guided by the sets of grooved rollers installed at the in-feed and out-feed of the grooved gears. For each wire diameter a separate set of grooved gears was used.

Tensile testing of the model bars was conducted using 120 kips (55 ton) Tinius Olsen Universal Testing Machine. A S-1000 Tinius Olsen Electronic Extensometer was used to plot the stress-strain curves of all model bars as shown in Fig. 2.18.

Table 2.8 indicates the geometrical properties of the model bars, and compares them to those of the prototype corresponding
bars, as they are specified by ASTM A-615[10] . As can be seen from this Table , excellent similitude was obtained for all dimensions .

All the rebars (models of #3, #4 & #5) were produced using the method described before. In order to meet the ASTM A-615 specifications concerning the strength characteristics, by achieving a one to one duplication of the mechanical properties of full-scale tests[19,44], the following was decided :

Model #3 Bar : The plain bar, used in this case had an initial yield strength of about 52 ksi (3600 kg/cm^2). After deforming it, its strength reached 68 ksi (4700 kg/cm^2) which is higher than the 56 ksi (3890 kg/cm^2) reported for the prototype bar yield strength. A heat treatment of 750 ^{o}F for 15 minutes, air cooled was carried out to improve the ductility and decrease the yield strength to be close to the yield strength of the prototype bar. A typical stress-strain curve is shown in Fig. 2.19.a .

Model #4 Bar : The plain bar, as it was delivered, had a yield strength of about 71.6 ksi (4975 kg/cm^2) and after deforming it, its strength reached 78 ksi (5400 kg/cm^2) which is too high with insufficient ductility. To lower the strength to the prototype strength level and

to increase the ductility, a heat treatment of 900 °F for 20 minutes with air cooling, was carried out. The typical mechanical properties and the stress-strain curve for a typical specimen are shown in Table 2.9 and Fig. 2.19.b respectively .

Model #5 Bar : The plain bar used had an initial yield strength of about 53.5 ksi (3700 kg/cm^2). After deformation it has an average yield strength of 64.8 ksi (4500 kg/cm^2) which was close to the yield strength of prototype bar. Typical stress-strain curve for model bar is shown in Fig. 2.19.c and Table 2.9 summarizes the mechanical properties .

Table 2.8 Geometric Properties[1] of Model and Prototype[2] Reinforcement

Bar designation		# 3	# 4	#5
Diameter	Prototype	0.375 (10)	0.500 (13)	0.625 (16)
in. (mm)	1/3-Scale	0.125 (3.2)	0.166 (4.2)	0.208 (5.3)
	Model	0.122 (3.1)	0.162 (4.1)	0.192 (4.9)
Cross-sectional area	Prototype	0.1100 (0.71)	0.200 (1.29)	0.3100 (2.00)
in.^{2} (cm^2)	1/3-Scale	0.0122 (0.079)	0.0222 (0.14)	0.0341 (0.22)
	Model	0.0117 (0.076)	0.0206 (0.13)	0.0289 (0.19)
Perimeter	Prototype	1.178 (3.0)	1.571 (4.0)	1.963 (5.00)
in. (cm)	1/3-Scale	0.392 (1.0)	0.523 (1.33)	0.654 (1.66)
	Model	0.383 (0.97)	0.508 (1.29)	0.604 (1.54)

(1) - Based on an average of 3 measurements

(2) - As specified in ASTM A-615

Table 2.9 Mechanical Properties of Model # 3, #4 & #5 Bars

Model	Plain Bar[1]	Deformed[1]	Heat Treat.[1]	Prototype[2]
Model # 3 Bar				
Yield Strength, ksi (t/cm^2)	52 (3.6)	68 (4.7)	57.6 (4)	56.1 (3.9)
Ultimate strength	58 (4)	72 (5)	63.8 (4.5)	81.3 (5.7)
Modulus of Elasticity	-	-	22300 (1560)	23500 (1633)
Yield Strain in./in.	-	-	0.0028	0.0024
Ultimate Strain in./in.	-	-	0.022	0.02
Model # 4 Bar				
Yield Strength, ksi (t/cm^2)	71.6 (5)	78 (5.45)	64.2 (4.5)	66.9 (4.65)
Ultimate strength	76 (5.3)	82.4 (5.75)	69.8 (4.85)	106.5 (7.4)
Modulus of Elasticity	-	-	25400 (1778)	27800 (1932)
Yield Strain in./in.	-	-	0.0025	0.0024
Ultimate Strain in./in.	-	-	0.034	0.028
Model # 5 Bar				
Yield Strength, ksi (t/cm^2)	53.5 (3.7)	64.8 (4.5)	-	64 (4.5)
Ultimate strength	57.2 (4)	71 (4.95)	-	103.4 (7.2)
Modulus of Elasticity	-	27000 (1890)	-	29000 (2015)
Yield Strain in./in.	-	0.0024	-	0.0022
Ultimate Strain in./in.	-	o.039	-	0.03

(1) - Based on an average of 3 specimens

(2) - From Referances [127 & 129]

2.7 CLOSURE

The methodology and techniques of using small scale direct models of masonry component material at 1/3-scale have been presented, along with correlation to available prototype component materials. The physical properties and mechanical characteristics of each model masonry component material, which will be used in this study have also been presented. In manufacturing the model units, the effects of method of vibration and grain size of aggregates on the physical and mechanical properties were investigated. Correlation of the model units and prototype results ranges from excellent to good.

The following conclusions can be drown from the tests of the model material properties :

1- Excellent correlation between model and prototype results in predicting the mechanical properties of masonry concrete blocks in terms of overall behavior is achieved. The modes of failure of model concrete blocks tested under axial compression and splitting tension matched the prototype failure modes very well. The tensile strength of prototype was found to be between four to seven times the square root of its compressive strength, and this was also observed in the current model results. The compressive and splitting tensile strength results of model masonry units fell within the range of prototype results especially for method 2 of vibration. Based on these observations, it is concluded that the modeling techniques are capable of predicting the mechanical and physical properties of masonry blocks .

2- The grain size of the aggregate for the same degree of compaction has a significant effect on the absorption, compressive strength, and splitting tensile strength of model concrete blocks .

3- In making model blocks, the last vibration period when the mold is turned down has a significant effect on the physical and mechanical properties of model concrete blocks. Method 2 of vibration (high compaction) yielded the smaller water absorption and larger compressive and splitting tensile strengths values compared with method 1 of vibration.

4- Strong correlation exists between water absorption of model units and mechanical

properties. As the water absorption decreases the compressive and tensile splitting strength increases. Therefore water absorption can be considered one of the estimating scales for the quality of the concrete masonry unit .

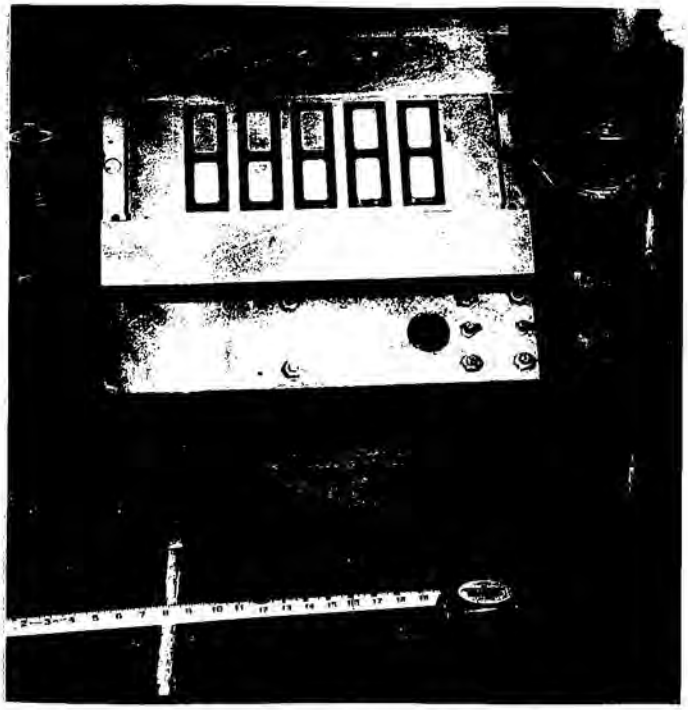

Fig. 2.1 Block-Making Mashine

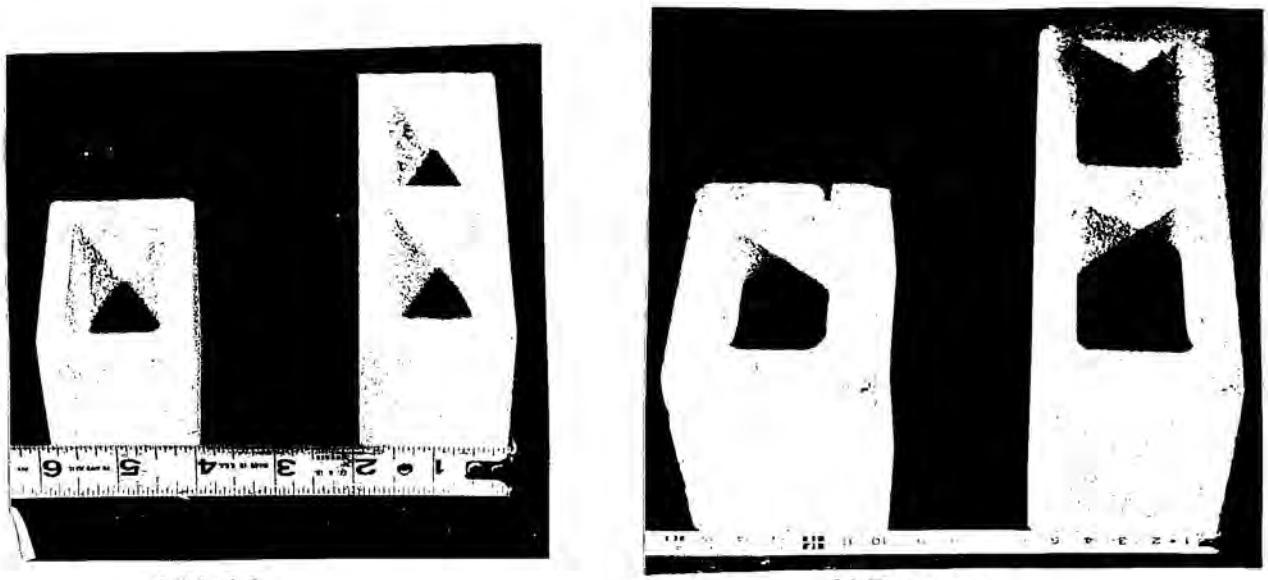

a) Model

b) Ptototype

Fig. 2.2 Photographs of Model and Prototype Units

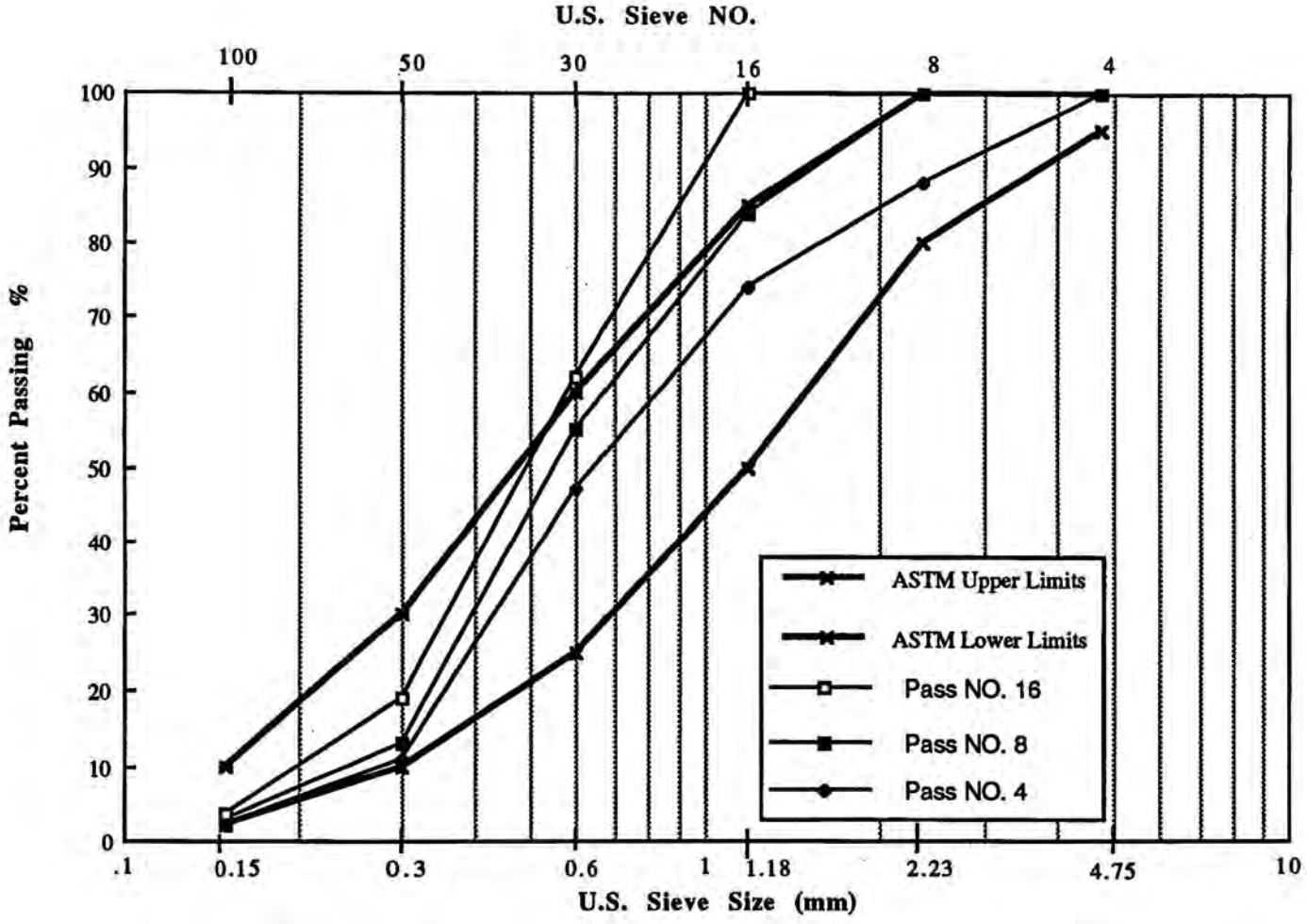

Fig. 2.3 Aggregate Gradation Curves For Model Concrete Block Masonry

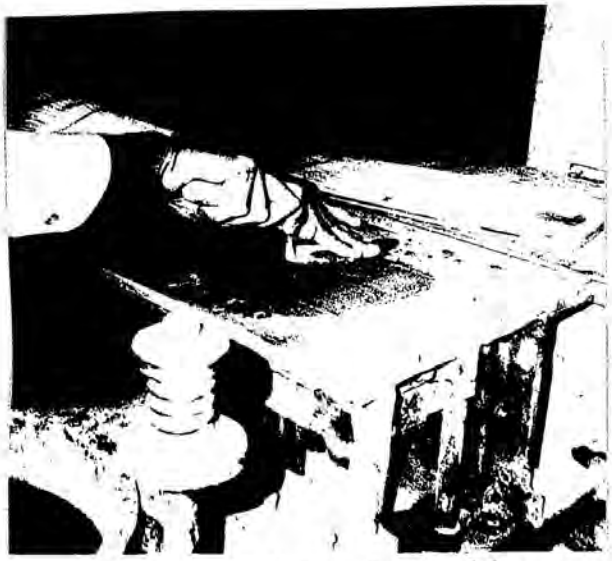

a) Hand compaction of the dry mix into the mold

b) Smoothing of the top surface

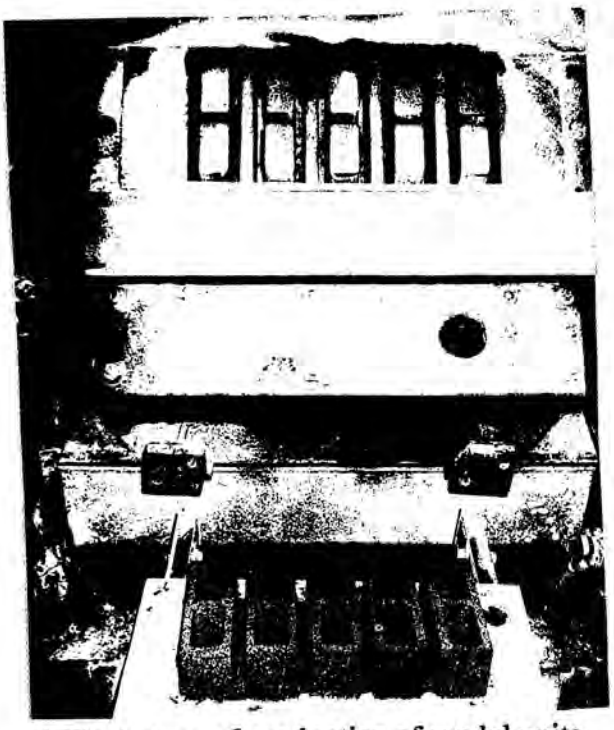

c) Final stage of production of model units

Fig. 2.4 Procedure for Manufacturing Model Blocks

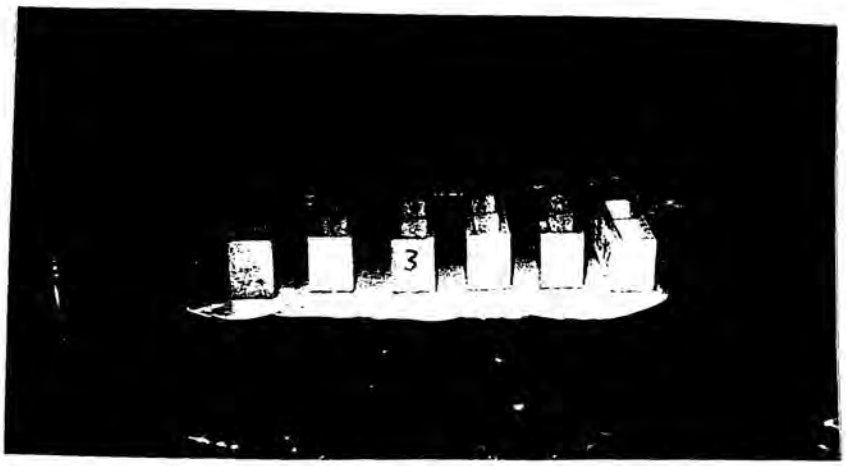

a) Capping of the bottom surface

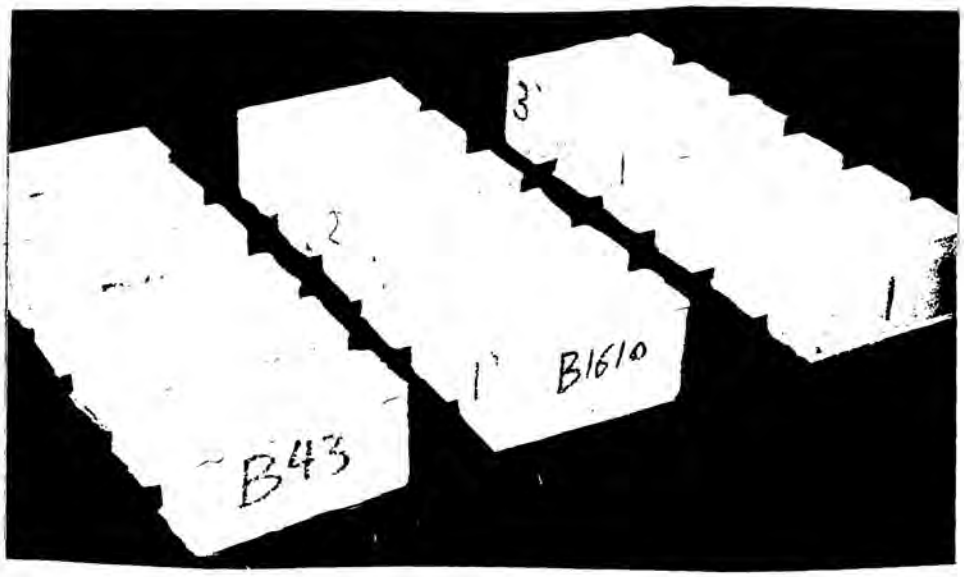

b) Blocks after capping

Fig. 2.6 Capping Blocks

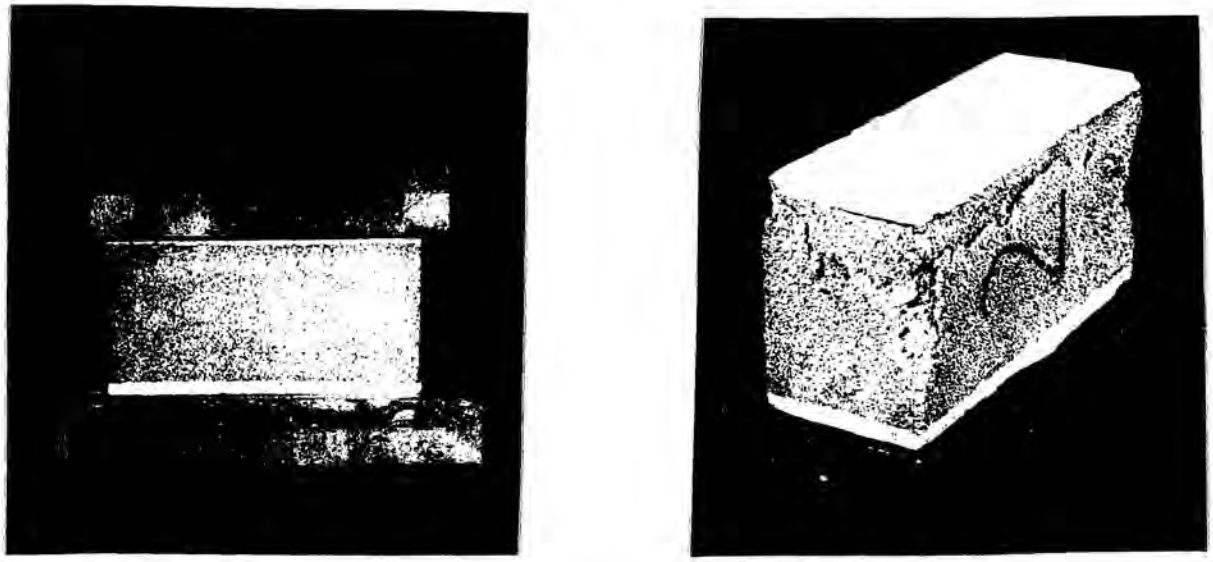

a) Test set-up b) Failure mode

Fig. 2.7 Model Blocks Under Axial Compression

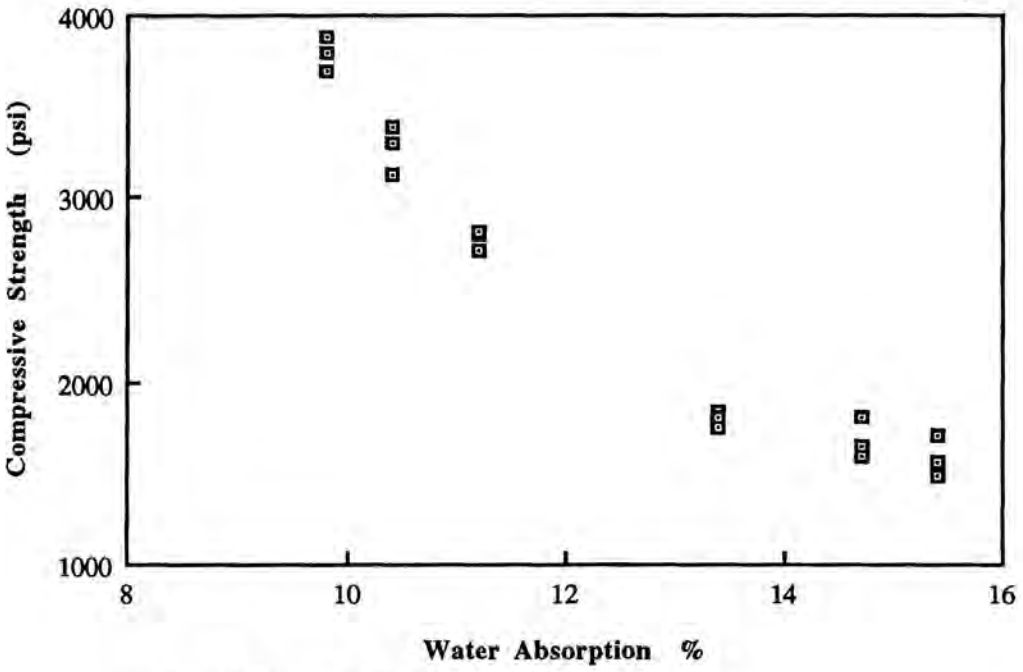

Note: 100 psi = 7 kg/cm2

Fig. 2.8 Effect of Water Absorption on the Compressive Strength of Model Units

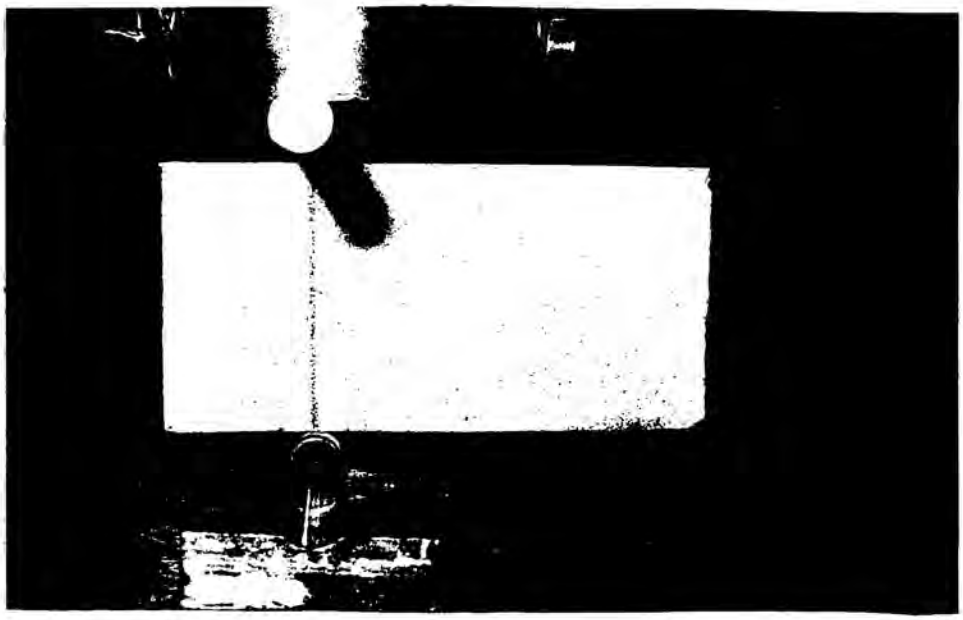

a) Test set-up

b) Failure Mode

Fig. 2.9 Model Blocks Under Splitting Tension

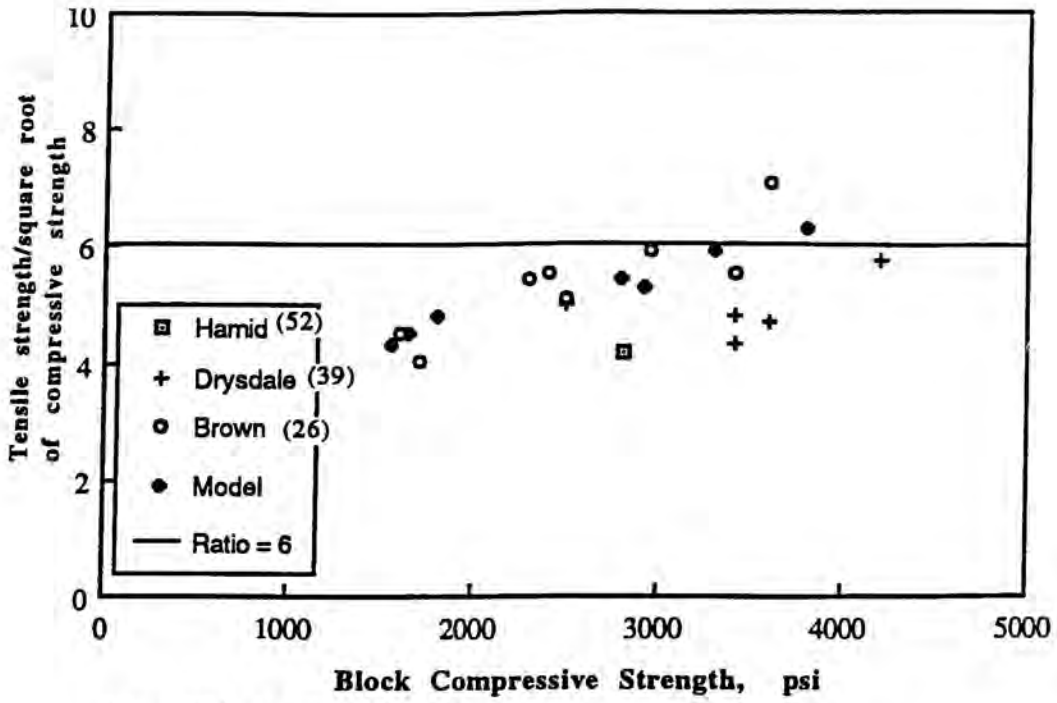

Note: 100 psi = 7 kg/cm2

Fig. 2.10 Comparison Between Model and Prototype Block Tensile Strength

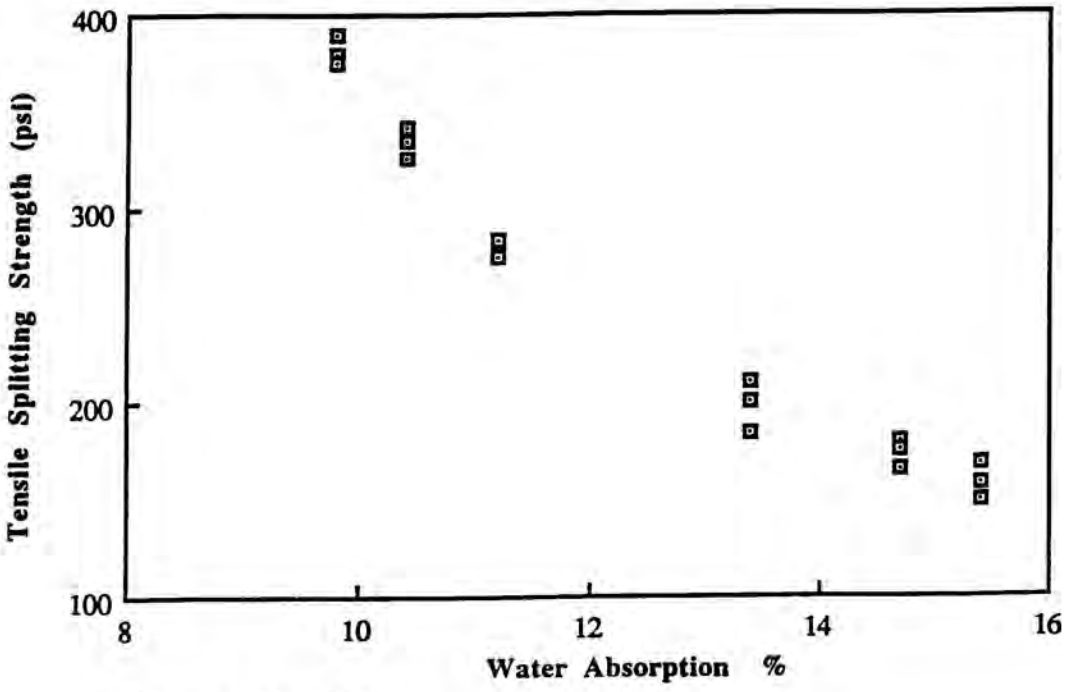

Note: 100 psi = 7 kg/cm2

Fig. 2.11 Effect of Absorption on the Splitting TensileStrength of Model Units

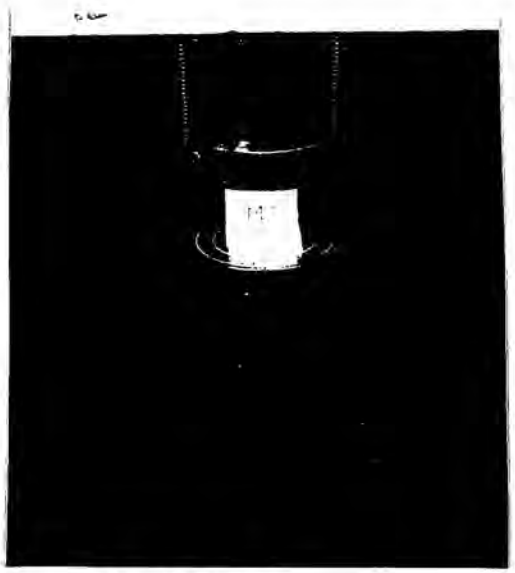

a) Test set-up

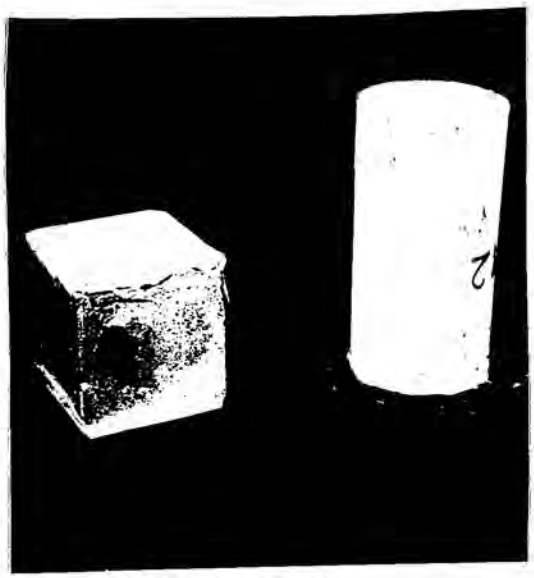

b) Failure Mode

Fig. 2.12 Model Mortar Under Axial Compression

a) Test set-up

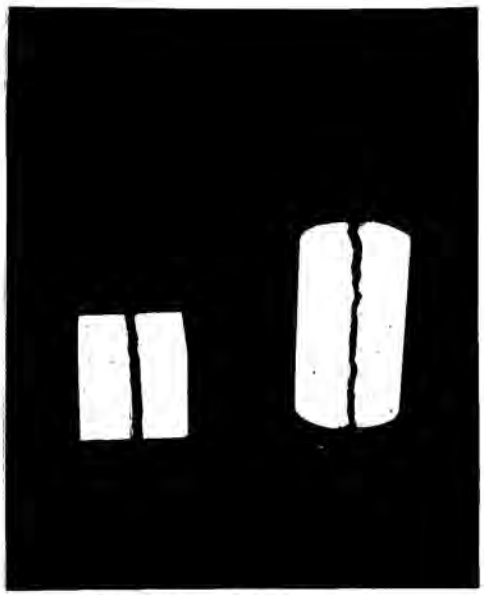

b) Failure Mode

Fig. 2.13 Model Mortar Under Splitting Tension

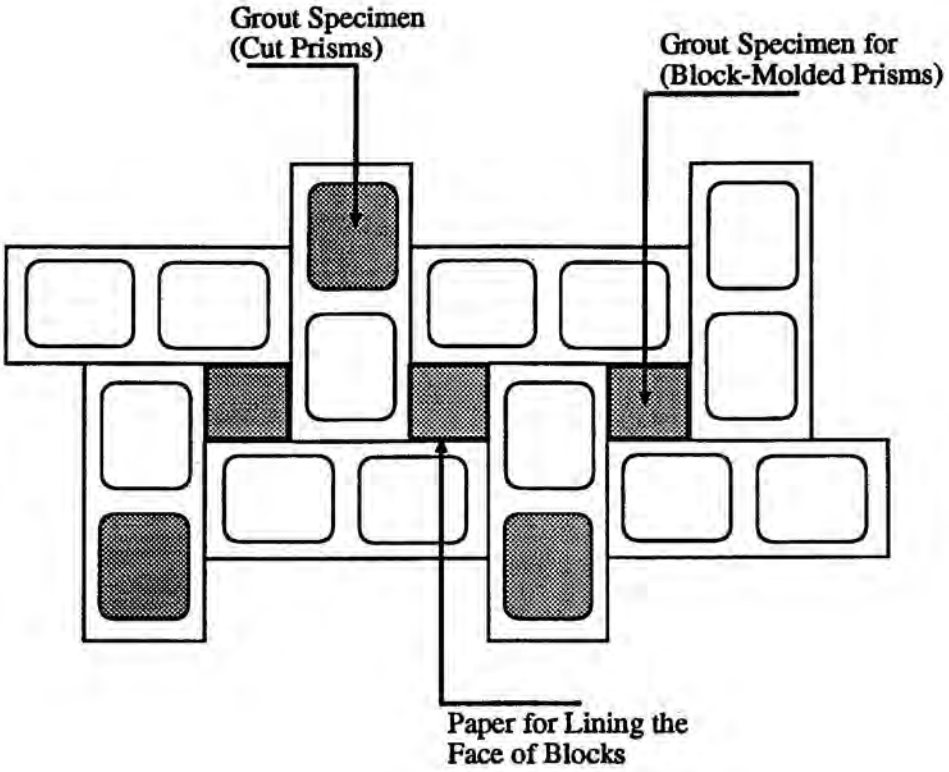

Fig. 2.14 Block-Molded Specimens for Grout

a) Test set-up

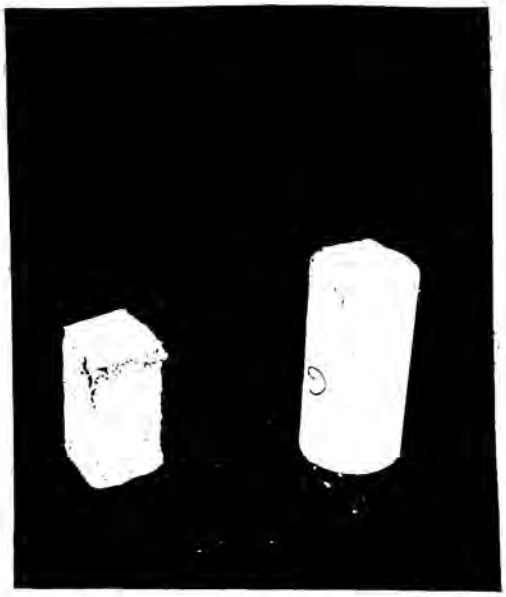

b) Failure Mode

Fig. 2.15 Model Grout Under Axial Compression

a) Test set-up

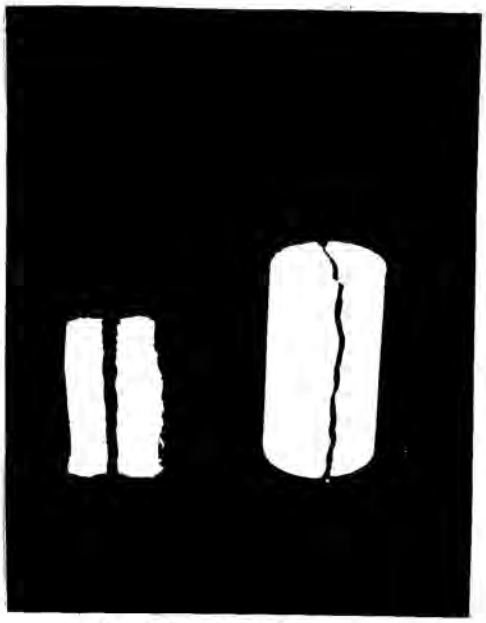

b) Failure Mode

Fig. 2.16 Model Grout Under Splitting Tension

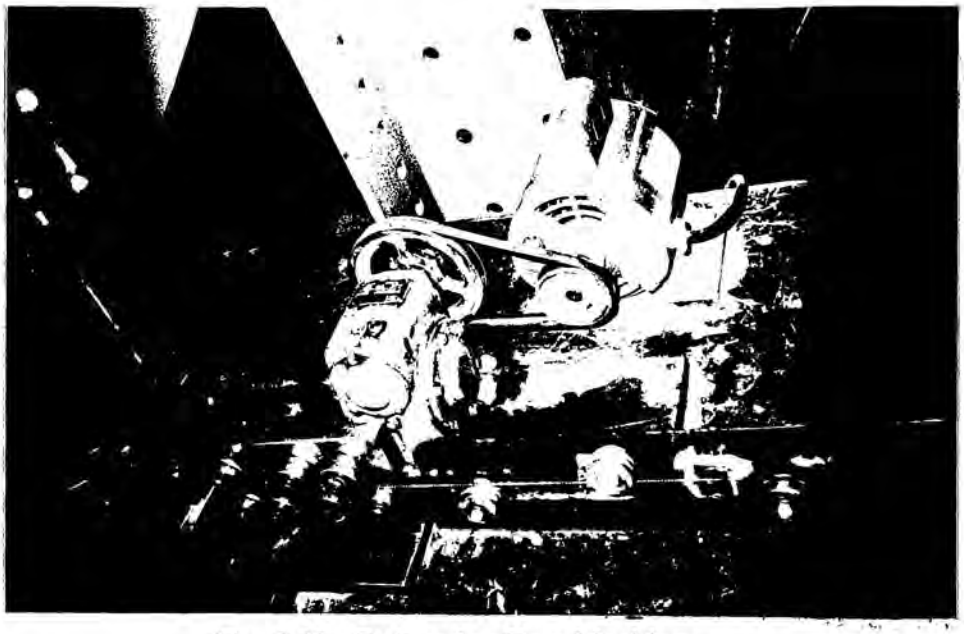

Fig. 2.17 Deforming Bars Machine

Fig. 2.18 Tensile Testing of the Model Bars

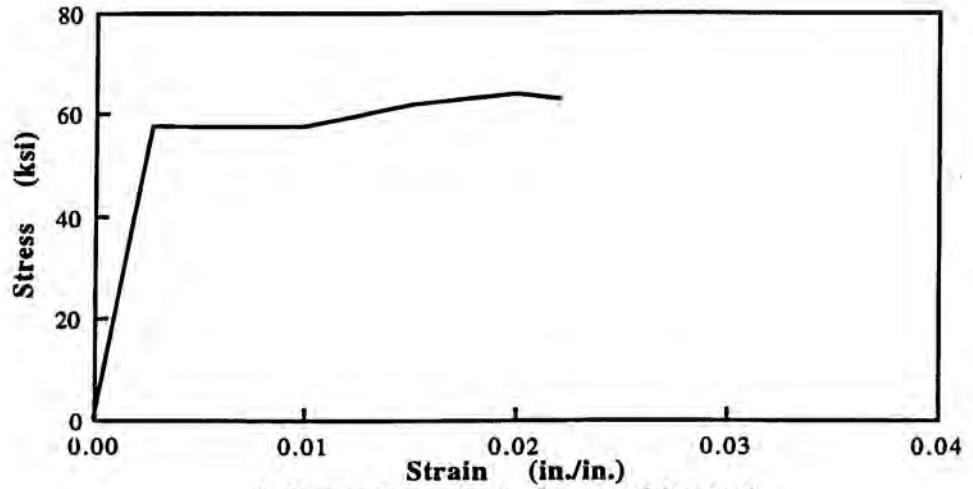

a) Typical Stress-Strain Curve for Model # 3

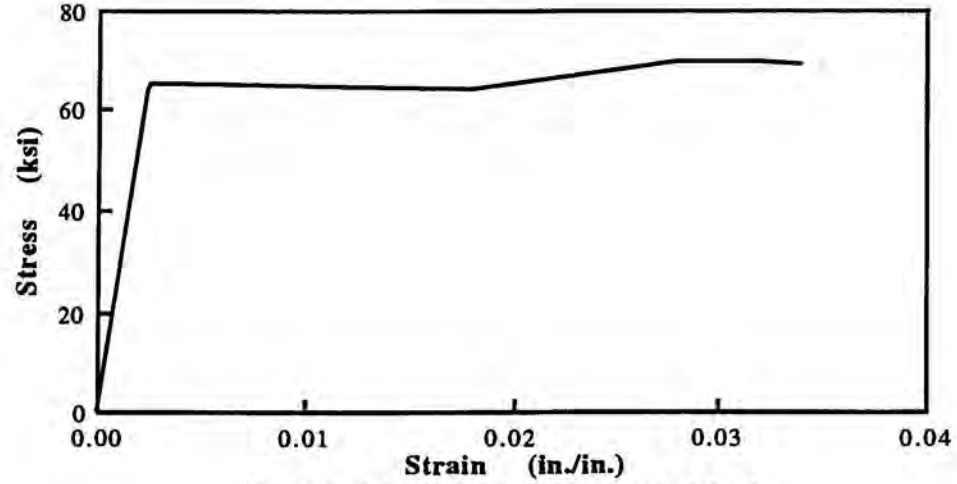

b) Typical Stress-Strain Curve for Model # 4

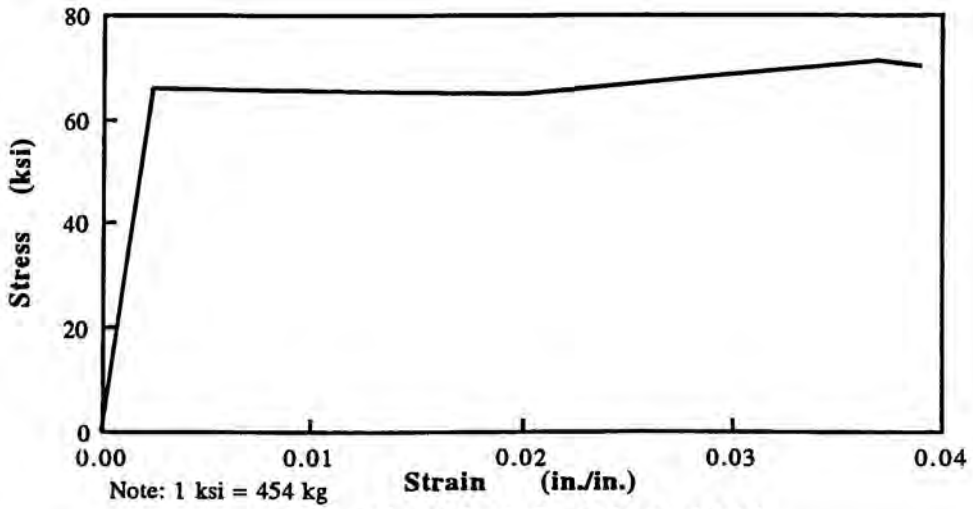

c) Typical Stress-Strain Curve for Model # 5

2.19 Stress-Strain Curves for Model Reinforcement

CHAPTER 3
ASSEMBLAGE PROPERTIES

3.1 INTRODUCTION

Generally, there are two possible modes of behavior that can be identified for masonry shear walls as indicated in Fig. 3.1. One is the flexural mode of failure which is characterized by the tensile yielding of the vertical steel, debonding of the bed joints at the tension side due to tension normal to the bed joints (splitting tensile strength) and compressive crushing of masonry at the toe of the wall (axial compression). The other mode is the shear mode of failure which is characterized by diagonal tensile cracking (splitting tensile strength and Joint shear). Therefore, the importance of studying and understanding the behavior of small assemblages under axial compression, joint shear and splitting tension can be recognized.

Masonry is a composite material made of units, mortar, grout and reinforcement. The interaction of these component determines the characteristics of masonry[24,30,32,48,52,70&125]. The compressive, bed joint shear, and splitting tensile tests with different load/bed joint orientations of small assemblages are commonly used to constitute the basic tests for determining different properties. A thorough knowledge and understanding of the behavior of the component materials will aid the researchers in understanding the behavior of wall panels subjected to more complex loading conditions. The basic tests are also important in that they provide practical methods for quality control by measuring the integrated effect of any variation in component materials by using small-scale modeling technique (Chapter 2).

In this experimental program, it was not feasible to model each components in the assemblages on a one-to-one basis. Each assemblage was modeled from the geometric characteristics of the prototype assemblage and the results of the model tests are briefly correlated to the available prototype results of failure modes and strength characteristics.

3.2 AXIAL COMPRESSION

3.2.1 General

The masonry has been traditionally used as a loadbearing material capable of transferring gravity loads to the foundation. This has made the topic of axial load bearing capacity of masonry walls the subject of extensive experimental research for many years. The need to determine allowable stresses in shear and tension might be also expressed in terms of the specified compressive strength (f'_m). The compressive strength of masonry could be evaluated either by a prism test or from tables that relate f'_m to the strength of the component masonry units and mortar type. However, the prism test is becoming the universal standard method in establishing the compressive strength of masonry and in predicting the failure mode of masonry structures under different loading conditions. Prism construction should reflect the masonry to be used in a building. This implies similar workmanship, joint thickness, bond pattern, thickness of the wall and curing .

In the current program, the prism test is chosen to examine the adequacy of modeling techniques in predicting the behavior and strength of masonry walls under axial compression .

The method used to determine the compressive strength of masonry assemblages complies with ASTM E-447[16] requirements. These methods specifies prisms with the length equal to or greater than the thickness of the prism and the height is at least twice the thickness, containing a minimum of two bed joints. These methods are recommended by various investigators[25,32,52&125] who reported that the compressive strength of concrete masonry may be evaluated using prisms with not less than two nor more than four mortar bed joints and also recommended that the compressive strength of prisms is primarily a function of the number of bed joints not the h/t ratio. Hegemier et al[70] investigated the influence of prism height, platen restraint, mortar strength, mortar joint thickness, bond pattern, and bearing plates on prism compression behavior. They observed that bond

pattern and platen restraint have a significant effect on prism strength and also observed a significant influence of prism height on strength and strain at peak .

A number of studies[24,30,52&125] have been undertaken to examine the behavior and factors influencing grout concrete masonry under uniaxial compression, and the interaction between grout, block, and mortar, from different view points. Some of their observations were that the geometric configuration of the vertical cross-sectional shape of block has a significant effect on the compressive strength of grouted prisms, on the other hand Hamid[26] showed that the horizontal shape of the block's cross-section has no significant influence on both the behavior and strength of grouted prisms.

Some attempts have also been made using finite element techniques for the purpose of studying the behavior and developing empirical formulas which can be used to predict compressive strength of concrete masonry[30&52] .

The Uniform Building Code[141] UBC-1991, Section 2405C, recommends a prism not less than 12 in. (300 mm) high with a height thickness ratio (h/t) of not less than 1.5 nor more than 5.0 . The values of f'_m are determined by multiplying the prism strength by a specified correction factor in terms of h/t in an attempt to normalize the compressive strength f'_m of concrete masonry to h/t ratio. These correction factors are given in Table 3.1 (comparison of code correction factors) .

The ASTM E-447[16] specify two different methods for determining f'_m of masonry. Method A is used to determine the compressive strength of masonry prisms built in the laboratory. This method specifies prisms of (h/t) ratios of 2 to 5 with correction factors for slenderness effects. Method B is used to determine the compressive strength of masonry prisms built at the job site. This method specifies prisms containing at least two mortar bed joints and a minimum of 15 in. (375 mm) high. Method B of ASTM E-447 seems to be more realistic than method A because it is more widely recommended by various investigators[24,52,70&125] who reported that 3 courses prisms minimize end platen effect and provide more realistic splitting mode of failure. Therefore, the three courses prism as

shown in Fig. 3.2 (2 bed joints) which has h/t = 4.2 was selected in this work to model the prototype at 1/3-scale because it gives more realistic results and allow adequate representation of the interaction of the mortar and the units .

Table 3.1 Comparison of Code Correction Factors

Source	h/t						
	1.5	2.0	2.5	3.0	4.0	5.0	6.0
UBC[141]	0.86	1.00	1.11	1.20			
Canadian Code[27]	0.86	1.00	1.11	1.20			
Australian Stand.	0.85	0.93	1.00	1.10	1.16	1.16	
New Zealand Stand.[136]	0.85	1.00	1.11	1.20	1.33	1.42	1.50
N. B. of Standard	0.85	1.00	1.11	1.20			
ACI 530.1/ASCE[2]	0.75	1.00	1.08	1.16	1.25		

3.2.2 Variables Affecting Prism Compressive Strength

There are two broad group of variables that affect the prism compressive strength[47]. The first group is the factors which interact to modify the stress pattern in prisms under test and lead to apparent masonry strength which differ from the results obtained on full size samples . These factors comprise prism shape or geometry, prism capping and type of masonry bond . The second group is the factors which interact to determine the actual mechanism of failure of the prism, these include unit strength, mortar, grout ,the joint thickness and workmanship.

Most of these factors were examined by many researchers[26,27,30,48&49]. However in this experimental program only the effects of block strength and grouting on the prism compressive strength were taken into consideration.

3.2.3 Objective of the Test Program

The main objective of prism tests are:

1- To determine the axial compressive strength of ungrouted (hollow) and grouted concrete masonry prisms.

2- To define the strength variation between model prisms of different block strengths.

3- To investigate the crack patterns, failure mode, deformational behavior and strength characteristics (initial and secant modulus of elasticity and strain at peak) for blocks of different strengths.

4- To establish correlations between the model and available prototype data.

3.2.4. Model Prism Specimens and Fabrication

A total of nine ungrouted and grouted 1/3-scale model prism were constructed in running bond using two full model units and two half model units for each prism (one unit long and three courses high) as shown in Fig. 3.2 with mortar face-shells bedded. The half model blocks were obtained by cutting the full model blocks with an electrical diamond edge saw. The bonding material used is Type S mortar for the construction of all model prisms. Two different block strengths were used for the model prisms. The first one has a net compressive strength value f_{b1} of 2800 psi (200 kg/cm^2), three ungrouted and three grouted prisms which represent a typical strength values in the United States and the second one has a lower compressive strength value f_{b2} of 1800 psi (125 kg/cm^2), three ungrouted and three grouted prisms which represent a typical strength values in the Arab Republic of Egypt. Details of the block units, mortar, and grout properties are presented in Chapter 2 . The construction of the prisms was identical to the one used in the field. They were built by an experienced and qualified mason, using a wooden plate, a small

rectangular trowel, and a spirit level. The construction procedures were simple and straight forward; the model units were placed flush on the wooden plate, mortar was then troweled all around the top of the outer shell of the unit. A unit was placed with firm pressure on top of the mortar, causing excess mortar to squeeze out of the joints. Gentle tapping with the trowel handle was sometimes required to further consolidate joints to the required 1/8 in. (3 mm) thickness and to ensure horizontal laying of the units. The final horizontal and vertical alignment was established by using a spirit level. Excess mortar around the joints was cleaned from the sides during construction. After being cast, joints were flushed from all sides. Care was taken to insure complete joint filling.

After 24 hours three prisms from block units which have f_{b1} strength were grouted. The grout was well puddled using an aluminum bar . All specimens as indicated in Fig. 3.3 were air cured under a controlled temperature of 70° F (21° C) and a humidity of 50 percent in the Structural Testing Laboratory, Department of Civil Engineering Drexel University .

Control specimens were made along with the construction of the model masonry prisms and were air cured in the laboratory under the same conditions as the corresponding assemblages. Two inch (50 mm) cubes and 2x4 in. (50x100 mm) cylinders, using six specimens from each type of control specimens were adopted as control specimens to determine compressive and tensile splitting strengths of type S mortar. For grout, three types of control specimens were used, block-molded grout prisms, cylindrical grout cores, and non-absorbent cylinders were fabricated along with the construction of model prisms using six specimens from each type of control specimens (the details of control specimens for model grout and mortar presented in chapter 2) .

3.2.5 Testing Procedure and Instrumentation

At the age of 28 to 40 days from fabrication the model prisms were capped using hydrostone gypsum plaster (ASTM C-447[16]) at top and bottom to achieve uniform load on the bearing surface (as shown in Fig. 3.3) and after 24 hours from capping they were

tested under axial compression. The load was applied uniformly in a constant intervals at the centroid of the face-shell area of the ungrouted prisms and at the center of the gross area of the grouted prisms, using a 120 kips Tinius-Olsen machine. A steel bearing plate 2/3 in. (17 mm) thick, satisfying the scaled down ASTM C-140 requirements, was placed between the 2 in. (50 mm) diameters spherically seated head block and the specimen .

Dial gages were attached to the face-shells on a stiff aluminum brackets using crazy glue as shown in Fig. 3.4. This is used for the measurement of the deformations in the vertical direction. Typical test set-up is shown in Fig. 3.5. The loading rate varied depending upon the specimen being tested with failure occurring in two or four minutes. The instrumented specimens, were loaded at a slower rate to permit the recording of the load increment and deformation data. The axial strain was calculated by dividing the average deformation readings by the initial distance between the attached aluminum brackets. The stresses were computed by dividing the load by the net area for ungrouted prisms and the gross area for grouted prisms .

3.2.6 Results and Discussions

Modes of Failure In Fig. 3.6 photographs of typical failure of the ungrouted prisms for each type of block strength (f_{b1}, f_{b2}) are shown. The mode of failure for the prisms having block strength f_{b1} was a vertical tensile splitting originated in the middle block away from the effect of platen restraint as indicated in Fig. 3.6.a. The vertical splitting of the prisms are related to the lateral strain of the mortar joints[52]. The modulus of elasticity of the mortar is lower than that of the block . Therefore, its free lateral deformation is substantially greater than that of the block assuming that poisson`s ratios are the same. Because the block at the mortar interface must undergo the same lateral expansion as the mortar, due to friction and bond, the lateral expansion of mortar is restrained producing tensile strain in the block units causing splitting failure under a tension-compression state of stress . On the other hand, the mode of failure for prisms which have block strength f_{b2} (smaller than the compressive strength of the mortar) was a shear failure for the units as shown in Fig.

3.6.b. The reason for such type of failure is that the compressive stress applied to the mortar is smaller than uniaxial compressive strength of the mortar and its lateral expansion is very small, hence the units reached full capacity and failed in shear before the tensile stress occurs .

For the model grouted prisms, the mode of failure was shear failure with tensile diagonal cracks crossing grout and units. A typical mode of failure for grouted prisms is shown in Fig. 3.7. The consistent mode of failure could be characterized as tensile splitting of the outer shells and compressive failure of the grout cores for both types of block strength. Because of the high lateral inelastic deformation of both the mortar and grout at high stress levels splitting failure of the shells occurred. The failure also originated in the central blocks free from the end confining effects. In addition, the grouted prisms showed a more gradual failure compared to the ungrouted prisms which showed sudden and explosive failure .

Effect of Block Strength The test results of Table 3.2 clearly indicate that block strength significantly affect prism strength. Since, the mode of failure is a tensile splitting of the outer shells of the units, as expected the compressive strength (f'_m) increases with the increase of the block strength. It can be noted that an increase of 55% in the block compressive strength results in a 64% increase of the prism strength which agree with results of other researchers[39,52,85&90].

The compressive strength of grouted prisms for model and prototype[56] having approximately the same grout strength (4500 psi = 315 kg/cm^2) were plotted against block strength as shown in Fig. 3.8. As clearly shown, for both model and prototype as the block strength increase the prism strength increases. It can be also observed that the block strength is the most important parameter affect on the prism compressive strength. Therefore, recent provisions for concrete masonry[2,27&141] values for the specified compressive strength f'_m which are based on the compressive strength of block and on the type of mortar .

Table 3.2 Charactersitics of Prism Compressive Strength

Type of Model Prisms	f_b [1] psi (kg/cm^2)	f'_m [2] Individual psi (kg/cm^2)	f'_m [2] Average psi (kg/cm^2)	E_{ini} [3] ksi (ton/cm^2)	E_{sec} [4] ksi (ton/cm^2)	ε_{ult} [5] %	E_{ini}/f'_m	E_{sec}/f'_m
Ungrouted (f_{b1})	2800 (195)	2180 2290 2430	2300 (155)	1980 (138)	1860 (130)	0.198	840	790
Ungrouted (f_{b2})	1800 (125)	1270 1420 1510	1450 (100)	1480 (103)	1360 (95)	0.228	1060	970
Grouted (f_{b1})	2800 (195)	2785 2905 3010	2900 (200)	2630 (184)	2360 (165)	0.216	910	815
Grouted (f_{b2})	1800 (125)	2250 2010 2190	2150 (150)	1920 (133)	1810 (126)	0.207	890	840

(1) Compressive Strength of Blocks Based on Net Area of Units
(2) Mean Compressive Strength of Prisms Based on Net Area of Ungrouted Prisms and Gross Area of Grouted Prisms
(3) Mean Initial Modulus of Elasticity at 5% and 33% of Maximum Compressive Strength of Prism
(4) Mean Secant Modulus of Elasticity at 50% of Maximum Compressive Strength of Prism
(5) Mean Strain at Maximum Compressive Strength of Prism

Effect of Grouting The axial compressive strength, f'_m of the model concrete masonry prisms was computed on the basis of the net area for ungrouted prisms and gross area for grouted prisms.

Priestley[110] presented an empirical formula based on experimental data, for predicting the strength of grouted masonry f'_m in terms of unit strength, percent solid and grout strength as follows:

$$f'_m = 0.59\ \phi\ \beta\ \sigma_{cb} + 0.9\ (1 - \beta)\ \sigma_{cg} \qquad (3.1)$$

where

σ_{cb} = Unit compressive strength

σ_{cg} = Grout compressive strength

ϕ = Strength reduction factor

β = Percent solid

From this Equation it can be noticed that the grouting and grout strength have a significant effect on the strength of grouted masonry (see Fig. 3.9).

The compressive strength of grouted prisms for different grout strength were calculated using Priestley's Equation. The calculated values were plotted against grout strength along with the experimental prototype results of Assis[56] and model results as shown in Fig. 3.9.

Compressive strengths of model prisms and companion mortar and grout control specimens are summarized in Table 3.2. The compressive strength of hollow prisms is lower than the compressive strength of model grouted prisms for the same block strength by approximately 26 percent. Therefore the compressive strength of model grout had

effected the compressive strength of model specimens which agree with various researchers findings[52,70,77&125] . It is worth noting that little increase in prism strength was achieved with large increase in grout strength. This indicated that the strength superposition concept highly overestimates the compressive capacity especially for high strength grout. This is because the lateral tension caused by grout tends to reduce the capacity of the prism than that calculated by superposition .

It is suggested[39&52] that at high stresses in the grout, the resulting inelastic deformation in the horizontal direction (due to the development of microcracking) produce higher bilateral tensile stresses in the outer shell as it tends to confine the grout. These tensile stresses in combination with the vertical compressive stress could be the cause of a premature splitting failure of the model blocks under a state of biaxial compressive tension stress. Hamid[52] found, that at any strain level, the load will be shared by the shell and the grout cores in proportion to their axial stiffness (compatibility of deformation in the vertical direction) . At a strain nearly equals to 0.002 in./in. the grout would reach its unconfined strength, then high lateral deformation occurs. At each strain level, the unit is able to accommodate more load, and therefore it acts to confine the grout. Failure occurs when the units are no longer capable of confining the grout (and the mortar as well) .

Deformation Characteristics of Model Prisms The axial deformation characteristics of ungrouted and grouted model prisms are illustrated in the stress-strain relationship curves shown in Fig. 3.10 . Each curve represents the average of three model prisms test results. It can be noted from this figure that the axial stiffness of grouted prisms is higher than that of ungrouted prisms and the axial stiffness of prisms that have block strength f_{b1} is higher than that of prisms that have block strength f_{b2}. Key deformation indicators are presented in Table 3.2 was derived from the stress-strain relationship curves. As it can be noted from the table for prisms that have block strength f_{b1} the peak strain (ε_{ult}) ranged between 0.00198 in/in (for ungrouted prisms) and 0.00216 in/in (for grouted prisms). The initial

modulus of elasticity E_{ini} varied between 840 f`m to 910 f'$_m$.

The secant modulus of elasticity E_{sec} between 5% and 33% of the peak compressive stress varied between 790 f'$_m$ to 815 f`m which agree with prototype results of Hamid[52] .

3.2.7 Correlation With Prototype Results

The axial compression test results of 1/3-scale model concrete masonry prisms were presented in this chapter. Correlation between model and prototype tests conducted by many investigators[24,52,85,110&125] on full-scale concrete block masonry under axial compression are described below :

The failure mode of ungrouted and grouted prisms as was described by Hamid et al[39] for full-scale blocks, is a splitting type of failure in the central block away from plate restraints. A similar mode of failure was observed in the model ungrouted prisms. On the other hand, the model grouted prisms had a shear or diagonal tensile failure through the face-shell of the block. This mode of failure was recognized by Boult[24] and Self[125] . Whereas the mode of failure for prisms having block strength f_{b2} (lower than the strength of mortar) is a shear failure ,therefore prototype failure mode was well duplicated by the model compression specimens using blocks f_{b1} .

The variation of compressive strength of model prisms with the grout strength is shown in Fig. 3.9 along with the prototype results of Hamid et al[39] and Priestley[110]. It can be noted from this figure that grouting had increased the compressive strength of model prisms, when the grout has a strength exceeding the unit strength. The model results showed a very good correlation with prototype results which were reported by Self[125] and Kingsley[85] . However prototype results by Hamid showed a decrease in prism strength with the addition of grout. Even when grout strength exceeded the unit strength, data indicated a loss of strength with grouting. The model results are also compared with the

recommended equation by Priestley[110] for estimating masonry strength f'_m .The results of the comparison is shown in Fig. 3.9 . As clearly shown in this figure , Priestly equation underestimates the model compressive strength by 6.8 percent. In general, the model results appears to be in a reasonable agreement with Priestly equation and also are in agreement with the results obtained by Kingsley[85] .

The variation of compressive strength of model prisms in terms of unit compressive strength is indicated in Fig. 3.11 along with the prototype results of Colville et al[81] and Maurenbrecher[90]. It can be noted that the ratio of prism strength to unit strength tested by Colville et al ranged between 0.84 to 0.855 and by Maurenbrecher ranges between 0.75 to 0.78 . In model masonry prisms, the ratio of prism strength to unit strength ranged between 0.79 to 0.82 which indicates that model results are close to that of the prototype results .

3.3 JOINT SHEAR

3.3.1 General

Joints or unit-mortar interfaces in concrete masonry shear walls constitute planes of weakness and a major source of stiffness degradation and damping[20,36,46,52,116,122&138]. Failure frequently initiate in joints and subsequent deformation and energy absorption may occur by relative slip across joint planes. Therefore, the possibility of a shear failure must be examined. This shear failure could be a slip along the bed joint at one or more courses.

3.3.2 Test Specimen

Many investigators[20,22,46,53,72,83,96,109&138] over the last two decades have used many different shapes of specimens associated with different test techniques. Benjamin and Benjamin[72] and Huizer[79] carried out tests on shear couplets composed of two bricks and a mortar joint illustrated in Fig. 3.12.a . The test set-up shown in Fig. 3.12.b was adopted by Haller[51] to determine the capacity of joints in solid brick masonry under shearing along with precompression (stresses normal to the bed joints) loading. Jolley[83] used the three unit specimen (triplet) shown in Fig. 3.12.c to evaluate the shear bond strength of brick masonry joints. A similar triplet specimen shown in Fig. 3.12.d was adopted by Stafford Smith and Carter[135]. Also test specimen used by Hegemier[72] were triplet that consists of three ungrouted blocks with either two bed joints or two head joints as shown in Fig. 3.12.e . These techniques have the disadvantage of developing flexural stresses over the mortar joint, so do not represent a state of pure shear over the joint. Balachandran[62] showed experimentally, that the flexural stresses developed from the external bending moments could considerably reduce the shear capacity of the joints. To avoid creating bending moments at the mortar joints Balachandran[20] adopted a triplet specimen supported and loaded in such a way as indicated in Fig. 3.12.f. Hamid[53] used four units assembled together to investigate the shear capacity of full-scale masonry joints

with and without precompression load. A similar specimen for testing mortar joints under shear and precompression loading has been reported by Rostampour[118] to evaluate the shear bond strength of solid brick masonry. The determination of the shear bond properties of mortar joints in masonry using five test set-up conducted by various authors[36,52,116,122&138] were results examined and compared by means of FE-calculations and documented in Ref [137]. Later Abboud[1] used the four units test specimen adopted by Hamid to investigate the shear capacity of 1/4-scale model masonry joints without precompression load .

In the present study a similar shape of shear test specimen assemblages used by Hamid et al[53] has been used to evaluate the shear capacity of 1/3-scale model concrete block masonry joints. The four block assemblage shown in Fig. 3.13 was adopted as the shear test specimen.

This type of specimens has the following advantages:

1- Flexural stresses at the joints are eliminated (the load is transferred by shear through these joints)

2- The test is relatively easy to set-up and simple to perform from universal testing machine

3- No stress concentration occur because the load is applied uniformly over an area far from the joints .

4- The shear deformation of the joint can be easily measured .

3.3.3 Objectives of the Test Program

The main objective of the shear test is to study the shear strength of concrete block masonry along the bed joints using small-scale direct modeling techniques. The effect of grouting, types of mortar bedding, and axial stress (normal to the bed joints) on the shear capacity of masonry joints are included in this work. Direct correlation between the model test results and available prototype results on similar specimens are carried out.

3.3.4 Fabrication of Test Specimen

A total of 12 model shear specimens were constructed by the same experienced mason. To help the mason in constructing these specimens, a special two plates with thickness of 1/8 in. (3.2 mm, which is the same thickness of mortar bed joint), small square trowel and two temporary units were used. The construction procedures were simple and straight forward, three units were placed flush on the wooden plate with 1/4 in. (6.5 mm) space between them. The two side units provided temporary support to the top central units and these were moved upon completing construction of the specimen as shown in Fig. 3.14. A steel spacer with the thickness of 1/8 in. (3.2 mm) was placed on the top of each side unit. The two central blocks were positioned in place as indicated in Fig. 3.14 with a firm pressure causing excess mortar to squeeze out of the joints. Gentle tapping with the wooden end of the trowel was applied to further consolidate the joints to the required 1/8 in. thickness and to assure horizontal laying of the units. The vertical cavity between the center blocks was achieved by placing a temporary steel bar of 1/2 in. (12.5 mm) between them. After the leveling and plumbing of the center units, a mortar bed was placed on top of the central units. The top block was placed in position as indicated in Fig. 3.14, plumbed vertically with the lower units and leveled horizontally to provide a 1/8 in. bed joint. Finally the joints were tooled on both sides of the specimens and the two side units were removed . Type S mortar was used for the construction of the assemblages .

After 24 hours three of the twelve specimens were grouted with grout. The proportions of the mortar and grout mixes were described in Chapter 2 . The grout was poured into the continuous cores and puddled with an aluminum bar. The grout was reconsolidated to provide good compaction and good bond to the masonry units. All the model shear specimens assemblages (shown in Fig. 3.15.a) were air cured in the Structural Testing Laboratory under controlled temperature and humidity .

Control specimens were made along with the assemblages and were air cured in the laboratory under the same conditions as the assemblages. For the mortar, two types of control specimens, six cubes and six cylinders were constructed and tested under

compression and splitting tension. For the grout, three types of control specimens, six drilled cores, six cylinders, and six molded-block were tested under compression and splitting tension .

3.3.5 Testing Procedure and Instrumentation

At the age of 28 to 40 days from fabrication, the ends of the central blocks were capped using hydrostone gypsum cement, the specimens were then tested after 24 hours. For the specimens without precompression, the test set-up is shown in Fig. 3.15.b. Each specimen was carefully aligned in the testing machine by centering the bearing plates with the vertical axis of the machine head. The load was applied at a constant speed using a 120 kips (55 ton) Tinius Olsen Machine in the Structural Testing Laboratory of Drexel University until failure occurred. Steel plates 1.85x2.6x0.1 in. (47x66x2.5 mm) were glued on each of the central blocks using 5-minute epoxy. To prevent the possibility of compressive failure of the central blocks before the joints reached their full capacity. The control specimens were tested at approximately the same age as the assemblages .

For the specimens with precompression stresses normal to the bed joints, the precompression load was applied first and maintained constant while the shear force was incrementally increased until failure. A photograph of the stressing spring assembly for providing precompression along with shear loading is shown in Fig. 3.15.c. It consists of two springs centered between two steel plates (1/2 inch thick bearing plates to provide a uniform distribution of the precompression load over the constant areas of the bearing blocks) with two stressing rods passing through the cells of the units. The spring is compressed between the plates by tightening the two nuts. There are also two nuts on the opposite end of the stressing rods which bears against its anchor plate. Tightening the nuts squeezes both the spring and the specimen. The force in the rod can be determined by simply measuring the spring deflection between the two plates and multiplying it by the spring constant. The spring constant was found to be 1333 lb/in. (1540 kg/cm) from the load deflection curve presented in Fig. 3.16. Spring deflection needed to produce

precompression stress 230 psi (0.1 f'm) in the specimen normal to the bed joint is 0.358 inch (9 mm). Typical test set-up for shear with precompression stress is shown in Fig. 3.15.c .

3.3.6 Experimental Results and Discussion

Modes of Failure : The mode of failure was a shear slip failure along two of the joints for both grouted and ungrouted model shear specimens. The failure initiated by a debonding at the model block and mortar interfaces for ungrouted masonry assemblages as shown in Fig. 3.17.a . For the grouted model specimens, a sudden failure occurred after the formation of a visible crack at the mortar-block interface. The failure surface of the grout had typical conical shape associated with diagonal tension failure as shown in Fig. 3.17.b. This failure mode agree with prototype results[52] The failed joints were mostly in one plane which was at the interface between the mortar and uppermost model block laid during fabrication. This may indicate the sensitivity of the mortar bond at early stages to any pressure normal to the bed joint even if it is only the result of the self weight of the upper courses .

Shear Strength: The test results of ungrouted and grouted shear joint specimens are listed in Table 3.3. The average shear stresses at failure are calculated using the following formula :

$$\tau = P / (2A) \qquad (3.2)$$

where

τ = average shear stress at failure

P = applied vertical load at failure, and

A = net area of contact (transfer bedded area) between two blocks for ungrouted

specimens, and gross area for grouted specimens .

Discussion of the effect of different parameters on the bed joint shear strength is presented in the following sections .

Effect of Grouting: The effect of grouting on the shear strength of the joints is shown graphically in Fig. 3.18. This figure shows grouted and ungrouted shear strength in terms of the grout tensile strength as calculated from splitting tests of block-molded grout prisms. It can be seen that grouting appreciably increased the average shear strength of the joints. An increase of 208% was achieved by grouting the cores with grout that has nearly a splitting strength of 180% the model block strength. The line in Fig. 3.18 shows the least squares fit of the test data, using a linear regression analysis, the following empirical formula was obtained:

$$\tau_g = 68 + 0.275\ \sigma_{tg} \qquad (3.3)$$

where

τ_g = shear stress for grouted masonry

σ_{tg} = grout tensile strength

It is interesting to observe that grouting helped significantly to decrease the variability of the shear test results. The coefficient of variation was reduced from 14.6 % for the ungrouted specimens to an average of 5 % for the grouted model shear specimens. This is due to the fact that the strength of ungrouted masonry is dependent on the mortar bond which is highly variable. However, shear strength of grouted specimens is controlled by the diagonal tensile strength of the grout which is considerably less variable than mortar bond.

Effect of Mortar Bedding : The average shear stresses at failure are calculated using the previous formula (3.4) which is depend mainly upon the contact area between the mortar and block interface for ungrouted specimens. Based on the results presented in Table 3.3, the average shear bond strength of the model masonry joints increased substantially with the addition of mortar bedding area. An increase of about 38% was accomplished by using full bed joint as presented in Table 3.3. This is attributed to the fact that adding web shell bed increase the contact area between mortar and block and also the web shell bedded area acts as a bracing increasing the stiffness of the diaphragm resisting the applied in-plane loads .

Effect of Precompression : Figure. 3.19 illustrates the relationship between the shear stress and normal compressive stress acting along the bed joints. As would be expected, increasing the normal compressive stress resulted in increased shear capacity along the bed joints. This increase in the shear capacity can be thought of as being similar to an increased internal frictional resistance (Coulomb theory of internal friction) .

The governing equation for the shear strength of masonry mortar-block joint is usually taken as a straight line relationship of the Mohr-Coulomb type as

$$\tau = \tau_o + \phi \sigma \qquad (3.4)$$

where

τ = the shear stress at failure

τ_o = the shear bond strength expressed as the shear stress at failure when $\sigma = 0$

σ = precompression stress, based on the net area of the slip plane

ϕ = a coefficient attributed to friction

Equation (3.6) has been used, as an empirical expression, to reasonably predict the shear strength for both solid brick masonry joints and hollow concrete masonry joints for the range of precompression up to 20% of the masonry compressive strength. Above this

Table 3.3 Summary of Joint Shear Test Results[1]

Type of Model Specimen	Mortar Strength[2] Compression psi (kg/cm^2)	Splitting	Grout Strength[3] Compression psi (kg/cm^2)	Splitting	Shear Strength[4] Individual psi (kg/cm^2)	Mean	C.O.V %
Ungrouted Mortar Face-shell Bedding	2250 (157)	215 (15)	-	-	71 57 77	68 (4.75)	14.6
Ungrouted Mortar Full Bedding	2250 (157)	215 (15)	-	-	87 93 102	94 (6.5)	7.9
Ungrouted[5] With Precompression Stress	2250 (157)	215 (15)	-	-	216 228 254	232 (16.2)	8.2
Grouted	2250 (157)	215 (15)	4500 (315)	515 (36)	200 221 209	210 (14.7)	5.0

(1) 1 psi = 6.9 x 10^{-3} MPa

(2) Mean Strength of 2 inches (51mm) Mortar Cubes

(3) Mean Strength of Block-Molded Grout Prisms

(4) Based on the Net Area of Ungrouted Specimens and Gross Area of Grouted Specimens

(5) Based on Mortar Face-shell Bedding

level, the failure mode changes from joint slip to a combined shear-tension mode and equation (3.4) no longer applies[52]. In the current work the proposed equation for shear strength of masonry mortar-block joints is taken from Fig. 3.19 as a straight line relationship with coefficient of friction equal to 0.71 and shear stress at zero precompression equal to 68 psi , this equation is

$$\tau = 68 + 0.71\ \sigma \qquad (3.5)$$

Hamid[52] developed empirical formulas based on curve fitting of experimental results to predict the shear strengths for both ungrouted and grouted concrete masonry joints for low level of precompression using linear regression analysis, these formulas are:

for ungrouted masonry $\tau_{un} = 76 + 1.07\ \sigma_n$ (3.6)

for masonry with weak grout, $\tau_g = 223$ psi = 15.6 kg/cm^2

$$\tau_g = 114 + 1.08\ \sigma_n \qquad (3.7)$$

for masonry with weak grout, $\tau_g = 500$ psi = 35 kg/cm^2

$$\tau_g = 156 + 1.54\ \sigma_n \qquad (3.8)$$

where

τ_{un} = average ungrouted shear stress at failure based on net area

τ_g = average grouted shear stress at failure based on gross area

σ_n = precompression stress

It is apparent from these Equations that there is a strong correlation between the increased precompression stresses and the increased joint shear strength of ungrouted and grouted masonry. Also it can be noticed that the first term of these Equations indicates the contribution of grout .

3.3.7 Correlation With Prototype Results

The shear stresses along the bed joints for model masonry assemblages were presented in this Chapter. Correlation between model and prototype conducted by Hamid[53] on shear along the bed joints are described below .

The model masonry assemblages are duplicated the modes of failure of prototype results reported by Hamid[53]. The prototype results indicated that the failure mode of ungrouted specimens was initiated by a debonding at the block-mortar interface, however grouted specimens failure was initiated by mortar debonding followed by diagonal tensile failure of the grout cores . Also, it was indicated that the failure plane was along one plane at the minimum interface contact area between the block and mortar.

The variation of shear strength of ungrouted and grouted masonry with grout tensile splitting strength for model and prototype shear specimens is shown in Fig. 3.20. It can be noted from this figure that the shear strength of masonry bed joints for model and prototype specimens was influenced by grouting. Also it can be noted that model results are higher than the prototype by about 26% specifically in the grouted specimens. This could be due to the higher tensile strength of model grout than the prototype .

The variation of shear strength with precompression stress for model and prototype shear specimens is illustrated in Fig. 3.21. Examination of the test data for both model and prototype revealed that precompression had substantially increased the shear strength of masonry bed joints. The similarity between model and prototype behavior indicates again the validity of direct modeling in predicting the behavior of masonry assemblages. It has been noted however, that the results of model specimens were approximately 5% higher than those of prototype results, the formula proposed by Hegemier overestimates the results by about 4.6% , and the formula proposed by Dawe underestimates the results by about 16% .

From the above discussions, it could be concluded that the use of modeling techniques at 1/3-scale in predicting the overall behavior of masonry assemblages under in-plane shear are feasible .

3.4 IN-PLANE TENSILE STRENGTH

3.4.1 General

The splitting tensile strength is one of the important parameters which affect the behavior of structural masonry elements such as shear walls. These walls are subjected to lateral forces which produce tensile stresses. The mode of failure generally occurs as a diagonal failure which is governed mainly by the tensile strength characteristics of masonry.

Tests of concrete masonry shear walls and observations of the actual failure following earthquakes indicate that the combination of axial load and in-plane shear and overturning moment often leads to various orientations of cracking rather than to slip along a bed joint. Therefore it should be expected that the cracking load or the tensile strength of such masonry walls will be influenced by the strength characteristics of the constituent blocks, mortar, and grout.

3.4.2 Test Specimen

A limited number of major investigations have been performed on the in-plane splitting tensile strength of masonry assemblages. The effect of tensile stresses in different directions was studied by Meli[96] with diagonal compression tests on small panels of different shapes. For square panels as indicated in Fig. 3.22.a, he concluded that failure was usually through the joints, except for very weak units where a pure tensile crack caused the failure. Johnson and Thompson[82] developed a diametral test produce to evaluate the tensile splitting strength of brickwork. Their test basically consisted of applying a compressive load along the diameter of a circular masonry disc 15 inches (380 mm) in diameter as indicated in Fig. 3.22.b. This test technique is similar to the indirect Brazilian test for determining the splitting tensile strength of concrete. It has many advantages over other techniques that outlined in Reference[7]. The greatest advantage of this test technique is the ability to test identical specimens under tensile stresses at different

orientations from the bed joints. For that Drysdale and Hamid[38] had adopted the diametral testing technique for concrete block masonry. They modified the circular shape into hexagonal shape as shown in Fig. 3.22.c for ease of preparation, handling, and testing. A finite element analysis was performed by Hamid[52] to investigate the stress distribution along the loaded plane of the suggested hexagonal shape. He indicated that the modified shape would provide a good approximation of the stress with a conventional circular disc, provided that the height of the specimen is equal to or greater than its length. Based on linear finite element analysis of masonry disc loaded at 45 degree to the bed joints, Balachandran[20] assumed that the tensile cracking of ungrouted concrete masonry occurs if the maximum principle tensile stress exceeds the tensile strength of the block or mortar, whichever is less.

The experimental technique used by Drysdale and Hamid[38] was used in this experimental program to determine the splitting tensile strength of concrete block masonry. The hexagonal shape was used for model specimens tested under a load plane oriented at 45 degrees from the mortar bed joints. However a square shape (the part of the wall between the reinforced cells of partially reinforced shear walls) was adopted for specimens tested at 0 and 90 degrees from the bed joints. The adopted shape is more convenient for preparation, handling, and testing. Typical dimensions of model test specimens under loads having three orientations with respect to the bed joint are indicated in Fig. 3.23 .

3.4.3 Objective of the Test Program

The aim of this experimental program is to use small-scale direct modeling techniques to investigate the splitting tensile strength characteristics of concrete block masonry discs under tensile stresses of different orientations ($\beta = 0, 45$ & 90) relative to the bed joint direction. The effects of block strength, grouting, and mortar bedding area on the tensile strength of concrete block masonry assemblages are considered in this investigation.

In the experimental work the validity and adequacy of the 1/3-scale direct modeling of concrete block masonry in predicting the in-plane tensile strength characteristics of concrete masonry were determined and documented in this Chapter through direct correlation between the model test results and available prototype test results[38] on similar tested specimens .

3.4.4 Fabrication of Test Specimens

A total of 24 model specimens were constructed in running bond 9 hexagonal shapes for load at $\beta = 45^{o}$ to examine the effect of block strength and grouting and 15 square shapes, 9 of them for load at $\beta = 90^{o}$ to examine the effect of grouting and mortar bedded area and the rest 6 for load at $\beta = 0^{o}$ to examine the effect of block strength . The model test specimens were 2 blocks long and 4 courses high i.e. they consist of 6 full blocks and 4 half blocks. For the hexagonal shape, the corner blocks were cut first with an electric diamond-edge blade saw and then the discs were built with block arrangement to provide the final hexagonal shape shown in Figs. 3.24 & 2.25. All the model specimens were fabricated by the same experienced mason using the same techniques described in section 3.3.4.1 . Type S mortar was used to assemble the specimens. The physical and mechanical properties of the model units, model grout, and model mortar are presented in Chapter 2 .

After completing the fabrication of each specimen, four model blocks were placed on top of the specimen to simulate enough pressure on the bed joints. After 24 hours, six specimens (3 of a square shape and 3 of a hexagonal shape) were grouted using the same grout techniques utilized for the other model masonry assemblages. All model specimens as shown in Fig. 3.26 were air cured in the laboratory under controlled temperature and humidity .

Control mortar and grout specimens were made along with the model masonry assemblages and air cured in the laboratory under the same conditions used for model

masonry assemblages described in the previous section .

3.4.5 Testing Procedure and Instrumentation

After 28 to 40 days the model masonry assemblages were capped with gypsum plaster and subsequently tested under splitting line loads having three different orientations with respect to the mortar bed joints direction as indicated in Fig. 3.23 , these orientations are:

a) Normal to the bed joints ($\beta = 90^{o}$) as indicated in Fig. 3.23.a . This allows measurements of tensile strength normal to the bed joints f'_{tn}. The parameters considered in this case, are the mortar bedding area and grouting (9 specimens) .

b) Diagonal to the bed joints ($\beta = 45^{o}$) as indicated in Fig. 3.23.c . This allows measurement of the diagonal tensile strength f'_{td}. The parameters studied in this case are the block strength and grouting (9 specimens) .

c) Parallel to the bed joints ($\beta = 0^{o}$) as indicated in Fig. 3.23.b . This allows measurement of tensile strength parallel to the bed joints f'_{tp}. The only parameter examined in this case is the block strength (6 specimens) .

Each model masonry specimen was carefully aligned in the testing machine by centering and plumbing the point of bearing with the vertical axis of the machine load. The load applied through roller bearing plates at top and bottom of the model panel. The typical test set-up for the model masonry assemblages for different orientations ($\beta = 0^{o}$, 45^{o} & 90^{o}) are shown in Fig. 3.27. To prevent local compression failure of the face-shells of the ungrouted hexagonal masonry panel, the cells of the bearing blocks adjacent to the load were filled with mortar . The load was applied until failure occurred and the patterns of the failure cracks were recorded. The control specimens for model mortar and model grout were tested at approximately the same age of the model assemblages .

3.4.6 Experimental Results and Discussion

Modes of Failure : The general mode of failure of the test specimens was that of a splitting along the central line (the line between the load points) due to the induced transverse tensile stresses. The failure plane was differentiated according to the load orientation as described below :

The specimens with the bed joints parallel to the loaded plane i.e. tensile stresses at $\beta = 90^{o}$, had failure planes passing along the mortar-block interfaces. The failure of the ungrouted specimens at the top surface of the mortar joint corresponding to the minimum contact area between the mortar and face-shell because the blocks have flared webs and face-shell (see Fig. 2.5). On the other hand the failure of the grouted specimens occurred along the bottom surface of the bed joint which was the weakest plane and had the minimum grouted areas. Typical modes of failure for ungrouted and grouted model specimens under tension normal to the bed joints are indicated in Fig. 3.28.

The specimens with the bed joints perpendicular to the loaded plane i.e. tensile stresses at $\beta = 0^{o}$, failed in a tension mode with the failure plane passing through the intercepted face-shells of the blocks and along the mortar-block interfaces at the head joints, in the most direct line between the load points. The two types of blocks had approximately the same mode of failure. Typical mode of failure for the two types of blocks model specimens under tensile stress parallel to the bed joints are indicated in Fig. 3.29.

The specimens with a line load applied at $\beta = 45^{o}$, the failure plane for ungrouted masonry discs was a fracture crack extending through the blocks and mortar joints in a direct path between the points of loading as shown in Fig. 3.30.a . But for grouted specimens, the fracture crack was occasionally similar to the ungrouted specimens, but more often partially followed the mortar- block interfaces in a zigzag plane of failure as shown in Fig. 3.30.b . In this case it was a mixed shear (slip at the block-mortar interface) and tension (splitting of block, mortar and grout) mode of failure .

Effect of Load Orientation on the Tensile Strength : The tensile strength at failure was calculated on the basis of the gross area of the splitting plane for both ungrouted and grouted specimens using the following equation :

$$f'_t = 2P / (\pi A) \quad (3.9)$$

where

f'_t = splitting tensile strength of masonry

P = applied failure load, and

A = gross area of the splitting plane

Table 3.4 summarizes the results of ungrouted and grouted model masonry specimens tested under splitting loads. The results of the corresponding control specimens are also presented in this table. Fig. 3.31 indicates the influence of the orientations of the principal tensile stresses with respect to the bed joints (measured by angle β) on the splitting tensile strength of masonry discs. This figure shows that the tensile strength of either ungrouted or grouted specimens is variable with the orientation of the principal tensile stresses. It is worth noting that the ungrouted specimens showed an increase of 112% in the tensile strength as the load changed direction from normal to diagonal. On the other hand grouted specimens showed an increase in tensile strength by only 14%. This behavior is expected because in case of grouted specimens, the grouted cores provide some continuity to the media which may help to give masonry the tendency towards a more isotropic behavior .

As presented by Hamid[63] the apparent tensile strength of the assemblage can be described by incorporating the resistance of the component material (grout, mortar, and block) as follows :

$$f_{tn} = \eta_h \sigma_{tbm} + (1-\eta_h) \sigma_{tg} \quad (3.10)$$

$$f_{tp} = 1/2 (\eta_{vm} \sigma_{tbm} + \eta_{vb} \sigma_{tbl}) \quad (3.11)$$

Table 3.4 Summary of Model Masonry Splitting Tension Test Results[1]

Type of Model	Block Strength[2] Comp.	Split.	Mortar Strength[3] Comp.	Split.	Grout Strength[4] Comp.	Split.	Tensile Strength[5] Parallel (f_{spp}) b = 0°			Diagonal (f_{spd}) b = 45°			Normal (f_{spn}) b = 90°		
Assemblages	psi (kg/cm^2)		psi (kg/cm^2)		psi (kg/cm^2)		Individ.	Mean	C.O.V.	Individ.	Mean	C.O.V.	Individ.	Mean	C.O.V.
							psi (kg/cm^2)		%	psi (kg/cm^2)		%	psi (kg/cm^2)		%
Ungrouted							126			115			52		
Mortar Face-	2800	282	2250	215	-	-	134	132	3.8	121	121	5.0	59	57	7.6
Shell Bedding	(195)	(19.7)	(157)	(15)			136	(9.2)		127	(8.5)		60	(4.0)	
Ungrouted							92			86					
Mortar Face-	1800	200	2250	215	-	-	99	98	7.0	91	91	5.5		-	
Shell Bedding	(125)	(14)	(157)	(15)			105	(6.85)		96	(6.4)				
Ungrouted													68		
Mortar Full	2800	282	2250	215	-	-		-			-		75	76	11.0
Bedding	(195)	(19.7)	(157)	(15)									85	(3.8)	
									216			192			
Grouted	2800	282	2250	215	4500	515		-		234	232	6.9	199	205	7.8
	(195)	(19.7)	(157)	(15)	(315)	(36)				248	(16.2)		224	(14.3)	

(1) 1 psi = 6.9 x 10^{-3} MPa
(2) Based on Net Area of Units
(3) Mean Strength of 2 inch (51 mm) Mortar Cubes
(4) Mean Strength of Block-Molded Prisms
(5)Based on Gross Area of the Splitting Plane

$$f_{td} = 2/3\ (f_{tn} + f_{tp}) \tag{3.12}$$

Based on the method of least squares to relate the diagonal tensile strength to prism strength. Balachandran[20] proposed a straight line relationship from his experimental data as follows:

$$f_{td} = K\ (f'_m)^{1/2} \tag{3.13}$$

where

f_{tn} = average normal tensile strength

σ_{tbm} = tensile bond strength of mortar

σ_{tg}= grout tensile strength (f_{tg} = 0 for ungrouted masonry)

η_h = maximum net to gross area ratio (in a horizontal plane)

f_{tp} = average parallel tensile strength

η_{vb} = maximum net to gross area ratio (in a vertical plane)

η_{vm} = ratio of mortar area of head joint to gross area

f_{tb} = splitting tensile strength of the block

f_{td} = average diagonal tensile strength

f'_m = nominal compressive strength

K = factor depends upon the type of units and grouting

Hamid's Equations 3.10, 3.11,and 3.12 contain the contribution of grouting to the normal and diagonal tensile strength. On the other hand there is no contribution for grouting to the parallel tensile strength as indicated in Equation 3.11. Balanchandran[84] suggested a K value of 3.8 for grouted concrete masonry piers regardless the grout, mortar and unit strength.

It is to be noted that Equation 3.10 can be used to predict tensile strength normal to the bed joint in terms of tensile bond strength of mortar acting along the block-mortar contact area (bed joint), percent solid and tensile strength of grout. This Equation is valid only for ungrouted and fully grouted masonry and can not be directly used for partially grouted masonry, so as Equation 3.12. Because Equation 3.11 is not dependent on grout strength, it can be used for partially grouted masonry without any modification .

Equation 3.10 should be modified to incorporate the grout strength for predicting the strength of partially grouted masonry as follows:

$$A_{pg}\, f_{tn} = A_{fs}\, \sigma_{tbm} + (A_{pg} - A_{fs})\, \sigma_{tg}$$

$$f_{tn} = (A_{fs} / A_{pg})\, \sigma_{tbm} + (1 - A_{fs} / A_{pg})\, \sigma_{tg}$$

Substituting for $A_{pg} / A_{fs} = (1 + 0.9\, n\, L_b/L_w)$ from Equation 7.3 leads to an expression for the average normal tensile strength of partially grouted masonry in the form:

$$f_{tn} = 1 / (1 + 0.9\, n\, L_b/L_w)\, \sigma_{tbm} + (1 - 1 / (1 + 0.9\, n\, L_b/L_w))\, \sigma_{tg} \qquad (3.14)$$

It can be noticed that this Equation contains two terms; the first one for the contributions of unit strength and ratio of ungrouted to effective area and the second term for the effect of grouting where it contributes to the tensile strength of the assemblages by its tensile capacity and the number of grouted cells or spacing of grouting .

Effect of Grouting : It is apparent that filling the cores with grout has the greatest effect on the tensile strength of masonry elements. The contribution of grout in increasing the tensile strength varied with the orientation of the bed joint as presented in Table 3.4. It has a maximum contribution when the principal tensile stresses are normal to the bed joints. This is attributed to the higher tensile strength of the grout compared to the low bond strength of

mortar. The maximum tensile capacity of the grouted specimens was reached in the case of diagonal tension, at $\beta = 45$ degree. In this case, the capacity was mainly influenced by the tensile strength of the block, mortar , and grout with no appreciable effect of the limited mortar bond strength. This is logical since the tensile crack must cross the grout whereas for tension parallel to the bed joint the crack can follow the path of least resistance i.e. interface between web and grout, for this reason the effect of grouting wasn't taken into account. From Table 3.4 , it can be seen that for grouted specimens the normal tensile strength (f'_{tn}) and diagonal tensile strength (f'_{td}) were higher than the ungrouted specimens by approximately 260 and 92 percent respectively .

Effect of Block Strength : The strength of the model blocks would be expected to have a significant effect, when the tensile crack passes through the face-shells of the block for splitting tension tests parallel and diagonal with the bed joint. To examine this effect, the results are plotted in Fig. 3.32, using the splitting tensile strengths of the blocks as the basis for comparison. It can be noted that the increase in the block strength caused an increase in tensile strength of the tested specimens. However, it is not possible to provide a direct correlation with block strength alone. The strength f'_{tp} and f'_{td} for specimens with unit strength of f_{b1} (2800 psi = 200 kg/cm^2) was higher than those with unit strength f_{b2} (1800 psi = 125 kg/cm^2) by approximately 36 % and 32 % respectively. This is because the cracking along the head joints initiates failure before the full tensile strength of the block can be developed[63]. Also it can be noted that the block strength has a higher effect in the case of parallel tensile strength than diagonal tensile strength because the first has a shear failure plane passes through the face-shells of the intercepted blocks whereas the second has a mixed shear failure (slip at the block-mortar interface) and tension failure (splitting of the block, mortar, and grout). From equations 3.10 and 3.11, it is worth noting that increasing the block strength resulted in an increase in the parallel and diagonal tensile strength, with the contribution of block strength being more effective in case of

parallel tensile strength.

Effect of Mortar Bedding Type : The mortar contributes to the tensile strength of masonry normal to the bed joints by its tensile bond strength and bedded area (full bedding or face-shell bedding). For tension perpendicular to the bed joints, it is logical that, based on the mortar-block interface, the tensile strength would increase with the increased mortar-block interface area because the specimens with tension normal to the bed joints failed by tensile debonding at the block-mortar interfaces. This is illustrated in Table 3.4, where it can be noted that the normal tensile strength for full bedding was higher than the normal tensile strength for face-shell bedding by about 33 percent .

3.4.7 Correlations Between Model and Prototype Results

The failure mode of ungrouted and grouted assemblages was a splitting type of failure along the line of the applied load (central portion caused by the transverse tensile stresses). The failure plane was determined by tensile stress orientation, the geometric components, and the strength characteristics. This mode of failure was observed and recognized by Drysdale and Hamid[38]. The variation of splitting tensile strength in terms of unit strength is illustrated in Fig. 3.33 along with the prototype results of Hamid and the Equation proposed by Hamid. Therefore, prototype failure was very well duplicated by the 1/3-scale model, showing the capability of modeling techniques in predicting the overall behavior of masonry blocks under in-plane splitting tension .

The average splitting strength for ungrouted model assemblages is very close to that of the prototype and this could be due to the fact that the splitting strength of model blocks is close to that of the prototype. The average splitting strength of model grouted assemblages is 38% higher than that of prototype assemblages, and this is mainly due to the highest model grout tensile strength.

When the tensile crack passes through the face-shells of the block for splitting tension tests parallel to the bed joints, the strength of the block have a significant effect.

Large increase in block strength do increase the tensile strength parallel to the bed joint for both model and prototype .

The general variation trend of the tensile strength with different orientations of the applied load for model results compares very well with the prototype results.

3.5 CLOSURE

The methodology of using small scale direct models of concrete masonry structures and techniques of fabrication and testing of small masonry assemblages at 1/3-scale have been presented. Basic strength evaluation tests on model grouted and ungrouted masonry assemblages along with their corresponding control specimens were carried out to determine compressive strength, shear capacity along the bed joints, and splitting tension at different orientations from the bed joints. Behavior characteristics of these model assemblages were investigated and discussed. The effects of grouting, type of mortar bedding, and block strength on the behavior of model masonry assemblages were investigated along with direct correlation to available prototype results on similar specimens .

From the experimental program presented in this chapter the following general conclusions can be drawn:

1) The modes of failure and crack patterns of ungrouted and grouted 1/3-scale models of small masonry assemblages duplicated the modes of failure and crack patterns of similar prototype masonry assemblages .

2) The strength and deformation characteristics of concrete masonry vary with the stress orientations with respect to the bed joints. This is a typical behavior of anisotropic composite material. Grouted masonry exhibits a more isotropic behavior because of the continuity provided by the grouted cores compared to ungrouted masonry .

3) Failure of concrete masonry assemblages can occur in one of the following modes :

a- Compression or a splitting failure the outer shell under high compression normal to the bed joints .

b- Debonding or joint slip failure at the block-mortar interfaces occurring under high shear stresses along the bed joints .

c- A splitting failure along the line between the load points under different orientations with respect to bed joint (diagonal, normal and parallel to the bed joint) .

4) Grouting significantly affect the compressive strength of model prisms, shear capacity of model joints, and tensile strength of specimens. This conclusion agrees with prototype results .

5) The strength of grouted small masonry assemblages was slightly higher than the corresponding prototype assemblages. This was due to the higher tensile strength of model grout control specimens .

6) Mortar bedding area has a significant effect on the bed joint shear and on the tensile strength under load parallel to the bed joints. This is true for mortar full bedding where the continuity provided by the mortar bedding acts as a diaphragm (high in-plane stiffness) to resist the shear along the bed joints (in-plane loads). Full mortar bedding exhibits more shear capacity compared to mortar face-shell bedding.

7) The block strength has a pronounced effect on the behavior of concrete block masonry. The block tensile strength is the most significant parameter influencing the compressive strength and splitting tensile strength parallel to the bed joint .

8) For ungrouted masonry the minimum capacity is obtained when the tensile stress was normal to the bed joints. In this case the capacity is only influenced by the mortar bond strength and contact area between mortar and block. Therefore, the normal splitting strength increases with increasing the contact mortar-block area. Under tensile stresses parallel to the bed joints, the block tensile strength and the tensile bond strength of the head joints contributed to the capacity, so that the parallel tensile strength increases as the block strength increases. For the diagonal tension case the capacity is governed by the block and mortar strength, but the tensile strength of the block has a much greater effect than the tensile bond strength of the mortar. Therefore, the higher the block strength, the higher the diagonal tensile strength capacity of the specimens is .

9) For grouted specimens, the anisotropic nature of behavior of the assemblages is also evident. However, it is less pronounced compared to the case of the ungrouted specimens. This behavior indicates that grouted cores provide some continuity which may help to give masonry the tendency towards a more isotropic behavior .

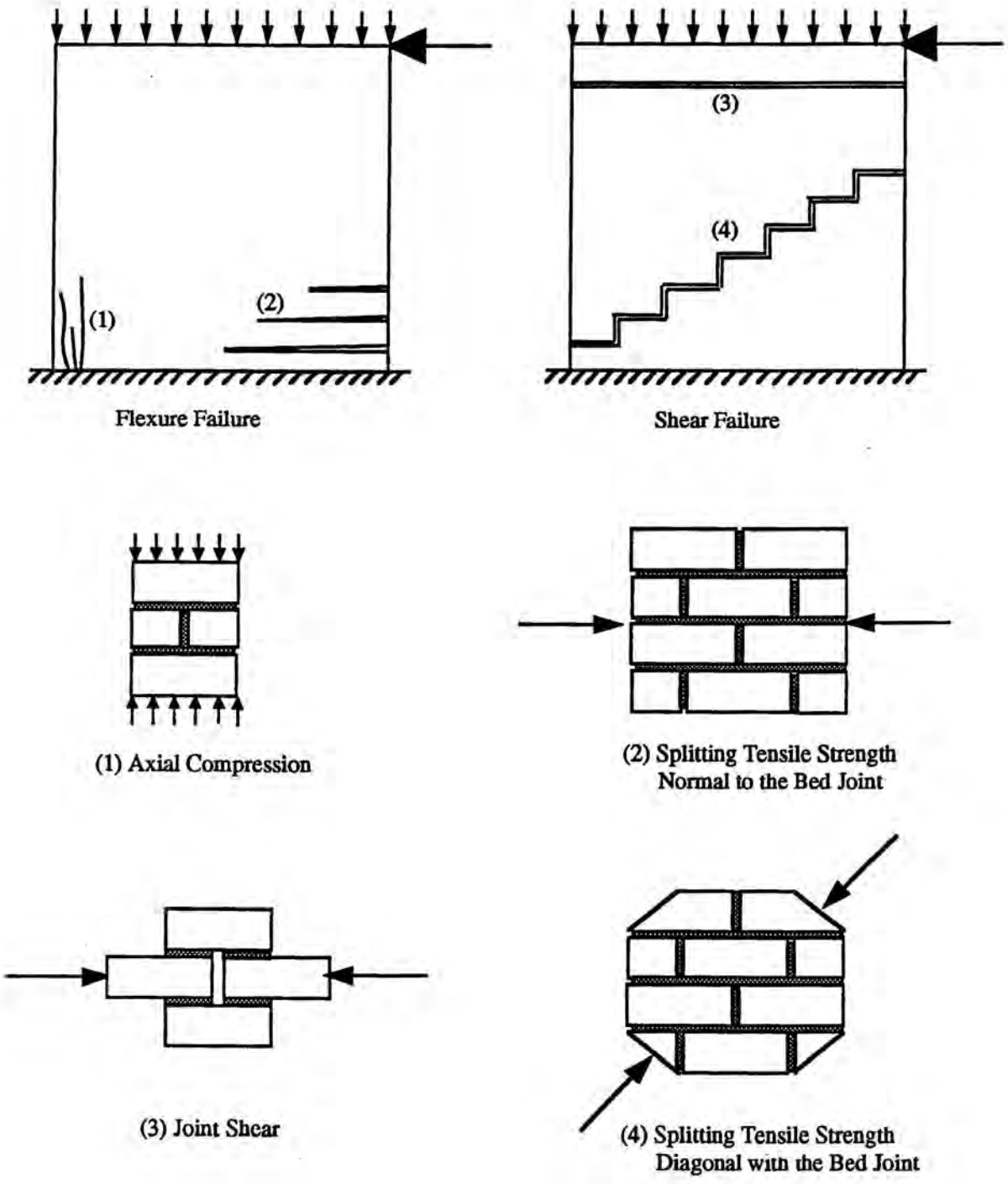

Fig. 3.1 Possible Failure Modes and Basic Test Assemblages

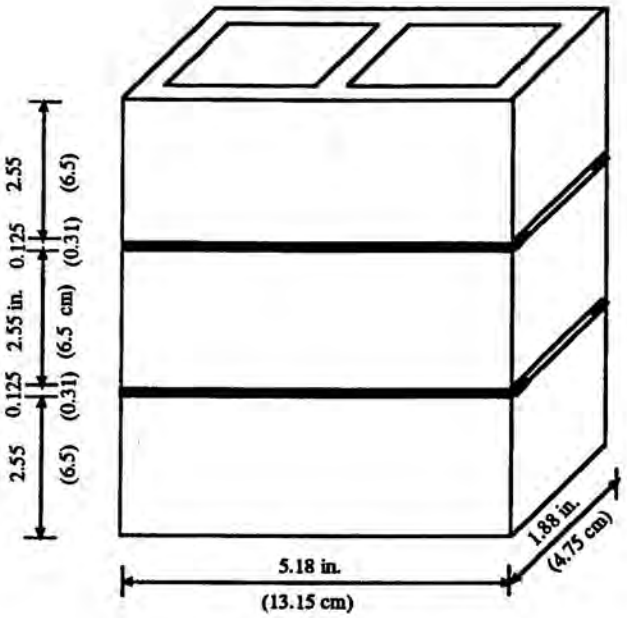

a) Ungrouted Specimen

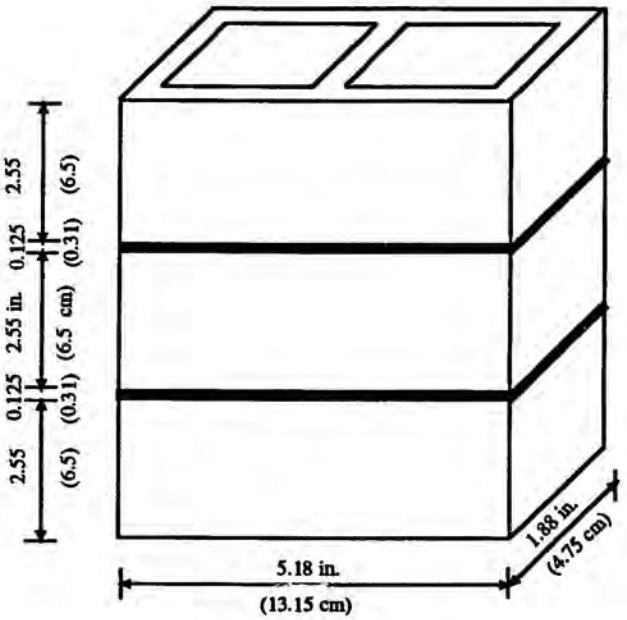

b) Grouted Specimen

Fig. 3.2 Model Prism for Axial Compression Test

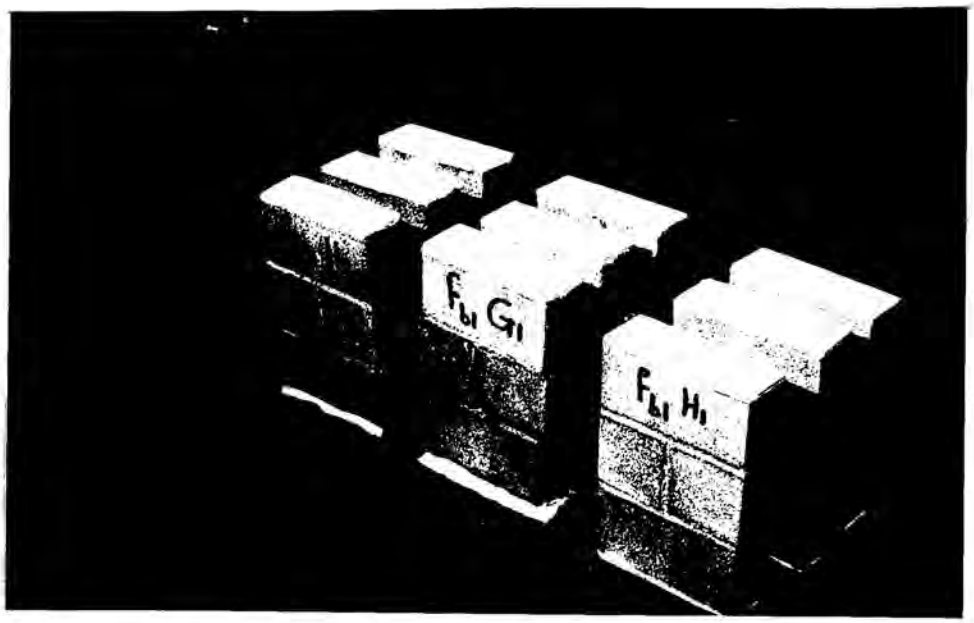

Fig. 3.3 Constructed Model Prisms for Axial Compression Test

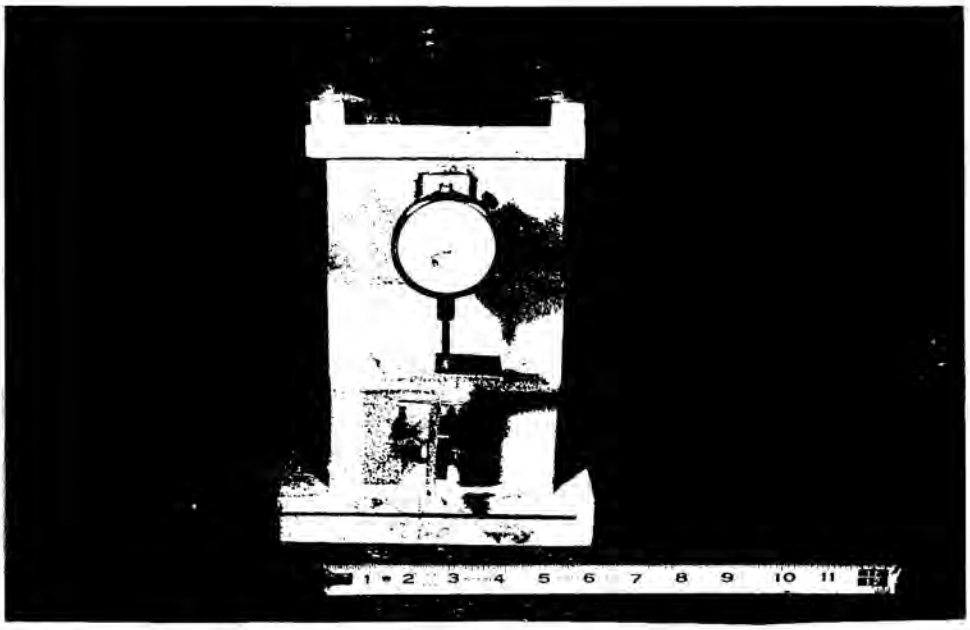

Fig. 3.4 Instrumentation for Model Prism

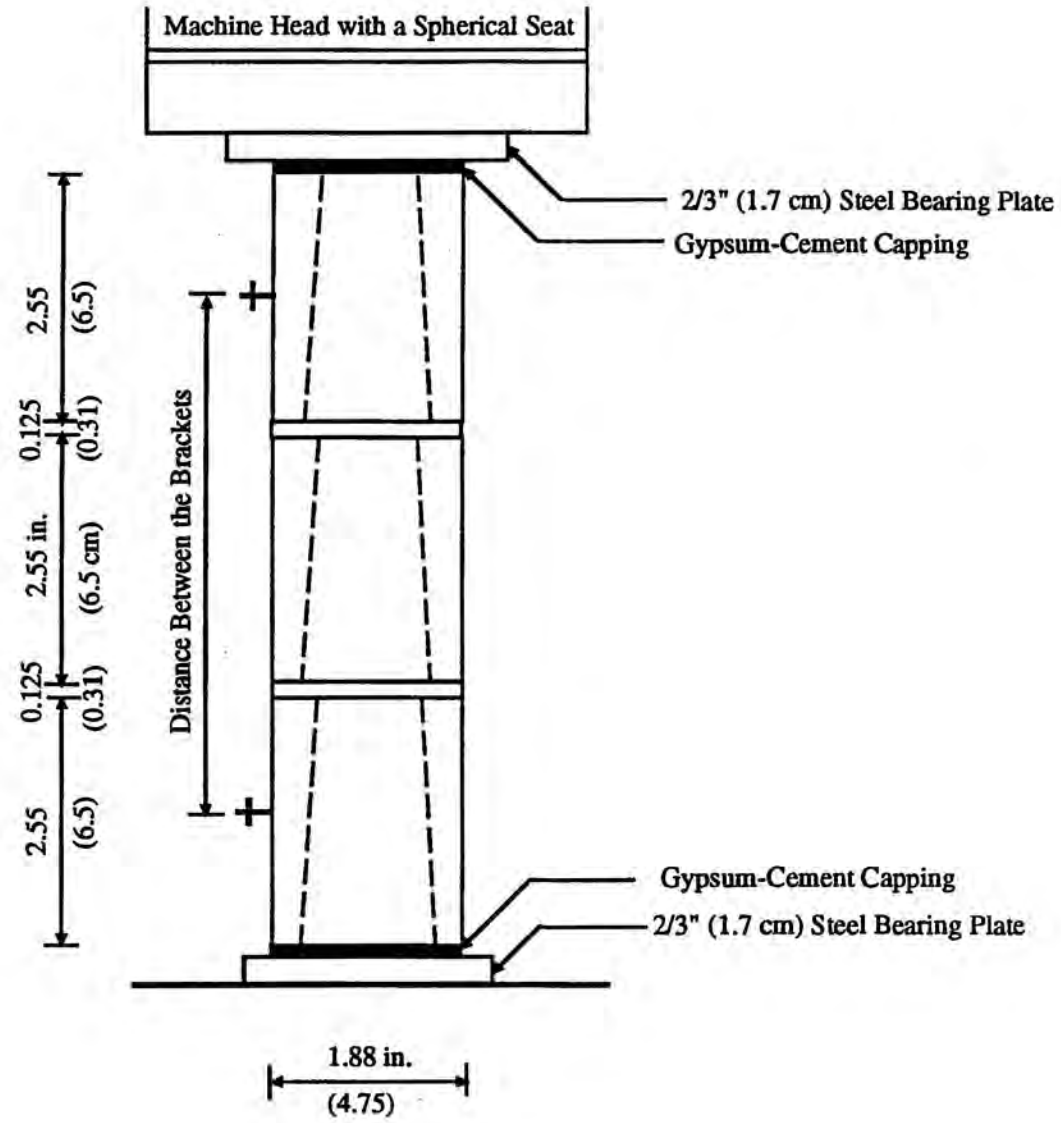

Fig. 3.5 Compression Test Set-Up for 3-Course Prisms

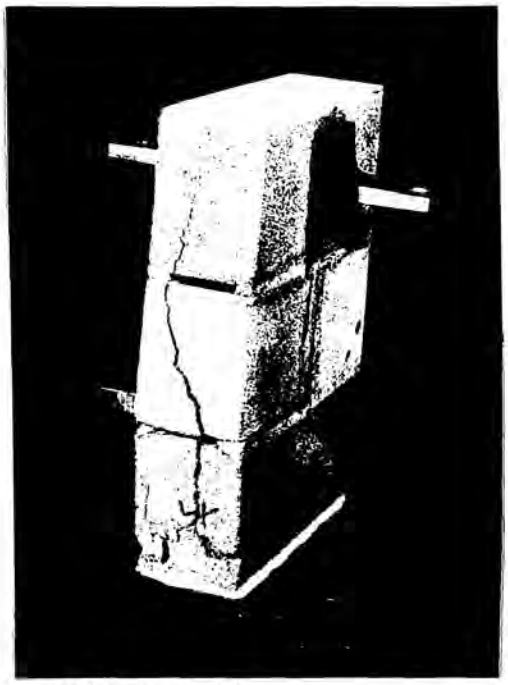

a) Ungrouted f_{b1}

a) Ungrouted f_{b2}

Fig. 3.6 Typical Modes of Failure for Ungrouted Prisms

a) Grouted f_{b1}

a) Grouted f_{b2}

Fig. 3.7 Typical Modes of Failure for Grouted Prisms

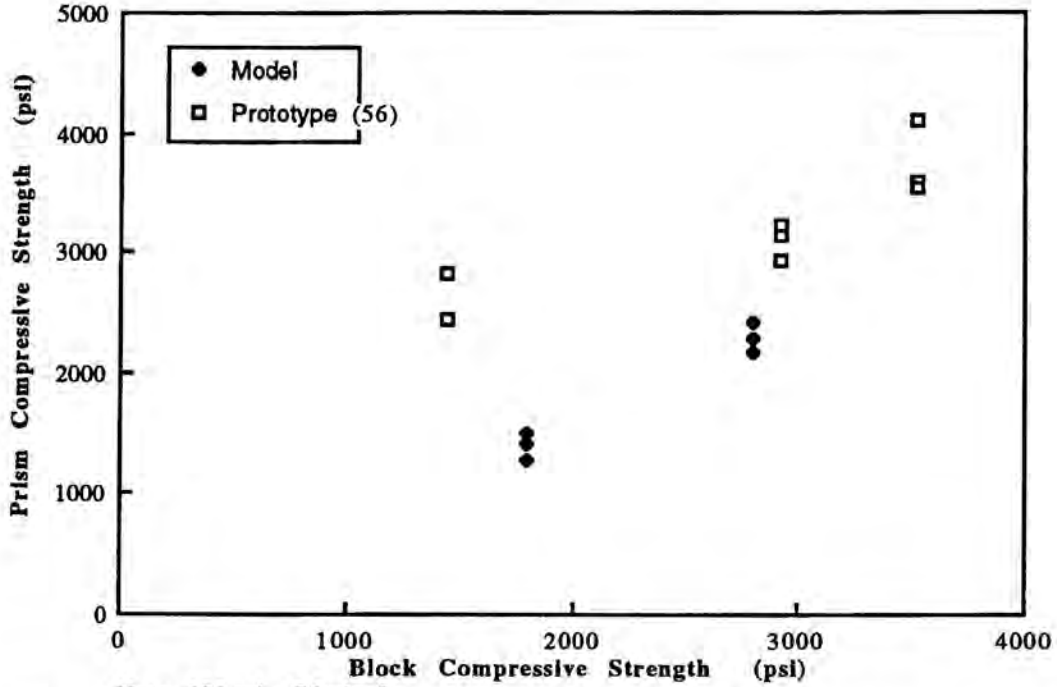

Note: 100 psi = 7 kg/cm2

Fig. 3.8 Effect of Block Strength on the Compressive Strength of Model Masonry

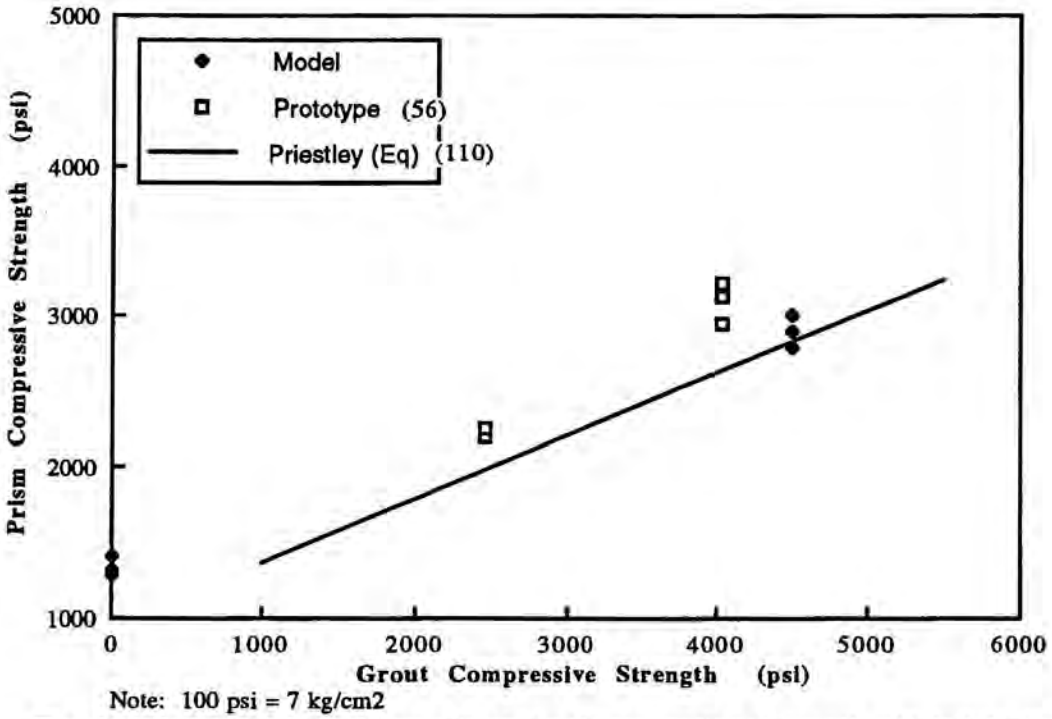

Note: 100 psi = 7 kg/cm2

Fig. 3.9 Effect of Grout Strength on the Compressive Strength of Model Masonry

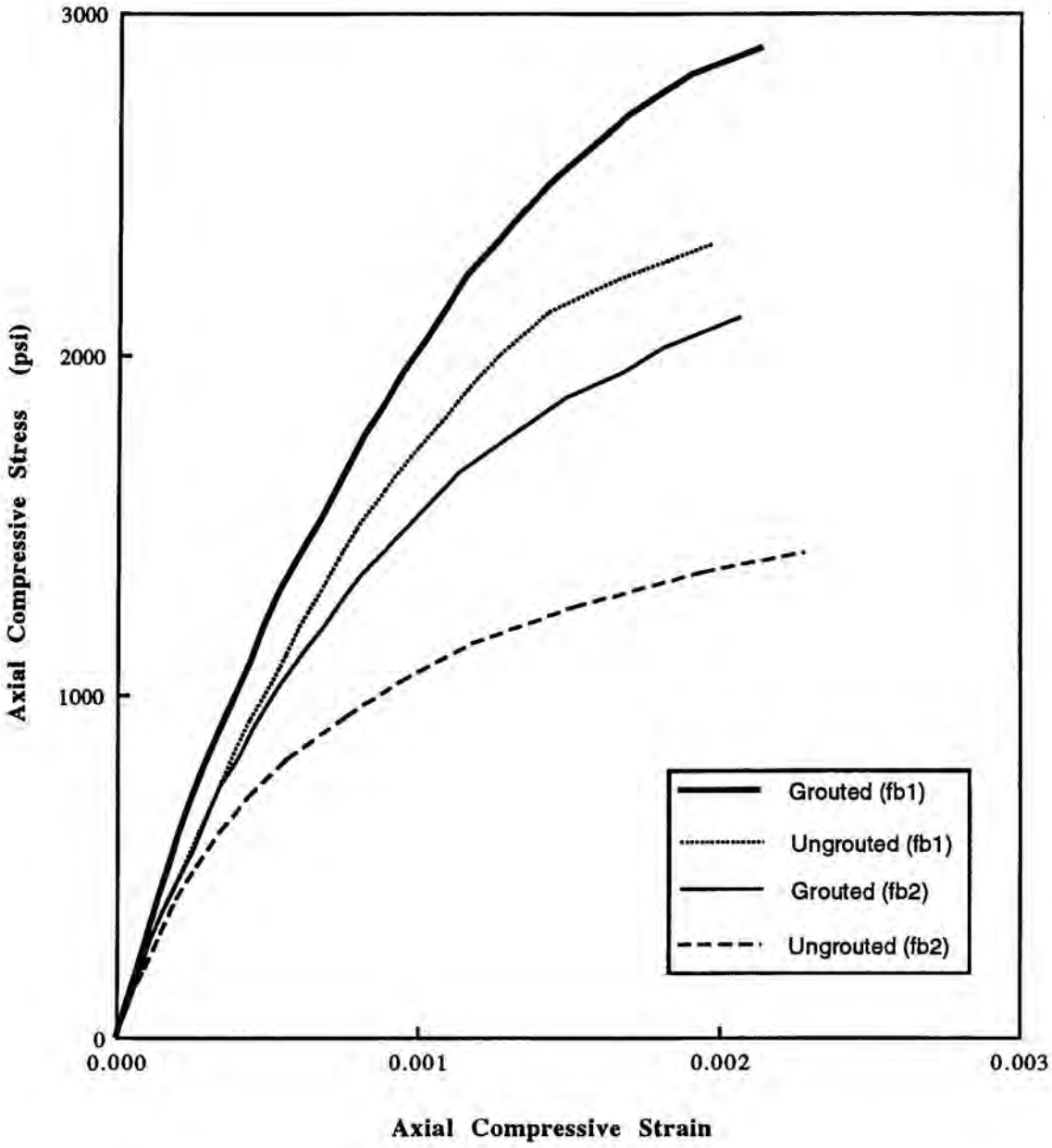

Note: 100 psi = 7 kg/cm2

Fig. 3.10 Stress Strain Curves for Model 3-Course Prisms

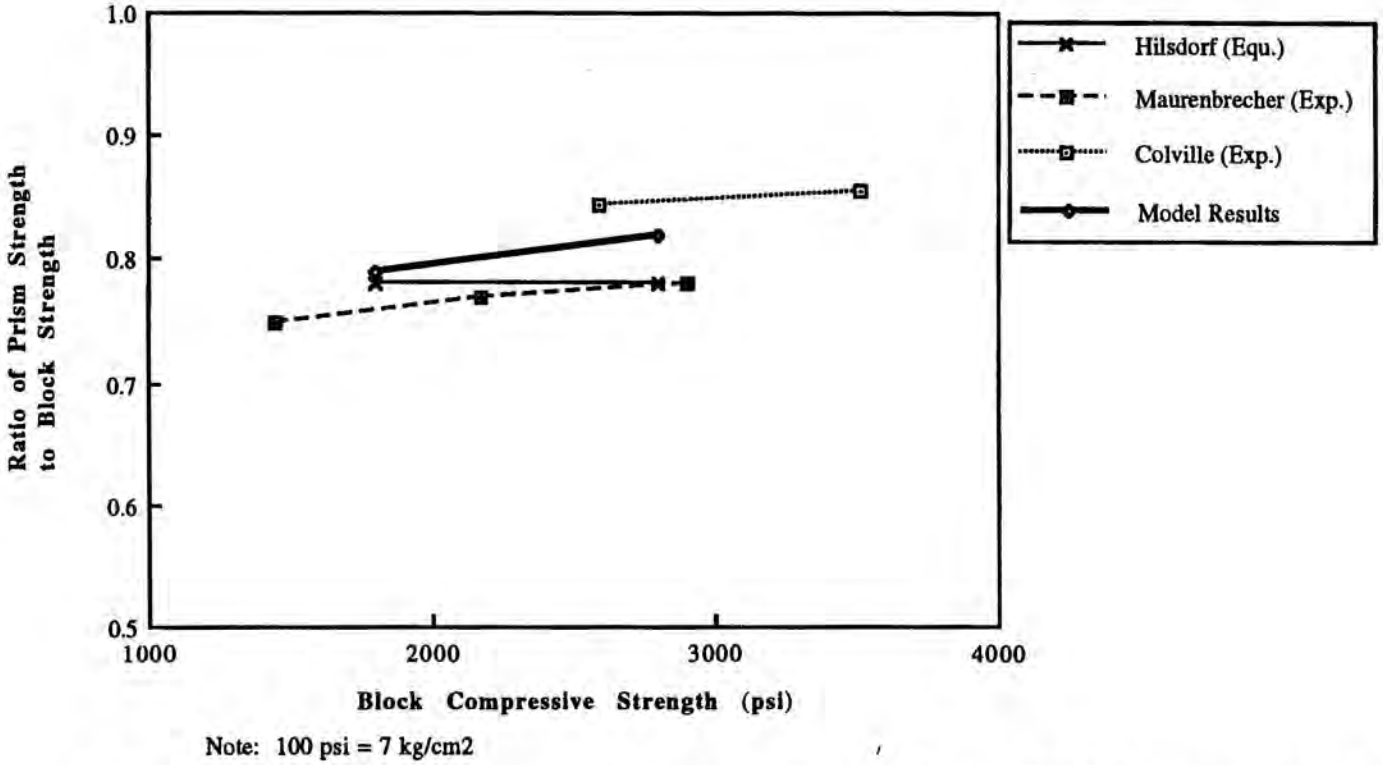

Fig. 3.11 Relationship Between Block Strength and Ratio of Prism to Block Strength for Model and Prototype

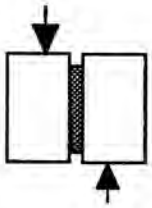

a) Couplet Shear Test Adopted by Benjamin and Williams

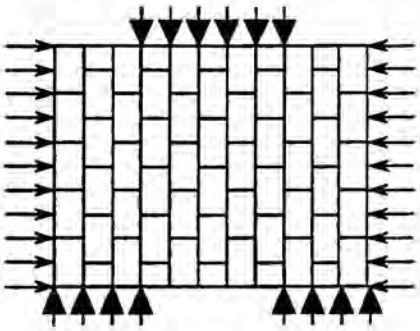

b) Shear Test Specimen Adopted by Haller

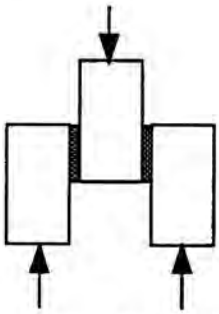

c) Triplet Shear Specimen Used by Jolley

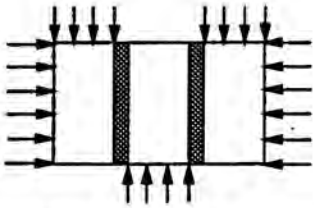

d) Triplet Shear Specimen Tested by Smith and Carter

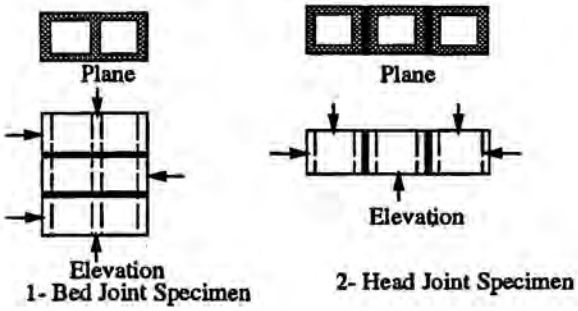

e) Triplet Shear Specimen Tested by Hegemier

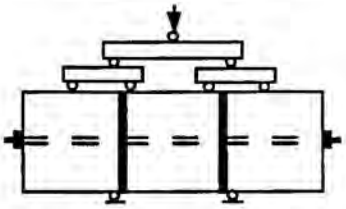

f) Shear Test Set-Up Adopted by Balachandran

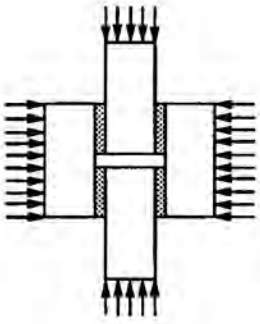

g) Test Arrangement Used by Hamid

Fig. 3.12 Shear Test Method

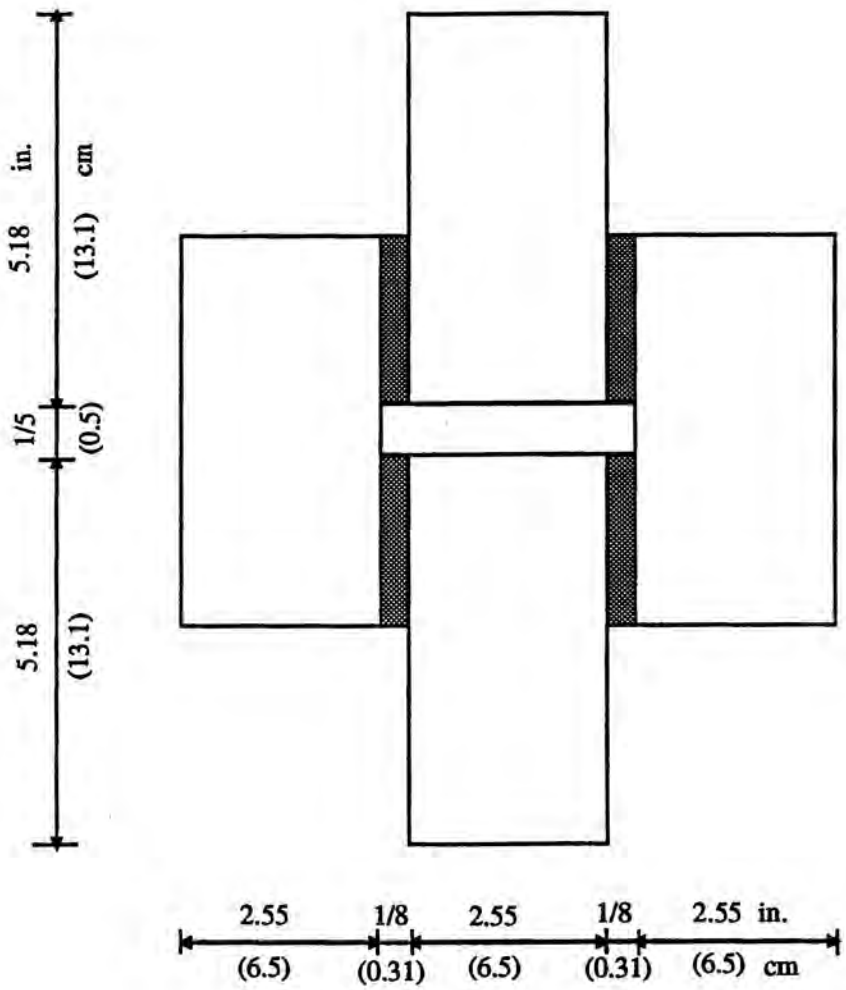

Figure 3.13 Model Shear Test Specimen Used in the Current Program

a)

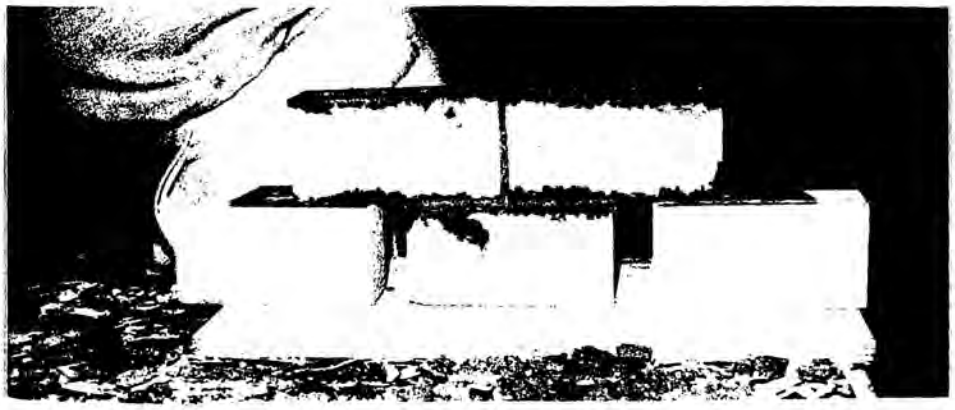

b)

c)

Fig. 3.14 Construction of Model Joint Shear Test Specimens

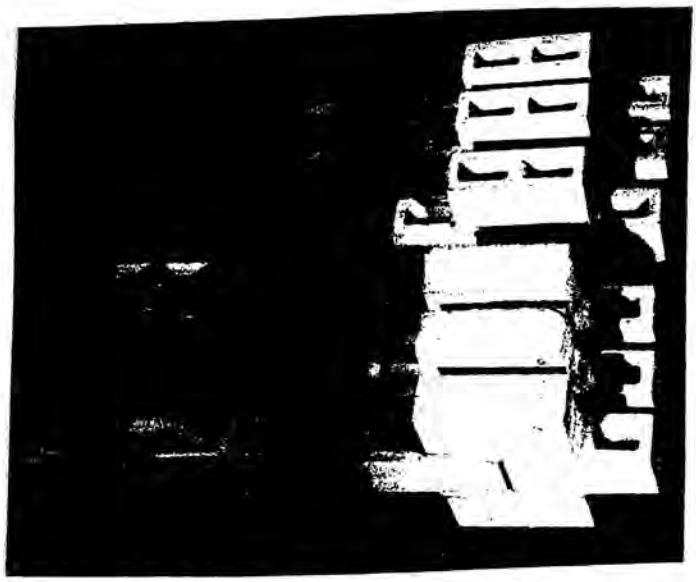

a) Constructed Model Assemblages for Joint Shear Test

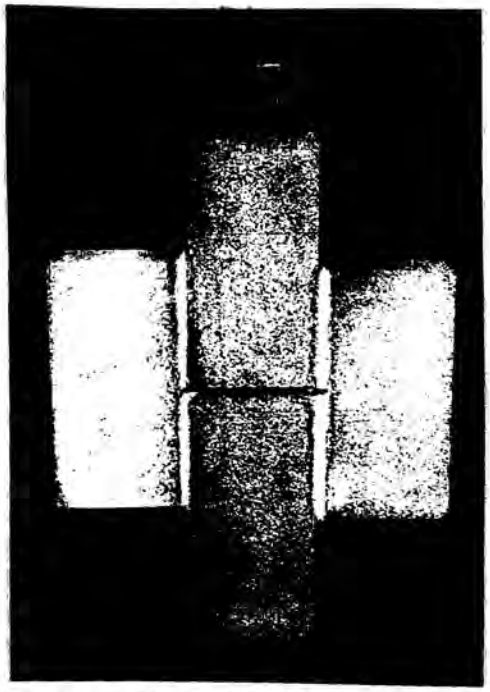

b) Test Set-Up for Model Shear Specimens Without Precompression

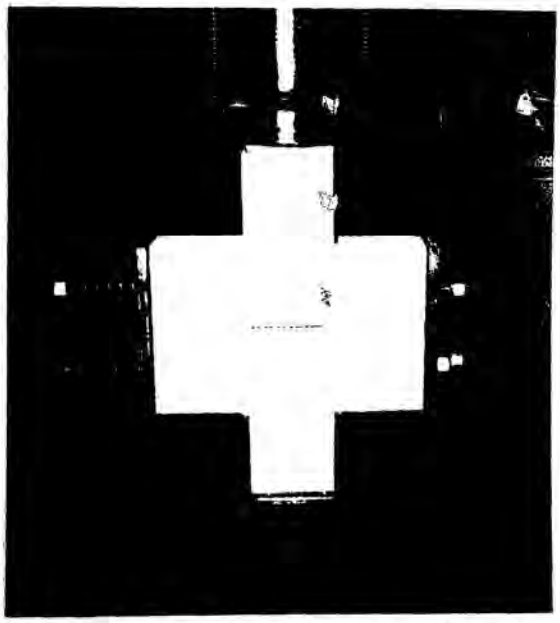

c) Test Set-Up for Model Shear Specimens With Precompression

Fig. 3.15 Joint Shear Test

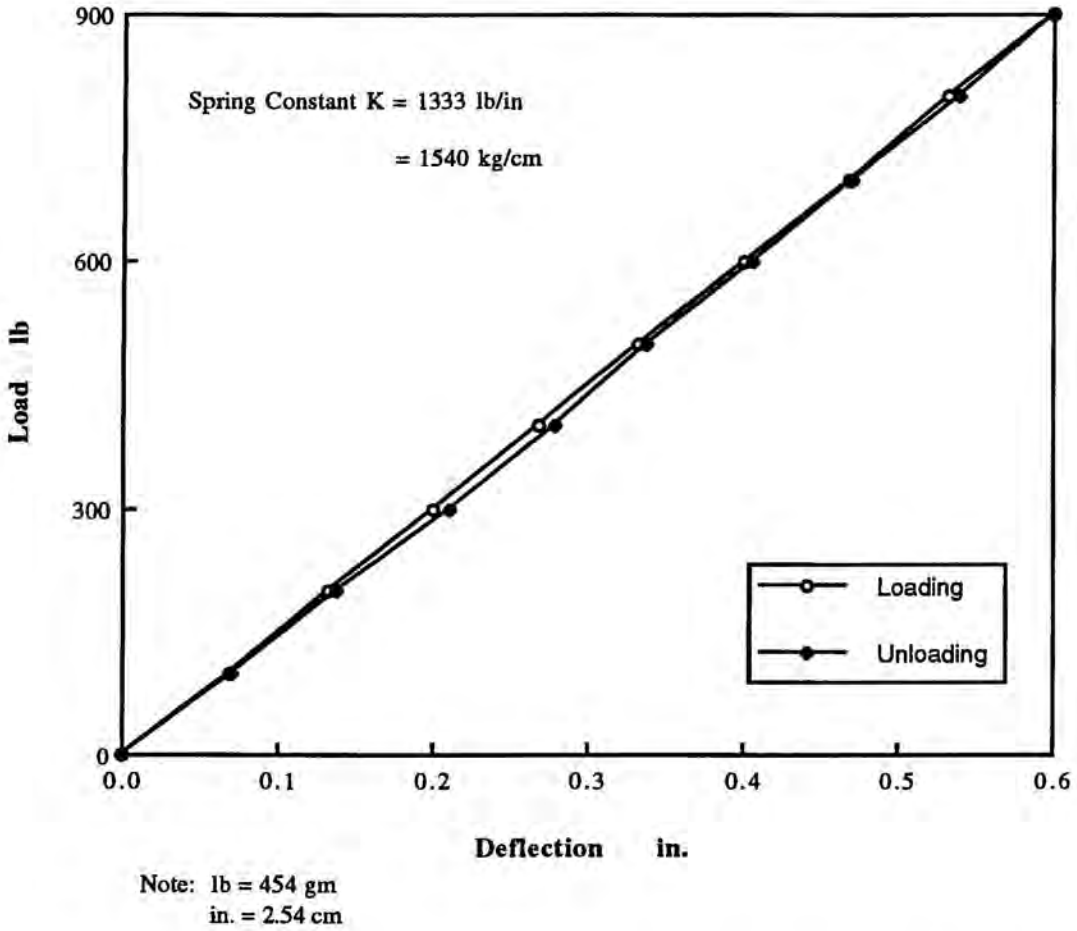

Fig. 3.16 Load Deflection Curve for the Spring (Experimental Spring Consrant)

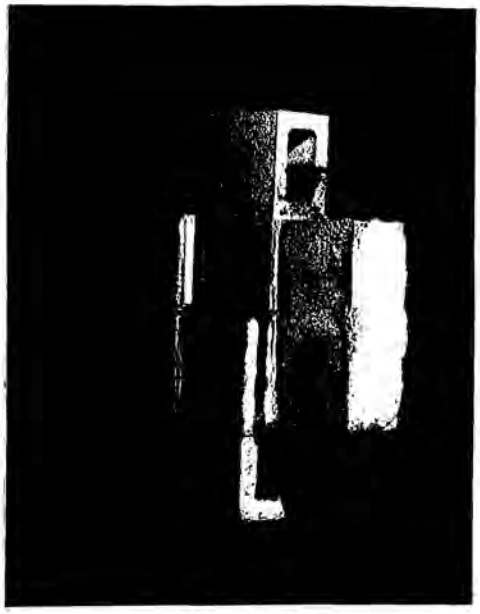

a) Grouted

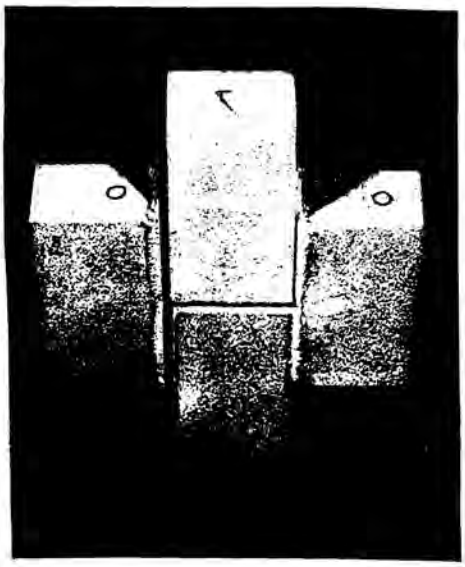

b) Ungrouted

Fig. 3.17 Typical Failure Modes for Shear Specimens

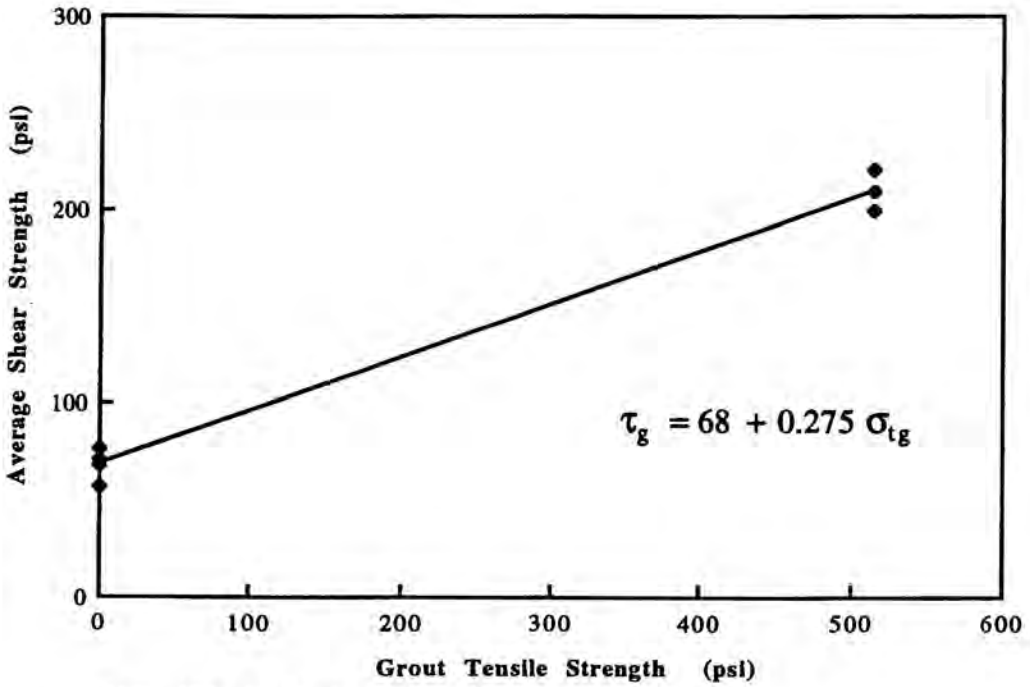

Note: 100 psi = 7 kg/cm2

Fig. 3.18 Effect of Grouting on Joint Shear Capacity of Model Masonry

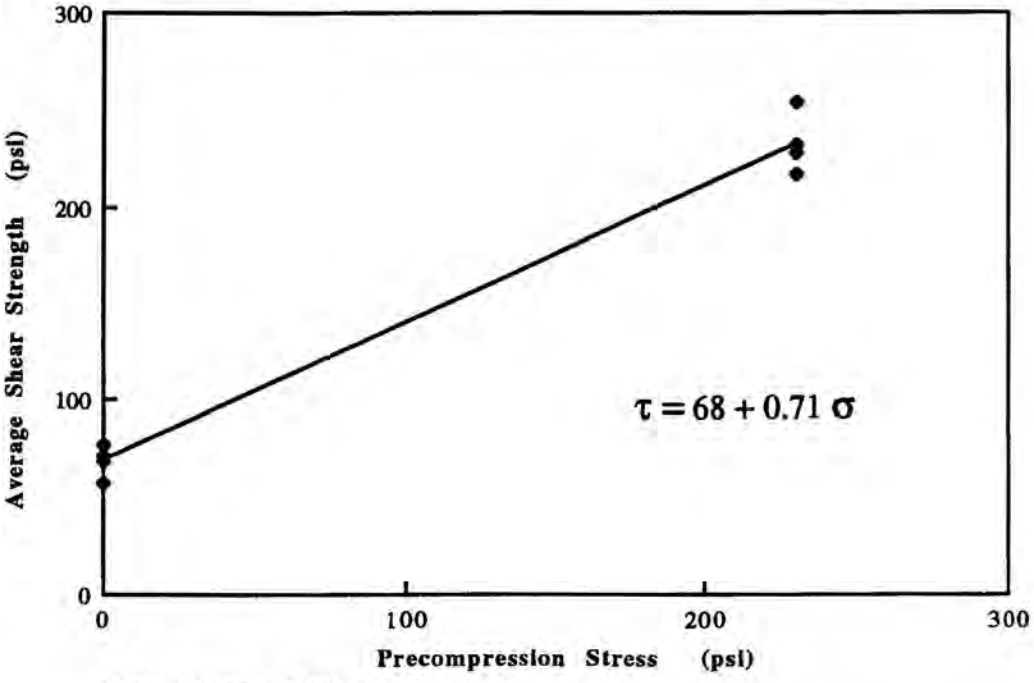

Note: 100 psi = 7 kg/cm2

Fig. 3.19 Effect of Precompression on Joint Shear Capacity of Model Masonry

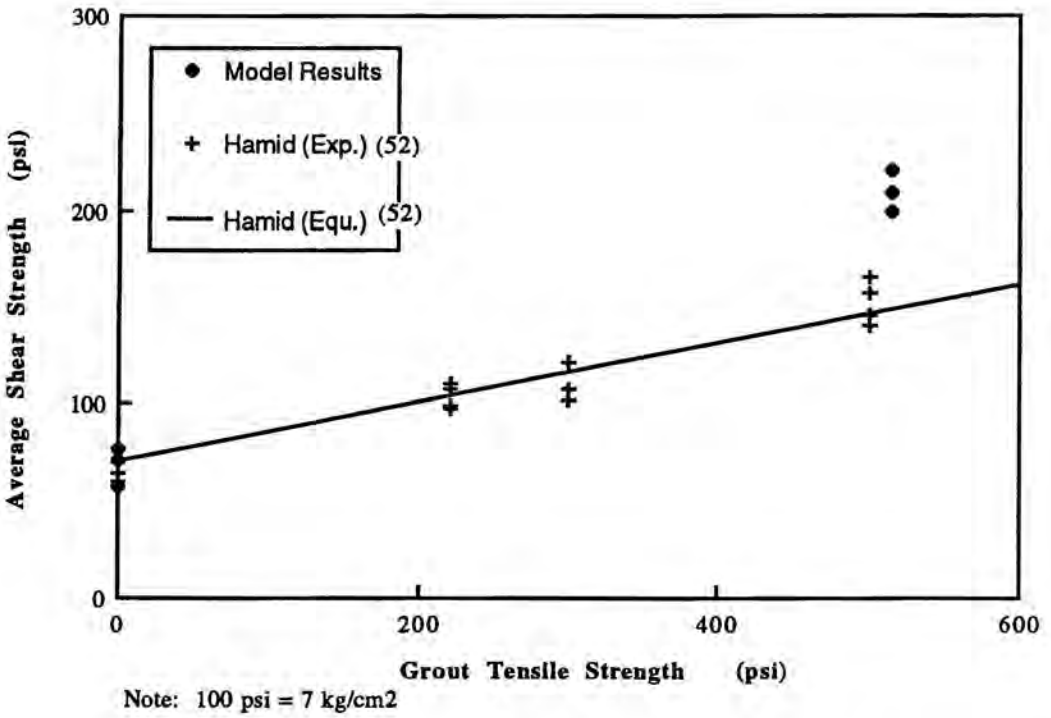

Fig. 3.20 Effect of Grouting on Shear Joint Capacity of Model Masonry Comparison of Model and Prototype Results

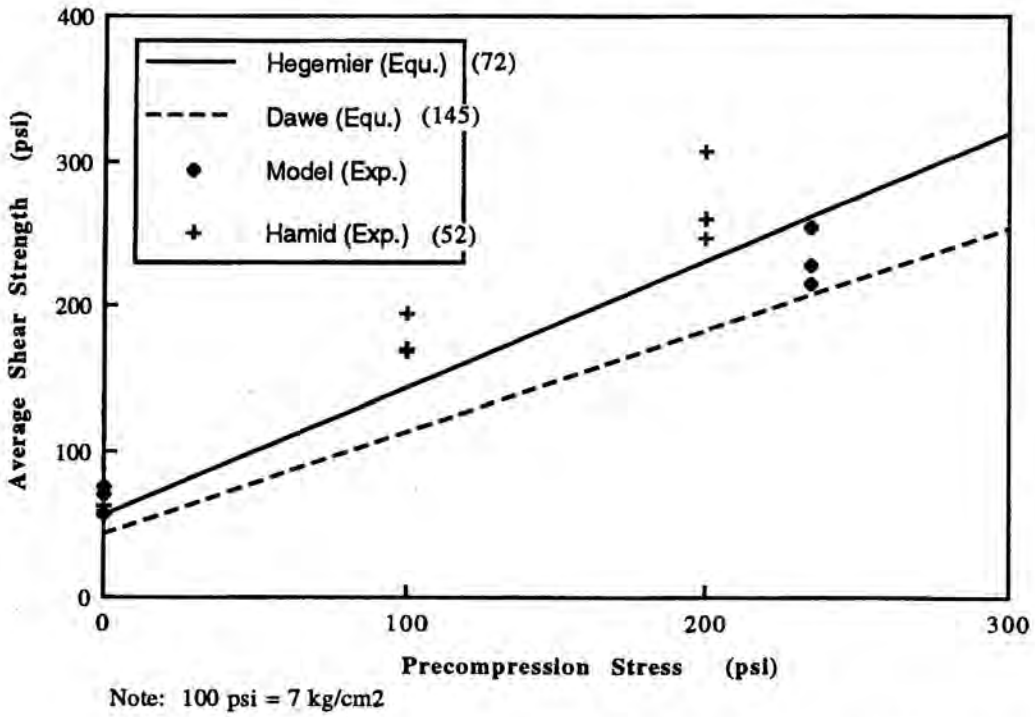

Fig. 3.21 Effect of Precompression on the Joint Shear Capacity Comparison of Model to Prototype Results

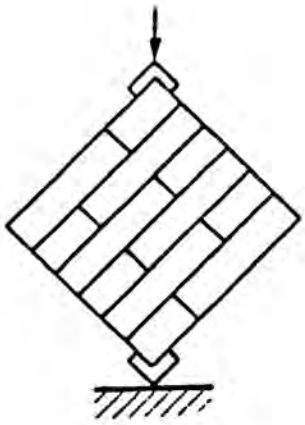

a) Test Specimen Adopted by Meli

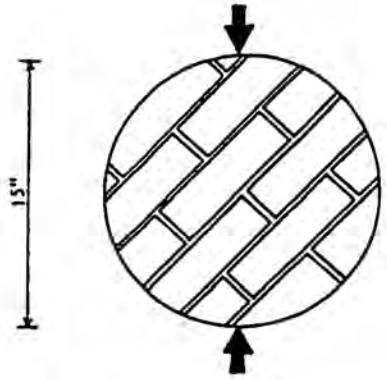

b) Test Specimen Adopted by Johnason and Thomapson

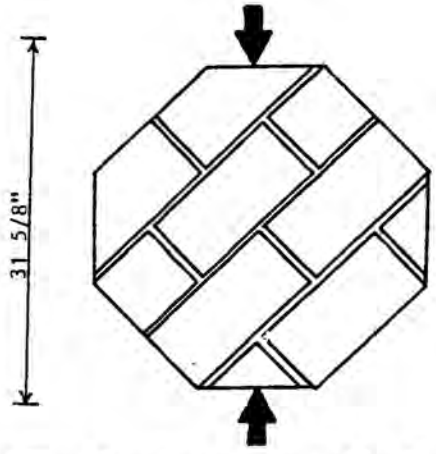

c) Test Specimen Adopted by Hamid

Fig. 3.22 Splitting Test Specimens

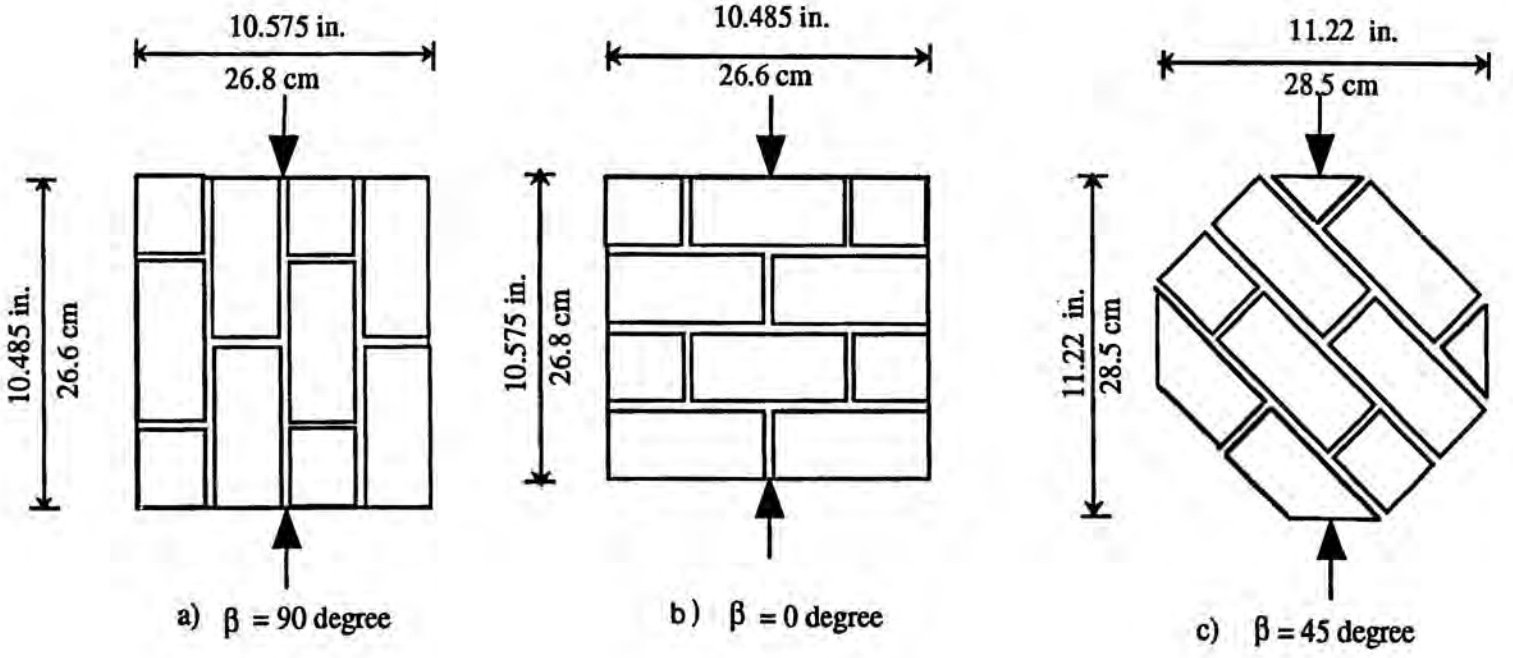

Fig. 3.23 Typical Dimensions of Model Splitting Test Specimens Under Loads Having Three Orientations With Respect to the Bed Joint

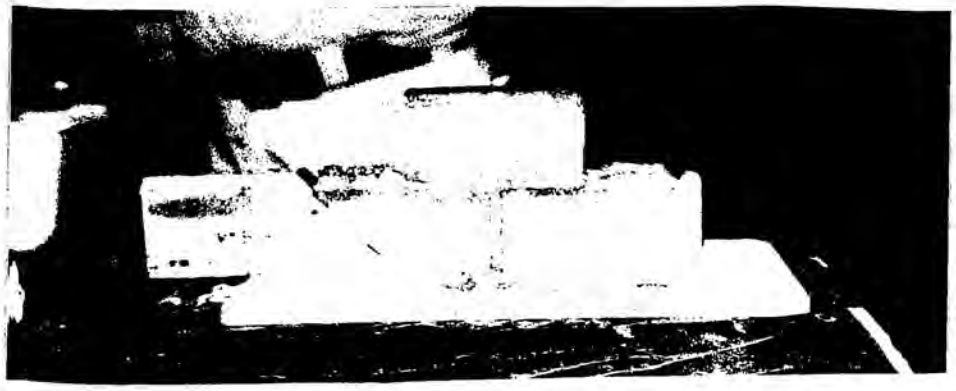

a)

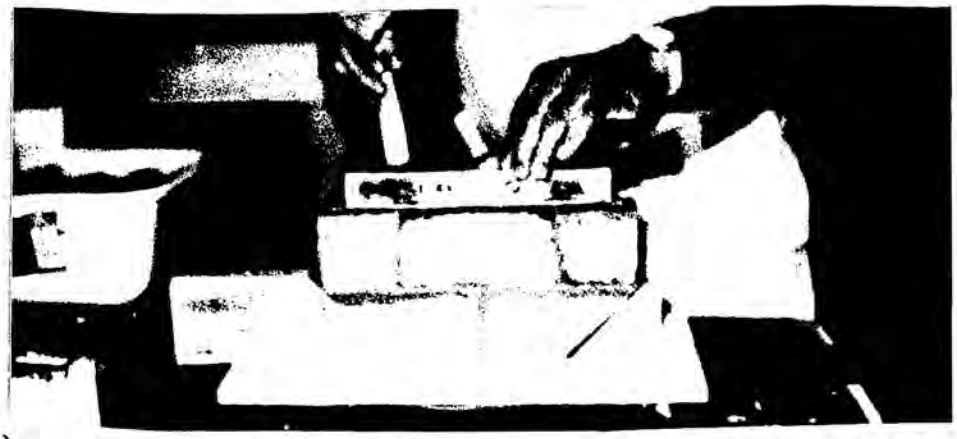

b)

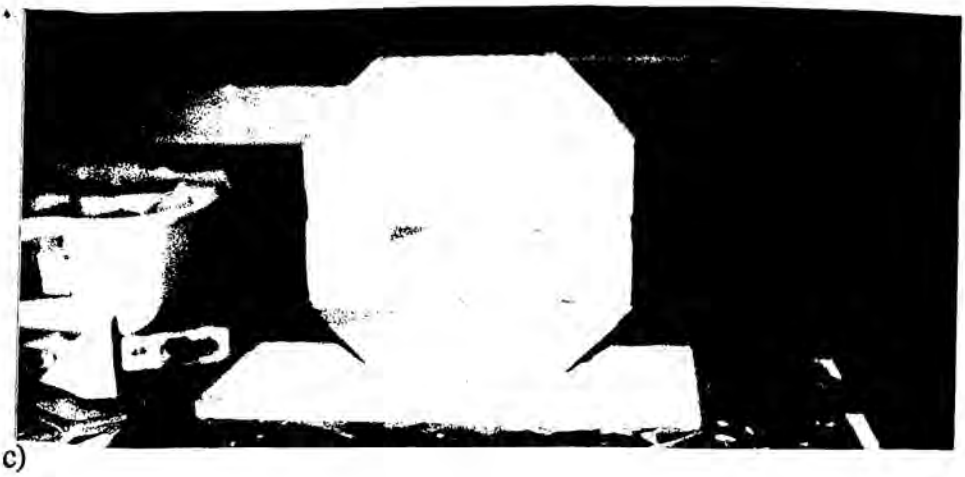

c)

Fig. 3.24 Construction of the Hexagonal Shape Splitting Test Specimens

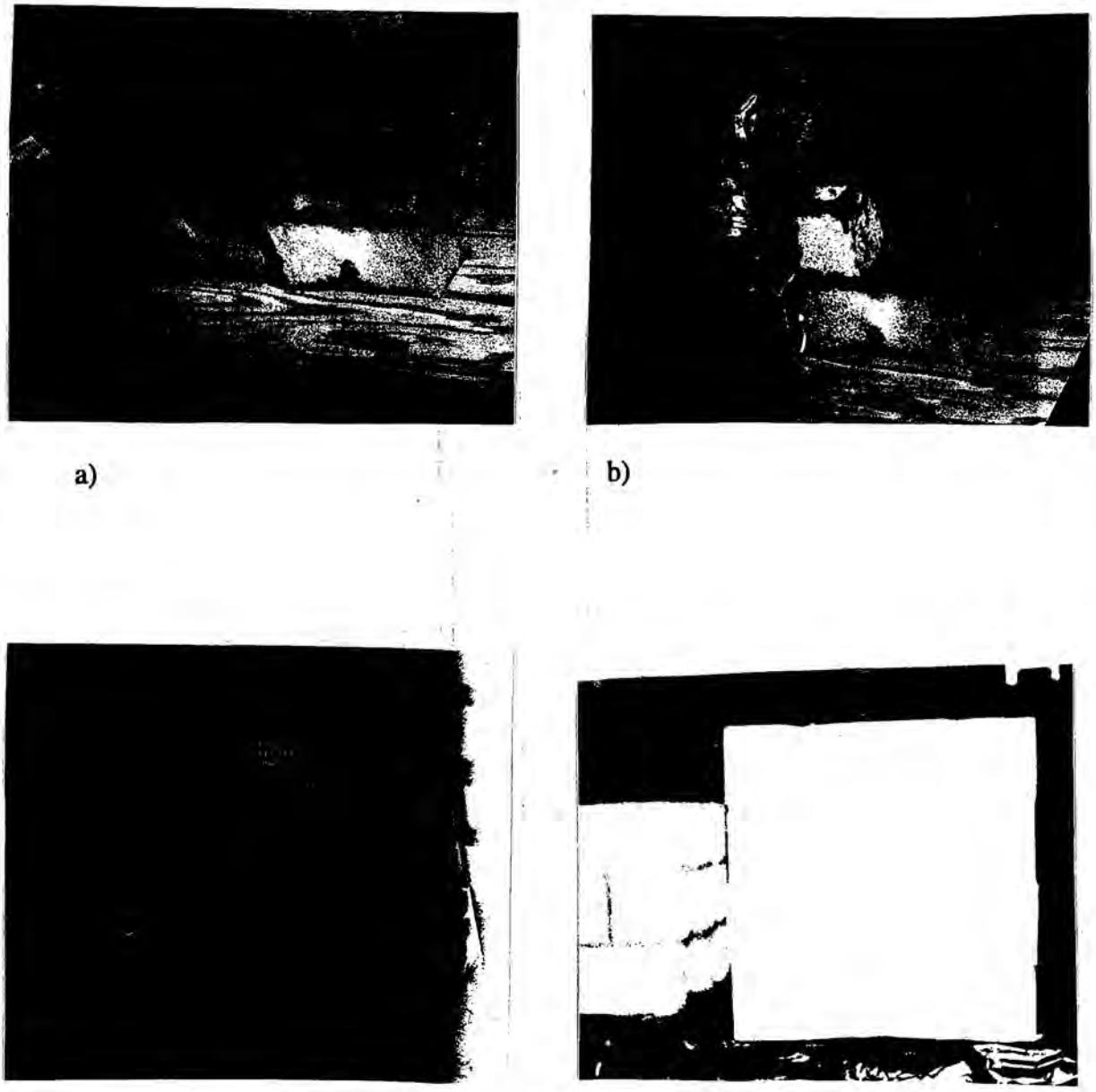

Fig. 3.25 Construction of the Squared Shape Splitting Test Specimens

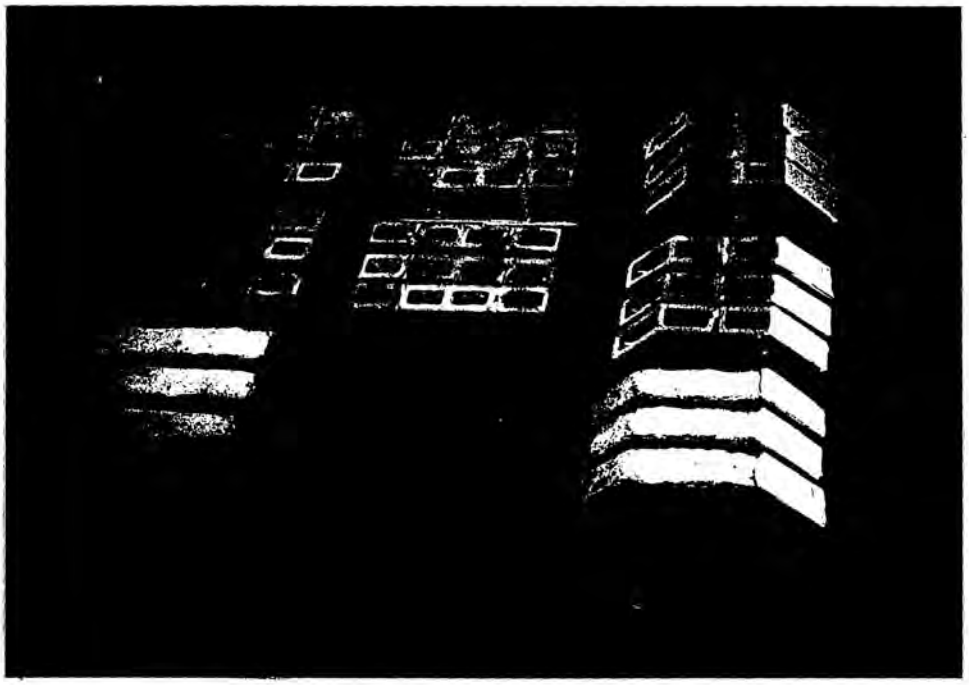

Fig. 3.26 Test Specimens for Splitting Tension

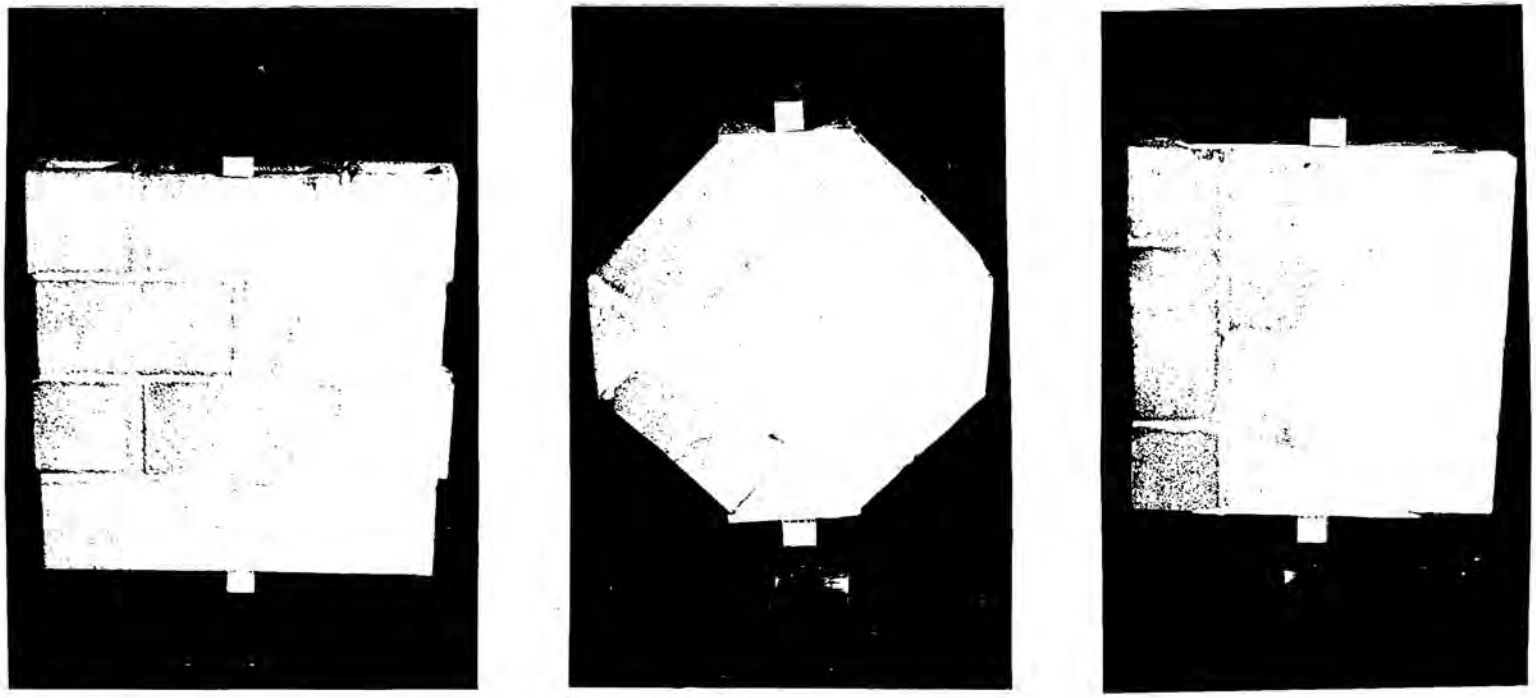

a) $\beta = 0^{o}$ b) $\beta = 45^{o}$ c) $\beta = 90^{o}$

Fig. 3.27 Splitting Tension Test Set-Up

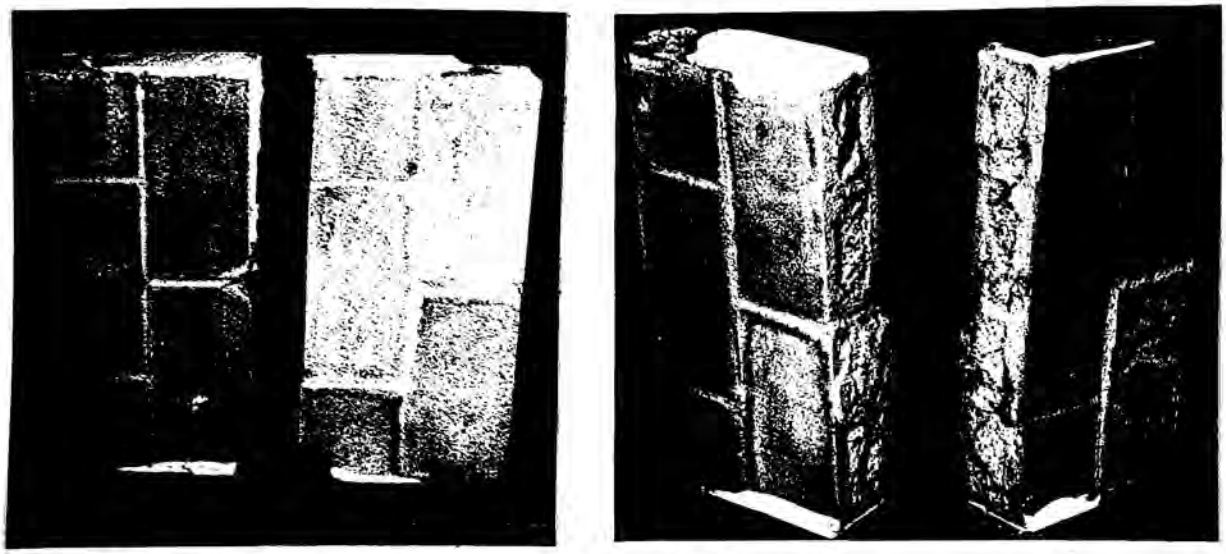

a) Ungrouted b) Grouted

Fig. 3.28 Typical Modes of Failure for Normal Splitting Stress ($\beta = 90^{o}$)

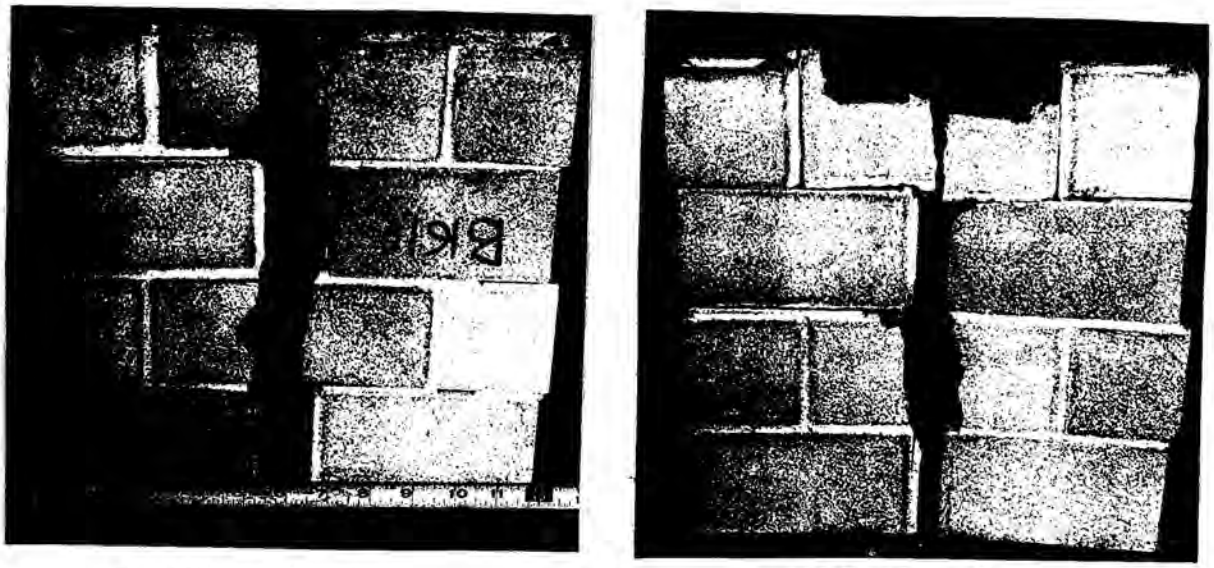

a) Specimen f_{b1} b) Specimen f_{b2}

Fig. 3.29 Typical Modes of Failure for Parallel Splitting Stress ($\beta = 0^{o}$)

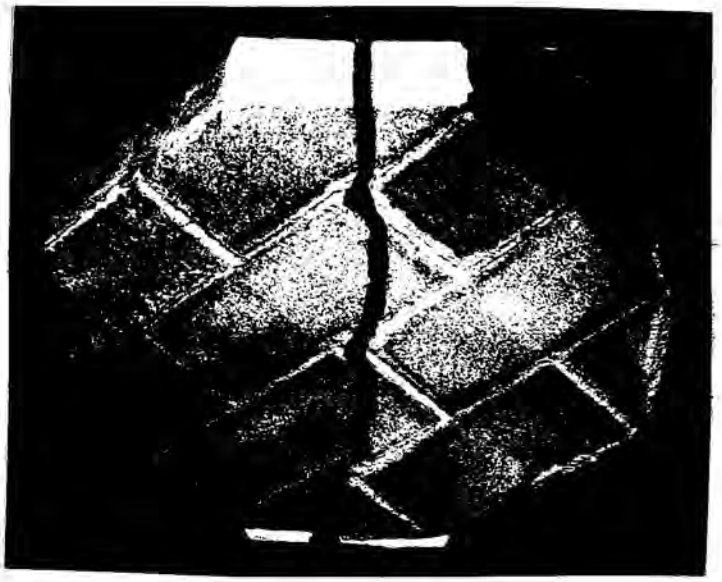

a) Ungrouted

b) Grouted

Fig. 3.30 Typical Modes of Failure for Diagonal Splitting Stress ($\beta = 45^{o}$)

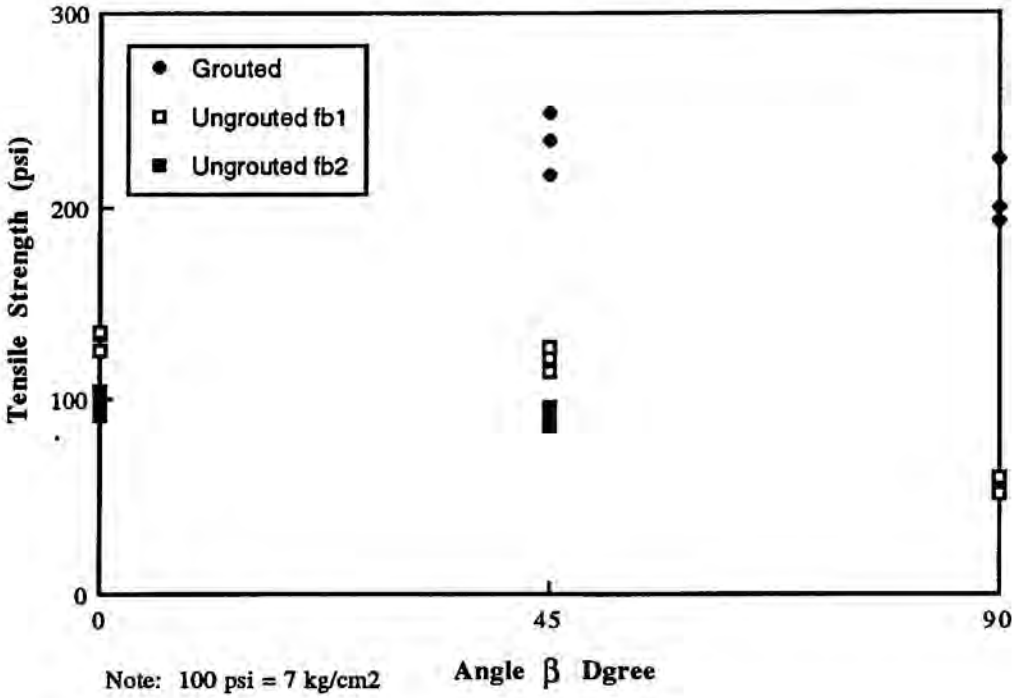

Fig. 3.31 Effect of Stress Orientation on the Tensile Strength of Model Masonry

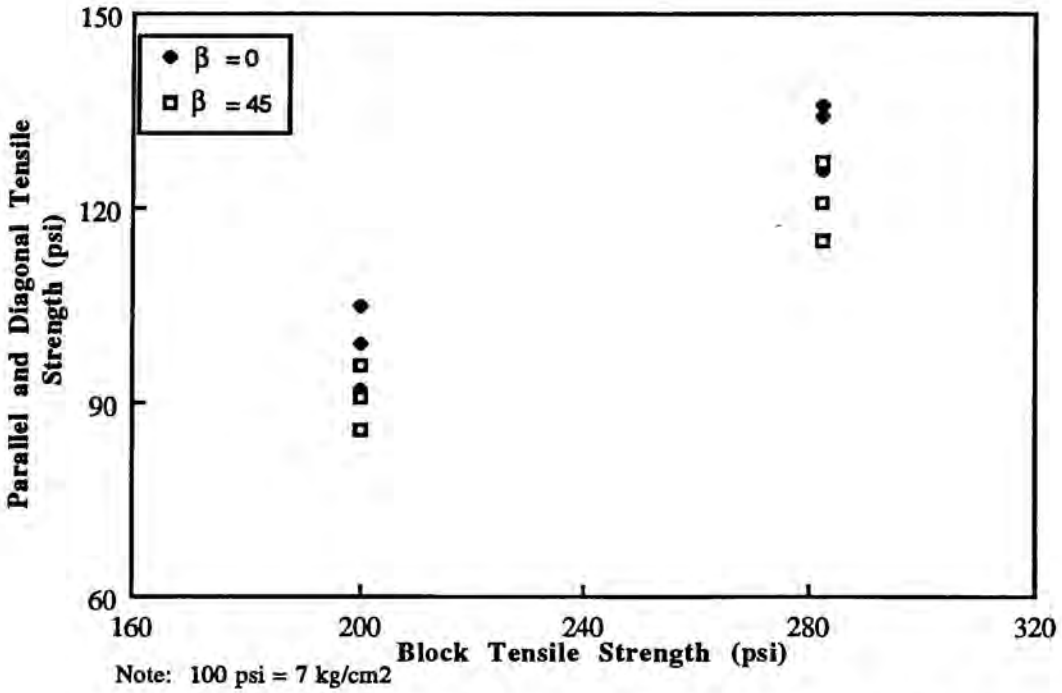

Fig. 3.32 Effect of Block Strength on the Tensile Strength of Model Specimens for the Same Bond Strength

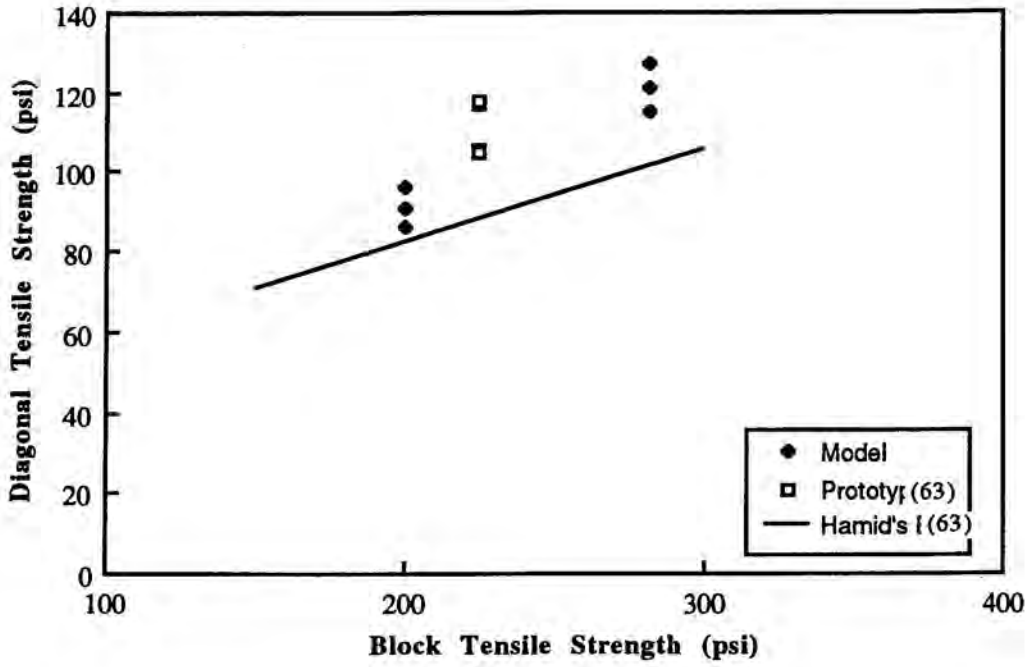

a) Diagonal

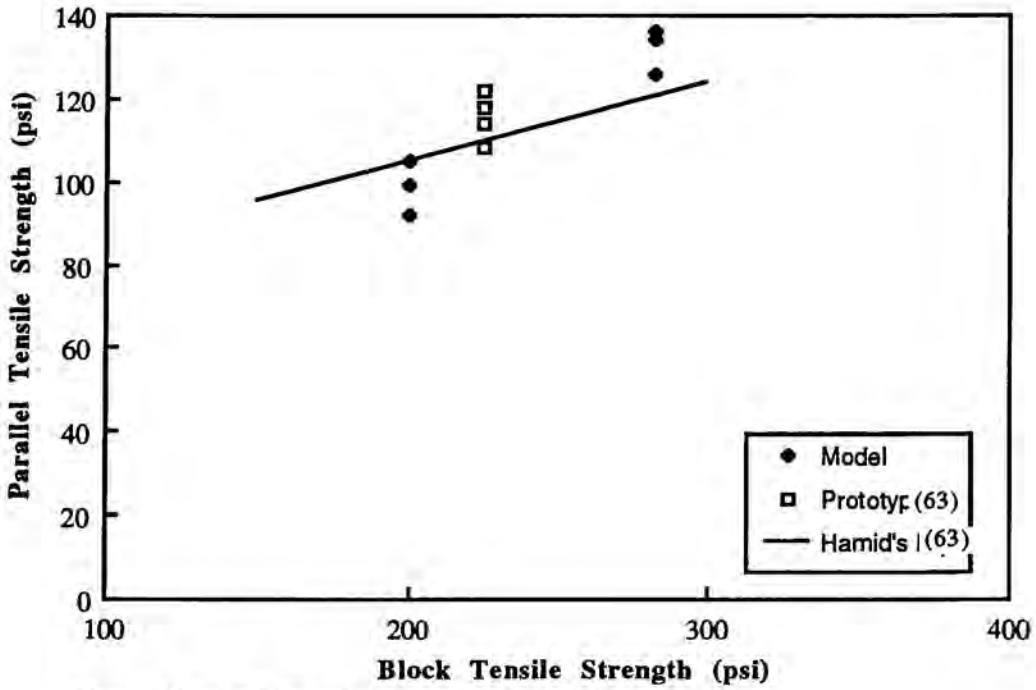

Note: 100 psi = 7 kg/cm2

b) Parallel

Fig. 3.33 Effect of Block Strength on Tensile Strength of Masonry

CHAPTER 4
EXPERIMENTAL PROGRAM FOR SHEAR WALLS

4.1 INTRODUCTION

An important consideration in the analysis of masonry buildings is the ability of the structure to withstand lateral loads due to wind and/or earthquakes. This has led engineers to choose reinforced and partially reinforced masonry for seismic area . The resistance of shear walls to lateral loads is provided predominantly by their in-plane shear or their flexural resistance depending on wall geometry (aspect ratio of the wall, type of block cross-section: solid, hollow or perforated, single-wythe or multi-wythe, and walls cross-section rectangular or flanged) , level of axial stresses, properties of the materials (strength of block units,type of grout, type of mortar, and type of steel reinforcement), and the percentage and distribution of the vertical and horizontal steel reinforcement. Also the behavior of masonry shear walls is significantly influenced by their boundary condition (cantilever or coupled) and the shape and distribution of openings .

In regions of low seismic loads or in areas where seismic forces are not considered to be critical, partially reinforced masonry system is a suitable and more economical system as compared to fully reinforced masonry.

Partially reinforced concrete masonry has the following characteristics: the reinforcement provided is less than 0.002 times the gross cross-sectional area of the wall or the spacing between steel bars either in the vertical or horizontal directions is more than 48 inches (1.2 m) and grouting is applied only to cavities containing the steel bars. In this case reinforcement provided is the minimum needed to control cracking and deflection, to carry tensile and shear stresses, and to increase ductility, and energy absorption, as compared to unreinforced masonry. The definition of partially reinforced masonry according to UBC-91 code[141] and Canadian CSA S304 code[27] is a masonry provided by reinforcement at spacing more than the upper limit of reinforced masonry even if the amount of steel is more than 0.002 times the gross area of the wall. Other codes contains

no information and have not addressed partially reinforced masonry system yet. The UBC-91[141] specifies the maximum spacing of vertical reinforcement in exterior partially reinforced masonry shear walls to be 8 feet (2.4 m) and reinforcement shall be provided each side of each opening and at each corner of the wall. Horizontal reinforcement not less than 0.2 $in.^2$ (1.3 cm^2) in area shall be provided at the top of the footings, at the bottom and top of wall openings, near roof and floor levels as indicated in Fig. 4.1, and at the top of the parapet walls .

The Canadian code[27] specifies that vertical and horizontal reinforcement required to resist flexural tensile stresses shall be continuous between lateral supports and shall be spaced not more than 2.4 m on center along the length and height of the wall, it shall be provided at each side of openings over than 1.2 m wide, it shall be provided at each side of control joints , and shall be provided at the corners and at the ends of the wall.

Partially reinforced masonry system which possesses improved compressive strength, tensile strength, flexibility and ductility is less costly than reinforced concrete masonry. Thus, this system offers considerable scope for widening the range of applications in situations where tension is small enough to require steel spaced more than 4 feet (1.2 m) on center .

From design stand point according to the UBC-91 code[141] and the CSA S304 code[27], partially reinforced masonry walls shall be designed as plain masonry walls spaning between the reinforcing cells except that reinforcement may be considered in resisting flexural tensile stresses and shear stresses. Masonry codes do not contain analytical formulas for estimating shear and flexural strength of partially reinforced concrete masonry. Analytical models to predict the behavior of partially reinforced masonry walls are not yet available. This indicate the need for more research to enable partially reinforced concrete masonry to achieve its full potential[49] .

Therefore, the present study focuses on the behavior of partially reinforced masonry shear walls subjected to in-plane monotonically increasing and reversed cyclic

loading representing wind or earthquake actions. The gravity loads transmitted from the above floors are represented by a constant axial load acting at the top of the shear walls. The aim of this study is to investigate the behavioral characteristics of partially reinforced shear walls, and to provide analytical expression for estimating the shear and flexural strength of partially reinforced masonry shear walls .

4.2 LITERATURE REVIEW

While there is a significant amount of research on reinforced masonry shear walls only a few number of investigations have been performed on partially reinforced concrete masonry walls with focus on the out-of-plane behavior. The in-plane behavior of partially reinforced masonry shear walls have not yet been addressed and no information is available on the design of such a system. Therefore, the available knowledge on the behavior of reinforced masonry walls will be utilized and modified for application to partially reinforced masonry walls .

4.2.1 Reinforced Masonry Shear Walls

Significant research on the behavior of masonry shear walls under in-plane lateral loads has been reported, especially during the last decade. These include both bricks and concrete blocks, unreinforced and reinforced. In what follows, a brief summary of some of the work on reinforced masonry shear walls is presented .

Schneider[121] carried out extensive tests to study the shear behavior of concrete piers, the parameters studied included: aspect ratio of the walls, presence of web reinforcement, and effect of axial compressive load. It was concluded that: shear strength increased with a decrease in aspect ratio of the wall and that the presence of horizontal web reinforcement improves the shear behavior of the pier. Some increase in shear strength and pier stiffness was observed when an external axial compressive load was applied .

Scrivener, et al[123&124] performed several tests on reinforced concrete masonry walls, where the major parameters studied were the amount and distribution of steel

reinforcement. Their effect on the stiffness and the failure load was investigated. It was demonstrated that: stiffness and failure load increase with increasing the amount of vertical reinforcement, with being more efficiency when used in the periphery of the wall. The inclusion of bond beams increased the wall strength by about 20 to 50 %.

Significant work was done by Blume[23] to evaluate the shear strength of grouted brick masonry walls and to observe the influence of the amount and orientation of the reinforcing steel upon the strength and ductility of the panels. He concluded that the minimum recommended grout core thickness is 2 in. (50 mm) for high-lift grouting, the reinforcement in excess of the minimum specified by the code is not justified on the basis of the slight increase in ductility and energy absorption capacity that is obtained, and the arbitrary use of large percentage of steel area or closely spaced bars in grouted masonry should not be encouraged .

An important effort on the shear strength of model shear walls was conducted by Sinha and Hendry[131] at University of Edinburgh. After demonstrating that the strengths of brick and mortar can be reproduced in a model test, shear strength tests were carried out on a 1/6-scale model structure. Compressive and racking loads were applied to test specimens. Two types of failure were observed: a shear failure at the brick-mortar interfaces, and a diagonal tension cracking through bricks and mortar .

In the early seventies, Williams[145] carried out tests to study the behavior of reinforced concrete masonry shear walls under static and dynamic loads. The parameters investigated included: distribution of steel reinforcement, magnitude of axial load, and the wall geometry and their effect on ductility, stiffness degradation and load capacity of the shear walls were examined. He concluded that for an aspect ratio of two or more (provided that the shear strength exceeds the ultimate flexural strength) a ductile behavior is observed and can be predicted. Such behavior is characterized by minor stiffness degradation and a negligible load deterioration under load repetition and generally can be obtained in cases of low reinforcement, high aspect ratio, low bearing load and low flexural strength. As the

energy dissipation capability of the shear walls behaving in a shear predominant mode is of great importance, attention should paid to construction details. Another important conclusion drawn by Williams was that for flexural brick walls that showed a satisfactory ductile behavior under static loading, a severe loss of structural capability occurred with load repetition, which suggests that results from static tests cannot be applied to dynamic situations. However, for the walls where shear effects prevailed, static and dynamic behavior were nearly the same .

Meli[94&95] investigated the behavior of 6x6 feet (1.82x1.82 m) cantilever concrete and clay brick walls subjected to monotonic lateral loads and to cycles of alternating lateral loads. He found that for a low vertical steel ratio the failure was governed by flexure. Extensive flexural cracking occurred and failure was due to toe crushing or rupture of extreme bars. Precompression of the wall increases the strength but for high vertical stresses the behavior tended to change to a brittle shear failure. For high steel ratio, failure was governed by shear. A high stiffness was maintained until a diagonal crack occurred. Cracking generally occurred at the joints, but for high precompression loads or low strength units cracks crossed the units .

At the University of California-Barkely, Mayes, et al[91&92] carried out series of tests on concrete block masonry walls subjected to lateral in-plane cyclic loading to examine the effect of rate of loading, presence of vertical and horizontal reinforcement and the effect of partially grouted and fully grouted on the behavior of reinforced masonry walls. It was concluded that: Sufficient amount of horizontal steel enhance the ductility of shear mode response significantly. Use of 1/8 inches perforated steel plates in the toe area improves flexural mode response. Partial grouting improves the elastic-plastic shear mode response compared with fully grouting.

Thirty walls were tested under cyclic and control axial load using lateral load test method with top and bottom of walls kept rotationally fixed by Sveinsson, B. I., et al[139]. The aim of the tests is to examine the type of masonry, distribution and amount of vertical

and horizontal reinforcement, and axial load. It was concluded that: Increasing axial load increases lateral load resistance significantly. Increasing axial load increases ductility. Increasing axial load changes the mode of response from flexural to shear. Amount of horizontal reinforcement is not a significant factor in hysteretic behavior. Effect of axial load and horizontal reinforcement on stiffness degradation is not very significant.

More recently a significant research on shear walls was carried out at the University of Colorado by Shing et al[126-130] as a part of the U.S-Japan Coordinated Program for Masonry Building Research. A total number of 22 reinforced concrete and brick masonry walls have been tested under quasi-static fully reversed cyclic loading. The parameters studied included: the amount of vertical and horizontal steel reinforcement, the distribution of the horizontal steel, the magnitude of the axial load, the displacement history of the applied load, and the wall geometry. Their effects on stiffness degradation, base slip, ductility, the capacity limit state, and energy dissipation capability were examined. Also the research aimed at evaluating the validity of the UBC-91 design formulas for ultimate shear capacity of reinforced masonry shear walls. Shing concluded that: wall specimens that exhibited a predominantly flexural behavior were more ductile than those dominated by diagonal shear cracking, except under high axial loads. The flexural ductility was reduced when the axial load was increased. The occurrence of the first major diagonal crack depends on the tensile strength of masonry, and not very much on the amount of reinforcement present. The postcracked resistance depends on the amount of horizontal and vertical steel. Increasing the amount of horizontal steel can change the inelastic behavior from a brittle shear mode to a flexural mode. However, the amount of horizontal steel required to inhibit brittle shear behavior depends on the flexural strength as well on the shear resistance provided by the dowel action of the vertical steel and the aggregate interlock mechanism. On the other hand, increasing the axial load can change the behavior from a mixed flexural/shear mode to a brittle mode. It was also concluded that the UBC-91 specification for the masonry shear strength is overly conservative for walls tested in this study.

Hirashi[78] performed tests on nine walls subjected to lateral cyclic load history to study the effect of type of masonry and horizontal reinforcement on the flexural behavior of reinforced masonry walls. He concluded that increasing the amount of horizontal reinforcement increases the maximum shear to flexural strength ratio and significantly improves deformation capacity, the ability to simultaneously develop large deformation with substantial strength degradation and also the ratio of maximum strength to cracking shear strength was in the range of 1.3 to 1.8 indicating that substantial post cracking strength gain is possible in shear mode failures, depending primarily on the effective use, rather than the amount of horizontal reinforcement.

Wakabayashi, M. and Nakamura, T.[144] tested six fully grouted hollow brick walls were axially loaded under dynamic lateral load, and six walls constructed with 1/3-scale solid and hollow brick units were tested under cyclic lateral load, to study the effect of size of units, axial stress and horizontal reinforcement on the behavior of reinforced brick masonry walls. It was concluded that: A horizontal reinforcement ratio of 0.85% or greater is required for ductile shear failure and that maximum shear capacity can be predicted reasonably by using a combination of truss and arch analogies and stress-strain relationship developed from diagonal compression and diagonal tension tests. It was also found that hysteretic response curve can be developed using a combination of slip, degrading and bilinear hysteretic models.

Matsumura, A.[89], carried out several tests on 57 concrete masonry and 23 brick masonry walls subjected to cyclic in-plane shear and constant axial loads aimed at deriving a formula for predicting the shear strength of reinforced masonry walls and to determine the difference in shear strength between fully grouted and partially grouted walls. He suggested a formula for prediction of the shear strength of reinforced masonry walls. This formula is a synthesis of the mathematical expressions derived to quantify the influences of the test variables. Reduction factors are introduced to account for the use of partial grouting and for the cantilever test set-up versus the fixed-fixed boundary condition.

Probably the most important work done in that area was carried out by Priestley[111&112], to study the seismic resistance of reinforced concrete masonry shear walls. The experimental ultimate loads were compared with theoretical ultimate loads. Priestley analyzed the influence of base-course slip and compared experimental displacement ductility with code required ductility. He proposed two formulas to predict the flexural strength of masonry shear walls with distributed and concentrated steel reinforcement. He concluded that when all shear stresses is carried by adequately anchored horizontal steel, higher maximum shear stresses should be allowed. The test results indicate that current New Zealand design practice overestimates the cracked stiffness of walls by a factor of more than 2. The current under capacity factor ø for walls subjected to axial compression and bending should be increased from 0.65 to 0.85.

Later at Drexel University, Larbi, A.[87] carried out tests on nine concrete block masonry shear walls under in-plane horizontal and vertical loads using 1/3-scale model. The parameters investigated were the vertical and horizontal reinforcement ratio. Seven walls were tested under monotonically increasing loads and two walls were subjected to reversed cyclic loads. All specimens were subjected to an axial precompression of 270 psi (19 kg/cm^2) and tested as cantilever walls. These parameters duplicate the parameters studied by Shing using full scale test panels to evaluate the using of 1/3-scale in predicting the behavior of fully reinforced masonry. This study concluded that: the overall behavior of the wall panels were very well duplicated to the prototype results conducted by Shing. Flexural and shear strengths increased with the amount of vertical reinforcement. Increasing the vertical reinforcement ratio , favored the shear failure, therefore decreased the wall ductility. The behavior changed from a shear (brittle) failure to a flexural (more ductile) failure when horizontal reinforcement was increased. Hence, with proper amount of horizontal reinforcement, the diagonal tensile failure (brittle) can be inhibited and consequently an improved behavior would result. Flexural strength can be predicted with a reasonable accuracy if the masonry and steel mechanical properties are accurately modeled.

A review of the technical literature on masonry shear wall tests was conducted by Yancey, et al[146] to determine the range and depth of available research and to identify areas in need of additional research. The review covers documents published from 1976 to 1989 and includes approximately seven hundred masonry wall tests.

4.2.2 Partially Grouted Masonry Walls

All the research outlined in the previous section dealt with fully grouted walls. As prerequisite to understanding the behavior of partially reinforced concrete masonry shear walls, the behavior of partially grouted masonry walls must be studied. Partially grouted masonry shear walls are constructed from hollow concrete masonry unit where the ends and intermediate cells are grouted with large spacing between them.

Most of the research studied on partially grouted concrete masonry is carried out as extensions of investigations[54-56] dealing with fully grouted concrete masonry where the extent of grouting was varied to include few configurations of partially reinforced concrete masonry. Both model and full scale test results are available, but the test results are few. These studies indicate that partially grouted concrete masonry is inferior to fully grouted reinforced concrete masonry and superior to hollow concrete masonry. Still partially reinforced concrete masonry, per se, remains to be researched.

An important study of partially grouted concrete masonry was carried out by Elnawawy and Hamid[41] and the investigation dealt with flexural tensile strength. This property influences the cracking moment and also helps to predict and control deflection of masonry walls under service loads. The results indicated that the extent of grouting significantly affects the flexural tensile strength of concrete masonry. The apparent factor of safety against cracking of concrete masonry calculated from allowable flexural stresses specified in ACI/530 ASCE 5 code[2] is not constant for different extents of grouting.

Vekey[36] and Hamid et al[57] studied grout placement and quality, which has an important influence on the strength of partially reinforced concrete masonry. The results

indicate that satisfactory grouting can be attained if suitable adjustments are made in the grout composition to accommodate the dewatering action by the absorptive surface of the masonry "shuttering" which may lead to fissures in the grout. Also pumping as well as hand compaction can be employed in the placement of grout.

Fouad[48] carried out experimental tests and developed a nonlinear finite element model to study the general behavior of partially grouted walls subjected to in-plane concentric and eccentric concentrated loads. They concluded that: grouting the two cells beneath the concentrated load had similar effect as that for fully grouted walls, since these two cells are quite enough and sufficient to increase the load carrying capacity of the walls therefore, there is no need for fully grouting the walls in this case. Grouting the two cores next to the loaded central cores had a negligible effect on the cracking load, failure load, deflections, and the distribution of the vertical and horizontal strains within the walls.

A significant work was done by Chandrakeerthy and Hamid[58] to evaluate the compressive strength of partially grouted concrete masonry using 1/3-scale model wall elements and to observe the influence of grout spacing on the failure mechanisms. They concluded that : the ultimate load per unit length in compression increases as grout spacing decreases. It was also concluded that compressive strength based on gross area is more suited for use with partially grouted concrete than that based on net area, since stresses are not distributed uniformly over the net area. They recommended the following formula for compressive strength of partially grouted wall

$$f'_{mpg} = 0.64\, f_b\, (1 - \beta) + 1.07\, \phi\, f_g \qquad (4.1)$$

where

f'_{mpg} = the compressive strength of partially grouted wall based on the gross area

f_b & f_g = the compressive strength of concrete block and grout, respectively

β = the ratio of net area to gross area of the unit

ϕ = the ratio of grouted area to gross area

This formula can be applied to concrete masonry shear walls as well as flexural walls with the same accuracy, since this equation defined by the ratio of grouted area to gross area and not dependent on the grout spacing .

They also proposed an equation based on the best fit of the experimental results to predict the compressive strength of partially grouted walls within the range of grout spacing ranging from 8 in. to 32 in.

$$f'_{mpg} / f'_{mg} = 1.08 - 0.01\ s \qquad (4.2)$$

where

f'_{mpg} & f'_{mg} are the compressive strength of partially and fully grouted walls based on the gross area

s is the grout spacing in inches

This formula can be modified for concrete masonry shear walls by replacing S by l_w/n as follows :

$$f'_{mpg} / f'_{mg} = 1.08 - 0.01\ (l_w / n) \qquad (4.3)$$

where

l_w is the total length of the shear wall

n is the number of grouted cells

ACI 530/ASTM 5 code[2] identifies partially grouted concrete masonry as a distinct material and specifies values for allowable flexural tensile stresses. However, codes give no information on properties or design of partially grouted concrete masonry elements under compression, or shear, or tension. Valuable information on grouting procedure is given in codes dealing with important aspects such as grout mixes, cleaning of grout space and removal of mortar projections, period of grouting, consolidation of grout, horizontal construction joints between two grout pours, size and height limit of grout space, provision of cleanouts, maximum grout lift, and placement of reinforcement. This information is applicable to partially grouted masonry as it is for fully grouted masonry construction .

As noted from the survey of the avialabe literature reported in this section, the behavior of partially reinforced masonry shear walls under in-plane vertical and lateral loads, has not been fully investigated, therefore this study was initiated at Drexel University in 1990 to investigate of the behavior characteristics of partially reinforced masonry shear walls under in-plane monotonic and cyclic loading .

4.3 OBJECTIVES AND SCOPE

The overall objective of this investigation is to evaluate the in-plane behavior of partially reinforced concrete block masonry shear walls under in-plane monotonically increasing and reversed cyclic loading using small-scale direct modeling techniques. The specific objectives of this experimental program are :

1- To have a better understanding of the behavioral characteristics of partially reinforced concrete block masonry shear walls under combined in-plane vertical and lateral loads .

2- To study the effect of block strength, axial stress, lateral load (monotonically increasing and reversed cyclically loading), and amount and distribution of vertical and horizontal steel reinforcement on :

- The load-deflection relationship ,
- Shear strength , in-plane flexure, and wall ductility ,
- Crack patterns and
- The stress distribution within the walls .

3- To provide a rotational design methodology for predicting both shear and flexural capacity of partially reinforced masonry shear walls .

The scope of the proposed research was limited to partially reinforced masonry shear walls. The test results for model partially reinforced concrete block masonry shear walls under in-plane loading are presented and discussed in this chapter. The failure modes and crack patterns along with load-deflection relationships, hysteretic response, ductility and ultimate capacity of masonry shear walls are presented. Due to the prohibitive cost of

full-scale testing of masonry walls, a more economical and feasible test method utilizing direct modeling techniques is needed. The main parameters studied in this investigation are:

1- The amount and distribution of vertical reinforcement .

2- The amount and distribution of horizontal reinforcement .

3- Level of axial stresses .

4- Unit strength .

5- Type of lateral loads (monotonic and cyclic).

4.4 EXPERIMENTAL PROGRAM

4.4.1 Scale Factor

A scale factor of three is selected for this experimental program to model the partially reinforced concrete masonry shear walls under in-plane loading. The selection of 1/3-scale model in this program based on the success of the previous studies using this scale and also to acquire wider knowledge in modeling masonry structures, to minimize the scale effect and to increase the accuracy of the detailing of the model.

The technique and approach adopted herein to model partially reinforced block masonry shear walls are similar to those described in Chapters 2 & 3 . The similitude requirements that have been already used for all assemblages of unreinforced masonry are again used to model the walls. The complete similitude requirements are indicated in Table 2.1 (Chapter 2)

4.4.2 Model wall Materials

Two types of model block units with 2800 and 1800 psi (195 and 125 kg/cm^2) were used. The physical and mechanical properties of units are listed in Tables 2.2 & 2.3 (Chapter 2). Type S mortar and type GN grout model were used in the construction of the model masonry shear walls. The proportion and properties of the mortar and grout are presented in Tables 2.4 , 2.5, 2.6 & 2.7 (Chapter 2) . The use of 2800 and 1800 psi block strength resulted in prism compressive strength (f'_m) of 2300 & 1450 psi (160 & 100 kg/cm^2) respectively .

Model deformed rebars whose physical and mechanical characteristics are described in article 2.6 and presented in Table 2.8 & 2.9 (Chapter 2) were used in the construction of the walls .

4.4.3 Test Specimens

A total of fourteen (not including a pilot wall) 1/3-scale model of partially reinforced concrete block masonry shear walls were constructed and tested under in-plane

lateral loads, with axial precompression. Eleven shear walls were tested under monotonically increasing loads and two shear walls were tested under fully reversed cyclically loading. Later, one infilled frame was chosen to be tested under monotonic loading .

Five parameters were investigated: axial stresses, block strength, lateral load, and amount and distribution of vertical and horizontal reinforcement. Table 4.1 presents the test matrix. Four groups can be classified as follows :

1. Specimens (SWA)

Ten shear walls (not including a pilot wall) were tested under in-plane loading. The main parameters investigated in this group were: axial stress, unit compressive strength, and amount and distribution of vertical and horizontal steel reinforcement. Eight walls were tested under monotonically increasing loading and two were tested under reversed cyclically loading to study the effect of the type of lateral load .

A typical shear wall panel is 3.08 feet (0.94 m) length (7 blocks) by 3.02 feet (0.92 m) height (13 courses) , corresponding to a 9.2 x 9.1 feet (2.9 x 2.8 m) full-scale wall. The walls were fabricated with a single wythe of 1/3-scale model units of the 6 in. (0.15 m) thick full-scale walls. Two ratios of vertical reinforcement (0.12% & 0.21%) were chosen with four ratios of horizontal reinforcement (0.05%, 0.09%, 0.12% & 0.21%) to study the effect of amount of vertical and horizontal reinforcement. The vertical and horizontal steel reinforcement were distributed in the periphery and the middle of the wall in both the vertical and horizontal directions as shown in Fig. 4.2, with an average spacing of 17.0 in. (1/3-scale of 51.0 in. = 1.3 m for full-scale). Nine walls were constructed from normal strength units with a prism compressive strength f'_m of 2300 psi (160 kg/cm^2) and one wall constructed from weaker units with prism compressive strength of 1450 psi (100 kg/cm^2) to study the effect of unit strength. Eight walls were tested under an axial stresses 100 psi (7 kg/cm^2) based on net area which is equivalent to 5% of the prism strength, one

Table 4.1 Test Matrix for the Shear Wall Specimens

Group	Wall Specimens	Vertical Steel # & Size	%(1)	Horizontal Steel # & Size	%	Masonry Strength psi (kg/cm^2)	Axial Stress psi (kg/cm^2)	Type of(2) Lateral Load
	SWA1	3#5	0.12	3#5	0.12	2350 (165)	100 (7)	M
	SWA2	3#5	0.12	3#3	0.05	2350 (165)	100 (7)	M
	SWA3	3#5	0.12	3#3	0.05	2350 (165)	0.0 (0)	M
	SWA4	3#5	0.12	3#3	0.05	2350 (165)	200 (14)	M
	SWA5	3#5	0.12	3#3	0.05	1400 (100)	100 (7)	M
	SWA6	3#5	0.12	3#4	0.09	2350 (165)	100 (7)	M
	SWA7	3#5+3#4	0.21	3#5+3#4	0.21	2350 (165)	100 (7)	M
	SWA8	3#5+3#4	0.21	3#5+3#4	0.21	2350 (165)	100 (7)	C
	SWA9	3#5+3#4	0.21	3#4	0.09	2350 (165)	100 (7)	M
	SWA10	3#5+3#4	0.21	3#5+3#4	0.21	2350 (165)	100 (7)	C
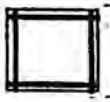	SWB1	4#4	0.12	4#4	0.12	2350 (165)	100 (7)	M
	SWC1	4#4	0.12	4#4	0.12	2350 (165)	100 (7)	M
	SWC2	4#4+2#5	0.20	4#4	0.12	2350 (165)	100 (7)	M
SWD1 (Infilled Frame)		4#4	0.12	4#4	0.12	2350 (165)	100 (7)	M

1- Percentage of Steel (Based on gross area)

2- M = Monotonic Loading ; C = Cyclic Loading

wall was tested under 200 psi (14 kg/cm^2) based on net area which is equivalent to 10% of the prism strength, and the last wall was tested without axial stresses .

2. Specimen (SWB)

One wall with steel bars distributed only on the periphery as shown in Fig. 4.3 was considered to study the effect of distribution of vertical and horizontal steel reinforcement. The ratio of both vertical and horizontal reinforcement is 0.12 % and the spacing between bars in both directions is about 34 in. (1/3-scale of 102 in. = 2.6 m full-scale). The wall was tested under in-plane monotonically increasing loading .

3. Specimens (SWC)

Two ratios of vertical reinforcement (0.12 & 0.21) and one ratio of horizontal reinforcement 0.12 % were considered with an average spacing equal to 11 in. (1/3-scale of 33 in.= 0.84 m full-scale). The reinforcing steel were distributed in the periphery, one-third and two-third of height and length of the wall as shown in Fig. 4.4 to study the effect of the amount and distribution of vertical and the amount of horizontal steel reinforcement. The two walls were tested under in-plane monotonically increasing load .

4. Specimen (SWD)

The 1/3-scale infilled frame shown in Fig. 4.5 was constructed and tested under in-plane monotonically increasing loading. The dimensions are the same as for the partially reinforced masonry walls and 4#3 steel reinforcement was chosen in each column and beam. The reinforcement ratio is the same as wall SWB in both the horizontal and vertical directions (0.12%). This wall was tested to compare the behavior and carrying load capacity of infilled frames to partially reinforced masonry shear walls with the same amount of steel .

4.4.3.1 Wall Construction

a) Reinforced Concrete Footing

A reinforced concrete footing as a base was used for the wall construction. The dimensions of this base is 5x5x43 inches (12.7x12.7x109 cm) and is reinforced with four 1/3-scale #5 bars (one at every corner) and with model gage # 8 black annealed wire ties as indicated in Fig. 4.7. The concrete used contained portland cement type III, concrete sand, pea gravel, in proportions of 1 : 3 : 2 : 0.58 (cement : sand : gravel : water) by weight. Water was added to obtain 4000 psi (280 kg/cm^2) compressive strength and a workable mix. The concrete beam was cast on the top of the steel beam (the base of the test set-up) to fit the bolts in the bottom of concrete beam into the holes on the top of the steel beam. The concrete was poured in three layers and was vibrated.

Vertical steel was held in place at the time of casting using a wooden frame as shown in Fig. 4.7. Sixteen 3/8 in. (10 mm) bolts, in two lines each line had eight bolts, were included at the bottom of concrete base beam , and were designed to tie the footing to a steel I-beam representing the base of the testing frame. The upper surface of the footing were smoothed and wet cured for a week and then air cured in the laboratory under controlled temperature and humidity of 70°F (21°C) and 50% respectively. Control specimens were taken during the construction and cured in the laboratory under the same condition .

b) Shear Wall Panels

The walls were constructed in the Structural Testing Laboratory of Drexel University by the same experienced and qualified mason who built the small assemblages presented in Chapter 3. Prior to wall construction, all footings were set and leveled in a horizontal position on a wooden base prepared especially to fit the bolts underneath the concrete beam, and marked to ease the laying of the first course. All the walls were constructed in running bond with half a block overlap. Type S mortar with face-shell mortar bedding was used for all walls. No mortar was placed on the webs except at the

ends of the grouted cells to create dykes to prevent grout from flowing out. Because vertical steel was already embedded in the footing, the units had to be threaded from the top after they were buttered with mortar. After the blocks were laid, the horizontal bars were slid down around the outmost vertical bars, and tied with thin wire in their final position. Extensions of the hooks were about 1.5 in. (38 mm) to ensure sufficient anchorage.

Two days after construction the reinforced cells were grouted with normal grout strength. The grout was poured into the cells and consolidated with an aluminum rod. Because of the difficulty of grouting the horizontal bond beams due to the spanning of the grouted vertical cells (case of partially grouted), testing of how far grout can flow in bond beam from pouring the vertical cells as indicated in Fig. 4.6 was conducted. For this reason the bond beams being grouted during the construction of the wall, had a hunches at the ends. This is due to ensure continuity at the joint where vertical cells intersects with horizontal bond beams. During grouting of the bond beams, wire mesh was placed on the top and the bottom of the grouted course to prevent grouting from spreading into the hollow part of the wall. All the joints in the model masonry shear walls were tooled on both sides to further compact the mortar joints. All shear wall panels were air cured in the Structural Testing Laboratory under controlled temperature and humidity of 70 oF and 50% respectively. Control hollow and grouted prisms from the two types of units were built during the construction. Mortar, and grout specimens were made along with the model masonry panels and cured in the laboratory under the same conditions as the corresponding shear wall panels. Figures 4.8 & 4.9 illustrate the different stages of the construction of shear wall specimens .

c) Infilled Frame

The 1/3-scale infilled frame used in this study is shown in Fig. 4.10. The concrete frame was cast first on the reinforced concrete footing and later the inside wall panel was built. The concrete used contained portland cement type III, concrete sand, and pea gravel

in the proportions of 1 : 3 : 2 : 0.58 (cement: sand:gravel:water) by weight to obtain 4000 psi (280 kg/cm^2) compressive strength. After 14 days the masonry panel was constructed inside the concrete frame using 1/3-scale concrete blocks with a prism compressive strength of 2300 psi (160 kg/cm^2) placed in running bond with half a block overlap and with face-shell mortar bedding. Type S mortar was used to assemble the panels. All joints were tooled on both sides to further compact the joints. The infilled frame was air cured in the laboratory under controlled temperature and humidity of 70°F (21°C) and 50%, respectively .

d) Reinforced Concrete Top Beam

A concrete beam was cast at the top of every shear wall specimen to serve as a distribution beam for application of vertical and lateral loads. The dimensions of this beam is 4x4x40 inches (10x10x100 cm) as indicated in Fig. 4.2. Twelve 3/8 in. (10 mm) bolts in two lines, each line had six bolts, were included to tie the concrete beam to a stiff steel beam designed to transmit the lateral load in a manner similar to that used for the base beam. A wood frame supported on a concrete base beam was provided to hold the concrete top beam during its construction. Reinforcement consisted of 1/3-scale four bars #4 and gage # 8 black annealed wire ties was used. The same concrete mix used for base beam was adopted to cast the top beam. It was poured in three layers and consolidated with a steel rod since no other means of vibration was available. Control specimens were made along with the construction of the beams. Curing was done under the same conditions as for the concrete base beam .

4.4.4 Test Setup

A typical test arrangement used for the 1/3-scale model partially reinforced concrete masonry shear wall is shown schematically in Fig. 4.11. The wall panels were tested as cantilever walls, under in-plane lateral and vertical loadings. The concrete base beam on

which the panel was built was bolted to a stiffened wide flanged steel beam (WF10x22). This steel beam was attached to the test frame by four 1 in. diameter bolts at each end (Fig. 4.11) and was also supported on another steel beam (WF12x87), resting on the reaction floor to ensure that all the loads were adequately transmitted to the reaction floor. The top distributing beam consisted of a wide flange steel beam (WF10x22) attached at two lines, each line had six 3/8 in. (10 mm) diameter bolts to the top concrete beam.

The vertical load was applied through a roller support made with 1.5 in. (38 mm) diameter steel rod at the middle of the wall. This allowed the free horizontal displacement of the wall during testing. The vertical precompression load was applied through a hydraulic jack supported at the top steel beam of the frame through a pin connection that consisted of 1 in. diameter rod as shown in Fig. 4.11. This connection has a limited rotation ability to accommodate the expected rotation due to horizontal displacement of the wall panel. This jack, an Enerpac double acting hydraulic cylinder of 49,100 lb (22 ton) pushing capacity had a stroke of + 5 in. (127 mm).

To fix the point of application of the lateral load at the top of the wall, a short bracket box cross-section steel was welded in the downward position, to the distributing beam as shown in Fig. 4.11. This bracket was connected to a lever arm having 1: 6 ratio by 1 in. (25 mm) diameter rod through three plates connected to the bracket. This lever arm was connected through 1 in. (25 mm) diameter rod at the top end of the short span to a two stiff steel beam fixed at the column of the frame to provide an adequate support at the top. Also the lever arm was connected by a 1 in. diameter rod at the bottom end of the long span to a load cell through a push-pull swivel permitted rotation in both ends to accommodate any movement without introducing bending into the load cell. The load cell was connected to a double acting hydraulic cylinder jack. The hydraulic jack, an Enerpac 17-kips (7.7 ton) ram, was modified into a servo-controlled actuator, by adding a Moog servo valve to the actuator. The actuator and the load cell were then coupled with the MTS servo-control system available at the Structural Testing Laboratory of Drexel University. This system resulted in the magnification of jack load by a factor of seven. The reason for

this design was that there was a lack of a small capacity jack connected to MTS system in the testing facility. The hydraulic jack was provided with a support that could slide along the vertical column of the test frame, and be fixed at any location. To allow any vertical movement of the wall, this support was equipped with a pin connection that consisted of 1 in. diameter rod .

Additional support for the wall in the out-of-plane position was provided by a set of two steel angles running horizontally on either side of the wall panel at the top and clamped with the two columns of the testing frame as illustrated in Fig. 4.12. Three tubes were riveted to the steel angles from one end and rubber casters from the other end which was in contact with the specimen. These casters have the ability to rotate in any direction, this system was provided to guide the wall and to prevent any out-of-plane deflection, particularly at high loads to allow in-plane movement of the walls during the testing .

4.4.5 Instrumentation

The in-plane deformations (deflections and strains) of the wall panel were measured and monitored by means of LVDTs (Linear Variable Differential Transducers), and dial gauges. The distribution and location of these instrumentations are indicated in Fig. 4.13. A total of seven LVDTs and three dial gauges were attached to the wall panel and used to monitor the deformation and displacement of each wall specimen. LVDT # 1 (one) was fasten to an external reference fixed support from one point and attached to the specimen at the top (the same lateral load level) from the other point to measure the lateral displacement at the top of the wall specimen. LVDT # 2 (two) were used to monitor the shear deformations on the two main diagonals of the specimen. LVDT # 3 (two) were used to measure the in-plane flexural deformations on the front face of the wall at the same location as end vertical bars, as shown in Fig. 4.13. LVDT # 4 (two) were used to measure the in-plane curvature of the specimen and therefore were placed on the edges of the specimen at the bottom. One dial gage was used to monitor any slip at the interface between the wall panel and the concrete footing, and another dial gauge was used to

monitor the slip at the interface between concrete footing and steel base beam and finally a third dial gage was used to monitor the slip at the interface between concrete top beam and wall panel as shown in Fig. 4.13. In this experimental program, all the measuring instruments, loading, and MTS equipment were connected to a computerized control station and data acquisition system.

4.4.6 Control Station and Data Acquisition System

The testing facility at the Structural Testing Laboratory of Drexel University contains three different parts: Control Station, Hydraulic Equipment and Testing Frame. A schematic illustration of the test equipment is shown in Fig. 4.14. The control station contains MTS computer controlled loading system where it is used for testing full-scale and small-scale building components using two dimensional loading history. Through this sophisticated control station, the operator interacts with the hydraulic actuators to control either loading or displacement, acquire test data and mathematically manipulate the test data to display the information in a meaningful engineering graphical display. The control station is basically an MTS control station with servo controllers, data acquisition equipment, computer control system, and computer peripherals such as a video terminal, X-Y plotter, printer and pin plotter. The unique feature of this control station is that the MTS control system can be coupled to or decoupled from the computer control system. In other words, the computer can act independently collecting and manipulating data while the MTS control system operates the test .

The computer initially receives instructions from the operator and then transmits responses to the operator through especially developed software. This software has the capability to acquire real-time data through a high speed-analogy-to-digital converter, control the hydraulic actuator through the servo-controllers, and manipulate the data. The distinctive feature of the software is that all three functions are integrated into a single command language and data architecture. In additional, the software can repeatedly pause and restart a physical test without loss of data or experimental continuity, and can perform

actuator motions based on feedback from other transducers mounted on the experimental specimen. Other capabilities such as post-test data processing and presentation are fundamentally retained .

4.4.7 Test Procedure

The shear wall specimens were tested under specified in-plane displacement using the MTS servo-hydraulic system driven by the data control station as indicated in Fig. 4.14. The load was applied under a displacement controlled actuator, the deflection and the strains were monitored through a computer control and data acquisition system. A constant rate was applied and the data were recorded at specific regular time increments .

Twelve specimens (not including pilot wall) were tested under monotonically increasing loads and constant axial stresses. The magnitudes of the axial stress for each model specimen are presented in Table 4.1. A displacement amplitude well exceeding the ultimate predicted value was specified through the computer, and the test was interrupted at failure.

Collection of the data was made at a rate of one point per second for a total of 800 seconds. Failure was considered to have occurred when the load-deflection curve monitored on the X-Y recorder showed a continuous drop in the load as displacement increased. The cracks were marked as they occurred and the mode of failure was recorded. The load and all the instrument measurements were continuously and automatically scanned and recorded on floppy discs .

Two specimens were tested under fully reserved cyclic loading. Each specimen was subjected to a constant axial stress, the magnitude of which is indicated in Table 4.1. To simulate the seismic response induced by earthquake ground motion, fully-reserved lateral displacement cycles of increasing amplitude were applied to each specimen by the horizontal actuator. The applied displacements consists of series of increasing increments with magnitudes equal to a ratio of the displacement corresponding to a first major event (first yield, first major crack, etc ...). In this study the first major event was represented by

the first major diagonal crack occurring in the wall panel. The displacement history consisted of sequences of fully reversed displacement cycles as shown in Fig. 4.15. The control actuator continuously pushed to a positive initial displacement amplitude of 0.35 in. (8.9 mm). The load was reduced to zero displacement and the wall then pulled to a negative displacement of 0.35 in. (8.9 mm). The operation of positive and negative displacement constitute one cycle. This procedure was continued until three cycles of the same amplitude had been completed. This is constitutes stage one. The maximum displacement during each subsequent stage of a cycle was increased in increments of 0.35 in (8.9 mm) up to a maximum displacement of 2.8 in. (71 mm) or the wall lost at least 50% 0f its maximum load, in this case the test was interrupted. Again, the failure mode and the corresponding measurements of all the instrumentations were scanned and recorded on a hard disc and later were copied on a floppy discs .

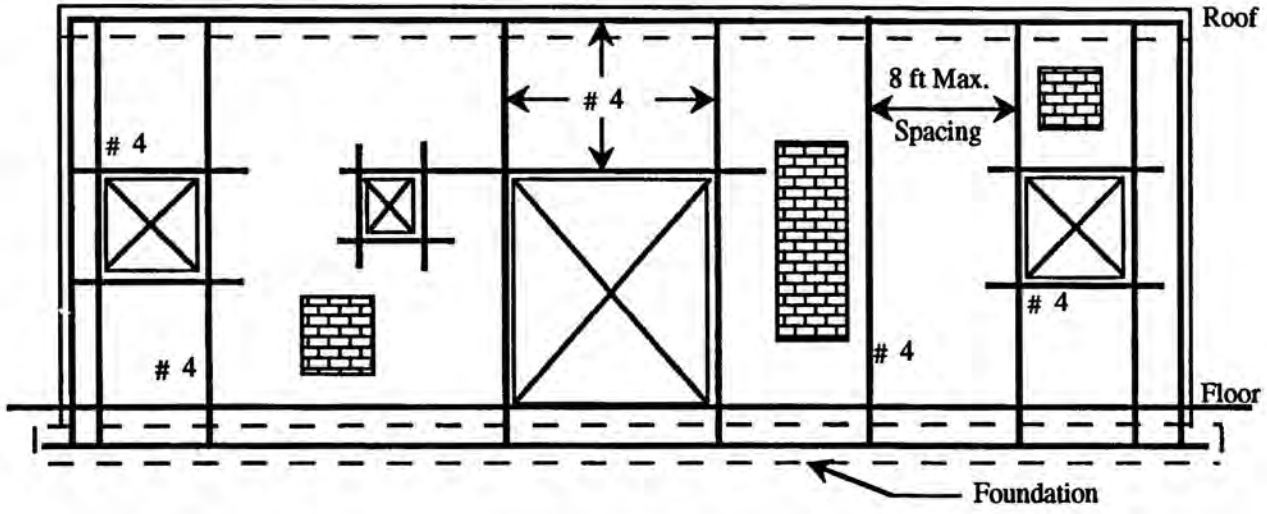

Figure 4.1 Code Requirement for Partially Reinforced Masonry[141]

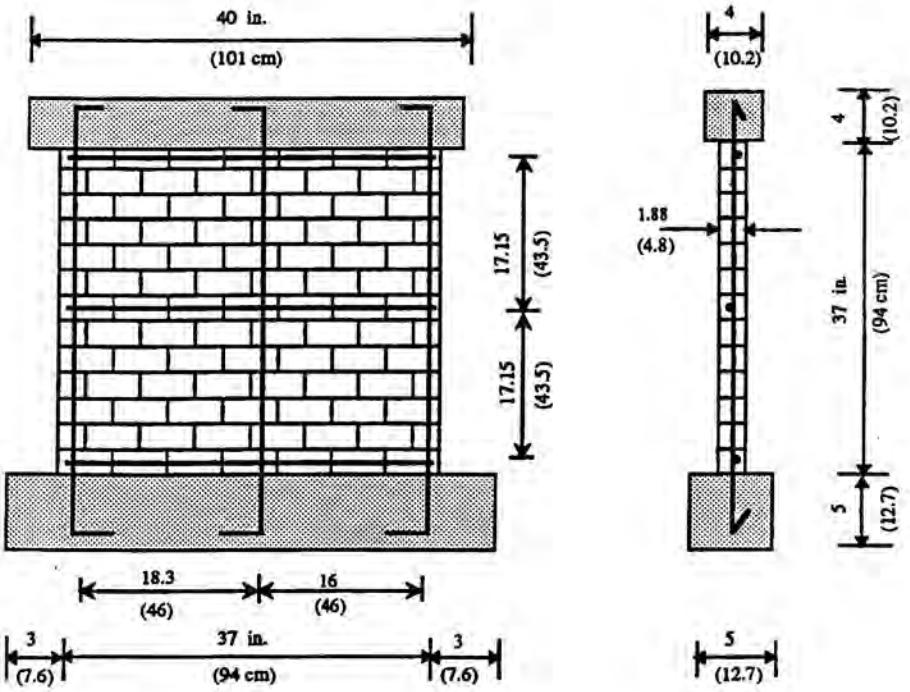

Fig. 4.2 Shear Wall Panel (SWA)

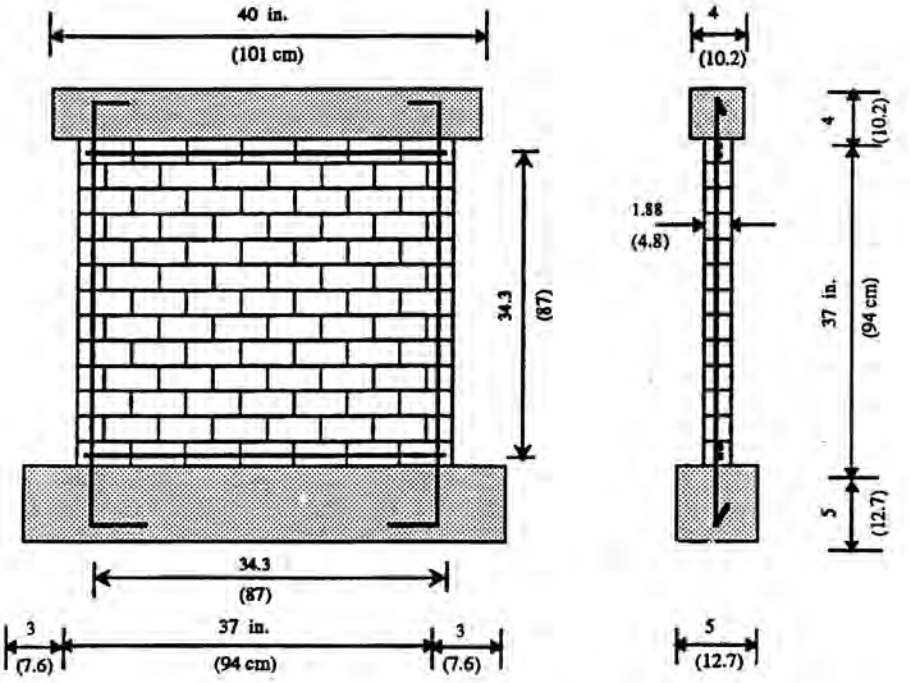

Fig. 4.3 Shear Wall Panel (SWB)

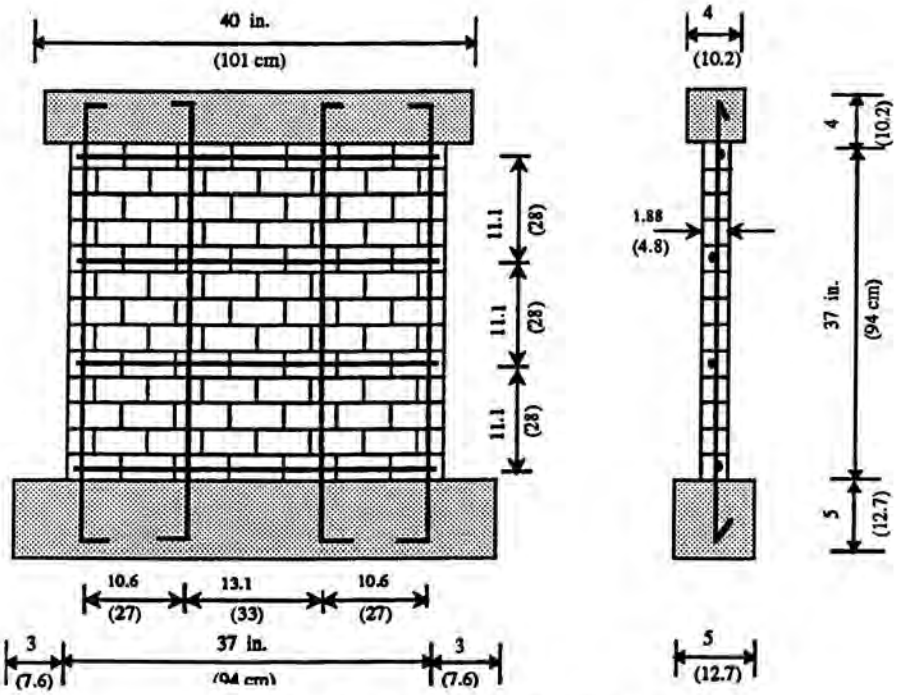

Fig. 4.4 Shear Wall Panel (SWC)

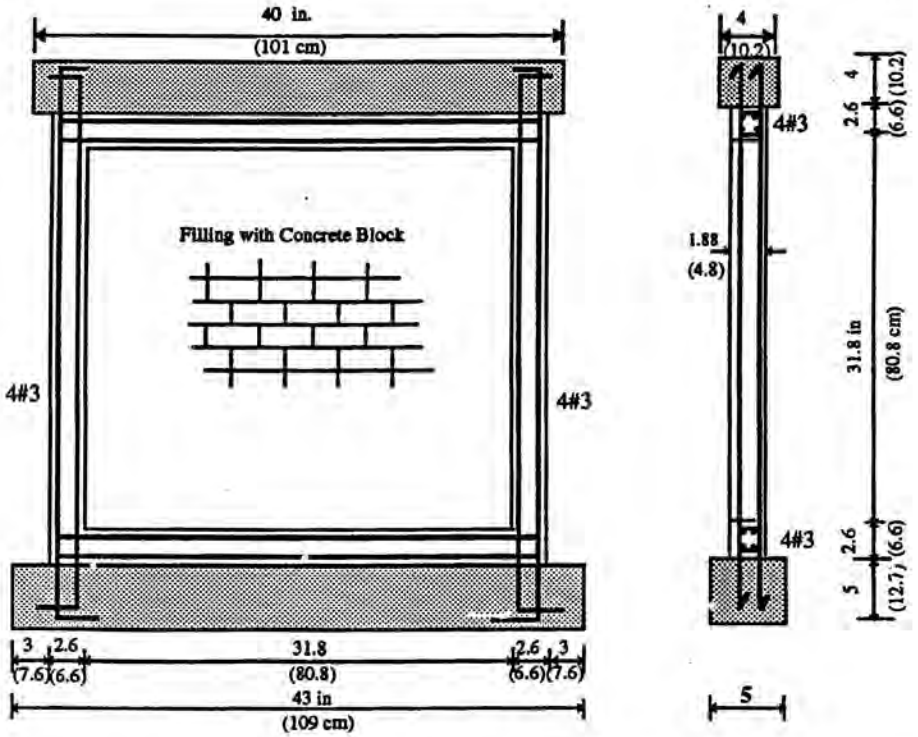

Fig. 4.5 Infilled Frame (SWD)

a) Grouting of the Vertical Cell

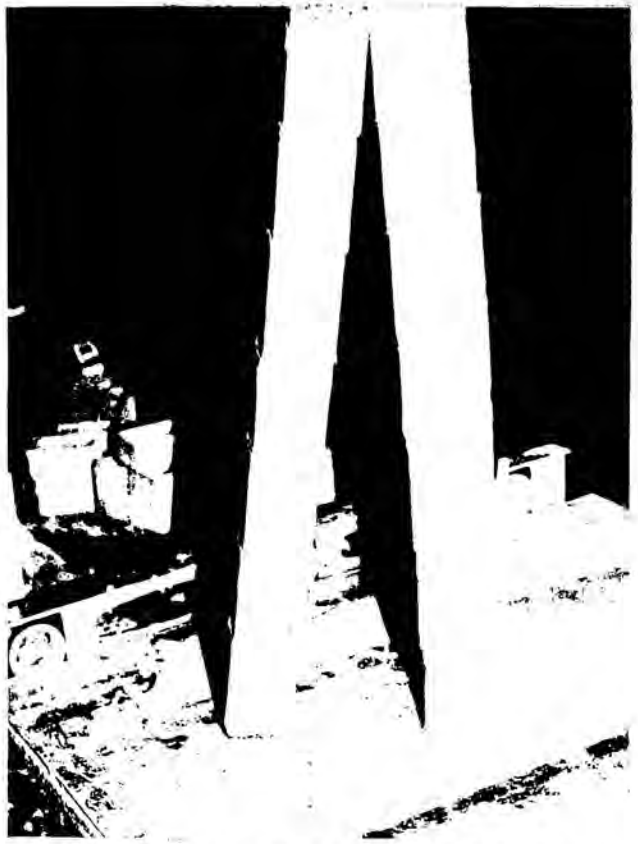

b) Cross-Section Illustrating the Interface Between the face-shells and grout core

Fig. 4.6 Experimental Procedure for Checking the Flow of Grout in Bond Beams

a) Reinforcement Cage of the Bond Beams and Bolts
Connecting the Wall to the Testing Frame

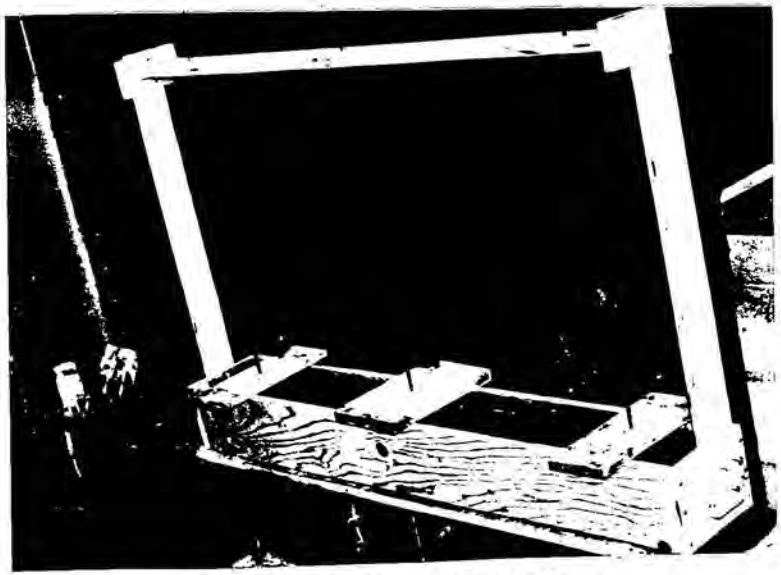

b) Securing the Vertical Steel in Place

c) Cast Concrete Base Beam

Fig. 4.7 Construction of Concrete Base Beam

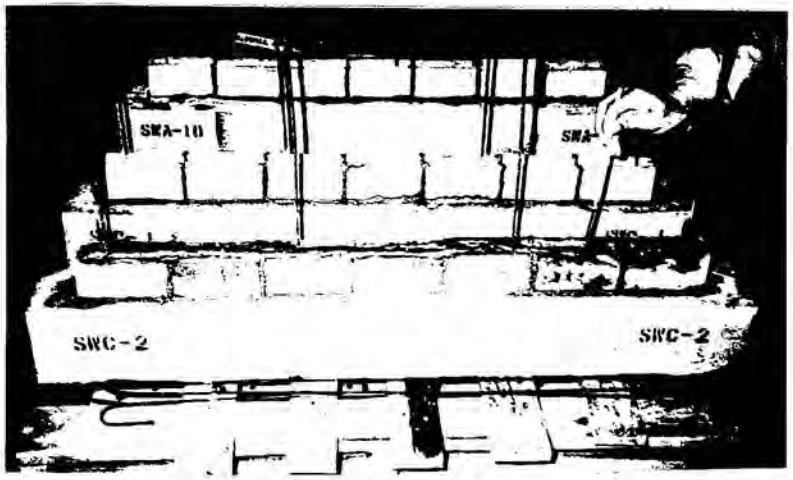

a) Grouting of the First Course

b) Grouting of an Intermediate Bond Beam

c) Placement of Mortar on Face-Shells and on Webs at Location of Vertical Steel

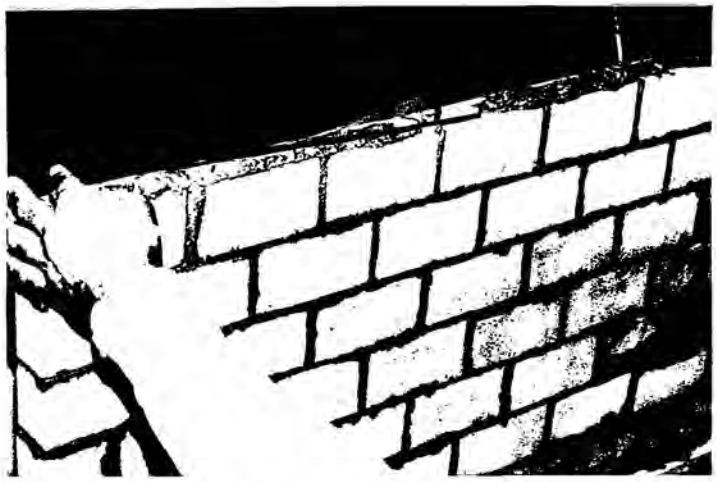

d) Placement of Horizontal Steel of Bond Beams

Fig. 4.8 First Stage of Construction of the Shear Wall Specimens

a) Water Absorption at Location of Grouted Cells

b) Construction of Top Portion of the Wall above Bond Beams

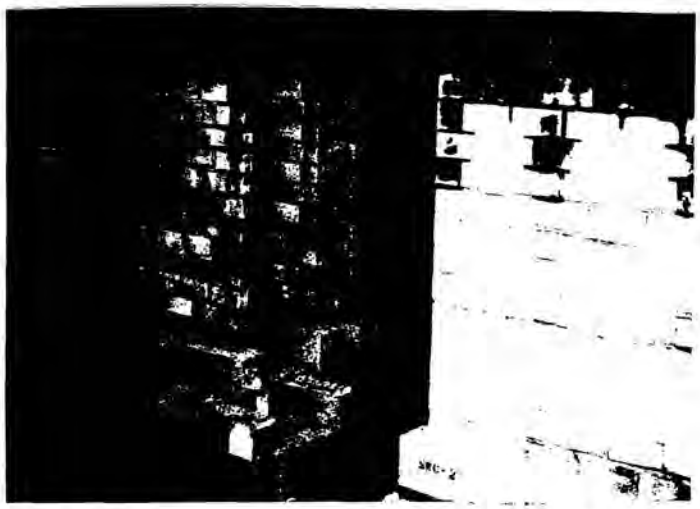

c) Completed Masonry Walls - Vertical Steel to be Embedded in the top beam

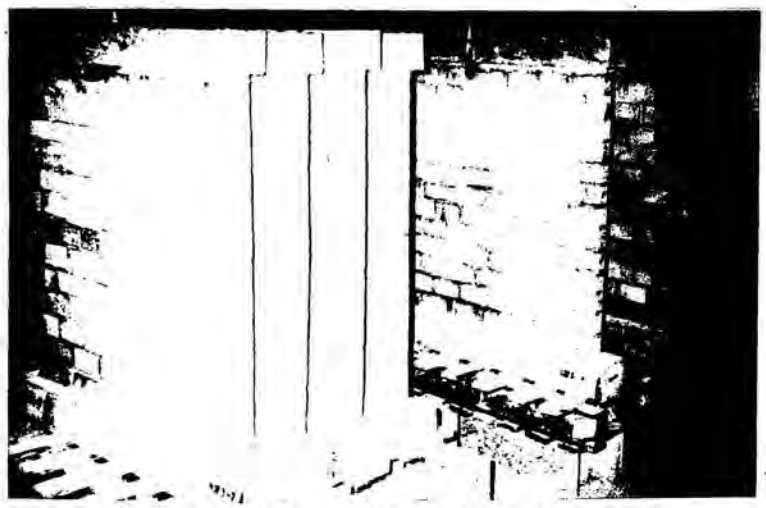

d) Complated Masonry Walls with Top Concrete Beams

Fig. 4.9 Final Stage of Construction of the Shear Wall Specimens

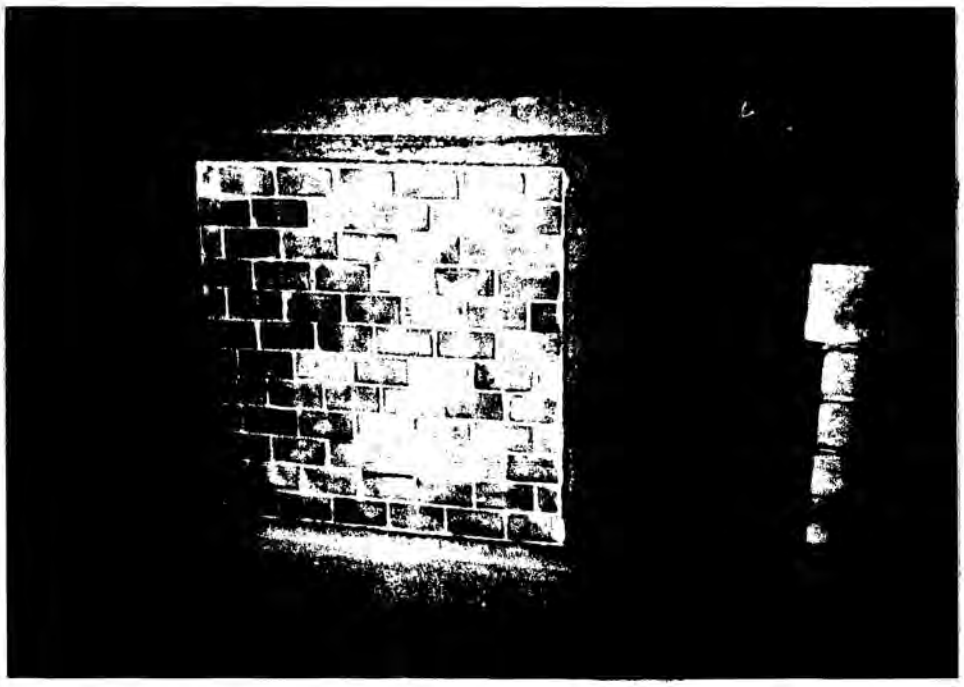

Fig. 4.10 Constructed Infilled Frame

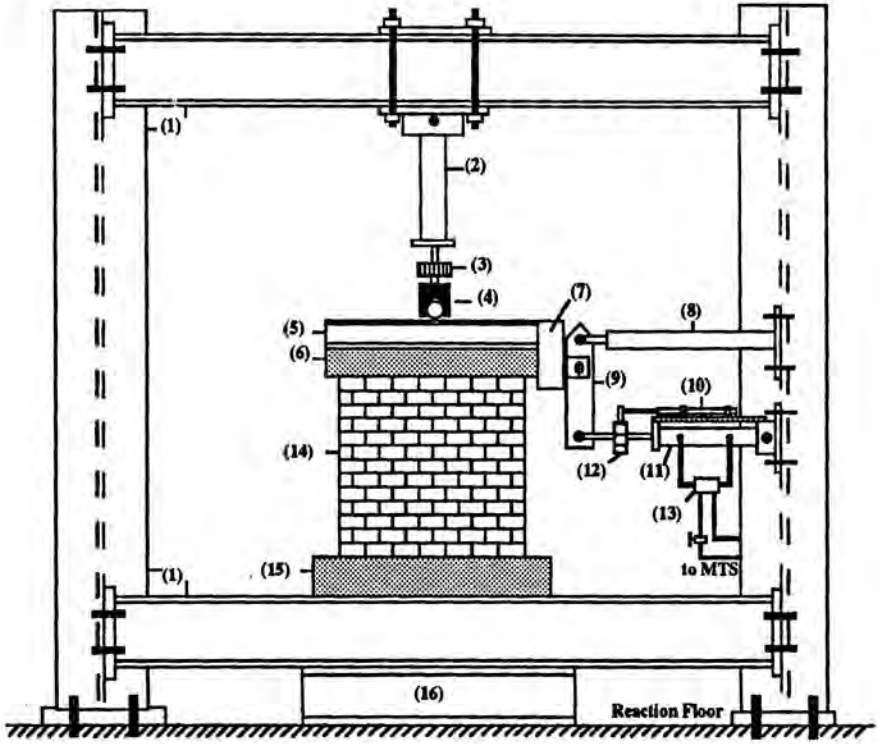

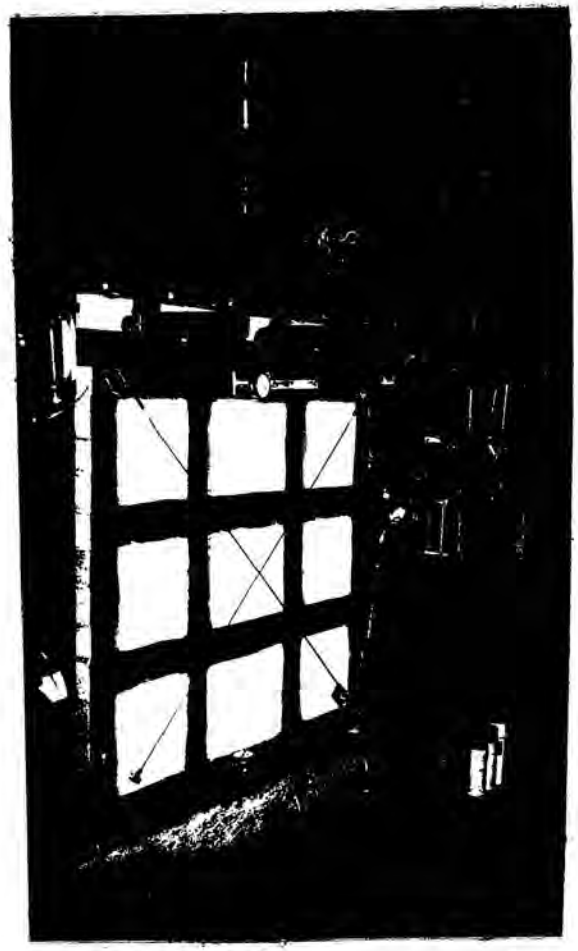

1-Testing Frame, 2-Jack for Axial Load, 3-Load Cell, 4-Roller Allowing Horizontal Displacement of the Wall, 5-Load Distributing Beam, 6-Reinforced Concrete Top Beam, 7-Bracket for Lateral Load, 8-Lateral Support for Lever Arm, 9-Lever Arm (Magnefication of Lateral Load), 10-Controlled LVDT, 11-Jack for Lateral Load, 12-Load Cell, 13-Servo-Valve, 14-Shear Wall Specimen, 15-Reinforced Concrete Base Beam, 16-Steel Beam

Figure 4.11 Test Set-Up

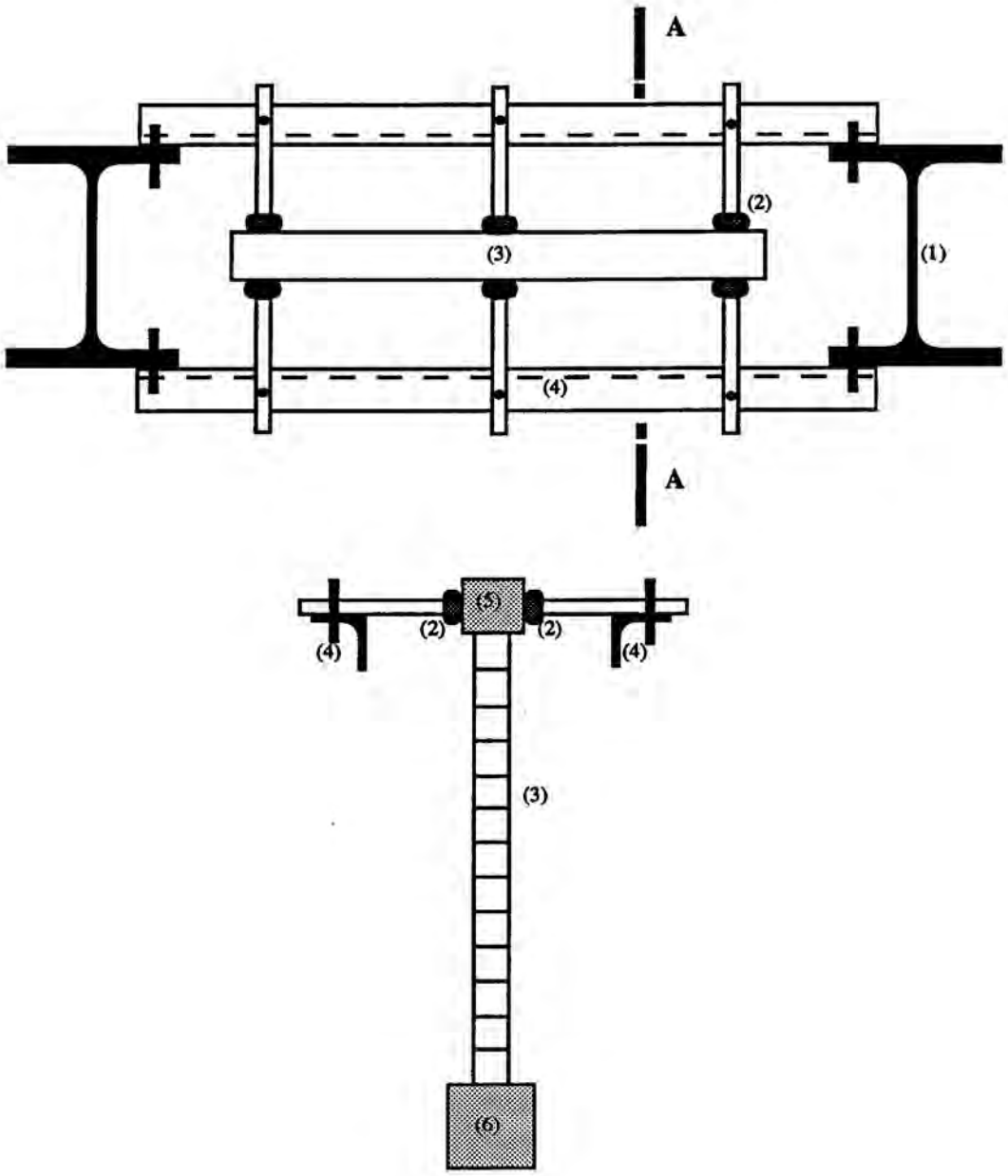

Sec. A-A

(1) Column of Testing Frame, (2) Rubber Caster, (3)Shear Wall Specimen,
(4) Steel Angle, (5) R.C. Top Beam, (6) R.C. Bottom Beam

Figure 4.12 Out-Of-Plane Bracing of Shear Wall Specimen

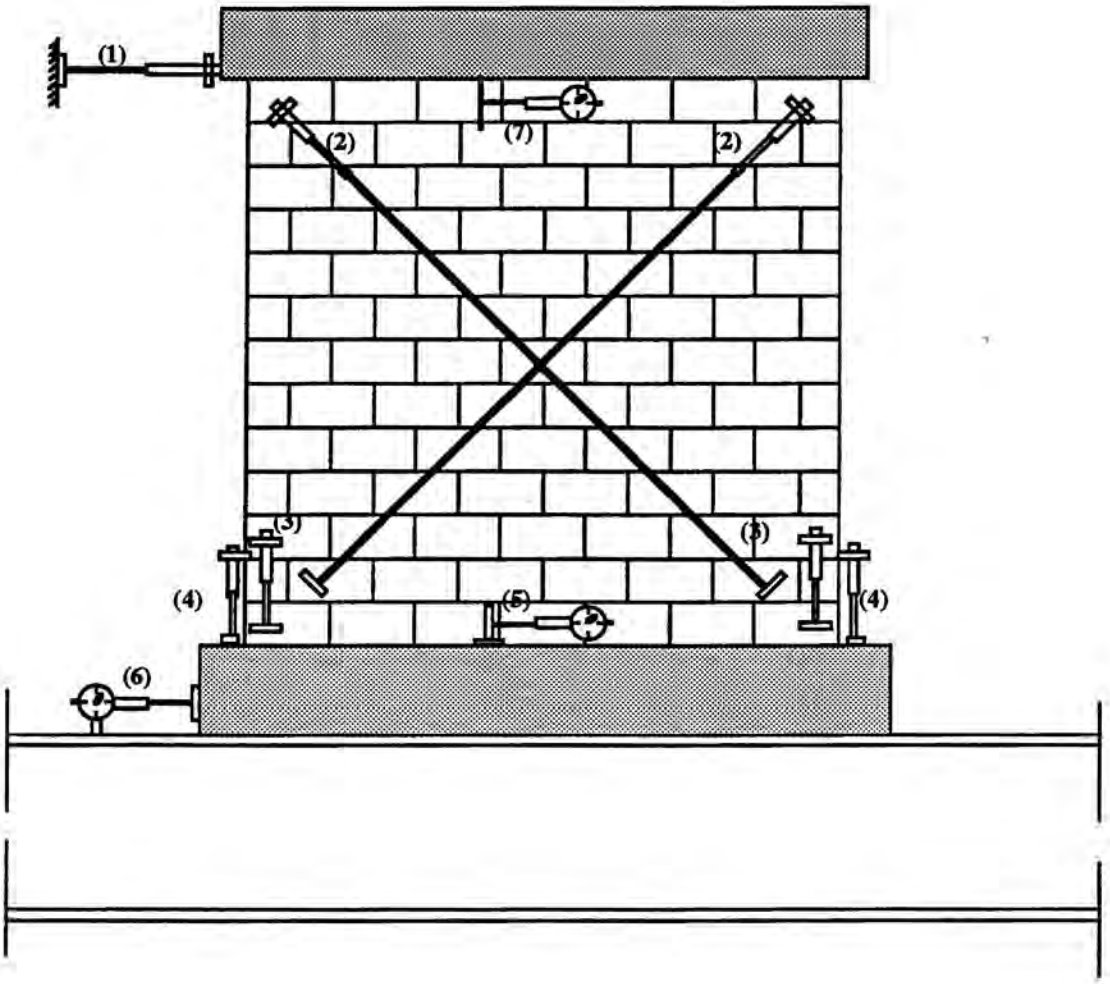

(1) Top Wall Deflection (LVDT), (2) Shear Deformation (LVDT), (3)Flexural Strain (LVDT), (4) In-Plane Wall Curvature (LVDT), (5) Slip Between Wall Specimen and Concrete Base Beam (Dial Gauge), (6) Slip Between Concrete Base Beam and Bottom Support (Dial Gauge), (7) Slip Between Concrete Top Beam and Wall Specimen (Dial Gauge)

Figure 4.13 Typical Instrumentation for Shear Wall Specimen

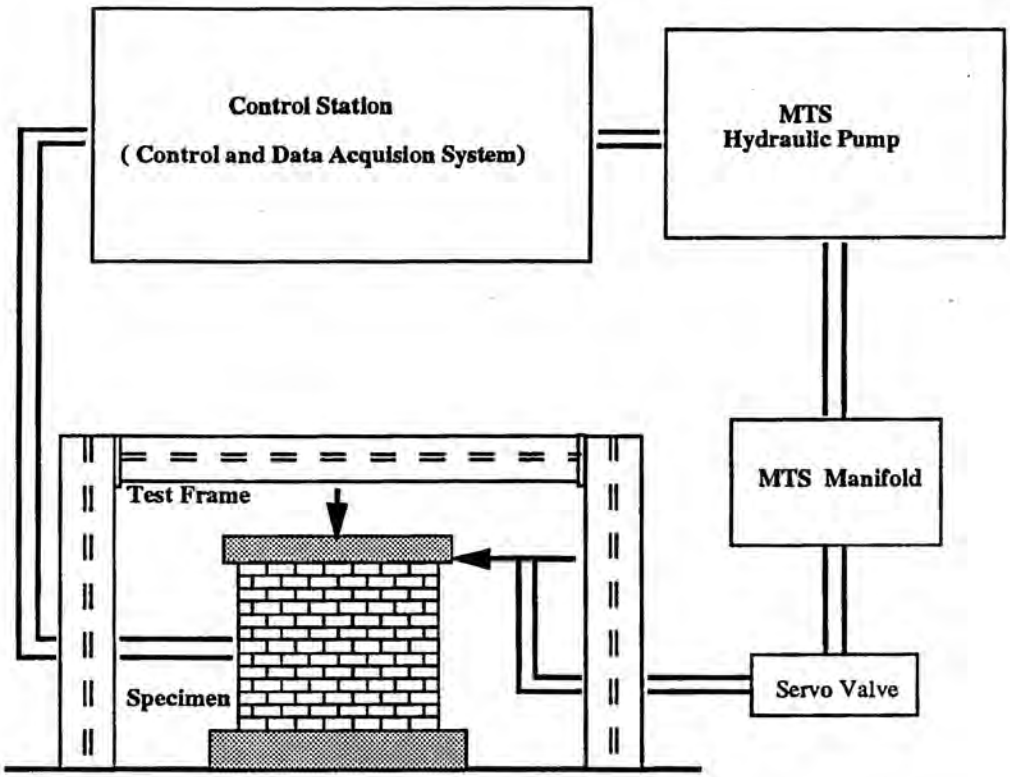

Figure 4.14 Test Bench, Hydraulic Equipment and Control Station

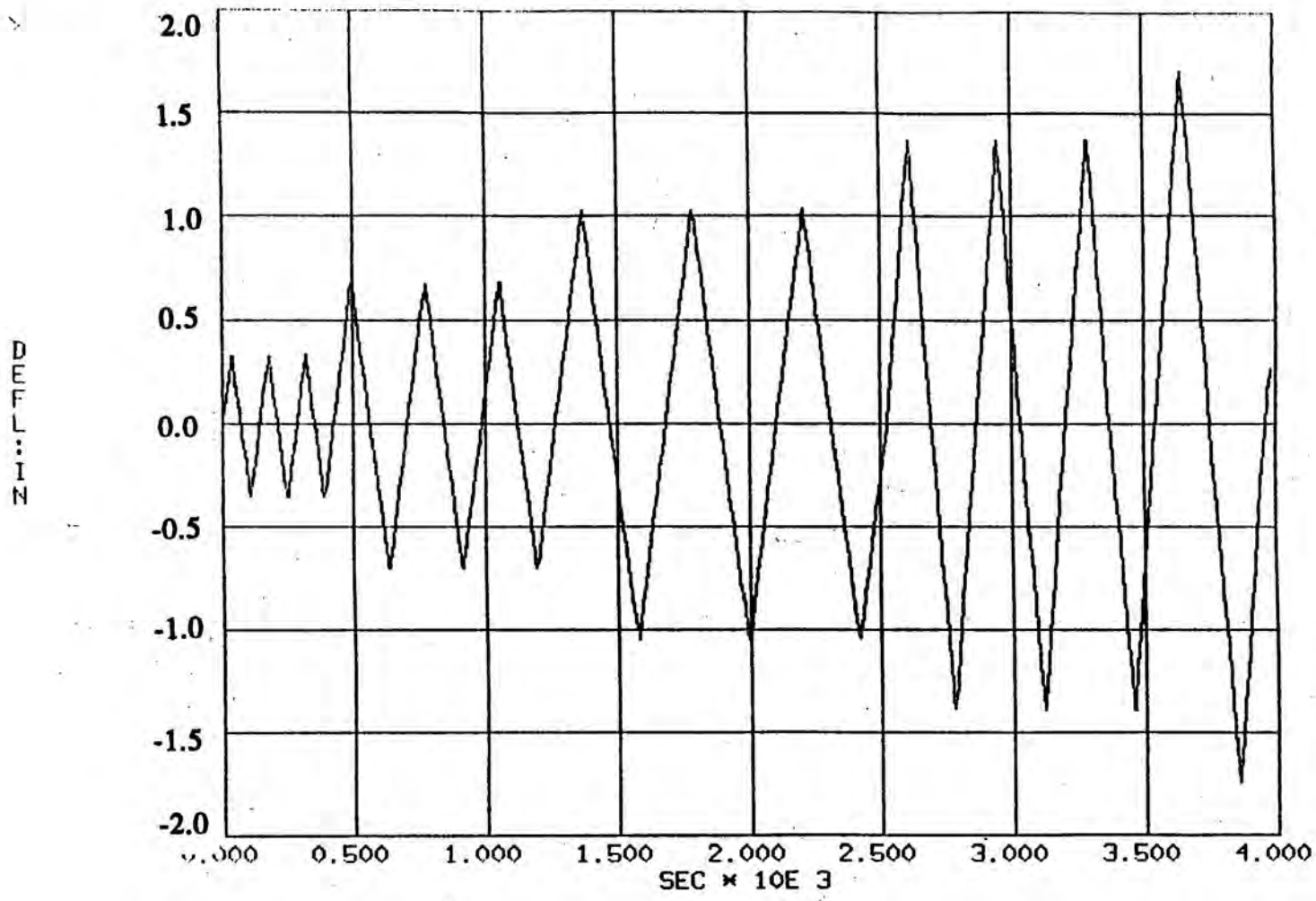

Fig. 4.15 Cyclic Input Displaciment

CHAPTER 5
EXPERIMENTAL RESULTS AND ANALYSIS OF SHEAR WALLS

5.1 INTRODUCTION

The experimental results for the fourteen walls having a height to width ratio of one are presented. The parameters that were varied during the tests include the amount and distribution of horizontal and vertical reinforcement , unit strength, and level of axial stress. The type of lateral load (monotonic verses cyclic) was also examined. The tested parameters are carefully chosen to provide demonstrate different modes of failure exhibited by the walls.

5.2 MONOTONIC TEST SPECIMENS

5.2.1 Crack Patterns and Modes of Failure

The crack patterns of the twelve walls are sketched in Figures 5.1 through 5.12. Included in the figures are photographs showing the cracking, spalling and toe crushing. Three modes of failure were observed during this test program:

1) Shear mode of failure for specimens SWA4, SWA5, SWA7, SWA8, SWA9, SWA10 and SWB1 where the behavior was governed by diagonal tensile cracking with very little or no flexural deformations.

2) Flexural mode of failure for specimens SWA2, SWC1, and SWC2 where their behavior was governed by a distinctly dominant flexural failure, i.e. horizontal bed joint cracks at the bottom courses yielding of the vertical reinforcement (indicated by horizontal crack at the tension side) followed by crushing of the masonry at the toe.

3) Specimens SWA3 and SWA6 exhibited a mixed flexural/shear behavior, which had significant flexural yielding, toe crushing as well as diagonal cracking.

Specimen SWD1 (infilled frame) had a completely different failure mode. It was characterized by full separation between the masonry panel and the concrete frame , shear failure of the beam-column connection at the bottom compression zone and crushing of the

toe of the wall at compression zone (see Fig. 5.12). Data on the ultimate load, type of the first crack, load at first crack as a percentage of the total load, and percentage of flexure deformation and diagonal deformation of the total deflection for the fourteen wall specimens are summarized in Table 5.1. The test results and major observations are described and discussed in the following paragraphs :

a) Walls With Predominant Shear Mode

The mode of failure of these specimens were governed by large diagonal cracks. These cracks occurred when diagonal tensile stress reached the tensile strength of the masonry. In this case the ratio of maximum diagonal deformation to the maximum flexural deformation of the tested walls varied between 3 -7 (Table 5.1) which indicates higher diagonal deformation leading to shear failure.

Specimen SWA4 ($p_v = 0.12$ % , $p_h = 0.05$%) This wall was subjected to 200 psi (14 kg/cm^2) axial stress. The major diagonal cracks occurred at 6.8 kips (3.1 ton) lateral load and 0.12 in. (3 mm) lateral displacement. Diagonal cracks extended from the top right corner to the base of the specimen at 45°. The ultimate load was 7.7 kips (3.5 ton) occurring at 0.2 in. (5.1 mm) lateral displacement as shown in Fig. 5.16. The high axial stress helped to sustain the ultimate load for a displacement in the range of 0.2 to 0.25 in. (5.1 to 6.3 mm) probably through the aggregate-interlock mechanism. The loss of the load resistance occurred suddenly at a lateral displacement of 0.25 in. (6.3 mm) as the diagonal crack opened substantially followed by a severe toe crushing over half unit length. Almost no slip occurred between the footing and the steel beam of the testing frame and no relative movement between wall panel and top concrete beam was recorded, probably due to the high axial stresses .

Specimen SWA5 ($p_v = 0.12$ % , $p_h = 0.05$%), this specimen had a very distinct shear failure with almost no flexural cracks. The first crack was a major diagonal crack at 2.8

Table 5.1 Experimental Wall Test Results

Wall Specimen	Load at First Crack, P_c kips(ton)	Ultimate Load, P_u kips(ton)	δ_u[1] in.(mm)	δ_d[2] in.(mm)	δ_f[3] in.(mm)	Ratio of P_c/P_u	δ_d/δ_u	δ_f/δ_u	δ_d/δ_f	Modes of Failure
SWA1	5.9 (2.7)	6.8 (3.1)	0.30 (7.6)	0.16 (4.0)	0.10 (2.5)	0.86	0.53	0.33	1.60	Shear/Flex.
SWA2	1.8 (0.8)	4.3 (2.0)	0.25 (6.4)	0.03 (0.8)	0.12 (3.0)	0.40	0.12	0.48	0.25	Flexure
SWA3	5.0 (2.3)	5.8 (2.6)	0.28 (7.1)	0.13 (3.3)	0.11 (2.8)	0.86	0.46	0.39	1.18	Shear/Flex.
SWA4	6.8 (3.1)	7.7 (3.5)	0.24 (6.1)	0.16 (4.1)	0.03 (0.8)	0.88	0.66	0.13	5.00	Shear
SWA5	2.5 (1.1)	4.6 (2.1)	0.20 (5.1)	0.12 (3.0)	0.04 (1.0)	0.54	0.60	0.23	3.00	Shear
SWA6	5.5 (2.5)	6.6 (3.0)	0.22 (5.6)	0.11 (2.8)	0.09 (2.3)	0.83	0.50	0.40	1.22	Shear/Flex.
SWA7	5.4 (2.5)	8.9 (4.0)	0.31 (7.9)	0.19 (4.8)	0.03 (0.8)	0.60	0.61	0.10	6.30	Shear
SWA8	4.9 (2.2)	7.9 (3.6)	0.20 (5.1)	0.08 (2.0)	0.02 (0.5)	0.61	0.40	0.07	4.00	Shear
SWA9	5.6 (2.5)	7.8 (3.5)	0.40 (10.2)	0.20 (5.1)	0.06 (1.5)	0.72	0.50	0.15	3.3	Shear
SWA10	5.3 (2.4)	7.3 (3.3)	0.20 (5.1)	0.11 (2.8)	0.02 (0.5)	0.73	0.55	0.10	5.00	Shear
SWB1	4.8 (2.2)	5.5 (2.5)	0.11 (2.8)	0.07 (1.8)	0.01 (0.3)	0.87	0.63	0.10	7.00	Shear
SWC1	5.0 (2.3)	7.8 (3.5)	0.40 (10.2)	0.08 (2.0)	0.20 (0.5)	0.64	0.20	0.50	0.44	Flexure
SWC2	6.0 (2.7)	9.8 (4.5)	0.38 (9.7)	0.06 (1.5)	0.18 (4.6)	0.61	0.16	0.33	0.50	Flexure
SWD1	3.8 (1.7)	6.7 (3.0)	0.30 (7.6)	0.10 (2.5)	0.08 (2.0)	0.60	0.33	0.26	1.25	Separ. bet. wall and frame

1 δ_u = Top deflection measured by LVDT no. 1. See figure 4.13

2 δ_d = Diagonal deformation measured by LVDT no. 2. See figure 4.13

3 δ_f = Flexural deformation measured by LVDT no. 3. See figure 4.13

kips (1.2 ton) lateral load and 0.08 in. (2.0 mm) lateral displacement. Further diagonal cracks at approximately the same inclination as the major crack (about 50°) occurred. The second major diagonal crack occurred at 4.25 kips (1.9 ton) and 0.17 in (4.3 mm). The diagonal cracks crossed the concrete block units, probably because of the low strength of the units compared to the mortar shear strength at the interface. The ultimate load was 4.6 kips (2.1 ton) at 0.2 in. (5 mm) lateral displacement. Load degradation occurred soon after the ultimate strength had been reached, due to the large opening of the diagonal cracks. The slip between footing and testing frame was 0.02 in. (0.5 mm).

Specimen SWA7 ($p_v = p_h = 0.21$ %). This specimen had a similar pattern of cracking and failure mode as specimen SWA1. As the load increased some of the horizontal cracks were occurred. The major diagonal crack was formed at 5.4 kips (2.5 ton) lateral load and 0.15 in. (3.8 mm) lateral displacement. More diagonal cracks at approximately the same inclination of the major crack took place especially near the toe causing severe damage. In this region, some face-shells spalling close to the toe at the compression corner took place. The ultimate load was 8.9 kips (4.0 ton) at 0.31 in (7.9 mm) lateral displacement. The diagonal cracks started from the top (point of application of lateral load) passing through the bed and head joints in a stepped-wise pattern and was interrupted at the intermediate bond beam. The bond beams with added stiffness due to grouting and reinforcement were capable of preventing cracking from passing through. Failure was not as brittle as other specimens (SWA4 & SWA5) because of the higher dowel action contribution by the vertical bars and the larger amount of horizontal steel. The slip between footing and the wall panel was 0.015 in. (0.38 mm) .

Specimen SWA9 (p_v =0.21 , p_h= 0.09%). This specimen behaved in a manner similar to that of SWA6 except that the stresses in the vertical steel did not reach yeilding. Significant diagonal tensile cracking caused failure. The first major diagonal crack formed at a lateral load of 5.6 kips (2.5 ton) and a corresponding lateral displacement of 0.09 in.

(2.3 mm) with some flexural cracks at 4.8 kips (2.2 ton) load. As the load increased other diagonal stepped-wise cracks formed near the toe. The ultimate load was reached at 7.8 kips (3.5 ton) which is 12% lower than that of wall SWA7, mainly because of the lower amount of horizontal steel. As the load increased the cracks widened until failure of the specimen took place. The slip between footing and testing frame was 0.015 in (0.38 mm).

Specimen SWB1 ($p_v = p_h = 0.12\%$). This specimen failed in a shear mode. The first major diagonal crack occurred at 4.8 kips (2.2 ton) lateral load and 0.08 in.(2 mm) lateral displacement and was inclined at 45° diagonally from top to bottom passing through bed and head joints. Further diagonal cracking formed followed by severe toe crushing at 5.5 kips (2.5 ton) lateral load and 0.2 in (5.1 mm) lateral displacement. This behavior was expected because of the low resistance by dowel action of the vertical rebars (distance between bars is increased) and because this specimen had no intermediate shear reinforcement to resist lateral load. It is to be noted that the top and bottom reinforcing bars do not have adequate development length to fully activate the steel to resist tension. Only the interior reinforcement can be activated by a diagonal crack[126]. The slip between footing and testing frame was 0.01 in. (0.25 mm) .

b) Walls With Predominant Flexure Mode

The mode of deformation of these specimens was governed predominantly by flexural yielding of the end vertical steel and crushing of the masonry at the toe of the compression zone. In this case the ratio of maximum diagonal deformation to the maximum flexural deformation varied between only 0.25 to 0.50 which is an indicative of higher flexural deformation leading to flexural failure.

Specimen SWA2 ($p_v = 0.12\%$, $p_h = 0.05\%$). This specimen has similar horizontal and vertical steel as SWA3 and SWA4 but without axial stresses. The first cracks were flexural (horizontal cracks) occurring at 1.8 kips (0.8 ton) lateral load and

0.04 in. (1.0 mm) lateral displacement and started at the bottom section. As the load increased, diagonal cracking followed immediately starting below the middle bond beam and extending to the bottom corner of the wall. The specimen was further cracked without any significant increase in lateral load because of the high ductility due to the absent of axial stress. The ultimate load was 4.3 kips (2.0 ton) at 0.25 in. (6.4 mm). Large flexural deformations took place after the ultimate load was reached. Due to difficulty of using strain gage in small rebars, yielding load of vertical steel is the load at horizontal plateau of the load-flexure deformation curve. End vertical steel started yielding at 3.6 kips (1.6 ton). The slip between footing and wall panel was 0.042 in. (0.11 mm) which is significantly higher compared to other specimens. This is attributed to the fact that this wall had no axial stress to resist wall sliding by friction.

Specimen SWC1 ($p_v = p_h = 0.12\%$) This wall had the same amount of vertical and horizontal steel as SWA1 & SWB1 but with different distribution. As shown by the load-deflection curve (Fig 5.23) the specimen exhibited a relatively ductile behavior. The first crack was flexure (horizontal crack at the bottom section of the tension side) at 5.0 kips (2.3 ton) and 0.13 in. (3.3 mm) lateral displacement. As the load increased a diagonal crack formed and larger deformations took place after the ultimate load was reached. The ultimate load at 7.8 kips (3.5 ton) and 0.4 in (10 mm) lateral displacement. The wall was able to accommodate lateral displacement greater than 0.5 in. indicating a more ductile behavior of the wall. Failure occurred by yielding of the end vertical rebars and crushing of the masonry at the wall toe over half block length. The sliding between footing and testing frame and the relative movement between the wall panel and top beam was negligible .

Specimen SWC2 ($p_v = 0.21$, $p_h = 0.12\%$). This wall had the same axial stress and horizontal steel as SWC1 with more vertical steel. The 75% increase in vertical steel did not force this wall to fail in shear but it failed in a rather unexpected flexural mode. The

first crack was a diagonal crack occurred at 6.0 kips (2.7 ton) and the major crack was a flexural crack formed at ultimate load of 9.8 kips (4.5 ton) and 0.36 in. (9 mm) lateral displacement. This load is 25% higher than that of SWC1 due to the larger amount of vertical steel. The higher contribution of dowel action of the vertical reinforcement and the bond beams in resisting the shear stresses resulted in a more ductile behavior. The specimen exhibited a rapid load degradation immediately after the ultimate capacity had been reached. Many cracks were distributed over the height of the wall until failure of the panel by steel yielding and toe crushing took place. Similar to wall SWC1 this wall was able to accommodate large displacement. The LVDT, which monitor the top deflection of the wall, reached its maximum limit. The Diagonal cracks in this specimen were more severe than those in specimen SWC1.

c) Walls With Predominant Shear/Flexure Mode

In this mode, shear failure was accompanied by yielding of the end vertical steel. In this case the ratio of maximum diagonal deformation to the maximum flexural deformation is 1.2 which indicates that both flexural and shear deformation have the same level leading to a mixed mode.

Specimen SWA1 ($p_h = p_v = 0.12$ %) had a distinct shear failure governed by diagonal cracks in bed and head joints and a horizontal crack at the tension side (Fig. 5.1) indicating a yielding of the vertical steel. A few flexural cracks occurred at the early stages of loading. The first flexural crack (horizontal crack) occurred at 3 kips (1.36 ton) lateral load and 0.13 in. (3.75 mm) deflection then two other cracks formed at the bottom half of the panel and extended towards the mid-section. The first major diagonal crack formed at 6.0 kips (2.7 ton) lateral load and 0.22 inches (5.6 mm) displacement. It was inclined at about 45^{o} to the bed joints and extended from top to bottom and passed through the bed and head joints in a stepped-wise pattern (due to high tensile strength of units compared to block/mortar bond strength). As the load increased, the cracks widened and then some

spalling of unit face-shells occurred just before failure. The end vertical steel yielded at 6.0 kips (2.7 ton). The ultimate load was 6.8 kips (3.1 ton) at 0.3 in. (7.6 mm) lateral displacement. A failure of the specimen took place with a sudden drop in the load capacity as shown in Fig. 5.13. The slip between footing and the steel beam of the testing frame was 0.02 in. (0.5 mm) and no relative movement between wall panel and top concrete (distributed) beam was recorded .

Specimen SWA3 ($p_v = 0.12\%$, $p_h = 0.05\%$). This specimen had a similar steel ratio as SWA4 but the difference was in the level of axial stress. The specimen was subjected to 100 psi (7 kg/cm^2) only which amounts to 5% of prism compressive strength. The wall exhibited a mixed flexure/shear mode with the first crack (flexural crack) observed at 2.8 kips (1.3 ton) and 0.07 in. (1.8 mm) lateral displacement. The end vertical steel started to yield at 5.4 kips (2.5 ton). Diagonal cracks started at 5.4 kips lateral load and the wall was still able to carry a load up to 5.8 kips (2.6 ton) and a corresponding 0.28 in. (7.1 mm) lateral displacement. At this level a major diagonal crack was formed. The load degradation was relatively moderate and was mainly caused by widening of the cracks until failure occurred. The slip between footing and testing frame was 0.015 in. (0.38 mm) and no relative movement between the wall panel and the top beam was recorded .

Specimen SWA6 ($p_v = 0.12\%$, $p_h = 0.09\%$). The crack pattern of this wall is shown in Fig. 5.6. The first crack was a flexural crack at 3 kips (1.4 ton) and the first major diagonal crack occurred at 5.5 kips (2.5 ton) lateral load and 0.13 in. (3.3 mm) lateral displacement. As the load increased more diagonal cracking developed with horizontal flexural cracks occurred at bed joints of the right side of the wall (side of load). The end vertical steel reached yielding at 6.4 kips (2.9 ton). Larger flexural deformation took place after the ultimate load was reached. The failure occurred by crushing of the masonry units at toe of the wall over half block length.

d) Infilled Frame (SWD1)

As expected, the main characteristic of the infilled frame is a separation between the wall and the frame which took place at 70% of the ultimate load. Failure was due to diagonal tension of the wall panel or crushing of the toe of the diagonal strut and a separation between the frame and the wall panel especially at the unloaded corners. But in this case the failure was due to crushing of the wall panel at the compression toe (toe of the diagonal compression strut) and shear of the frame at the beam-column connection as indicated in Figure 5.12. Also, a full separation between the concrete frame and the wall panel occurred at the unloaded corners and hair line cracks appeared at the loaded corners. This is because the stiffness of the concrete frame is too small compared to the stiffness of the wall panel. The ultimate load of this specimen was 7.2 kips (3.3 ton) which is about 25% higher than the load carried by the partially reinforced masonry wall SWB1 with the same amount and location of steel. However, the first crack occurred earlier in the infilled frame at 3.8 kips (1.7 ton) compared to 4.8 kips (2.2 ton) for the masonry wall. The difference in the cracking load indicates a different serviceability condition for the two types of construction .

5.2.2 Load-Deflection Relationships

The lateral load-top deflection relationships for the wall panels tested under monotonic loading are presented in Figures 5.13 through 5.24. In all curves shown, the plotted deflection is the horizontal top deflection (measured by LVDT #1) without any correction for the slip, if any, at the base of the wall. The shape of the load-deflection curve beyond the ultimate load varies from one wall to another depending upon the amount and distribution of vertical and horizontal steel reinforcement and level of axial load.

As mentioned earlier, the shear mode is characterized by early flexural cracks at the bottom followed by diagonal cracks. The major diagonal cracks formed at a load ranging from 60 to 80 percent of the ultimate load. A significant drop in the load carrying capacity occurred at ultimate load, followed by a change in the slope of the load-deflection curve,

indicating a severe stiffness and strength degradation of the wall. Development of further cracks caused further degradation until a sudden failure occurred as illustrated by the sudden drop of the load-deflection curves shown in Figures 5.13, 5.16, 5.17, and 5.19 through 5.21.

The flexure mode is characterized by early flexure and diagonal cracks. The first crack occurred at load ranging from 40 to 60 percent of the ultimate load of the ultimate load and then the load continued to increase with a reduced slope of load-deflection curve indicating stiffness degradation of the wall panel. After the ultimate is reached, a drop in the load occurred with a decrease in the slope of the curve due to the higher contribution of the flexural steel. Due to the limited range (0.5 in.) of the LVDT used to monitor the top deflection of the walls, the maximum deflection of walls SWC1 & SWC2 could not reached which indicated as vertical dashed line in the curves presented in Figures 5.23 and 5.24. This implies more deflection at ultimate load and a more ductile behavior .

For the flexure/shear mode, the load-deflection curve showed a distinct response to cracking. The first flexural cracks occurred at a load level of about 50% of the ultimate load and the first major diagonal cracks occurred at a load level of 85% of the ultimate load. As the load increased the deflection increased until failure occurred with a sudden drop in load carrying capacity as can be seen in Figure 5.15 and Figure 5.18. The drop in the load capacity and stiffness degradation was not as severe as the case of the shear mode due to the contribution of the vertical bars which made the specimen relatively ductile.

The infilled frame showed a distinguished load-deflection curve (Fig. 5.22), where hair-line cracks at the frame infill interface were developed at approximately 70% of the ultimate load. Further increase of the load caused almost complete separation between the frame and the wall at 80% of the ultimate load. In this case all the load was carried by the diagonal strut until failure occurred due to crushing of the diagonal strut at the toe and shear of the frame at the connection between frame and beam as shown in Figure 5.22. Beyond this point further deflection of the wall occurred without any load increase and therefore the test was halted .

Walls SWA1, SWB1 & SWC1 have the same ratio of vertical and horizontal steel (0.12%) and was subjected to 100 psi axial stress but having different steel distribution as shown in Figures 4.2, 4.3 and 4.4. The first major crack for these walls occurred at about 5.9, 4.8, and 5 kips (2.7, 2.2, and 2.3 tons) and 0.21, 0.1, and 0.15 in (5.3, 2.5, and 3.8 mm) lateral deflection. A sudden drop in the load carrying capacity occurred after reaching the ultimate loads at 6.8, 5.5, and 7.8 kips (3.1, 2.5, and 3.5 tons) and 0.3, 0.2, and 0.4 in (7.6, 5, and 10 mm) lateral deflection, respectively. As the deflection increased up to the controlled deflection (0.5 in.), the load decreased as indicated in Figures 5.13, 5.21, and 5.23.

For walls SWA2, SWA3 and SWA4 having the same amount and distribution of steel but with different axial stresses 0, 100 & 200 psi, it can be seen from Figs 5.14 through 5.16 that at 0.1 in. (2.5 mm) lateral deflection the corresponding lateral load were 3, 4, and 6 kips (1.4, 1.8, and 2.7 tons), respectively. This indicates that axial stress results in an increase in wall stiffness. Also the high axial stress helped to sustain the maximum load for a limited amount of deflection. However, the loss of load resistance occurred very suddenly at 0.25 in. (6.4 mm) lateral deflection as the diagonal cracks substantially opened.

Walls SWA3 & SWA5 have the same amount and distribution of steel and the same axial stress but with different unit strength. At 0.1 in. (2.5 mm) deflection the corresponding lateral loads were 4.1 and 2.9 kips (1.9 and 1.3 tons) for walls SWA3 and SWA5, respectively. This indicates that the higher block (masonry) strength the higher wall stiffness is due to the increase in aggregate interlock forces in resisting shear. The first crack in wall SWA3 occurred at 5.0 kips (2.3 ton) whereas in wall SWA5 it occurred at 2.8 kips (1.3 ton). This is attributed to the fact that increasing the tensile strength of the block increases the in-plane tensile strength of masonry[126] .

Walls SWA7 and SWA9 have the same vertical steel and axial stress but have different amount of horizontal steel. The first major crack for both walls occurred at 5.5 kips (2.5 ton) and 0.1 in. (2.5 mm) lateral deflection but the ultimate loads were 8.9 and

7.8 kips (4.0 and 3.55 tons), respectively. This is evidently due to the larger amount of horizontal steel in wall SWA7.

Both walls SWC1 and SWC2 have the same horizontal steel and axial stress but have different vertical steel ratios of 0.12 and 0.21%, respectively. A complete curve could not be obtained because of the limitation of the range of LVDT available (0.5 in.). In wall SWC2 the major crack occurred near 9.2 kips (4.2 tons) ultimate load while in wall SWC1 it was only 5.2 kips (2.4 tons). The ultimate loads were 9.8 kips and 7.8 kips (4.5 and 3.5 tons) at 0.40 in. and 0.38 in. (10.2 and 9.8 mm) lateral deflection, respectively. This is because SWC2 has more vertical steel which results in an increase in the flexural resistance of the wall panel.

Most flexural (horizontal) cracks occurred in the linear portion of the L-D curves of the wall panels, causing very small drop without any significant decrease in stiffness as shown in Figures 5.14, 5.23, and 5.24.

Comparing the three modes of deformations (shear, flexure, and flexure/shear), it can be noticed that, for the walls that behaved predominantly in a shear mode the load dropped in a much faster rate after attaining the peak load without showing appreciable inelastic deformation because of the brittle nature of the debonding failure at the bed and head joints. The post-peak behavior of these walls is characterized by severe degradation in load and stiffness. On the other hand, the walls behaved in flexure mode, because of the higher contribution of the bond beams and the dowel actions of the vertical bars in resisting shear stresses developed in the wall, showed a more ductile behavior .

The lateral load at which the first major crack occurred is dependent upon both the diagonal tensile strength of the masonry and the level of axial stress. For walls having similar masonry strength and axial stress the cracking load was consistent and varied in a narrow range between 5 to 5.9 kips. The wall with 60% reduction in masonry strength showed a decrease in the cracking load of about 50%. Also the wall which had a 100% increase in axial stress showed an increase in cracking load of about 25% .

From the observations of the dial gages, which were used to monitor the relative

movement between wall panel and top and bottom concrete beams, no slip was recorded. This indicates a full bond between the wall panels and top and bottom beams.

5.3 CYCLIC TEST SPECIMENS

Two specimens, SWA8 and SWA10 were tested under fully reversed cyclic loading, following the specified displacement history shown in Figure 4.15. The two walls have the same quantity of vertical steel but different amount of horizontal steel as indicated in Table 4.1. The effect of load cycles on the load-deflection relationship, stiffness degradation and ductility are discussed in the following sections .

5.3.1 Modes of Failure

Walls SWA8 and SWA10 were tested under cyclically reversed in-plane loads. As shown in Figures 5.25 and 5.26 they failed in a shear brittle mode similar to their companion monotonic walls. The first major diagonal cracks for both SWA8 and SWA10 occurred approximately at 80 percent of the ultimate load. As the cycles repeated and the load increased other diagonal cracks occurred. These cracks were opened and widened from both directions as the load increased which is expected due to the nature of cyclic loading.

The pull-push ultimate load for wall SWA10 was 7.3 kips (3.3 tons) which is 10 percent lower than that of specimen SWA8, while the diagonal cracking loads are almost identical. However, as shown in Figure 5.28 the hysteresis curves are not symmetrical where the resistance of the wall in the push direction is higher than the pull direction. This may be attributed to the possible variation in stiffness and strength properties of the units placed in the two sides of the wall. The diagonal cracks crossed all the grouted cells and the bond beams, especially at the head and bed joints. However, the load degradation of this wall appears to be more rapid than that of wall SWA8. This could be due to the severe opening of the diagonal cracks in wall SWA10 .

5.3.2 Load-Deflection Relationships

The ultimate load of the wall was reached after a successive number of stages of cycles, the displacement at the ultimate load was 0.2 in. (5.1 mm). Beyond this point the load started to decrease as the number of cycles increased. It is worth noticing that the load in each stage of cycles dropped sharply between the first and second cycles.

Specimen SWA8 has 0.21% vertical and horizontal steel and was subjected to 100 psi axial stress. The first major diagonal crack occurred at a lateral load of 4.7 kips (2.2 tons) and a displacement of 0.08 in. (2.0 mm) in the negative direction. This crack extended from the top left corner to the bottom right corner ending with splitting tension failure of the toe as shown in Figure 5.25. In the positive direction, the major diagonal crack occurred at 5.2 kips (2.4 tons) and corresponding 0.10 in. (2.8 mm) displacement. The ultimate loads were 7.8 kips (3.5 tons) and 7.9 kips (3.6 tons) occurring at 0.2 in. (5.1 mm) lateral displacement in the positive and negative directions. Load degradation occurred soon after the maximum strengths were reached. This is attributed to the opening of the diagonal cracks leading to crushing of the wall at the toe. The hysteresis curves in Figure 5.27 shows that the loops are symmetrical indicating similar resistance in the two directions. The relative slip between the top concrete beam and the wall panel was 0.01 in. (0.25 mm), but base sliding was negligible.

Specimen SWA10 had the same amount of vertical steel and axial stress as specimen SWA8. The horizontal reinforcement ratio is 0.09% . The first major diagonal crack occurred at about 6.4 kips (2.9 tons) and 0.085 in. (2.1mm) displacement in the push direction and 4.2 kips (1.9 tons) and 0.11 in. (2.8 mm) displacement in the pull direction.The ultimate loads were 9.3 kips (4.2 tons) and 5.3 kips (2.4 tons) and 0.21 in. and 0.18 in. (5.3 and 4.5 mm) top displacement in the positive and negative directions, respectively. The loss of load resistance, which is governed by the opening of the diagonal cracks, occurred suddenly after the ultimate load was attained. The relative slip between the wall and the top and base concrete beams were negligible .

It can be noticed from the L-D curves shown in Figures 5.27 and 5.28 that before

cracking the loads of the three cycles of the same stage are almost equal. After cracking the load always dropped by about 5% after the first cycle of each stage of cycles. This drop is primarily due to the widening of the cracks as the load increased. After the ultimate load was reached, the load dropped sharply by approximately 20% from one cycle to another until the test was interrupted. This severe degradation is attributed to the opening and widening of the major cracks and crushing of the toe of the wall.

5.4 PARAMETRIC STUDY

5.4.1 Effect of Reinforcement

The results from the experimental work have indicated that the behavior and load carrying capacity of partially reinforced masonry shear walls are highly sensitive to the amount and distribution of horizontal and vertical steel reinforcement present. The effects of these parameters on the flexural and shear strengths and ductility capabilities of the wall specimens are examined in this section[128].

It is well documented that the flexural strength of a partially reinforced masonry wall panel depends on the amount and distribution of vertical reinforcement present. On the other hand the shear strength is mainly dependent on the amount and distribution of horizontal reinforcement.

Figure 5.29 shows the load-deflection curves of wall panels SWA1, SWA6 and SWA3 having 0.12%, 0.09% and 0.05% horizontal steel, respectively. The three walls have the same amount of vertical steel (0.12%), axial stress and unit strength. Wall SWA1 showed a higher ultimate strength than that of walls SWA6 and SWA3 by about 13% and 23%, respectively. This is because ultimate strength wall SWA1 was governed by the horizontal steel and the dowel action of the vertical steel rather than by the flexural mechanism. It can be seen that for walls having the same vertical steel, the ultimate strength increases with increasing the amount of horizontal steel. Specimens SWA7 and SWA9 have the same vertical steel (0.21%) but their horizontal steel ratios were 0.21% and 0.09%, respectively. It can be noticed that SWA7 showed higher ultimate load than

SWA9 by 15%. It was evident from the tests that the first crack in SWA7 was a flexure crack whereas it was a shear crack for wall SWA9. This is due to the higher percentage of horizontal steel in wall SWA7. Unexpected increase in the stiffness of wall SWB1 was noticed. This may be attributed to a number of reasons including inconsistency in the top deflection measurement, a slight change in the position of the LVDT, an increase in axial stresses or high variability in unit strength .

A comparison of the load-deflection curves of the two walls having different amount of vertical steel is presented in Figure 5.30. The two walls have similar amount of horizontal steel and experienced similar mode of failure. As can be seen, the ultimate flexure strength increases with increasing amount of vertical steel. An increase of percentage of vertical steel by 75% resulted in a 25% increase in ultimate load. This is due to the increase in the contribution of the vertical steel by dowel action and truss action .

To examine the effect of distribution of vertical and horizontal steel wall panels SWA1, SWB1, and SWC1 were chosen with the same amount of vertical and horizontal steel but with different steel distributions. The load carrying capacity of the wall panels tends to increase with the decrease in the spacing of vertical and horizontal steel. It is apparent from Figure 5.31 that wall SWC1, which has 4 columns of vertical steel and 4 rows of horizontal steel, showed a 15% higher ultimate load than wall SWA1 which has 3 columns of vertical steel and 3 rows of horizontal steel and 42% higher than wall SWB1 which has 2 columns of vertical steel and 2 rows of horizontal steel. The most significant effect was in the wall behavior. Wall SWC1 failed in flexural; this is owing to the more distribution of dowel and truss actions of the vertical steel and the higher shear resistance of the horizontal steel. On the other hand wall SWB1 failed in shear; this is because it has no intermediate shear reinforcement (horizontal reinforcement is concentrated only at top and bottom). The top and bottom bars do not have adequate development length to fully activate the steel to resist tension[129]. It is only the interior reinforcement that can be activated by diagonal cracks[129]. The vertical steel concentrated at the ends is more efficient for flexure than for shear. On 0ther hand, wall SWA1 with intermediate intermediate bond

beam and column offers almost equal contribution to shear and flexure developed. Thereby, the wall failed in shear/flexure .

Test results indicate that increasing the amount of vertical steel increases the flexural capacity of the wall panel especially when the reinforcement is concentrated at the ends and no intermediate bond beams, thereby, leading to diagonal tensile failure. Increasing the amount of horizontal steel increases the shear capacity of the wall panels especially when the reinforcement is distributed through the wall height, resulting in diagonal cracks crossing larger amount of steel. The amount of reinforcement (horizontal or vertical) does not appear to have an effect on the shear cracking load, because before diagonal cracking occurs the reinforcement carries no load and the shear cracking is governed to a large extent by the tensile strength of the masonry, the block/mortar bond strength and axial stress .

5.4.2 Effect of Axial Stress

The experimental results indicate that the behavior of partially reinforced masonry shear walls is highly sensitive to the magnitude of the applied axial stress. As shown in Fig. 5.32, for wall panels having 0.12% vertical steel and 0.05% horizontal steel, as the axial stress increased the load carrying capacity increased. Wall SWA4 subjected to 200 psi (14 kg/cm^2) axial stress showed higher carrying load capacity by about 80% and 36% than wall SWA2 with axial stress and wall SWA3 with 100 psi (7 kg/cm^2), respectively. Figure 5.32 shows the effect of axial stress on the normalized ultimate shear strength of shear walls (τ_u/f'_m). It can be seen that the ratio τ_u/f'_m for walls with 0, 100 & 200 psi axial stresses were 2.5, 3.5 & 4.6, respectively.

It can be noticed that for walls without axial stress, extensive flexural cracking occurred and the strength was governed by yielding and toe crushing. Axial stress changed the wall response from a ductile flexural mode (SWA2) to a brittle shear mode (SWA4). This indicates that the higher the axial stress the larger is the tendency of the

walls to fail in shear .

The cracking strength increased with the increase in axial stresses as shown in Fig. 5.33. The walls having the same masonry strength and axial stress showed a consistent values among them, these values varied between 5 to 5.9 kips. While the wall with higher axial stress (100% increase) showed an increase in cracking load about 25%. This is attributed to the fact that the axial stress increases the aggregate-interlock force which increases the tensile strength of the masonry .

5.4.3 Effect of Block Strength

The shear cracking mechanism of partially reinforced masonry walls is complex. Before diagonal cracking occurs, the horizontal steel carries almost no force, and thus has little contribution in resisting the stress in a wall panel. Therefore, the first occurrence of a diagonal crack is governed to a large extent by the tensile strength of masonry, hence the resistance to cracking increases with the increase in the block strength. As illustrated in Figure 5.34 the load at first crack for wall SWA3 (which has 2300 psi prism compressive strength) was higher than wall SWA5 (which has 1450 psi prism compressive strength) by about 75 % and also the ultimate load was higher by about 26%. Crack patterns shown in Figure 5.5 indicates that in case of low strength block, the diagonal cracks crossed the units because of its lower strength compared to the interface bond at the joints. On the contrary, for high block strengths, diagonal cracks passed through the weak head and bed joints in a stepped-wise pattern .

5.5 SHEAR STIFFNESS

The estimation of the overall shear stiffness of a wall panel under service load is very important for the design of partially reinforced masonry shear walls. A simple theoretical solution is not possible due to the occurrence of flexural and shear cracks at moderate load levels. However, before cracking a wall panel can be considered linearly elastic and homogeneous. In this case, the shear stiffness of an elastic cantilever wall with

a rectangular section can be expressed as

$$K_s = (A_{pg} E_m) / [2.4 h (1 + \upsilon)] \quad (5.1)$$

Where

A_{pg} = the area of partially grouted shear walls calculated from Eq. 5.1

E_m = elastic modulus of masonry

h = the height of the wall

υ = the Poisson's ratio

The influence of the steel reinforcement on the shear stiffness in the uncracked stage can be neglected. However, when the shear or flexural cracks occur, the shear stiffness is substantially reduced and the influence of the steel reinforcement and axial stress becomes important[130]. In general, it can be expected that increasing the quantity of vertical and horizontal steel and/or the magnitude of the axial stress reduces crack opening and thereby, increases the shear stiffness.

The elastic shear stiffness represented by Equation 5.1 only applied within a very small lateral load . To illustrate this the shear stiffness K of the wall panels measured at various lateral loads (10%, 50%, major diagonal crack and ultimate load) are normalized by the elastic stiffness K_s and plotted against the applied axial stress in Figure 5.35. As can be seen from this figure the normalized shear stiffness of the wall panels tends to decrease as the lateral load increases due to the development of more severe flexural and shear cracks. The ratio K/K_s varied between 0.15 and 0.9 depending on the lateral load level and axial stress. There is also a distinct trend that the shear stiffness measured at lateral loads greater than or equal to 50% of the maximum shear increases as the axial stress increases. The experimental results do not show any consistent influence of the distribution and quantity of vertical and horizontal steel on the post-cracked shear stiffness. Further experimental studies are necessary to develop an equation for predicting the shear stiffness of the partially reinforced masonry walls under service loading.

5.6 DUCTILITY

Ductility is the capability of a structure to deform beyond its elastic limit. Ductility is a major design consideration especially in a seismic design. However, it is considered in this study only to demonstrate the capability of partially reinforced masonry shear walls as a new system to deform beyond the elastic limit. Wall ductility is considered a measure of the inelastic performance. Greater ductility is translated into higher energy absorption, and less possibility of brittle behavior.

Ductility of a structural component can be measured from the load-deflection curve. It is traditionally defined as the ratio of the ultimate deflection to the deflection at first yield. However, initiation of yielding is not always well defined, and the ultimate deflection should be rather based on the level of damage permitted for the given type of structure according to its use. For reinforced masonry shear walls, UBC Code[141] recommends a minimum ductility value of two. According to current building code provisions, the design loads can be substantially reduced if the structure is able to provide a good deformation capability beyond the elastic limit. Ductility can be calculated by two methods. The first method used by Shing[126], is defined as $\partial_{50}/(\partial_y e_p)$ where ∂_{50} is the displacement at 50% post peak lateral resistance and $\partial_y e_p$ is the yield displacement of the equivalent elastic-perfectly-plastic system (Fig. 5.36). The second method, presented by Priestly[110], defines the ductility as ∂_{80}/∂_y, where ∂_{80} is the displacement at 50% post peak lateral resistance, and ∂y is defined as shown in Fig. 5.36. The displacement at first yield was measured from the load-deflection curve assuming an equivalent elasto-plastic system. In this study, ductility was calculated using the second method because wall displacements were limited to approximately 70% (not 50%) of the ultimate resistance of the wall specimen due to the limitation on the controlled LVDT range. In addition the first method is intended to represent a specific damage state of a specimen.

Ductility of the flexural, shear and flexural/shear specimens are plotted against the axial stress in Figure 5.37. It is evident that the flexural specimens had larger ductilities

than the shear specimens, while the ductility of the flexural/shear specimen lie between the two. As presented in Table 5.1 by specimens SWA2, SWA3,and SWA4, the increase of axial stress tends to reduce the ductility and change the behavior from flexural to flexural/shear to shear modes. This is probably due to the fact that the increase of the axial load enhances the aggregate-interlock mechanism, thereby, increases the post-cracked shear resistance[129].

It has been demonstrated that increasing the amount of vertical or horizontal steel especially for wall panels type (SWA) which have only one intermediate bond beam and column, slightly increased the ductility but did not change the wall behavior. On the other hand, more distribution of vertical and horizontal steel (wall panels type SWC) changed the behavior from a brittle shear mode to a ductile flexural mode due to increasing the shear resistance provided by bond beams and the dowel action of the vertical steel .

For the same level of axial load and the same quantities and distributions of vertical and horizontal steel the ductility of the walls under cyclic loading were almost half the ductility of the wall under monotonic loading. This reduction could be attributed to the repetitive opening and closing of the cracks under reversed loading. This indicates that the ability of partially reinforced masonry shear walls to develop a large deformation capacity under cyclic load is limited. Therefore, it is not recommended for use in a moderate or high seismic areas.

5.7 COMPARISON BETWEEN MONOTONIC AND CYCLIC TESTS

Two walls out of fourteen walls were chosen to be tested under cyclic loading to examine effect of type of lateral loads on the behavior of partially reinforced masonry shear walls. The response of the two walls subjected to in-plane cyclically reversed loading was compared to the response of companion walls loaded under monotonic loading. Figure 5.39 shows a comparison of the L-D curves for wall SWA8 (cyclic) and wall SWA7 (monotonic). The load deflection envelope for the cyclic test was determined from the maximum positive loads and the corresponding lateral displacement for each

stage of three cycles of loading. As can be seen from this figure the curves have similar shapes. The cracking load were almost the same for the two walls and the ultimate load for the monotonic loading was higher than the cyclic loading by about 13%. However the deflection at cracking load for the cyclic loading was lower than monotonic loading by about 25% whereas the deflection at ultimate was 60% higher for monotonic loading than for cyclic loading. This represents almost a 40% reduction in ductility ratio as a result of cyclically reversed loading. The reduction in ductility ratio may be attributed to the repetitive opening and closing of the diagonal cracks.

Figure 5.40 shows the comparison of L-D curves for wall SWA10 tested cyclically and wall SWA9 tested monotonically. The load deflection envelope for the cyclic test was determined from the average of maximum positive and negative loads (average load resistance of the wall panel due to the variability of the unit strength used in one side to other side). The wall tested under cyclic loading had a lower cracking load by about 14% than that for the wall tested under monotonic loading. Also the ultimate load was lower by about 10%. On the other hand the deflection at ultimate load for cyclically loaded wall was almost half the deflection for the monotonically loaded wall. Again this reduction in ultimate deflection means reduction in the ductility ratio by about 50% due to opening and closing of diagonal cracks under cyclic loading.

From Figures 5.27 and 5.28 it can be observed that the slope of the L-D curves continued to decrease indicating a stiffness degradation. Wall panels suffered substantial stiffness degradation when subjected to cyclically reversed lateral loads. Wall stiffness was measured for different cycles at different lateral displacement and plotted against the corresponding lateral displacement in Figure 5.31. It can be noticed from this figure that as the lateral displacement increased the stiffness of the wall decreased. The initial stiffness of wall SWA8 was higher than the initial stiffness of wall SWA10 by about 6%. This small variation is expected due to the variability of unit strength. Also wall SWA10 showed a higher rate of stiffness degradation than wall SWA8. Which may be attributed to the widening and opening of the severe cracks occurred in wall SWA10.

5.8 CLOSURE

A modeling techniques was used to experimentally investigate the behavioral characteristics of partially reinforced masonry shear walls. A total of fourteen 1/3-scale models of partially reinforced concrete masonry shear walls were constructed and tested at the Structural Testing Laboratory of Drexel University under in-plane lateral loads, with and without axial precompression. Eleven shear walls were tested under monotonic loading, two shear walls were tested under fully reserved cyclic loading and one infilled frame was chosen to be tested under monotonic loading. Five types of parameters were investigated; axial precompression, block strength, lateral load, amount and distribution of vertical and horizontal steel. The experimental results provide detailed information on the strength, shear stiffness, ductility and deformational characteristics of partially reinforced masonry shear walls.

The following conclusions can be drawn from the tests of 1/3-scale partially reinforced masonry shear walls :

1- Partially reinforced masonry shear walls with large spacing of horizontal steel subjected to in-plane lateral loads and axial precompression possess a shear (brittle) behavior. On the other hand, shear walls with small spacing of horizontal steel possess a flexure (ductile) behavior, regardless the amount of vertical steel.

2- The amount of reinforcement (horizontal or vertical) does not appear to have an effect on the shear cracking load, since the shear cracking is governed to a large extent by the tensile strength of the masonry, the block/mortar bond strength and level axial stress .

3- Axial stress changed the wall response from a ductile flexural mode to a relatively ductile shear/flexural mode to a brittle shear mode depending upon the level of axial stress. This indicates that the higher the axial stress the larger is the tendency to fail in shear (brittle) mode .

4- The first occurrence of a diagonal crack is governed to a large extent by the level of the

tensile strength of masonry and axial stress. Hence the resistance to cracking increases with the increase in axial stress and block strength. In case of low strength block, the diagonal cracks crossed the units because of its lower strength compared to the interface bond at the joints. On the contrary, for high block strength, diagonal cracks passed through the weak head and bed joints in a stepped-wise pattern .

5- The load carrying capacity of wall panels tends to increase with the decrease in the spacing of vertical and horizontal steel for the same amount of vertical and horizontal steel.

6- The behavior of partially reinforced masonry shear walls was highly sensitive to the distribution (spacing) of horizontal and vertical steel reinforcement present. The distribution of horizontal and vertical steel controls the mode of failure. The larger spacing the more the tendency of flexural failure whereas the smaller the spacing the higher the tendency of shear failure.

7- The flexural strength of partially reinforced masonry shear walls depends on the amount and distribution of vertical steel present. On the other hand the shear strength is mainly dependent on the distribution and amount of horizontal steel .

8- The first crack occurred at load ranging from 40-60 percent of the ultimate load for wall exhibited a flexure mode. However, for walls with shear mode the range is 60-80 percent.

9- The infilled frame showed a 25% reduction in cracking load compared to the partially reinforced masonry wall having the same amount and location of steel. This indicates a different serviceability condition under service load.

10- The ductility of the walls under cyclic loading were almost half the ductility of the wall under monotonic loading due to the repetitive opening and closing of the cracks under reversed loading. This indicates that the ability of partially reinforced masonry shear walls to develop a large deformation capacity under cyclic load is limited.

11- The shear stiffness measured at lateral loads greater than or equal to 50% of the maximum load increases as the axial stress increases.

Considering the results of these fourteen tests on shear walls having aspect ratio of one, it is important to realize that the above conclusions which are valid for these tests may

not hold for tests on shear walls with other aspect (height to width) ratios. The complexity of the problem requires an extension of the test program especially for walls with aspect ratios less than one because their shear behavior may be quite different from the tested walls .

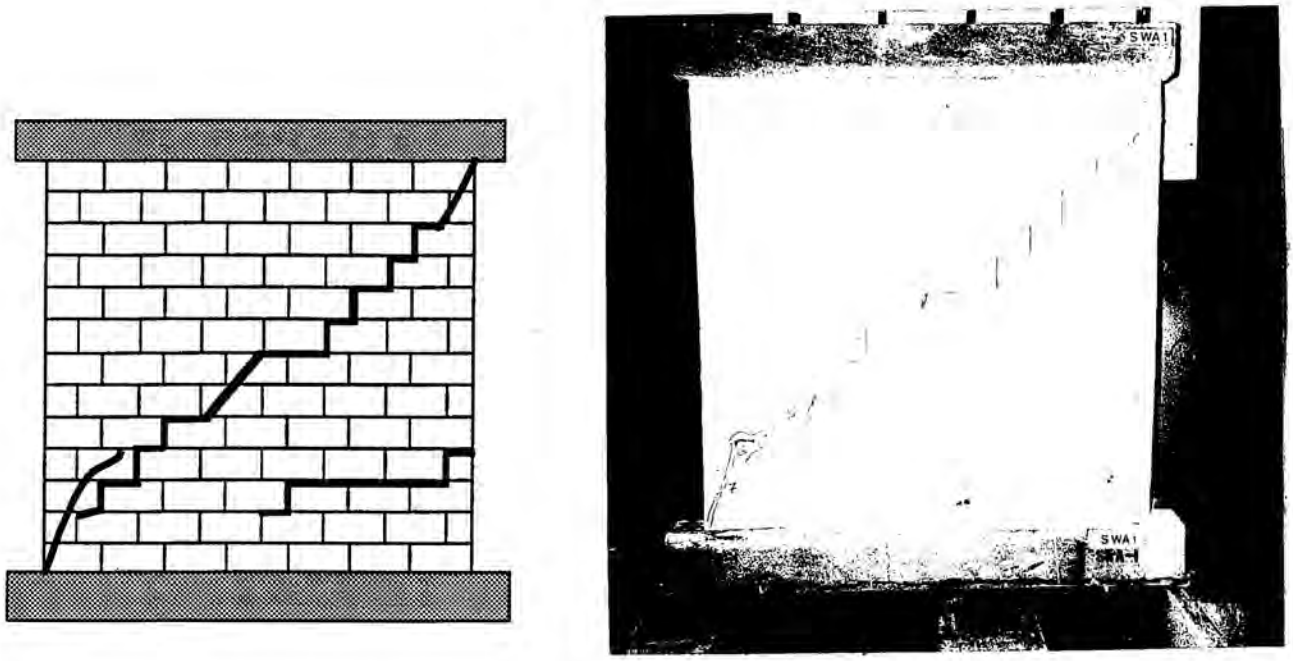

Fig. 5.1 Crack Patterns of Wall SWA1

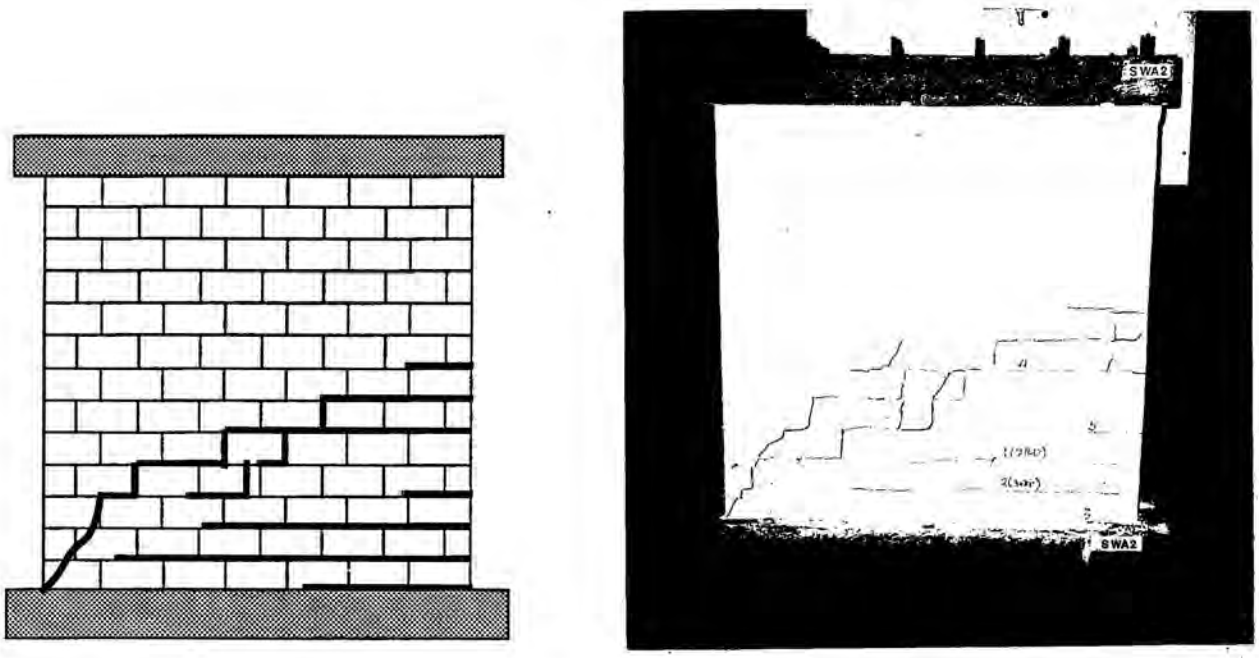

Fig. 5.2 Crack Patterns of Wall SWA2

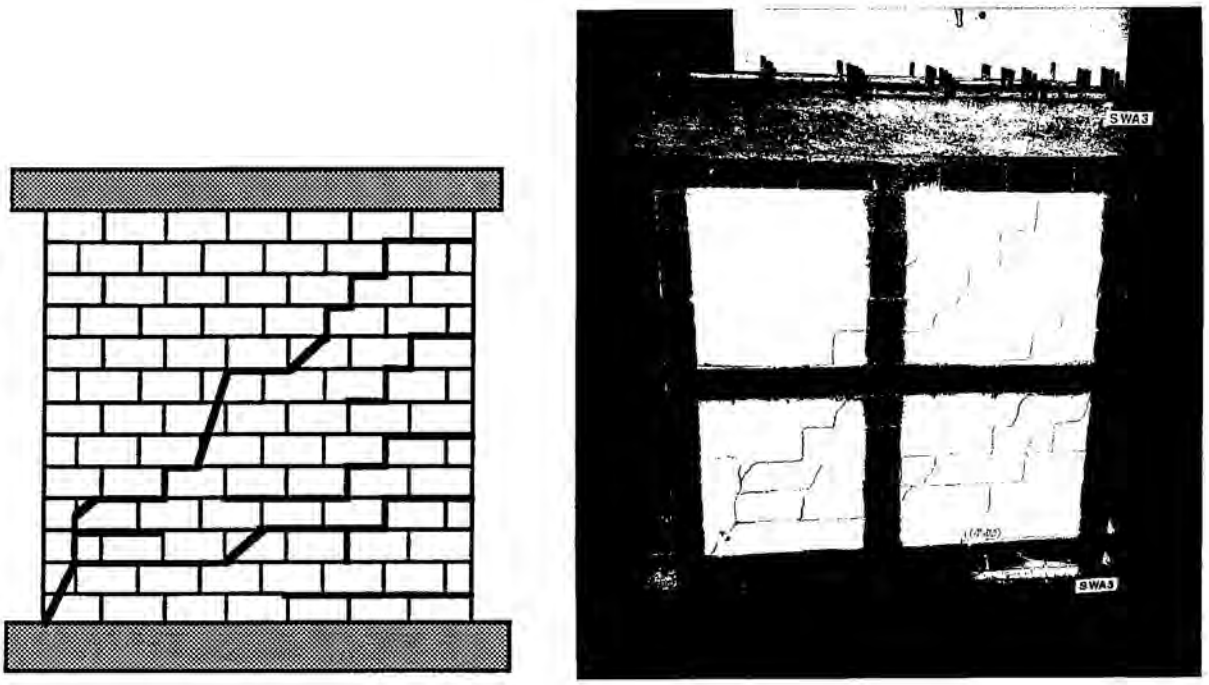

Fig. 5.3 Crack Patterns of Wall SWA3

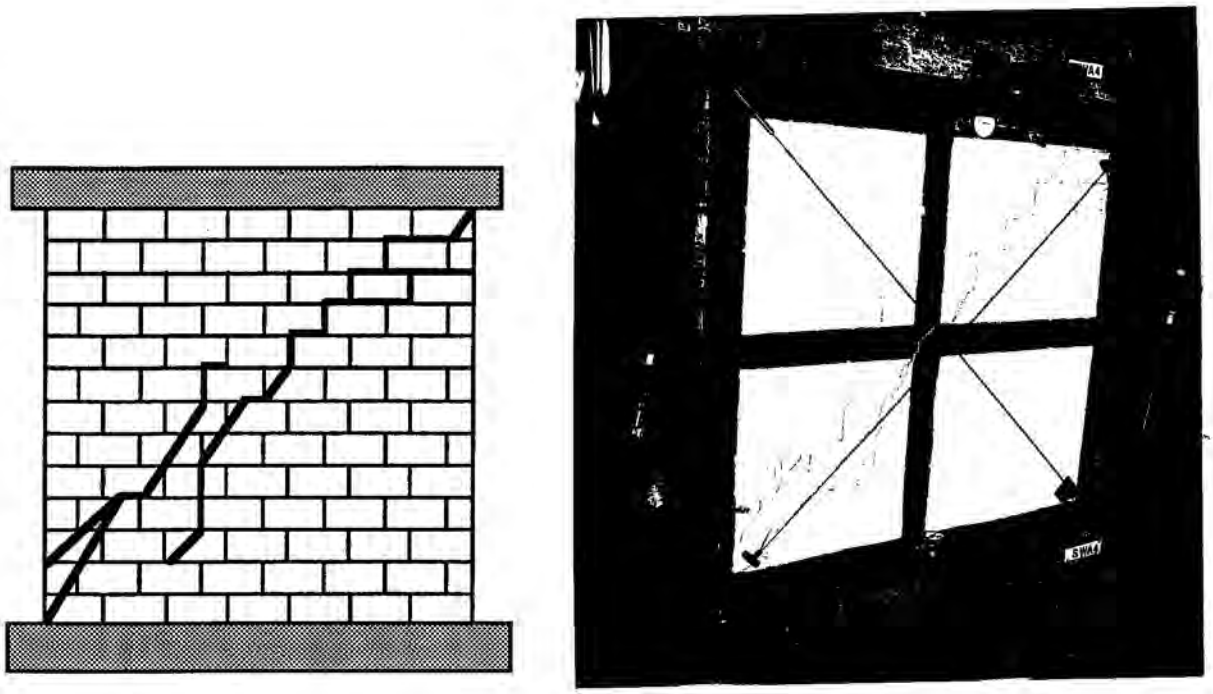

Fig. 5.4 Crack Patterns of Wall SWA4

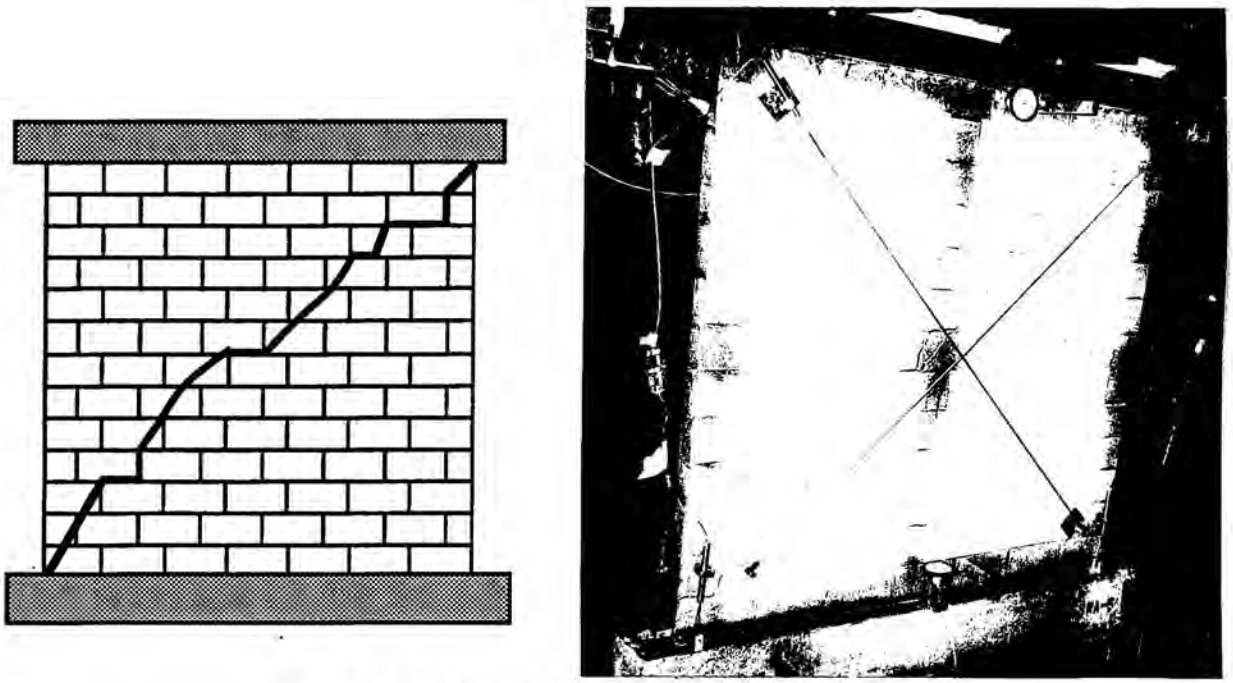

Fig. 5.5 Crack Patterns of Wall SWA5

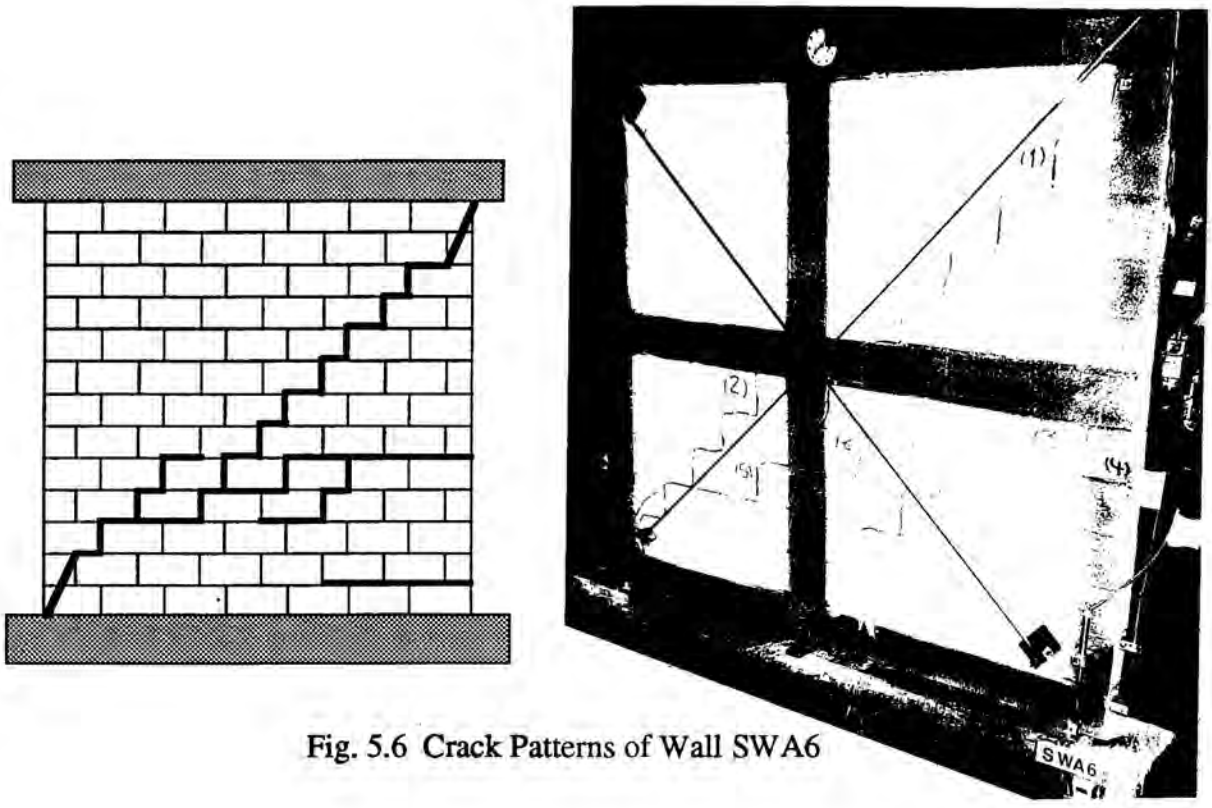

Fig. 5.6 Crack Patterns of Wall SWA6

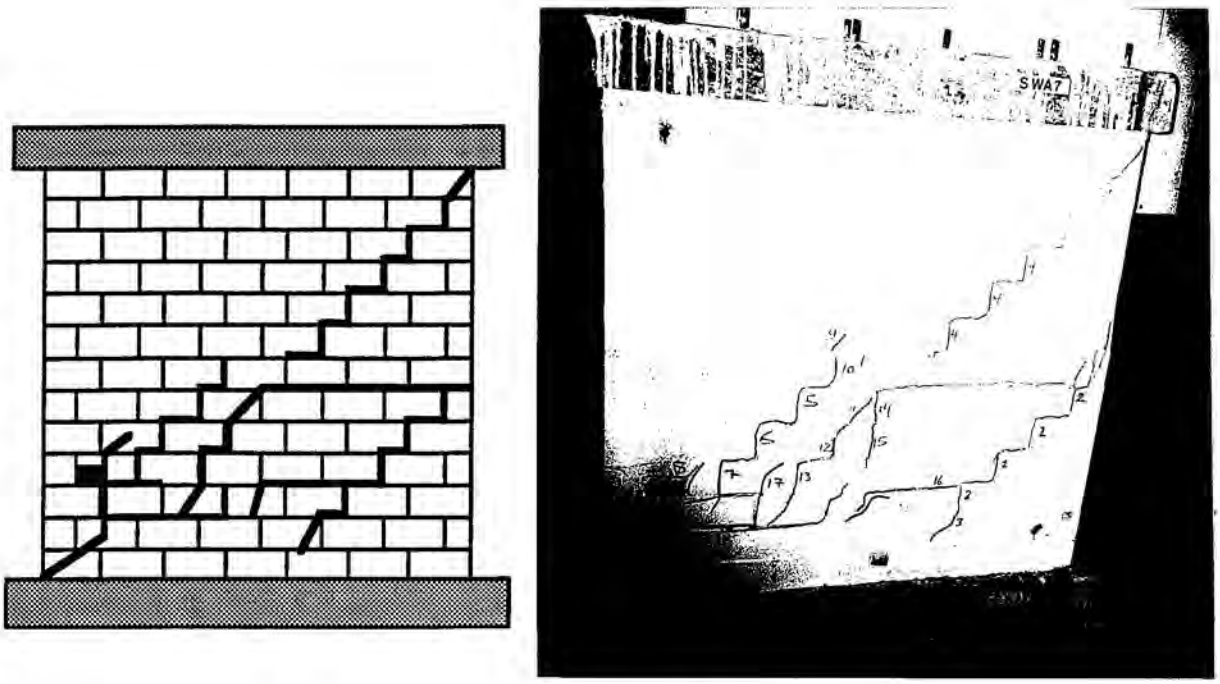

Fig. 5.7 Crack Patterns of Wall SWA7

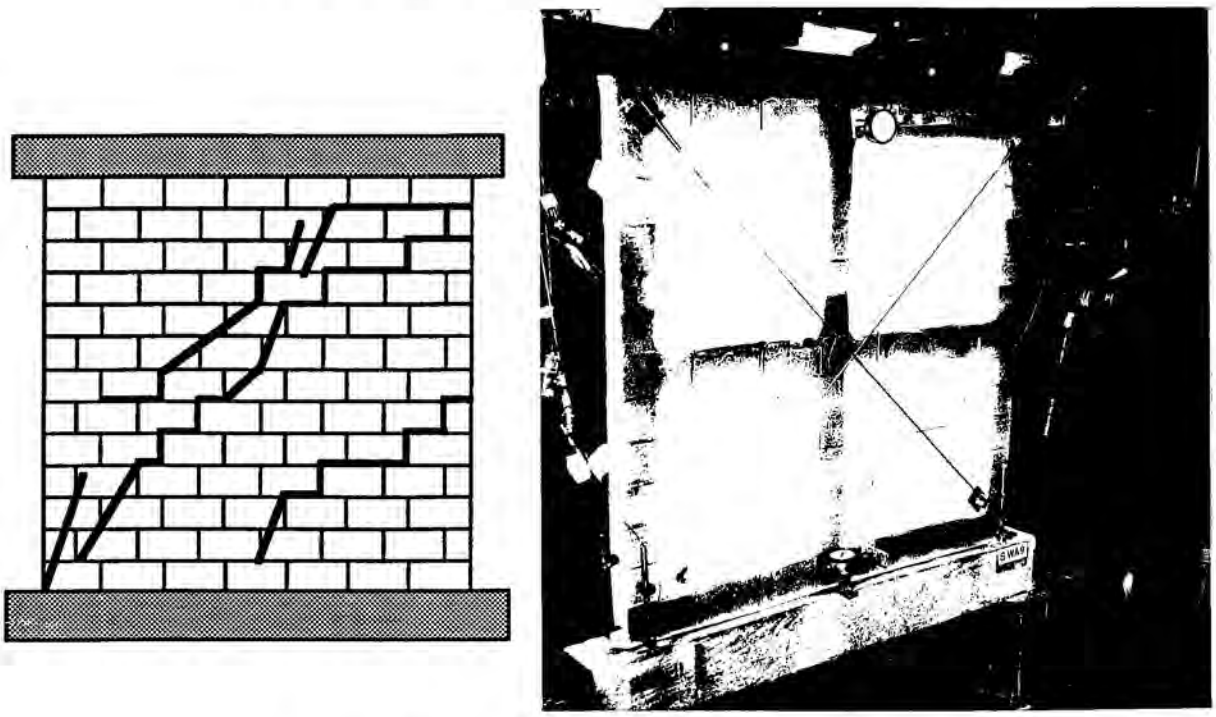

Fig. 5.8 Crack Patterns of Wall SWA9

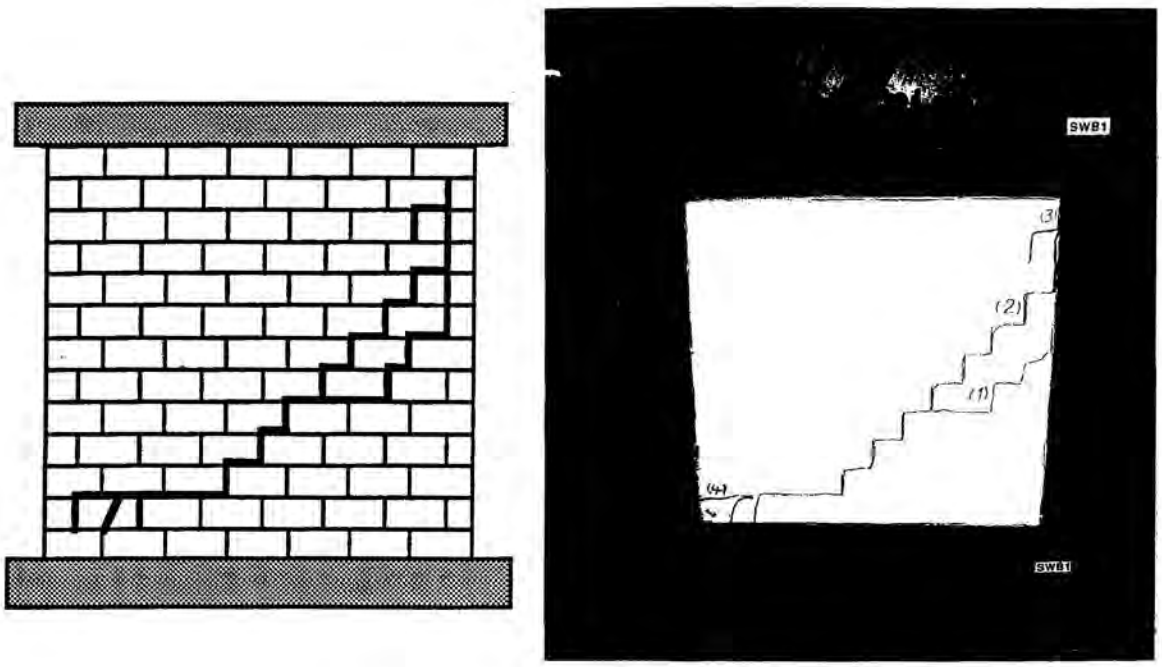

Fig. 5.9 Crack Patterns of Wall SWB1

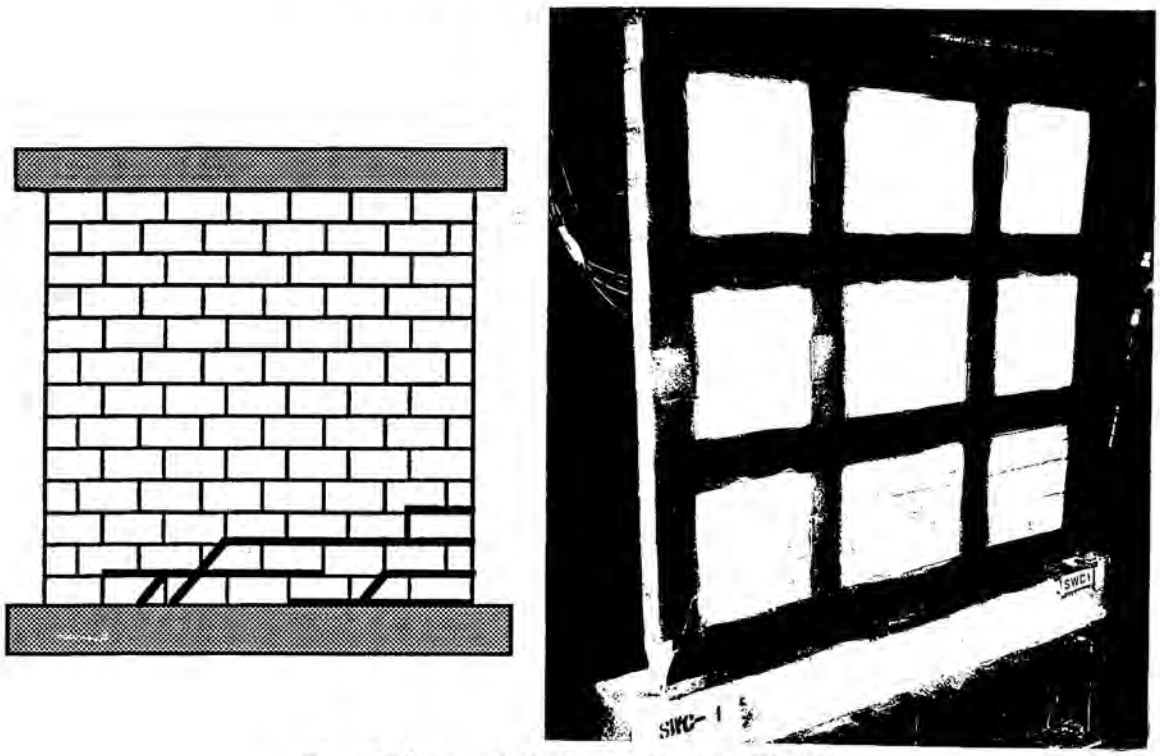

Fig. 5.10 Crack Patterns of Wall SWC1

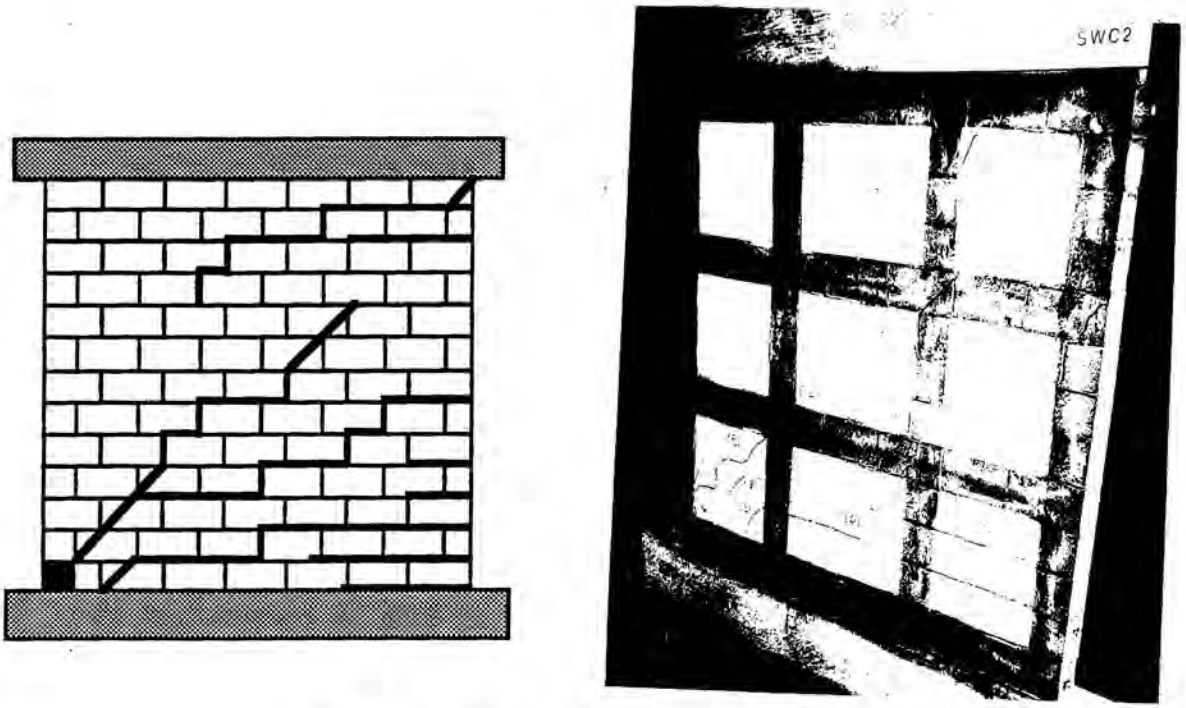

Fig. 5.11 Crack Patterns of Wall SWC2

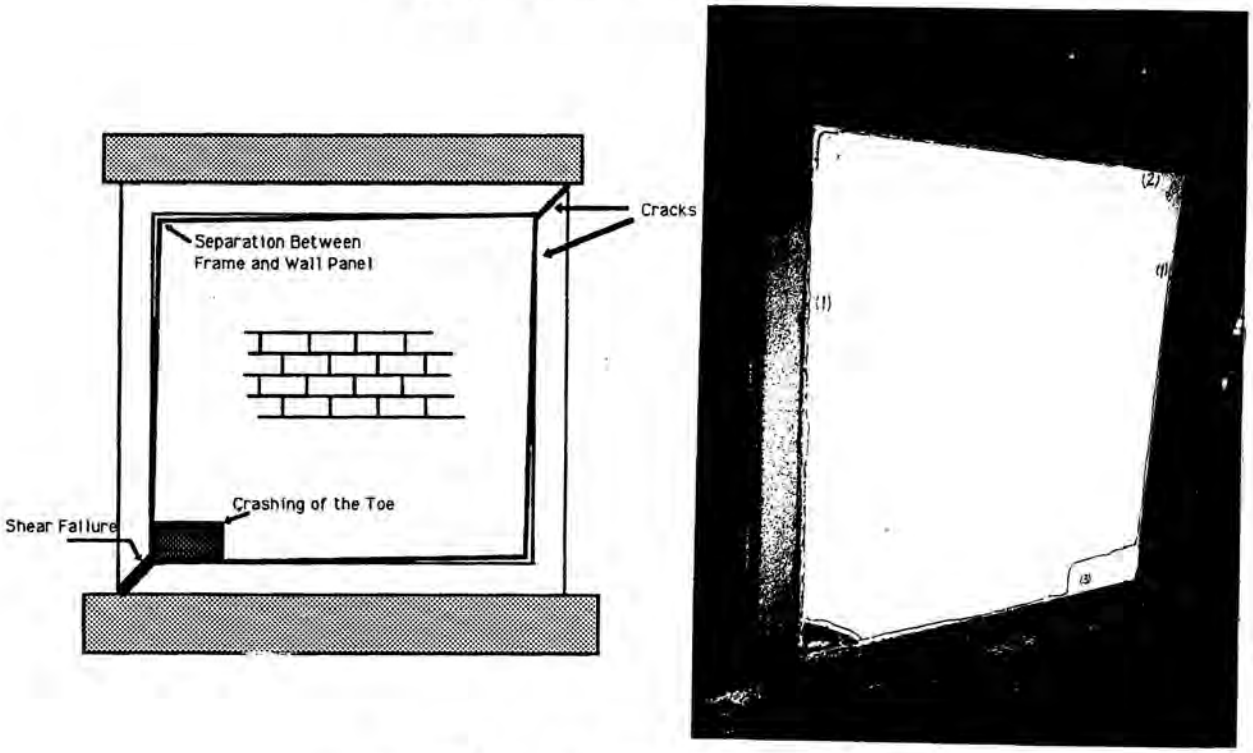

Fig. 5.12 Crack Patterns of Infilled Frame (SWD1)

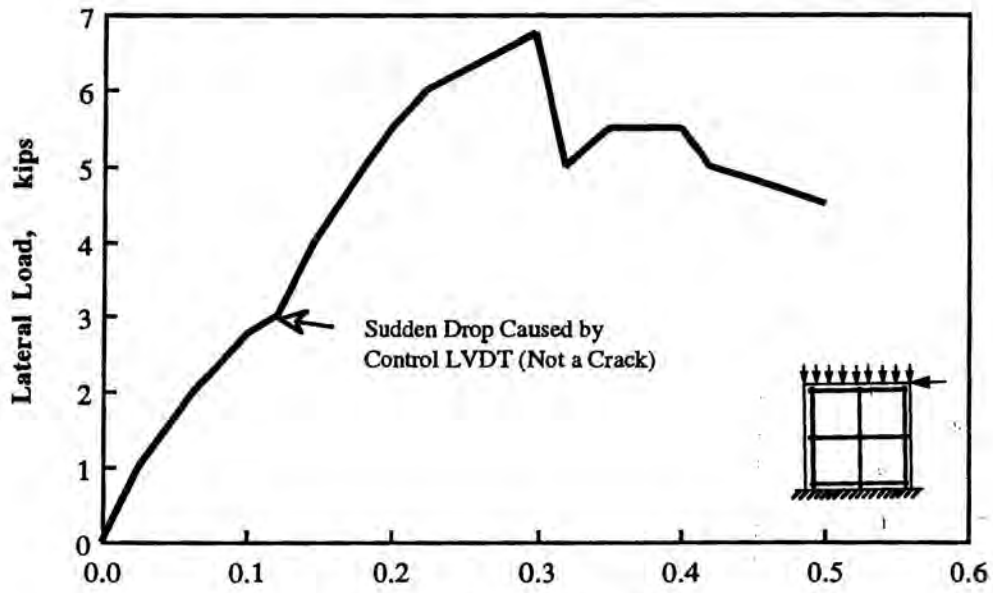

Note: 1 kip = 454 kg
1 in. = 2.54 cm

Fig. 5.13 Load-Deflection Curve for Wall SWA1

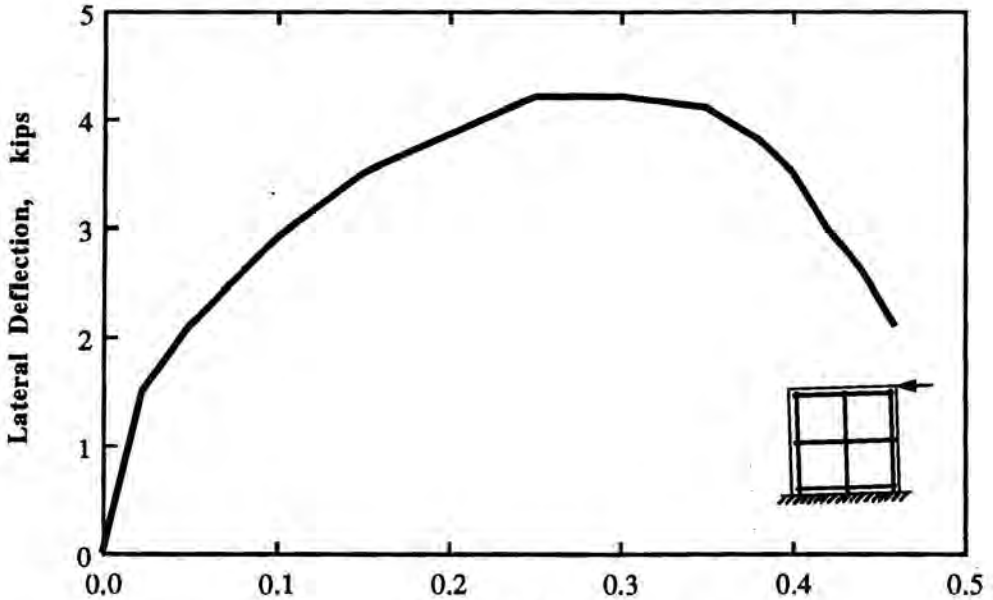

Note: 1 kip = 454 kg
1 in. = 2.54 cm

Fig. 5.14 Load-Deflection Curve for Wall SWA2

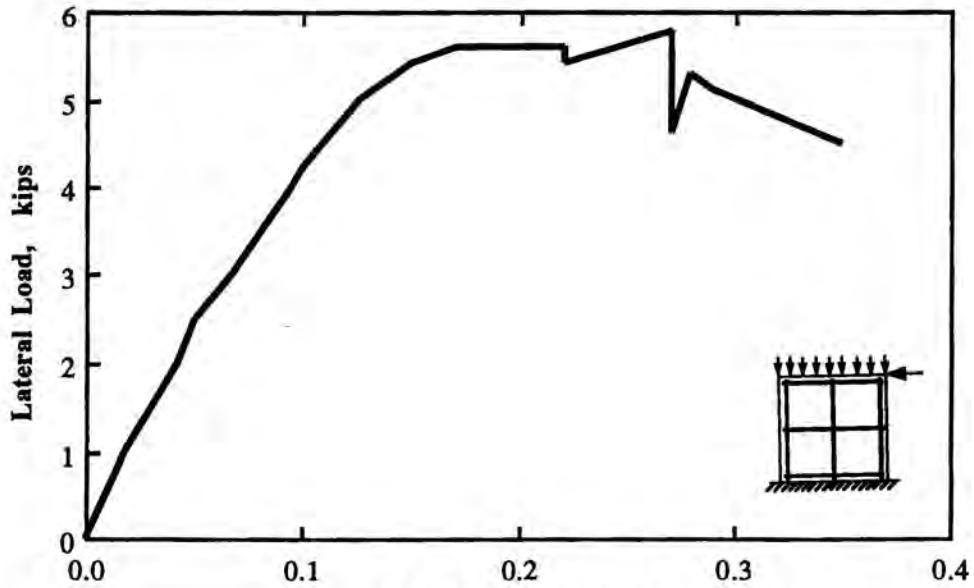

Note: 1 kip = 454 kg
1 in. = 2.54 cm

Fig. 5.15 Load-Deflection Curve for Wall SWA3

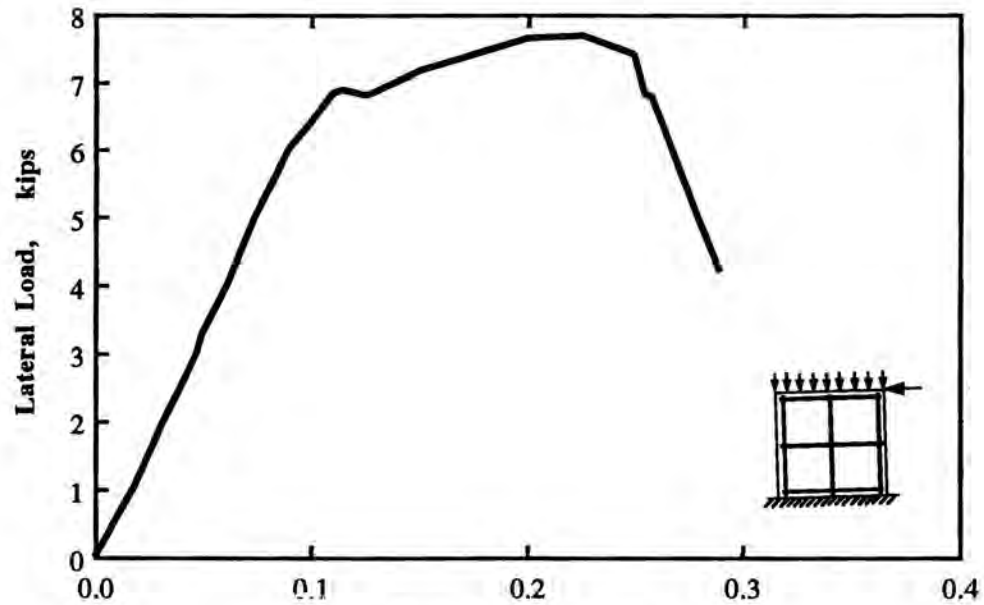

Note: 1 kip = 454 kg
1 in. = 2.54 cm

Fig. 5.16 Load-Deflection Curve for Wall SWA4

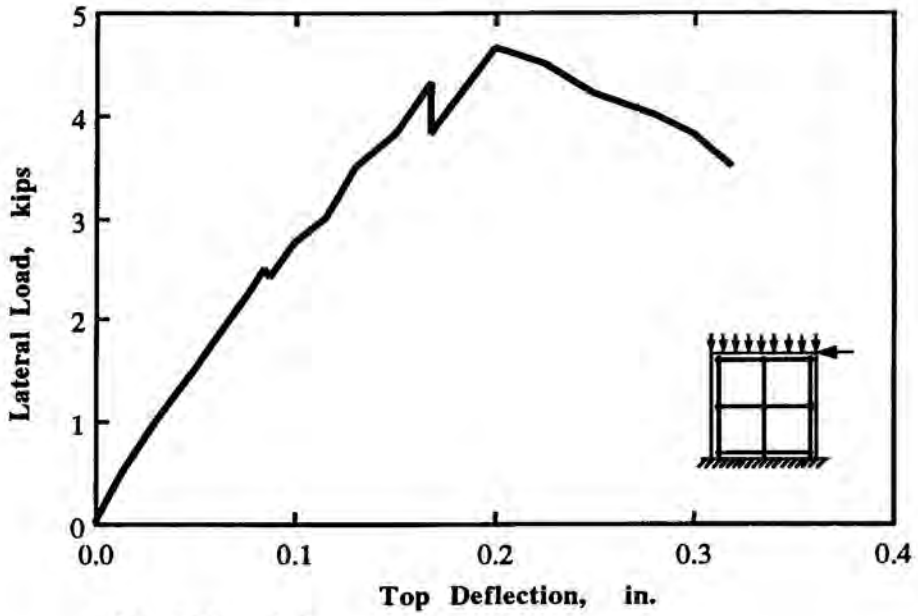

Note: 1 kip = 454 kg
1 in. = 2.54 cm

Fig. 5.17 Load-Deflection Curve for Wall SWA5

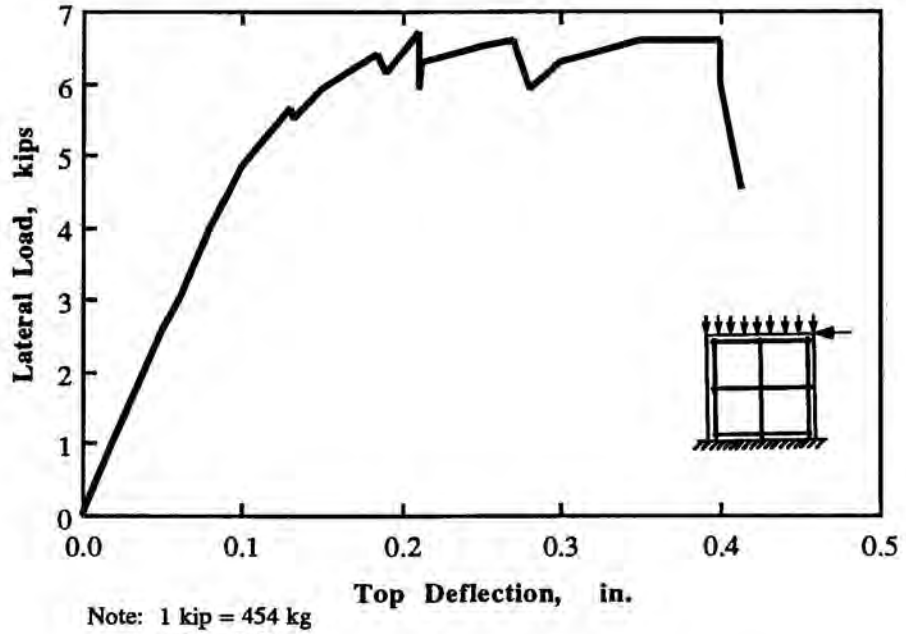

Note: 1 kip = 454 kg
1 in. = 2.54 cm

Fig. 5.18 Load-Deflection Curve for Wall SWA6

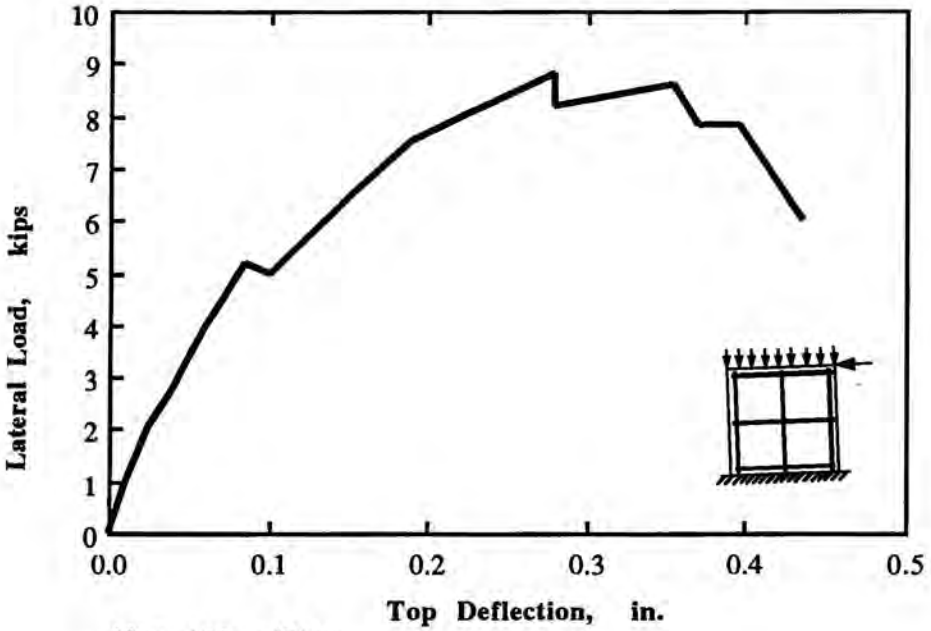

Fig. 5.19 Load-Deflection Curve for Wall SWA7

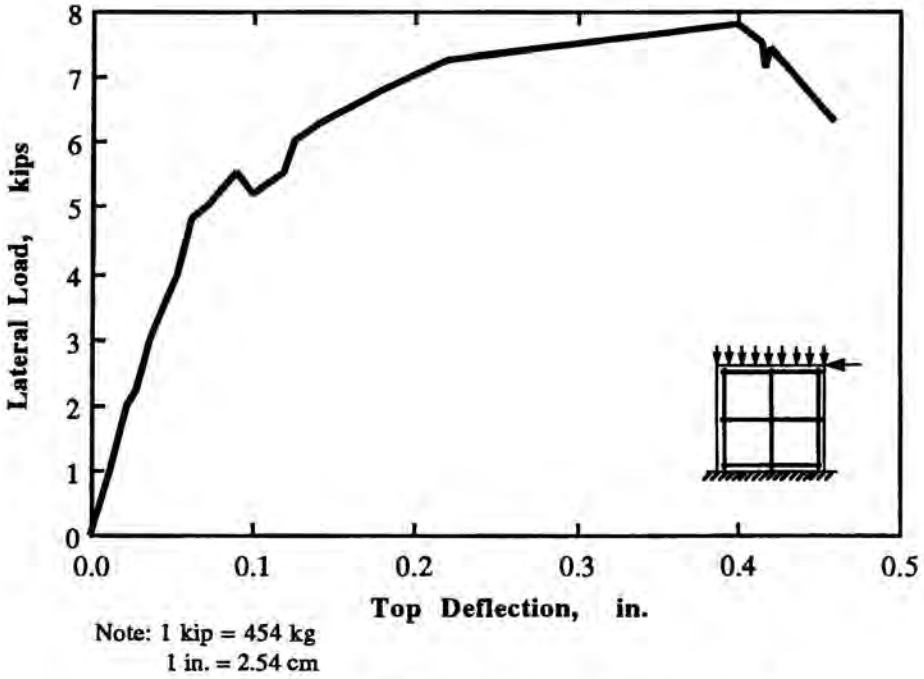

Fig. 5.20 Load-Deflection Curve for Wall SWA9

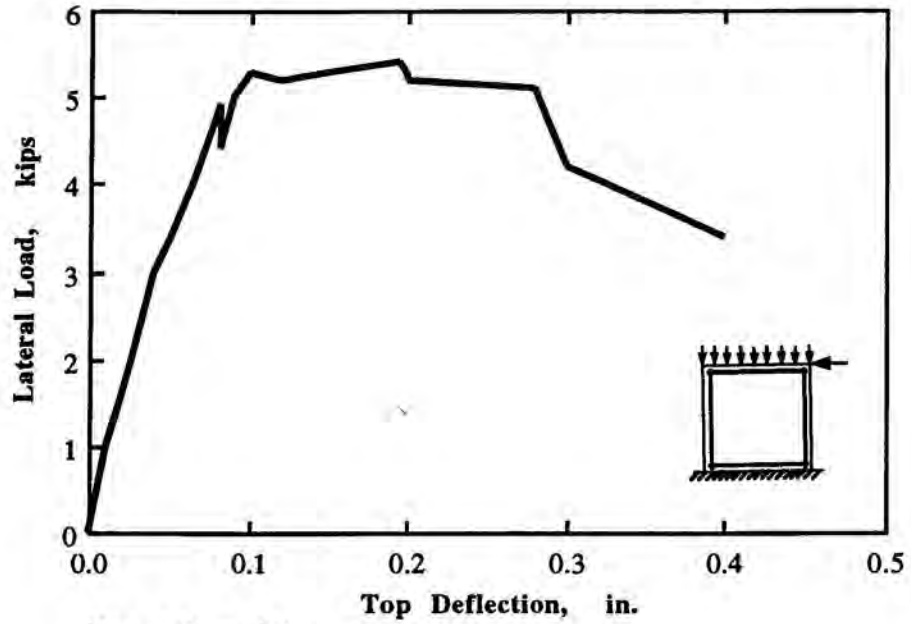

Note: 1 kip = 454 kg
1 in. = 2.54 cm

Fig. 5.21 Load-Deflection Curve for Wall SWB1

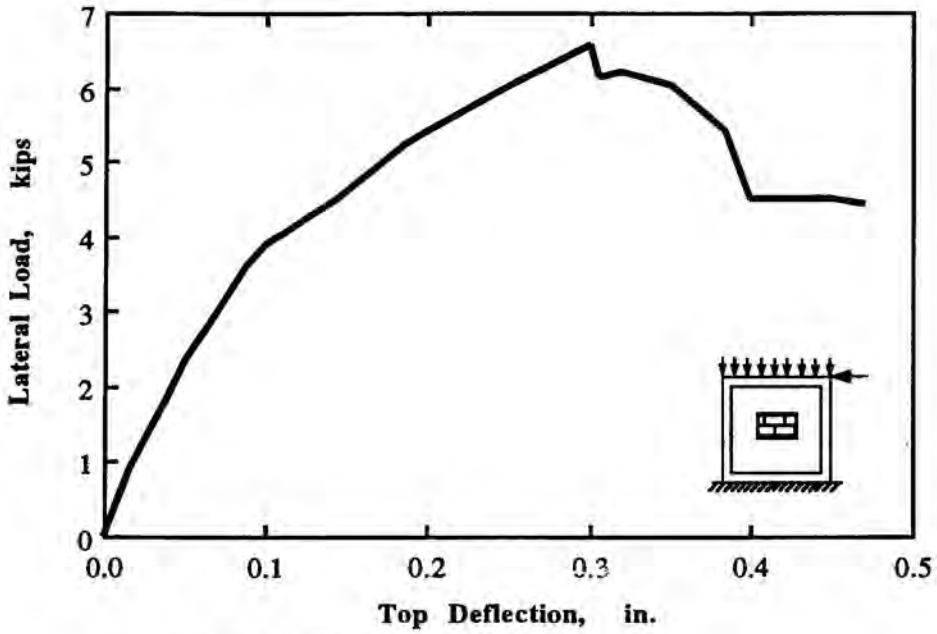

Note: 1 kip = 454 kg
1 in. = 2.54 cm

Fig. 5.22 Load-Deflection Curve for Wall SWD1

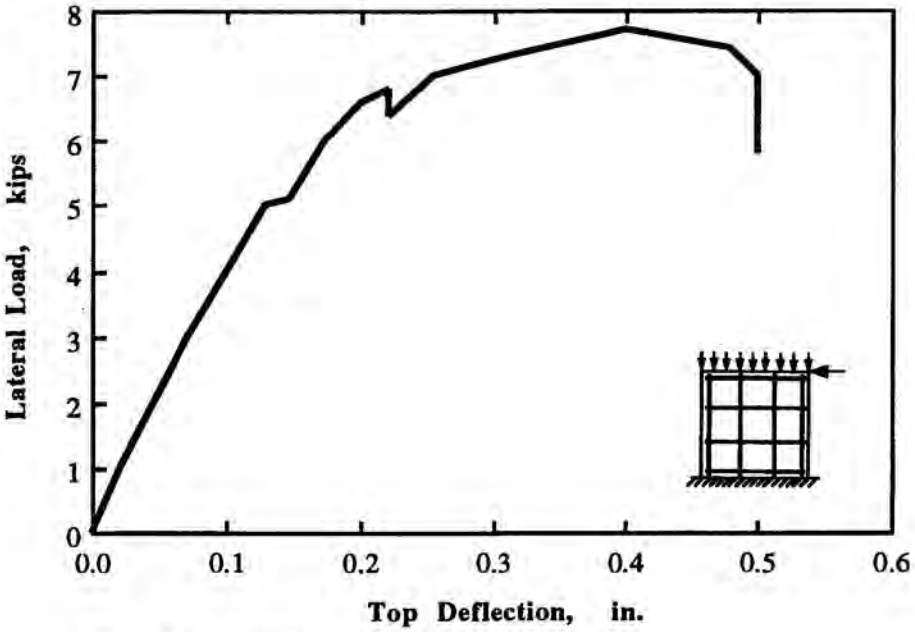

Note: 1 kip = 454 kg
1 in. = 2.54 cm

Fig. 5.23 Load-Deflection Curve for Wall SWC1

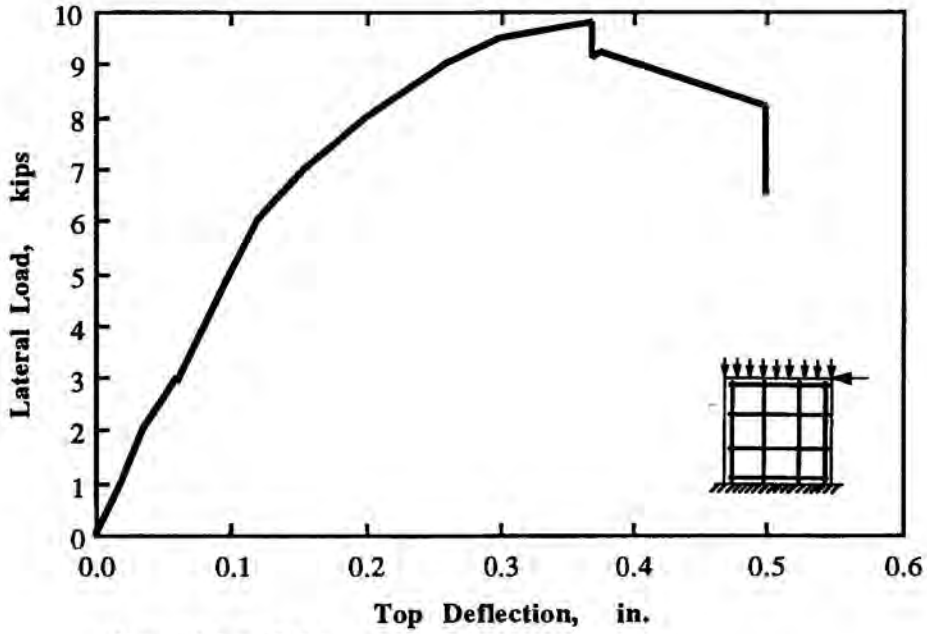

Note: 1 kip = 454 kg
1 in. = 2.54 cm

Fig. 5.24 Load-Deflection Curve for Wall SWC2

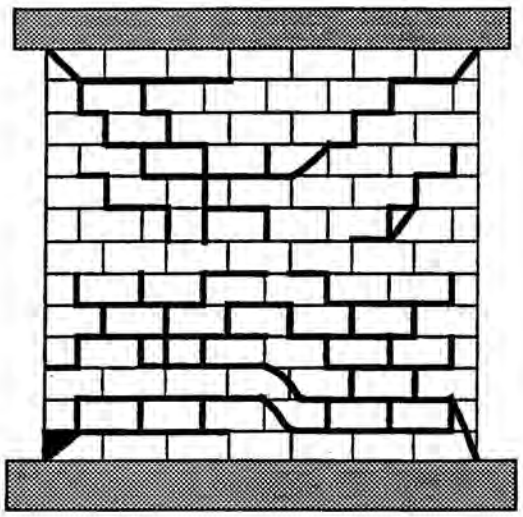

Fig. 5.25 Crack Patterns of Wall SWA8

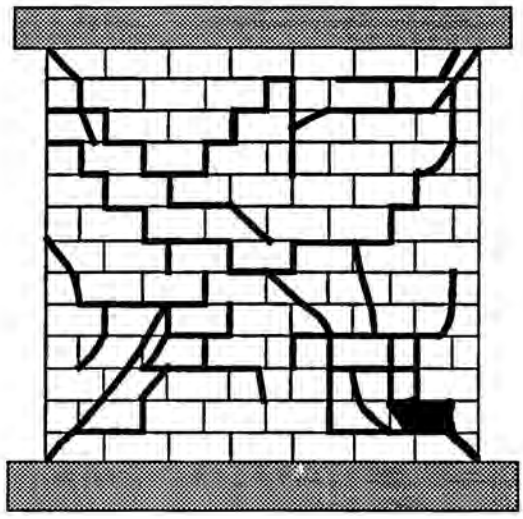

Fig. 5.26 Crack Patterns of Wall SWA10

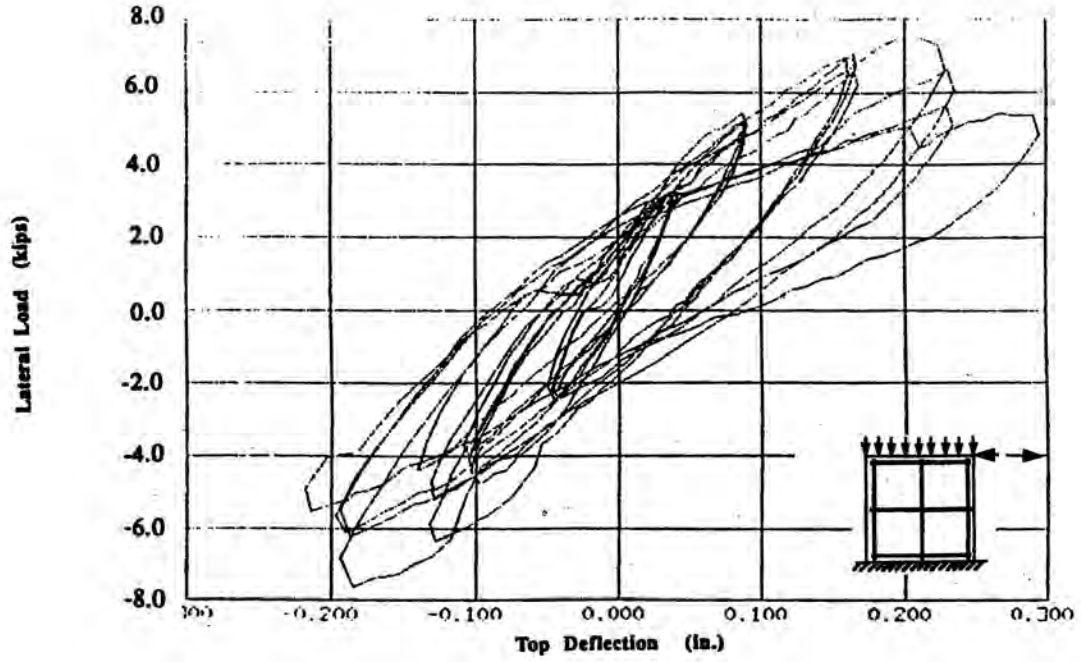

Fig. 5.27 Hysteresis Load-Deflection Curves for Wall SWA8

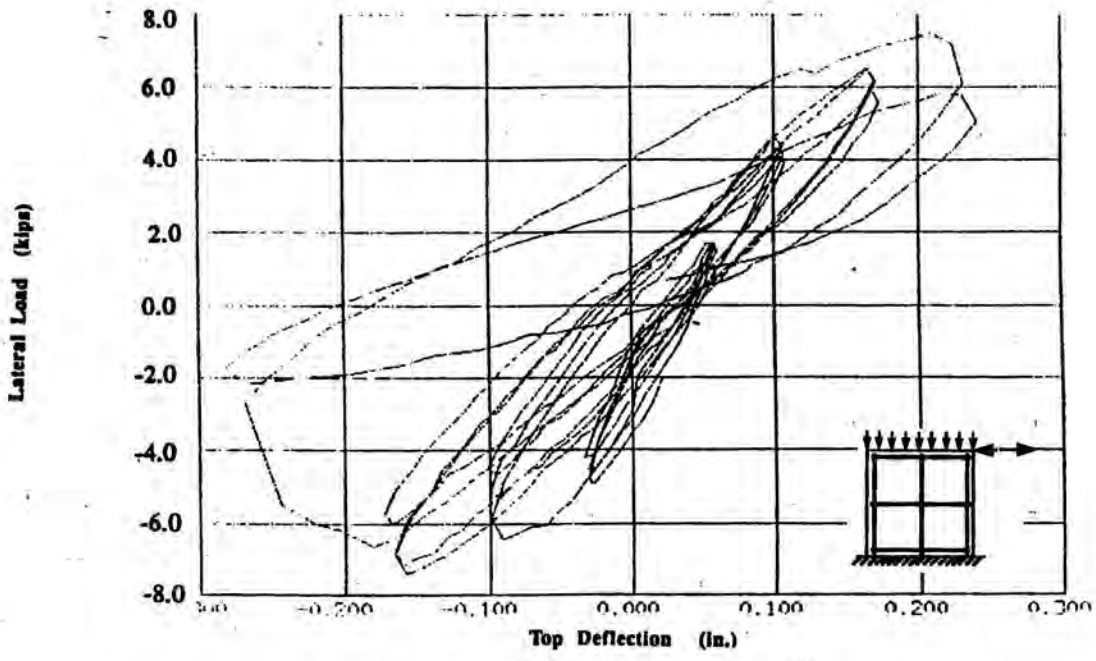

Fig. 5.28 Hysteresis Load-Deflection Curves for Wall SWA10

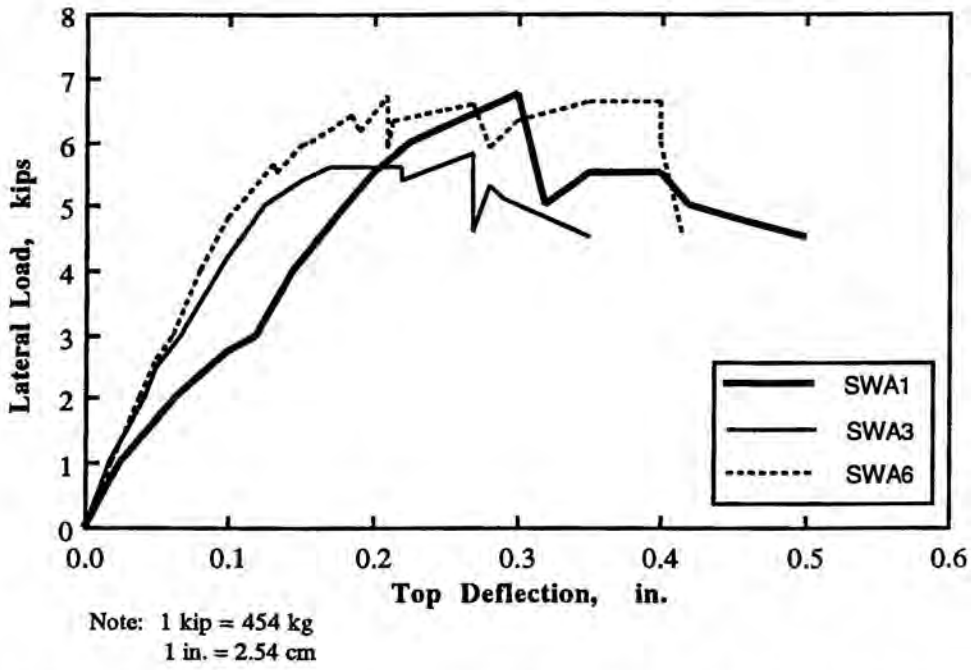

Note: 1 kip = 454 kg
1 in. = 2.54 cm

Fig. 5.29 Effect of Amount of Horizontal Steel on the Ultimate Load of the Shear Walls

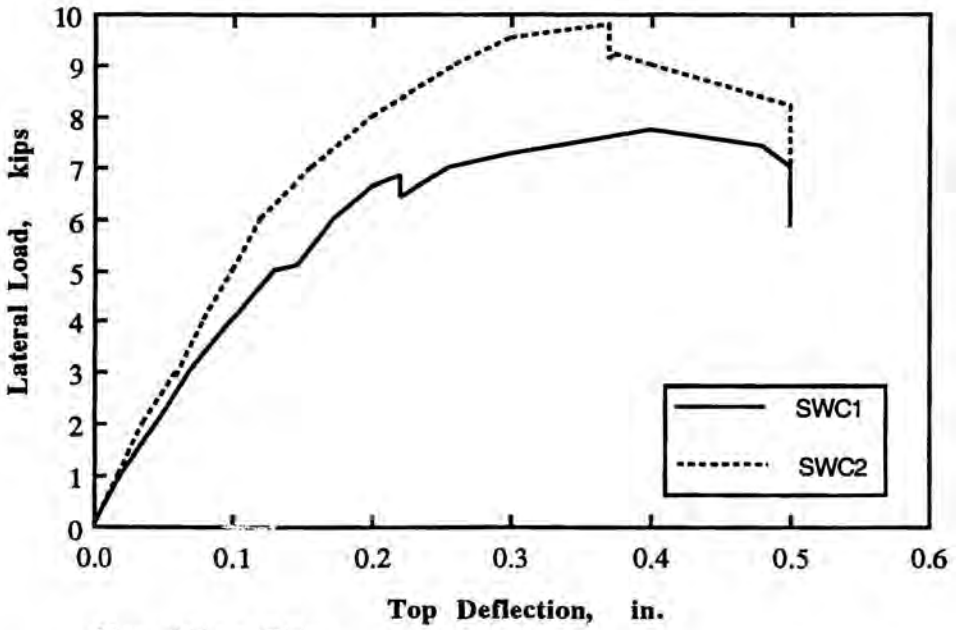

Note: 1 kip = 454 kg
1 in. = 2.54 cm

Fig. 5.30 Effect of Vertical Steel on the Flexural Capacity of Shear Walls

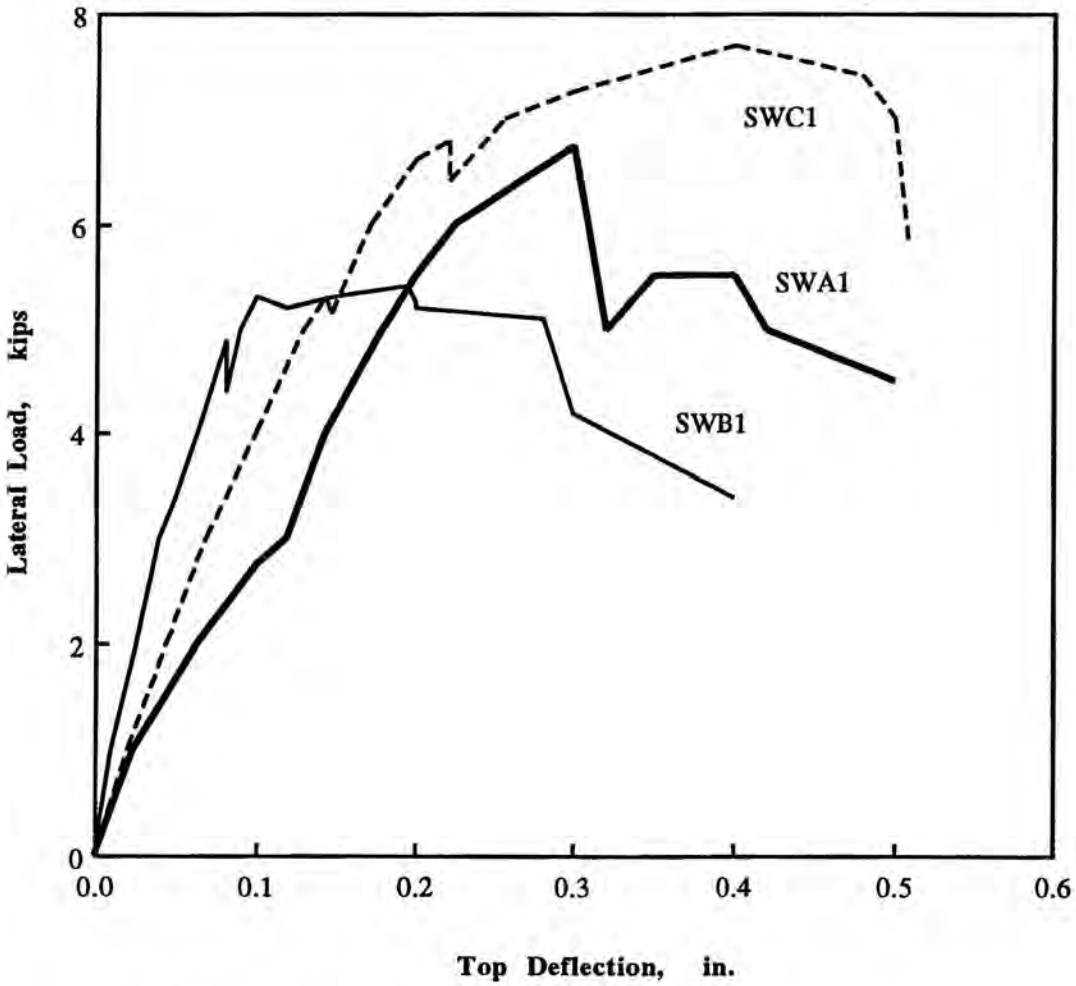

Note: 1 kip = 454 kg
1 in. = 2.54 cm

Figure 5.31 Load-Deflection Relationships of Walls SWA1, SWB1 and SWC1 Effect of distribution of Steel

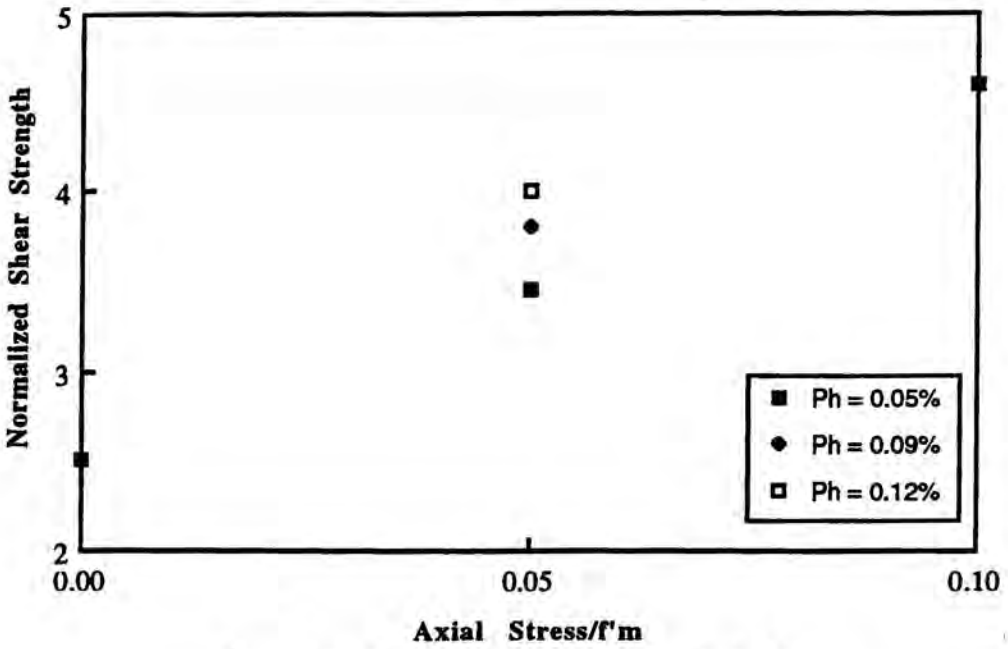

Normalized Shear Strength Versus Axial Stress

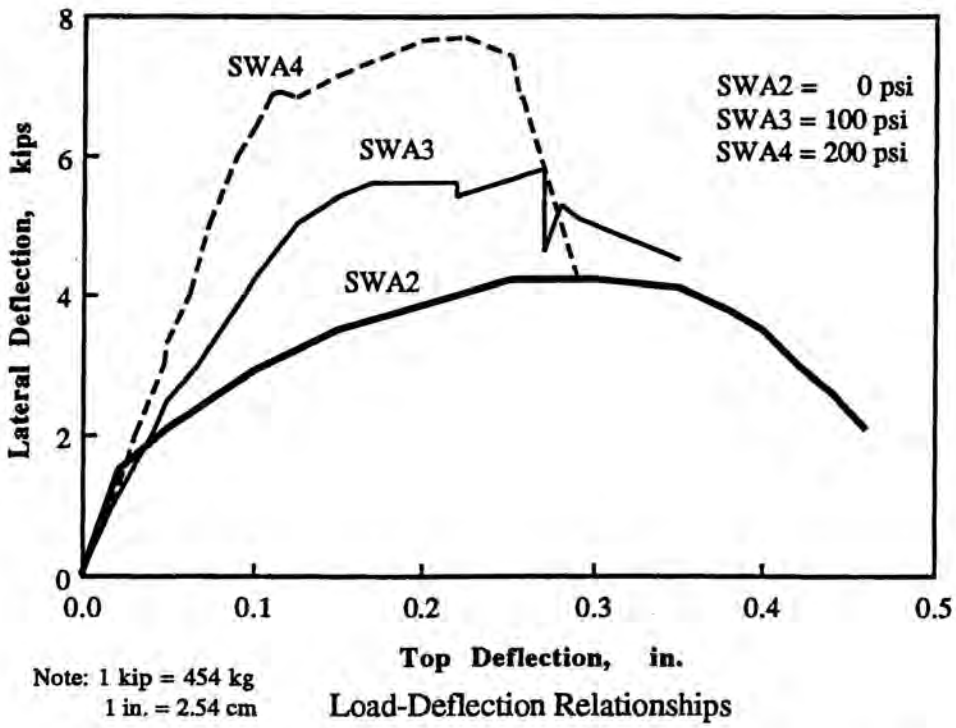

Note: 1 kip = 454 kg
1 in. = 2.54 cm

Load-Deflection Relationships

Fig. 5.32 Effect of Axial Stress on Wall Behavior and Strength

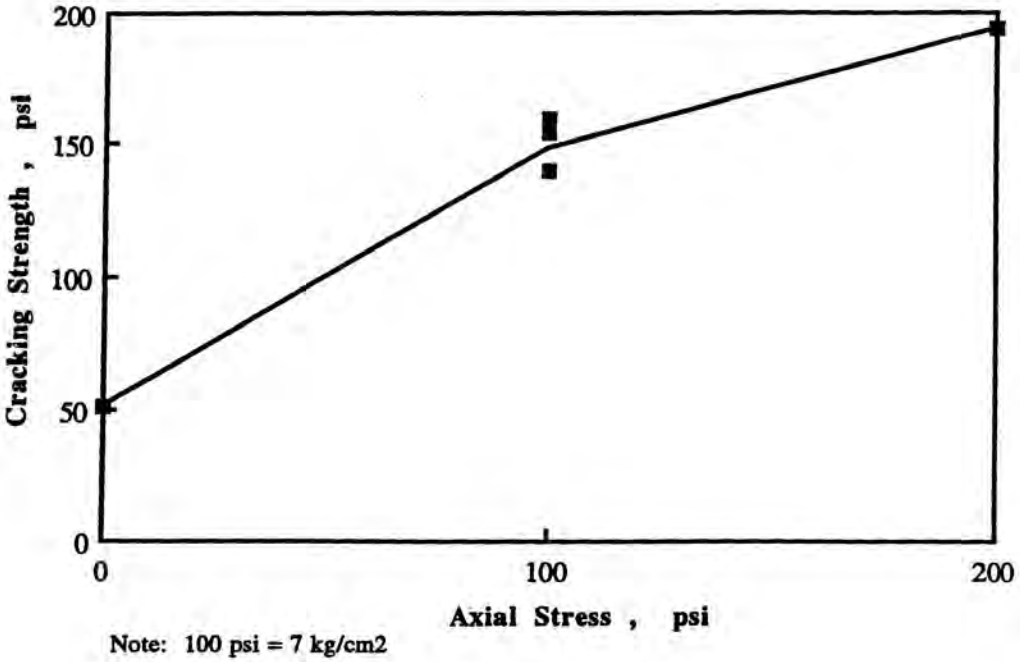

Fig. 5.33 Effect of Axial Stress on the Cracking Strength

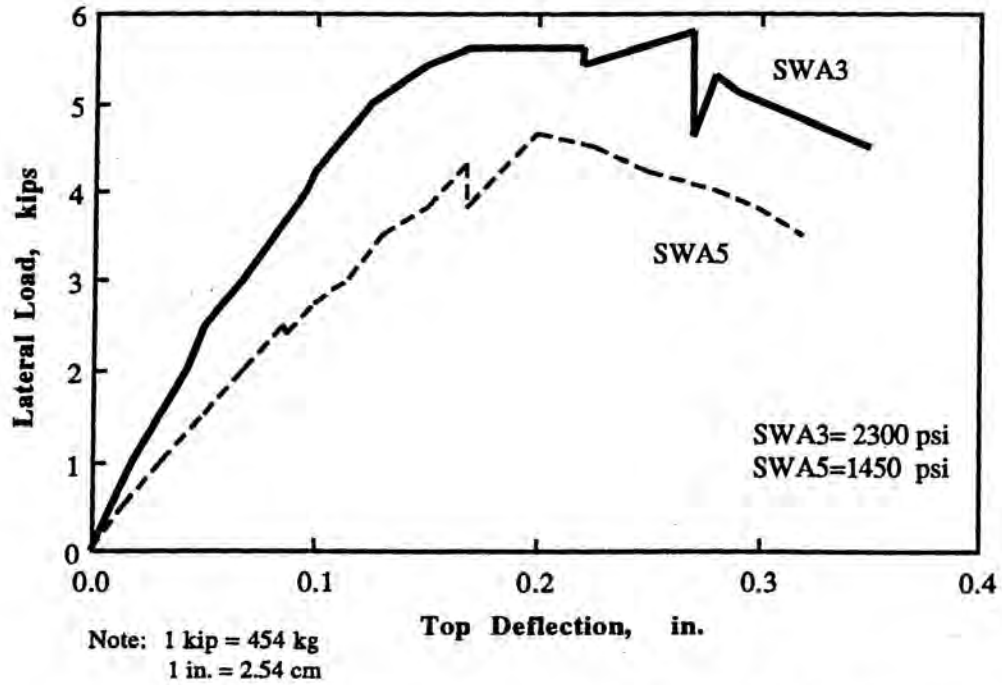

Fig. 5.34 Effect of Block Strength on Load-Deflection Curves

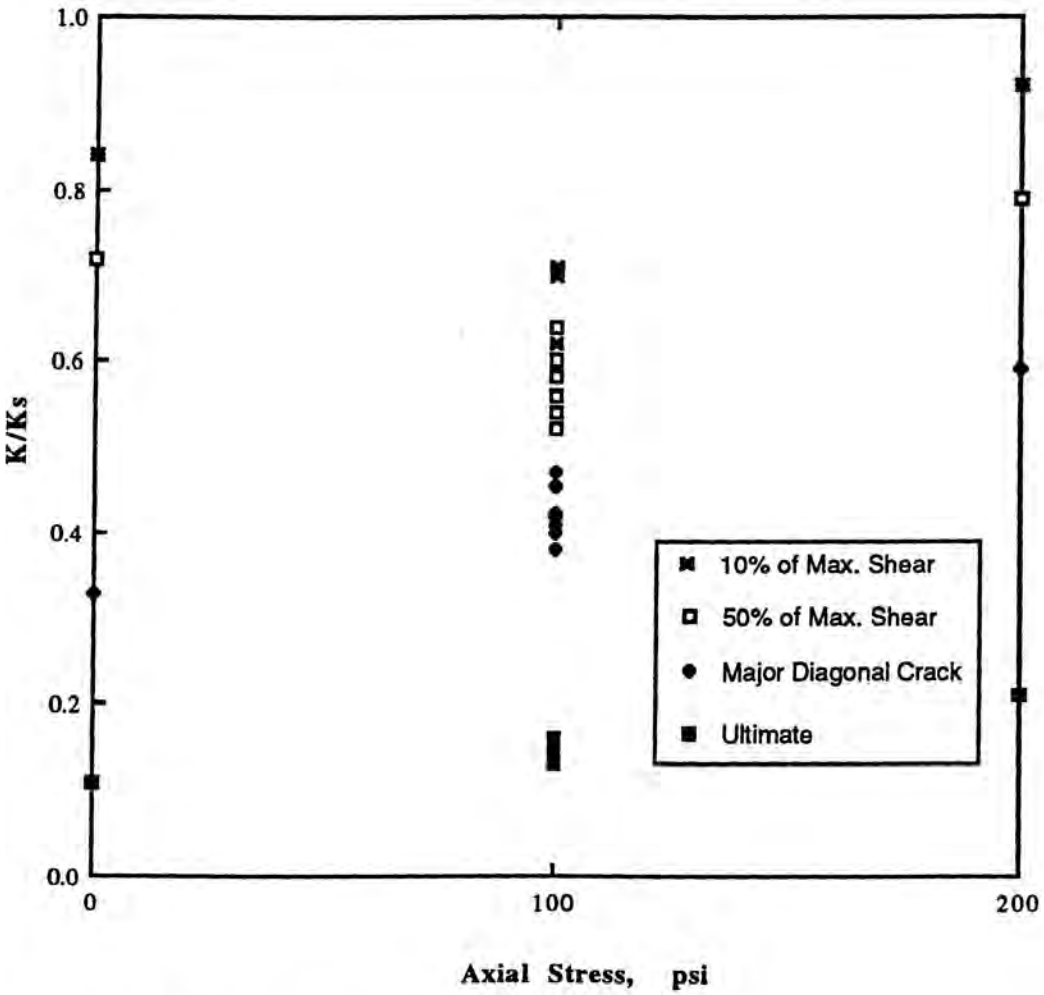

Note: 100 psi = 7 kg/cm2

Fig. 5.35 Normalized Shear Stiffness Versus Axial Stress

126

Shing

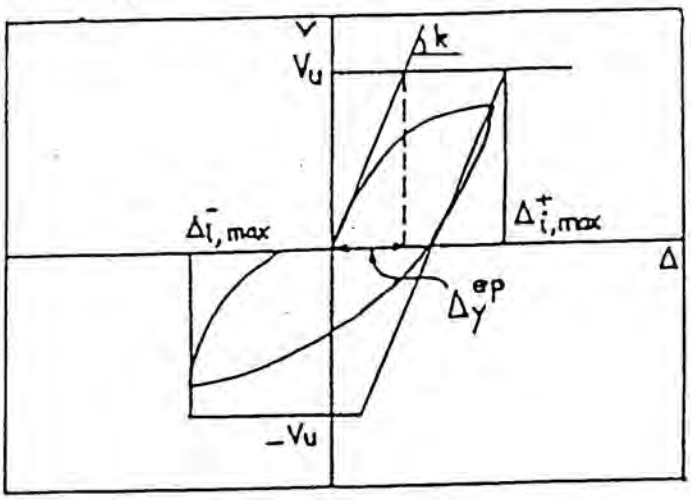

k = Average initial stiffness measured at a small displacement cycle in which the peak load is 50% of the ultimate load

110

Priestley and Park

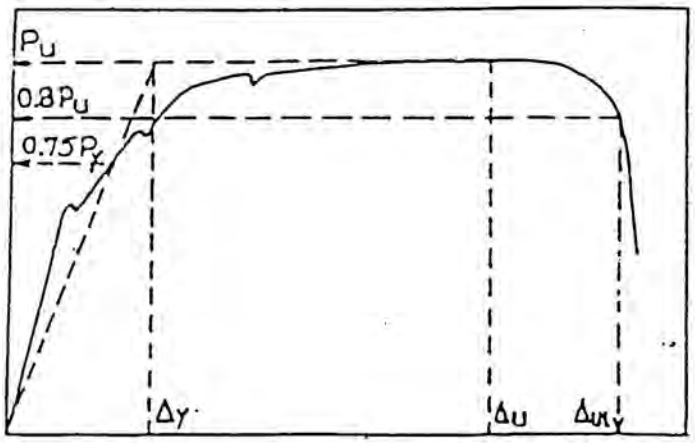

Fig. 5.36 Detrmination of Wall Ductility

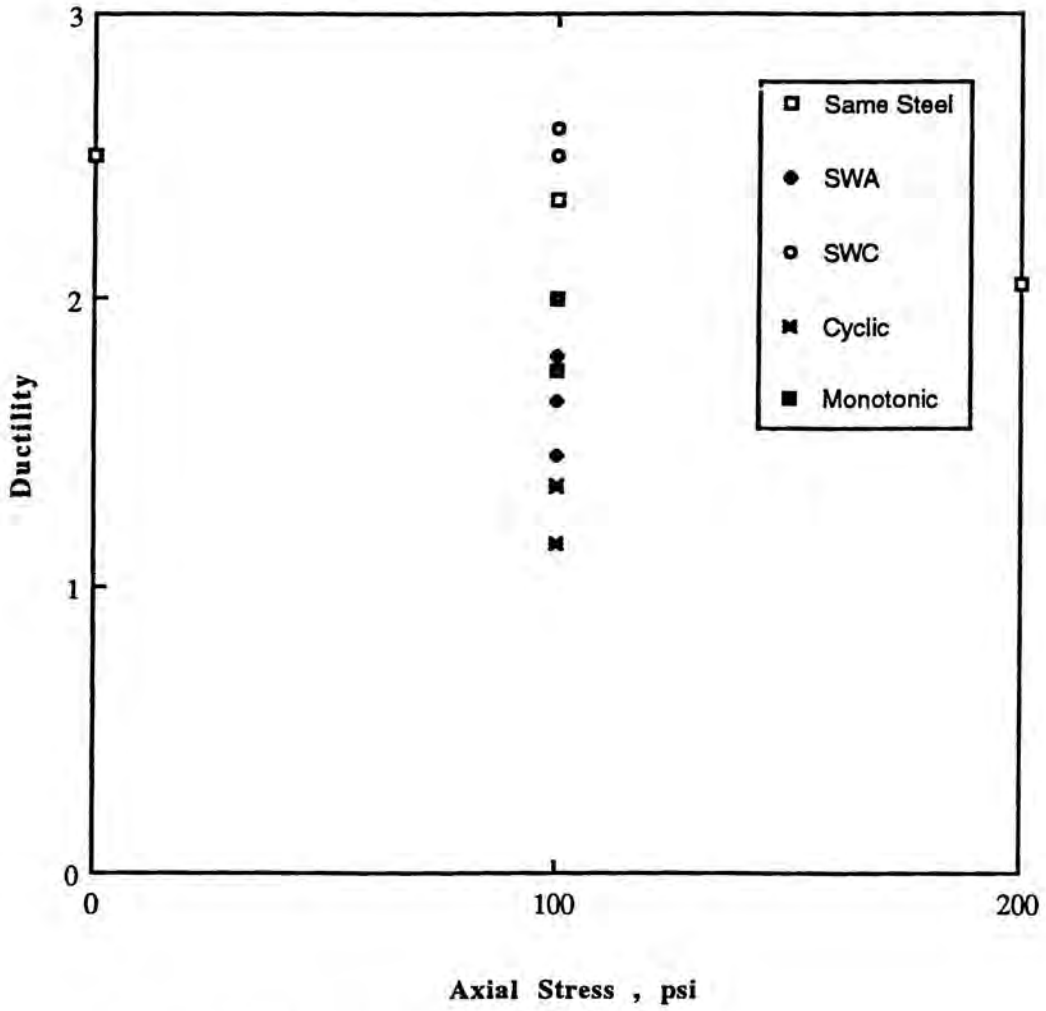

Note: 100 psi = 7 kg/cm2

Fig. 5.37 Effect of Axial Stress on Wall Ductility

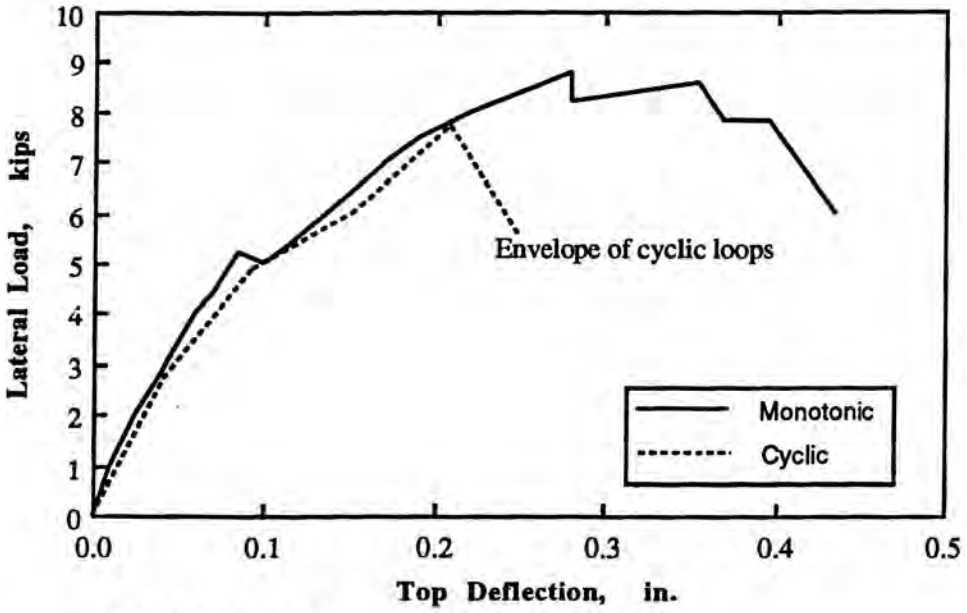

Note: 1 kip = 454 kg
1 in. = 2.54 cm

Fig. 5.38 Comparison Between Monotonic and Cyclic Tests for Walls SWA7 & SWA8

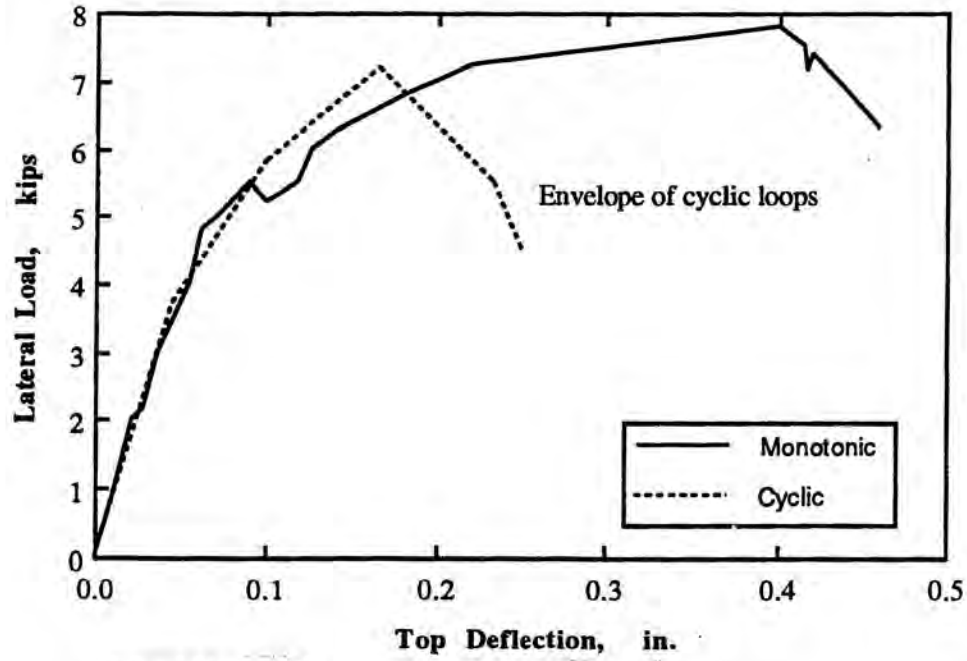

Note: 1 kip = 454 kg
1 in. = 2.54 cm

Fig. 5.39 Comparison Between Monotonic and Cyclic Tests for Walls SWA9 & SWA10

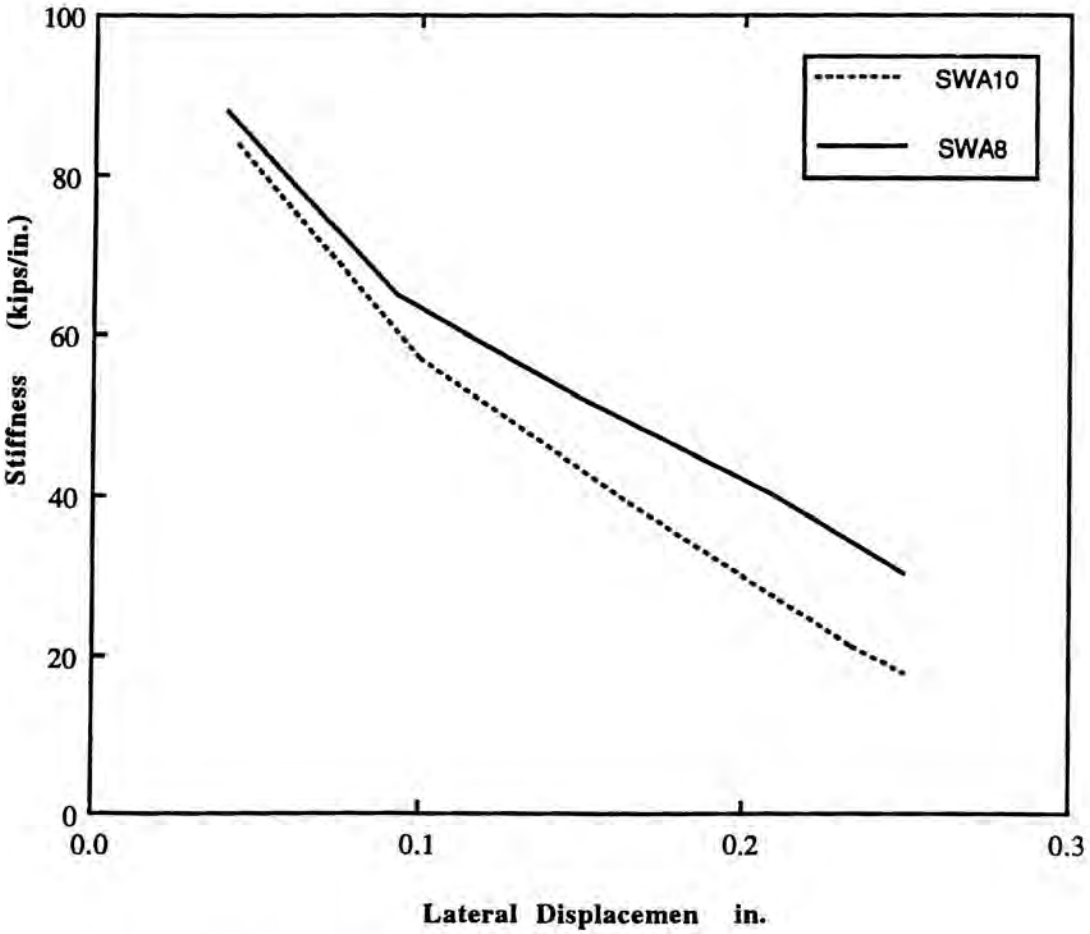

Note: 1 kip/in. = 179 kg/cm
1 in. = 2.54 cm

Fig. 5.40 Stiffness Degradation Diagrams of Cyclic Tests

CHAPTER 6

ANALYTICAL STUDY

6.1 INTRODUCTION

Due to cost and time constraints the experimental investigation did not cover all important parameters needed to develop a rational design methodology of partially reinforced masonry shear walls. An analytical study using the finite element method is conducted to perform parametric study of the effect of different factors on the behavior and strength of partially reinforced walls. Furthermore, the analytical model is used to check the adequacy of the design methodology proposed in Chapter 7.

The development of a nonlinear finite element model for the analysis of reinforced masonry or reinforced concrete structures involves the selection and formulation of appropriate analytical models and computational algorithms and the programming of a computer code or program that incorporates these models and algorithms. The analytical model must employ physical properties that are representative of these materials.

The nonlinear finite element analysis of reinforced masonry has recently been an active field of research. This is mainly due the high cost and difficulty of performing full-scale tests particularly for combined loading. The finite element method is a very powerful, modern computational tool to predict the complex behavior of reinforced masonry. Reinforced masonry is composed of different material, namely, concrete blocks, mortar, grout, and steel reinforcement. Each element has different properties which make the behavior of the wall panel more complex. In addition, the existence of bed and head joints makes the material non-isotropic.

The analytical model presented in this chapter is intended to be used for the prediction of load-displacement relationships, stresses and strains of masonry and reinforcement and first and major cracks of the tested walls (having aspect ratio of 1.0). The analytical results are correlated with experimental results presented in Chapter 5. The analytical model is also utilized to investigate the behavioral characteristics of partially

reinforced masonry shear walls having aspect ratios (h/d) of 0.5 and 3.0 which are out of the scope of the experimental work.

6.2 COMPUTER PROGRAM BACKGROUND

Masonry is first treated [120] as a linear elastic material, although tests [35] indicated that the stress-strain relationship is nonlinear. Such linear analysis may be considered satisfactory in predicting deformations at low stress levels in the working stress range, but is not expected to be adequate at higher stress levels when extensive stress redistribution occurs. This redistribution is caused by the non-linearity of the material and the localized failure due to loss bond between mortar, grout, reinforcement and units.

The idealization of masonry is a complex problem, not only because of its non-homogeneity but also due to bed and head joints acting as planes of weakness. To consider the presence of mortar joints as planes of weakness, a model was proposed by Balachandran [20] using different continuum elements to separately model the mortar joint and masonry unit materials. Since masonry usually experiences failure by debonding along mortar joints, this procedure avoided modeling the mortar/unit interface. A second element model was proposed by Hegmier et al.[71] to model masonry as a discontinuous system along the mortar joints. Besides separate modeling of mortar and masonry unit materials, the physical behavior of the interfaces between different materials was added by introducing double node pairs. The interconnection between the double nodes was specified to simulate the interface behavior. This model is capable of introducing the effects of material nonlinearity and progressive failure. A third element model was developed by Page [103,104&105] from the analogy of the behavior of masonry assemblages and jointed rock. In this approach, the masonry units were modeled as linear elastic continuum elements and the mortar joints were modeled as joint elements. This element accounted for the composite nature of masonry and incorporated the inherent nonlinearity due to both mortar joint behavior and progressive joint failure. However, application of these models

for the analysis of large structural masonry elements and structures is extremely difficult due to the very large number of elements needed to separately model the component materials and their interfaces.

Page and Kleemen [106] proposed an in-plane finite element model for brick masonry. This model included the nonlinear deformations and progressive local failure either through joints or in modes involving both bricks and joints. The deformation relationships and failure criterion proposed in this model were derived from biaxial test results of half scale brick masonry panels with different bed joints orientations. The presence of the mortar joints as particular planes of weakness was considered in the failure criterion adopted in this model. However, this model was limited to in-plane isotropic behavior of one wythe solid walls.

Essawy [42] proposed a model in a generalized form to handle both in-plane and out-of-plane loading conditions so that it can be used for analysis of most masonry assemblages. This was achieved by incorporating both in-plane and out-of-plane degrees of freedom in element formulation. Also this model can be used for the analysis of hollow masonry and multiwythe walls by adopting a layered plate approach in the finite element formulation. Moreover, orthotropic properties were included for each layer to improve the acceptability of the macroscopic approach because, this element is applied for plain masonry it has to be modified to account for the effect of reinforcement.

Ali, A.[4] presented a of finite element mode for the analysis of reinforced masonry walls subjected to in-plane concentrated load with the following elements: 1)rectangular plane stress element with four nodes with two degrees of freedom at each node to represent the grout block element with average properties; 2)joint element to represent bed and head joints, this element transfers shear and normal forces only; 3)truss element to represent vertical and horizontal steel. This model neglects the connection between vertical steel and grout and also between horizontal steel and mortar for representing bond and dowel actions. The model did not introduce the inelastic behavior of units and grout.

A layered finite element was developed by Fouad,H.A.[48] to study the behavior of partially grouted masonry walls under in-plane concentrated loads. The model treats the blocks and joints separately. It also allows for nonlinear deformation characteristics and progressive failure of both units and joints. The load is applied incrementally allowing the behavior of the wall to be traced from the first crack until failure.

It is well documented in the literature and prior research that the use of nonlinear finite element models is the most comprehensive analytical approach for the investigation of the inelastic behavior of reinforced concrete or reinforced masonry.

The reported research on nonlinear finite element models for reinforced concrete walls and panels demonstrates that these models can reasonably reproduce the degrading force-displacement envelopes up to peak load as well as the relative degrees of associated damage. However, the researchers reported difficulties in reproducing the post peak behavior. The deficiencies that were noted by some researchers include difficulty in passing over the limit points, convergency, problem associated with nonpositive definite stiffness matrices and, compression behavior past peak strength. The developed model used in this chapter had the advantages to overcome many of the deficiencies noted by previous researchers, as well as incorporate modeling capabilities that specifically represent the behavior observed for reinforced masonry. Since prior testing has shown similarities between reinforced masonry and reinforced concrete, it is generally agreed that a technology transfer between these two materials is appropriate. Accordingly, the models presented in this Chapter make use of the work done in reinforced concrete.

6.3 DESCRIPTION OF THE FINITE ELEMENT PROGRAM

The computer program is based on the VISCOUNT family of computer programs originally developed by E. Hinton and D.R.J. Owen[102]. The VISCOUNT program was subsequently modified and improved by others[5] and the FEM/I program utilizes some of the features of the original and improved versions. However, the program has been

extensively modified and improved for application to reinforced masonry building components by Ewing[43]. This program is operational on IBM compatible personal computers, since a large main frame computer is not required.

The program is a two-dimensional, four nodes parabolic isoparametric quadrilateral finite element (as indicated in Fig. 6.1) with idealized nonlinear stress-strain relations for reinforced masonry used in this model as shown in Figures 6.2 & 6.3. The model have been driven by either forces and/or displacements and strain have been used in the constitutive properties. The constitutive relations generally follow the research of Vecchio and Collins[142] on reinforced concrete. The material models are formulated in terms of element principal strains. The masonry and reinforcement are modeled separately, and their interaction is included by using four node isoparametric plane stress overlay elements and specialized stress-strain relations. In the layered model, two quadrilateral elements occupy the same space, overlaying each other, where one layer represents the masonry and the other represents the reinforcement. A typical overlay finite element model of a reinforced masonry is shown in Fig. 6.4. Although the material models for masonry and reinforcement are described separately, the element is considered to be smeared hybrid element, where the computed strains are assigned to both materials. The smeared model assumes that the reinforcement is distributed over the whole element and that the two components (reinforcement and masonry) are in full bond at the nodes. The bond slip between the two components is considered to be a material property of the masonry component in tension, and this property is defined by a tension stiffening model. The reinforcement is represented by an orthotropic material with a bilinear stress-strain relationship and includes unloading. The masonry is represented by a material with bimodular orthotropy, and includes tension stiffening, compression softening, and strain softening, as well as a degrading unloading rule. The pre-cracking strength of the masonry under a biaxial state of stress is given in Fig. 6.5 and indicates a reduction in compressive strength and stiffness after tensile cracking, as well as a tension stiffening effect. The stress-strain curves were described by two second order polynomial, one for the pre-

cracking branch and the other for the post-peak branch. The tension stiffening was described by an exponential function as indicated in Fig. 6.6. The masonry model incorporates a tension crack orientation adjustment approach, where the orientation of the final cracks can be different from the initial cracks (a smeared crack rather than a discrete crack approach). Experiments have shown that the final cracks do not coincide with their original orientations (fixed crack approach is theoretically incorrect). The model also includes a compressive strength reduction after tensile cracking normal to the principal compressive strains as presented by Collins[142]. The strength reduction is a function of the magnitude of the principal strains that are normal to the principal compressive strains. Moreover, the model includes a compressive strength increase due to lateral compressive confinement when both principal strains are in compression. The strength increase depends on the magnitude of the principal compressive strains that are normal to the principal compressive strains. The pre-cracking strength of the masonry is determined from the principal stresses/strains using Fig. 6.5, which shows a reduction in compressive strength in a tension-compression region. The post-cracking strength is determined from the current ratio of principal tensile strain to principal compressive strain, as

$$f_p = f'_m / b$$

$$e_p = e_0 / b$$

where

f_p = post-cracking peak strength

f'_m = unconfined compressive strength

e_p = post-cracking peak strain

e_0 = peak strain at unconfined compressive strength

$b = A - B\,(e_t / e_c)$

e_t = biaxial tensile strain

e_c = biaxial compressive strain

A & B = coefficients depend upon reinforcement properties (yield stress and yield strain)

Also, the integrity of the Gauss points is preserved in each element, where individual Gauss points can be in a different state of principal strain, thereby allowing strain gradients to occur across an element. This permits the use of relatively large elements when compared to approaches that assume average stresses and strains.

Both an incremental load - tangent stiffness and a total load - secant stiffness formulation were also being evaluated by Ewing[43] to verify that the solution is independent of the relative grid size. The type of nonlinearities dealt with in this analysis are material nonlinearity type.

The finite element method (FEM) is capable of tracing the envelope of load-deflection (L-D) curve of a monotonic loading. The most important predictions include stiffness degradation prior to peak strength, peak strength and post peak strength. The model also is capable of tracing elastic and inelastic unloading stiffness at any displacement. The model is not capable of tracing displacements related to translations parallel to cracks that are held open by inelastic strains in the reinforcement, but it is reflect the point in the unloading cycle where such displacements occur. However, the model is capable of recognizing when the applied axial loads prevent or limit displacements parallel to a crack.

As mentioned before this element is used for reinforced masonry walls. But it can be used also for partially reinforced masonry by considering an equivalent thickness for the hollow parts of the wall panel (Fig. 6.4.a). In this case one layer only should be used (masonry layer) by considering the ratio of vertical and horizontal reinforcement is zero and two layers of elements for the reinforced parts with the total thickness of the wall (Fig. 6.4.b).

The finite element models can be subjected to any combination of several static excitations including nodal concentrated loads, gravity loads, normal and tangential distributed edge loads, and prescribed nodal point displacements.

The program has three criteria for the unbalanced residual force that are used to exit

from iteration loops:

(1) convergence: when the unbalanced residual force is less than or equal to a prescribed percentage of the total applied force (this was specified as 1% for the parametric studies); (2) iterations: when the maximum number of iterations are exceeded before convergence is reached; and (3) slow convergence: when the difference between successive iterations is less than on-tenth of the convergence tolerances.

The output available from the program consists of selective printed responses and a data file suitable for postprocessing by a companion program. The printed output includes: nodal displacement, nodal reactions, global and principal stresses, principal strains and reinforcing steel stresses and strains. In addition, the program produces a force-deflection file and a major event file.

Force-Deflection File: contains a component of the reaction force and the deflection at a node that has prescribed displacement; this force-deflection file is updated at each loading increment.

Major Event File: contains a record of the major events for each element of the finite element model; load increment at which first tensile cracking occurs in masonry, maximum and minimum values of the tensile crack orientation in the masonry, load increment at which the masonry peak strength is reached; load increment at which the masonry crushing occurs; load increment at which yielding of vertical and horizontal reinforcement occurs, and maximum strains in the vertical and horizontal reinforcement.

6.4 COMPUTATIONAL ALGORITHM AND STEPS OF SOLUTION

The program uses an initial stiffness formulation with an incremental solution method, where displacements and/or forces can be used as the primary excitation. This method convergent for softening systems when prescribed displacements are used as primary excitation. The computational procedure is described in steps. These steps are given in the following paragraphs.

Step 1- Calculate an initial stiffness using the material properties of the element components

in the initial stages of loading. Assuming that the initial material modulus for masonry is the same in compression and tension.

Step 2- Apply a load increment composed of displacements and/or forces. An incremental force can be used if limit points are not to be passed.

Step 3- Calculate the incremental and total nodal point displacements. At nodes where displacements are prescribed, reaction are computed.

Step 4- Evaluate the total strains at Gauss points.

Step 4- Evaluate the principal total strains at the Gauss points using the total strains computed in the above step.

Step 6- Compute the orthotropic secant moduli in the principal directions. These moduli are determined from the compressive or the tensile stress-strain relations depending on whether the strains are tensile or compressive.

Step 7- Form a secant material matrix for the masonry at the Gauss points, using the secant moduli computed in the above step. This matrix is based on two different constitutive laws, one for the uncracked case and the other for the cracked case.

Step 8- Transform the material matrix for the masonry component from the orthotropic coordinates into the local element coordinates.

Step 9- Evaluate the secant material matrix for the reinforcement component. This matrix is based on the strain values in the x and y directions since the steel is assumed to behave in a uniaxial fashion.

Step 10- Obtain a combined material matrix based on the strain states at the Gauss points by combining the matrices for the two components. Assuming that the two components share the same nodal points strains.

Step 11- Compute the true stresses at the Gauss points using the secant material matrix constructed in the previous step.

Step 12- Calculate the residual force vector, which is the measure of load imbalance between external forces and internal resistance forces.

Step 13- Check the convergence of the iterative solution process. A convergence criterion

can be based on either nodal displacement or on residual forces.

Step 14 - If the convergence criteria are not met, the external force vector is updated and the solution is iterated. If the convergence criteria are met, the loads are incremented and the solution process is continued.

6.5 VERIFICATION OF THE COMPUTER PROGRAM

To evaluate the computer program and to be sure that the program operates satisfactory, Ewing compared the results of one story reinforced masonry shear walls with the experiments conducted at the University of Colorado[43]. There was good agreement between peak strengths for experimental and analytical shear walls results. The load-deflection curves taken from the experiments were consistent with monotonic envelope curves taken from the analytical results. The program is very easy to distinguish between different modes of failure. For flexure response, it shows tensile cracking in the masonry followed by yielding of vertical steel and crushing of the masonry in the compression toe, and for shear response, the program shows a major diagonal cracks associated by yielding of the horizontal steel.

As a part of the validation process for the developed computer code, Ewing compared the results of two story reinforced masonry shear walls with coupling beam were compared with the experiments conducted at Texas University[43]. The analytical results indicated that displacement comparisons are not possible until the measured displacements are corrected for base slip. However, preliminary comparisons of peak base shear indicate that the full width of the floor diaphragms may not be effective in the two-dimensional finite element simulation of the coupled walls. To indicate the capability of this program, the author has also tested the program by comparing it with another computer program using small cantilever wall. The results obtained from this program are agreeable with the analytical results obtained from ANSYS program.

6.6 CORRELATION BETWEEN ANALYTICAL AND CURRENT EXPERIMENTAL RESULTS

The correlations reported herein are attempts to extend the direct small scale modeling technique to study the behavior of partially reinforced masonry shear walls and to demonstrate that this technique is feasible and reliable and therefore, can represent an economical alternative to full-scale testing. First, one must demonstrate that the modes of wall response and most relevant strength values obtained from the experimental and analytical results correlate in an acceptable manner. This is attempted in the comparison presented in the following sections.

The finite element meshes used in the analysis of walls having different distribution of reinforcement, SWA, SWB & SWC are shown in Fig. 6.7. The model has 244 nodal points and 212 elements, and has a maximum front width of 38. In order to correlate as closely as possible with the experiment, the boundary conditions for the bottom and top concrete beams were included in the finite element model. The analytical model was loaded using the same procedure that was used in the test where the axial stresses was applied using normal distributed edge load at the top elements and the lateral monotonic displacement was applied at all the top nodal points. There are three different materials in this model: reinforced concrete elements representing the footing of the shear wall, reinforced masonry representing the reinforced parts of the wall panel, and plain masonry representing the hollow parts of the wall panel. Properties of the different materials for the analysis were taken directly from component tests conducted in Chapters 2, 3 & 5.

The analytical results of wall groups SWA, SWB and SWC (presented in Table 6.1) were compared with those obtained experimentally using small-scale modeling technique (Chapter 5). The comparison and major observations are described and discussed in the following paragraphs .

Table 6.1 Comparison Between Experimental and Analytical Results

Wall Number	Experimental			Analytical		
	Load at First Crack kips (ton)	Ultimate Load kips (ton)	Failure Mode	Load at First Crack kips (ton)	Ultimate Load kips (ton)	Failure Mode
SWA1	5.9 (2.7)	6.8 (3.1)	Shear/Flexure	6.4 (2.9)	7.3 (3.3)	Shear/Flexure
SWA2	1.8 (0.8)	4.3 (2.0)	Flexure	2.2 (1.0)	4.7 (2.1)	Flexure
SWA3	5.0 (2.3)	5.8 (2.6)	Shear/Flexure	5.8 (2.6)	6.5 (3.0)	Shear/Flexure
SWA4	6.8 (3.1)	7.7 (3.5)	Shear	7.5 (3.4)	8.9 (4.0)	Shear
SWA5	2.5 (1.1)	4.6 (2.1)	Shear	3.1 (1.4)	5.5 (2.5)	Shear
SWA6	5.5 (2.2)	6.6 (3.0)	Shear/Flexure	6.0 (2.7)	7.3 (3.3)	Shear/Flexure
SWA7	5.4 (2.5)	8.9 (4.0)	Shear	8.1 (3.7)	10.6 (4.8)	Shear
SWA8	4.9 (2.2)	7.9 (3.6)	Shear	8.1 (3.7)	10.6 (4.8)	Shear
SWA9	5.6 (2.5)	7.8 (3.5)	Shear	6.1 (2.8)	8.7 (4.0)	Shear
SWA10	5.3 (2.4)	7.3 (3.3)	Shear	6.1 (2.8)	8.7 (4.0)	Shear
SWB1	4.8 (2.2)	5.5 (2.5)	Shear	5.5 (2.5)	6.5 (3.0)	Shear
SWC1	5.0 (2.3)	7.8 (3.5)	Flexure	5.3 (2.4)	8.8 (4.0)	Flexure
SWC2	6.0 (2.7)	9.8 (4.5,	Flexure	7.5 (3.4)	11.6 (5.3)	Flexure

6.6.1 Wall Behavior

In accordance with the governing load resistance mechanisms, crack patterns and overall shape of the L-D curve, three types of behavior modes can be identified from the analytical results of wall specimens. Wall specimens SWA2, SWC1 and SWC2 with a flexural response mode shown in Figures 6.9, 6.17 and 6.18 respectively, show tensile cracking in the masonry (indicated by change in wall stiffness in the elastic range) followed by yielding of the vertical reinforcement (indicated by a horizontal plateau in the L-D curve), softening to a peak strength, and crushing of the masonry in the compression toe (indicated by sharp drop in the L-D curve). Wall specimens SWA4, SWA5, SWA7, SWA9 and SWB1 with a shear response mode shown in Figures 6.11, 6.12, 6.14, 6.15 and 6.16 respectively, show a major diagonal crack (indicated by sudden drop in the L-D curve just after peak load) with associated yielding of the horizontal reinforcement (indicated by picking up the load after a major crack occurred by activating the horizontal steel up to yielding). Wall specimens SWA1, SWA3 and SWA6 with a mixed flexural/shear response mode shown in Figures 6.8, 6.10 and 6.13 respectively, show yielding of both vertical and horizontal reinforcement and a major diagonal crack, sometimes accomplished by a crushing of the compression toe.

It has been found from the analytical results, which are comparable with the experimental results, that the inelastic behavior of a wall panel is sensitive to the applied axial compression stress, the distribution and amount of vertical and horizontal steel present and compressive strength of masonry for example, specimens that had a vertical steel ratio of 0.1% and a horizontal steel ratio of 0.1% but different steel distribution, SWA1 (with one column and one bond beam in the middle of the wall panel) exhibited a shear/flexure response, SWB1 (without interior columns and bond beams) exhibited a shear response, while SWC1 (with two columns and two bond beams in 1/3 and 2/3 of the height and length of the wall panel) exhibited a flexure response.

Wall SWA2, subjected to no axial stress, had a significant flexure response and wall SWA3, which was subjected to 100 psi (7 kg/cm^2), exhibited a mixed shear/flexure

response, while wall SWA4, which was subjected to 200 psi (14 kg/cm^2), exhibited a brittle shear response. The amount of vertical and horizontal steel and the compressive strength of masonry have a little significant effect on wall response, but have a significant effect on the peak load. Moreover, the compressive strength of masonry has a significant effect on the cracking strength of masonry.

Finally, based on the results presented in Table 6.1 and the L-D curves shown in Fig 6.8 through Fig. 6.18, it is evident that the failure mechanisms of walls SWA4, SWA5, SWA7, SWA9 and SWB1 were dominated by shear mode which are identical to those observed from the experimental results. The failure mechanism of walls SWA2, SWC1 and SWC2 was dominated by the flexure mode which agreed well with the experimental observations. Also, the wall response dominated by the shear/flexure mode (SWA1, SWA3 and SWA6) obtained analytically was similar to that obtained experimentally.

6.6.2 Load-Deflection Curves

Figures 6.8 through 6.18 present the comparison of load-deflection curves obtained experimentally and analytically for each wall. The load at first crack and the ultimate load were reasonably compared. Consistent with the experimental observations, the analytical results show significant effect of the applied axial compressive stress, the distribution and amount of reinforcement present and the masonry strength on wall behavior. The L-D curves obtained experimentally and analytically were similar. Furthermore, the analytical initial stiffness were higher than those obtained from the experimental results.

The comparison of the load-deflection curves is further discussed through the following four main points:

1- Load at first crack: it can be observed that the load at first crack obtained analytically was higher than those obtained experimentally. This increase varied between 5% to 25% except for wall SWA7, where the increase was 50%. This variation may be due to expected variation in the interface bond between the units and mortar. It is to be noted that the model considers the block and mortar as one element (neglect mortar joints).

2- Wall stiffness: it can be clearly noticed from the load-deflection curves that there is a large difference between the analytical and experimental results. The model results gives higher stiffness than the experimental results in the elastic range by about 50% to 190%. However, the elastic stiffness of walls SWA2, SWA9 and SWB1 were approximately the same for both. The difference may be attributed to possible slip between a wall panel and the testing frame and possible large variation of material properties. The analytically stress-strain curve is based on the uniaxial properties of masonry prisms, which does not reflect the actual strength of the wall panels where a strength increase due to lateral confinement and a strength reduction after tensile cracking normal to the principal compressive strains exist. In addition, the rising branch from the origin to the peak load of the stress strain curve is controlled by a shape factor, this factor is compatible with fully grouted masonry and may not be as accurate for partially reinforced masonry.

3- Yield load: the yield load can be observed directly from major event file which defines the load increment at yielding of either vertical or horizontal reinforcement. However, this load could be observed experimentally using LVDT to measure the masonry strain at the outmost location of the vertical bars at the tension side since it is difficult to use strain gages on small scale reinforcement. The analytically yield load was about 8% to 15% high than the experimental yield load.

4- Ultimate load: the analytical results show higher load carrying capacity than those obtained from experimentally by about 7% to 20%. This is expected due to the variation of unit properties.

The plots presented in Figures 6.8-6.18, show that the experimental post ultimate behavior of the wall panels do not compare well with the analytical results. This may be due to differences in the material properties after cracking and/or yielding of the steel reinforcement as compared to those used analytically. For example, the analytical curves show a higher displacement ductility, reflecting a more ductile steel reinforcement and/or probably a larger maximum usable masonry compressive strain.

It is observed that the analytical models reveals excessive deformation due to

yielding of vertical steel which is indicated by a long horizontal plateau of the L-D curve. Overall, the comparison presented above indicates that the 1/3-scale modeling technique can be used successfully to investigate the behavioral characteristics of partially reinforced masonry shear walls.

6.7 PARAMETRIC STUDY

Because of the budget and time restraint, the experimental investigation presented in Chapters 4 & 5 was limited to a defined set of parameters which are not comprehensive enough for the development of design methodology (Chapter 7). Therefore, a parametric study covering a wide practical range of parameters are considered. The parametric study presented in Table 6.2 contains a wider range of parameters covered in the experimental study, namely, distribution and amount of vertical and horizontal reinforcement, axial compressive stresses, and masonry strength. In addition, the effect of wall aspect ratio and extent of grouting of the unreinforced parts of the wall panel which were not covered experimentally, is included in the parametric study .

This study was conducted using full-scale wall dimensions as shown in Figures 6.19, 6.20 & 6.21 and representative material properties.

The finite element meshes used in the analysis are shown in Figures 6.19 to 6.21. The dimension of the wall panel for wall having aspect ratio of 1.0 is 136x136 in. (3.4x3.4 m), for wall having aspect ratio of 3.0 is 400x136 in. (12.0x3.4 m) and for wall having aspect ratio of 0.5 is 136x264 in. (3.4x6.7 m). The loading used in the analytical model is similar to that used earlier (Section 6.6).

6.7.1 Effect of Distribution of Vertical and Horizontal Reinforcement

The distribution of reinforcement plays an important role in the behavior and load carrying capacity of partially reinforced masonry shear walls[49&59]. To obtain a more comprehensive treatment of the effects of distribution of vertical and horizontal reinforcement, the analysis were carried out using different spacing of 16, 32 & 64 in. (0.4, 0.8 & 1.6 m). All the specimens had a height/length (aspect) ratio of one, axial stress of 100 psi (7 kg/cm^2), masonry strength of 2000 psi (140 kg/cm^2), percentage of vertical reinforcement of 0.2% and horizontal reinforcement of 0.1%. The unreinforced parts of the wall panel were left ungrouted as presented in Table 6.2. The effect of distribution of vertical and horizontal steel is shown if Figure 6.22. It can be seen from the figure that the

Table 6.2 Analytical Parametric Study

Wall NO.	Aspect Ratio	Spacing 64 (3.2) in. (m)	Spacing 32 (1.6) in. (m)	Spacing 16 (0.8) in. (m)	Grouting Partially	Grouting Fully	Masonry Strength 1000 (70) psi (kg/cm2)	Masonry Strength 2000 (140) psi (kg/cm2)	Masonry Strength 3000 (210) psi (kg/cm2)	Axial Stress 0 (0) psi (kg/cm2)	Axial Stress 100 (7) psi (kg/cm2)	Axial Stress 200 (14) psi (kg/cm2)	VL Steel 0.05 %	VL Steel 0.1 %	VL Steel 0.2 %	HL Steel 0.05 %	HL Steel 0.1 %	HL Steel 0.2 %
SW1		-			-			-			-		-				-	
SW2		-			-			-			-			-			-	
SW3		-			-			-			-				-		-	
SW4		-			-			-			-			-		-		
SW5		-			-			-			-			-				-
SW6	1	-			-			-		-				-			-	
SW7		-			-			-				-		-			-	
SW8		-			-		-				-			-			-	
SW9		-			-				-		-			-			-	
SW10			-		-			-			-				-		-	
SW11			-			-		-			-				-		-	
SW12				-		-		-			-				-		-	
SW13	3	-			-			-			-			-			-	
SW14	0.5	-			-			-			-			-			-	

Table 6.3 Results of Analytical Parametric Study

Wall Number	Load at First Unseen Crack	Load at First Major Crack kips (ton)	Ultimate Load kips (ton)	Load at Yield. of V$_l$ Steel kips (ton)	Load at Yield. of H$_l$ Steel kips (ton)	Failure Mode kips (ton)
SW1	18.7 (8.5)	37.4 (17.0)	47.2 (21.5)	46.0 (20.9)	-	Flexure
SW2	19.1 (8.7)	52.5 (23.9)	59.0 (26.8)	55.9 (25.4)	58.5 (26.6)	Shear/Flexure
SW3	19.7 (9.0)	72.5 (33.0)	77.5 (25.2)	-	74.8 (34.0)	Shear
SW4	18.0 (8.2)	40.9 (18.6)	54.8 (24.9)	-	54.7 (24.9)	Shear
SW5	20.3 (9.2)	51.2 (23.3)	63.1 (28.7)	61.8 (28.1)	-	Flexure
SW6	8.3 (3.8)	22.3 (10.1)	33.8 (15.4)	24.0 (10.9)	-	Flexure
SW7	20.8 (9.5)	75.6 (34.4)	79.2 (36.0)	-	77.8 (35.4)	Shear
SW8	11.5 (5.2)	43.8 (19.9)	48.1 (21.9)	-	47.3 (21.5)	Shear
SW9	30.2 (13.7)	52.2 (23.7)	67.3 (30.6)	65.2 (29.6)	-	Flexure
SW10	24.1 (11.0)	68.6 (31.2)	79.3 (36.0)	75.3 (34.2)	67.4 (30.6)	Shear/Flexure
SW11	36.0 (16.4)	81.1 (36.9)	87.9 (40.0)	85.0 (38.6)	76.8 (34.9)	Shear/Flexure
SW12	36.0 (16.4)	88.8 (40.4)	88.8 (40.4)	85.0 (38.6)	-	Flexure
SW13	1.3 (0.6)	5.9 (2.7)	21.0 (9.5)	17.8 (8.1)	-	Flexure
SW14	54.6 (24.8)	151.7 (69.0)	176.7 (80.0)	-	163.0 (74.1)	Shear

ultimate load for wall SW3 having spacing of 64 is lower than for walls SW10 & SW12 with spacing 32 & 16 by about 3% & 15%, respectively. It can be noted that as the spacing of reinforcement increases the behavior of the wall changes from a ductile flexural behavior to a brittle shear behavior. This is because in the case of small spacing, there is adequate number of bond beams activated to resist shear stresses developed in the middle of the wall. The distribution of vertical and horizontal reinforcement results in a more distribution of dowel and truss actions to resist the shear stresses and hence, wall is expected to fail in flexure. On the other hand, in the case of large spacing, there are not enough bond beams to resist the shear stresses and the wall is likely to fail in shear. Therefore, the spacing of horizontal reinforcement has a significant effect on the behavior (changing the wall response from brittle to ductile).

6.7.2 Effect of Amount of Vertical and Horizontal Reinforcement

The effect of the amount of the vertical and horizontal reinforcement on the flexural and shear strengths can be observed from the load-deflection curves of walls SWA1 through SWA5 presented in Figures 6.23 & 6.24. As presented in Table 6.2 three percentages of vertical and horizontal reinforcement were chosen (0.05, 0.1 & 0.2%). It can be noticed from Fig. 6.23 that the load carrying capacity of wall SW2 (A_{sv} = 0.05%) is lower than wall SW3 (A_{sv} = 0.1%) and wall SW3 (A_{sv} = 0.2%) by about 25% & 60%, respectively. On the other hand, as shown in Fig. 6.24, wall SW4 (A_{sh} = 0.05%) is lower than wall SW2 (A_{sh} = 0.1%) and wall SW5 (A_{sh} = 0.2%) by about 8% & 15% respectively. It is well documented[129] that the amount of vertical reinforcement has a more significant effect on the load carrying capacity rather than on the amount of horizontal reinforcement. It is apparent from Fig. 6.23 that increasing the vertical reinforcement ratio, favored the shear failure, and therefore decreased the wall ductility. The behavior changed from a brittle shear failure to a ductile flexural failure as the vertical reinforcement ratio decreased. This is owing to the contribution of vertical steel by dowel action and truss action. The flexural strength of partially reinforced masonry wall increases with the

increase of vertical steel, while the shear strength increases with the increase of horizontal steel. It is apparent that the amount of vertical reinforcement influence more wall behavior and mode of failure than the amount of horizontal reinforcement .

6.7.3 Effect of Axial Stress

The effect of axial stress is shown graphically in Fig. 6.25. It is apparent from the experimental results that the axial stress has a significant effect on the behavior of partially reinforced masonry shear walls and the load carrying capacity of the wall. To assist the evaluation of this parameter, three values of axial stresses were chosen as indicated in Table 6.2 while other parameters were kept constant. The ultimate load of wall SW6, which has zero axial stress, is lower than that of wall SW2 (axial stress = 100 psi) and wall SW7 (axial stress = 200 psi)by about 74% and 133%, respectively. Moreover, the axial stress has a significant effect on the behavior of the walls, the higher the axial stress the more the tendency of the wall to fail in shear and the smaller the axial stress the more tendency to fail in flexure. The first occurrence of a diagonal crack is influenced to a large extent by the applied axial load. The cracking load of wall SW6 is lower than the cracking loads of walls SW2 and SW7 by about 126% and 137%, respectively. This is because once diagonal crack occurs, a redistribution takes place and the shear resistance is shared between the horizontal steel and the aggregate interlock mechanisms. The resistance provided by the aggregate interlock depends mainly on the applied axial stress since it increases the aggregate interlock forces which in turn increases the tensile strength of the masonry. This characteristic behavior results in a significant drop in ductility. Wall SW6 with no axial load had an average ductility of 6.0 whereas wall SW2 and SW7, with 100 psi (7 kg/cm^2) and 200 psi (14 kg/cm^2) axial stress, had a ductility ratio of 3.6 and 2.4, respectively (ductility ratio was calculated using Priestley method[56] as presented in Chapter 5). This represents a drop in ductility by about 66% and 150%. This trend can be explained on the basis of limited deflection beyond the yield load due to the increase of axial stress. The major crack

for walls SW6, SW2 and SW7 occurred at 66%, 12% and 5% of the peak load, respectively. This indicate that the higher the axial stress the closer the major crack to the peak load is. The axial stress has a significant effect on the stiffness of the wall, where higher axial stress results in higher wall stiffness.

6.7.4 Effect of Block Strength

The effect of masonry compressive strength is studied by comparing the cracking load, the load carrying capacity, crack pattern and deflection at ultimate load of walls SW2, SW8 & SW9 having different strengths. The wall with higher prism strength has the tendency for an increase in crack load and ultimate load. The ultimate load of wall SW8, which has a prism strength of 1000 psi (70 kg/cm^2), is lower than the ultimate load of wall SW2 (2000 psi = 140 kg/cm^2) and wall SW9 (3000 psi = 210 kg/cm^2) by about 22% & 40%, respectively. The load at 0.1 in. (25 mm) deflection are 20.6, 28.9 and 40.6 kips (9.4, 13.1 and 18.5 ton) for walls SW8, SW2 and SW9, respectively indicating the effect of masonry strength affect on wall stiffness. Wall stiffness increased by about 40% and 97% as the block strength increased from 1000 to 3000 psi. From the major event file of the computer code it can be observed that the crack propagation for these wall were quite different due to the variation of the tensile strength of the block. The crack load is affected, to a large extent, by the tensile strength of masonry. The cracking load of wall SW8 is lower than the cracking loads of walls SW2 and SW9 by about 65% and 160%, respectively. This is because shear strength is governed by the residual strength of masonry, which depends on the tensile strength of masonry.

6.7.5 Effect of Grouting

The effect of grouting (fully grouted) and ungrouting (partially grouted) of the unreinforced part of the wall panel on the behavior of partially reinforced masonry shear walls can be studied directly by comparing the load-deflection curves shown in Fig. 6.27 and the ultimate load of walls SW10 & SW11 respectively. The walls have the same

amount and distribution of reinforcement and substantially the same masonry strength and level of axial stress. As can be seen from Fig. 6.27, an increase in the ultimate strength by about 12 % due to grouting of the unreinforced part of the wall was achieved. The grouting of the unreinforced parts of the wall panel has no significant effect on the behavior of wall. However, it has a significant effect on the stiffness of the wall and the post ultimate behavior of the wall as shown in Fig. 6.27. In the case of full grouting, after the major crack the load increased as the deflection increased due to increasing the tensile strength of the wall. While in the case of ungrouted, once the crack occurred, the load degredated due to opening of these cracks the bed and head joints act as planes of weakness. Moreover, the nonisotropic characteristics of masonry increases in the absent of grout. The hollow masonry as a brittle material is very sensitive to tensile stresses. The continuity of the grouted cores across the bed joint planes increases the homogeneity and the isotropy of the wall .

It can be concluded that the ability of partially grouted masonry shear walls to resist moderate lateral loads is far less than fully grouted masonry shear walls.

6.7.6 Effect of Aspect Ratio of the Wall Panel

The effect of the aspect ratio (height/length) on the behavior of the wall and the load carrying capacity can be obtained by comparing walls SW2, SW13 and SW14. It is apparent from Fig. 6.28 that wall SW2 which has an aspect ratio of 1.0, exhibited a shear/flexure failure, wall SW13 which has an aspect ratio of 3.0, exhibited a ductile flexure failure, while SW14, which has an aspect ratio of 0.5, exhibited a brittle shear failure. It can be concluded that increasing the aspect ratio of the wall panel resulted in an increase in the ductility of the wall and a decrease in the load carrying capacity or the resisted shear strength. From Fig. 6.28 it can be noticed that as the aspect ratio increases the load carrying capacity decreases. However, from the stress standpoint, the resisted shear stress in wall SW14 (h/d = 0.5) is higher than wall SW2 (h/d = 1.0) and wall SW13 (h/d = 3.0) by about 45% and 300% respectively. This means that the shear strength, as

measured by the developed shear stress, decrease significantly as the height to thickness ratio h/d ratio increase as indicated in Fig. 6.28.

6.8 CLOSURE

A finite element method is used to analytically investigate the behavioral characteristics of partially reinforced masonry shear walls. A correlation between experimental results and analytical results were carried out to demonstrate that the analytical model is reliable and feasible and therefore, can represent an economical alternative to full-scale testing. A parametric study were carried out to cover a wide practical range of parameters; namely; distribution of vertical and horizontal reinforcement, amount of vertical and horizontal reinforcement, axial compression, extent of grouting (fully grouting versus ungrouting of the unreinforced parts of the wall panel) and wall aspect ratio. The following conclusions can be drawn from the analytical study in this chapter:

1- The failure mode and wall behavior obtained analytically are similar to those observed experimentally.

2- Consistent with the experimental observations, the analytical results show the significant effect of the applied axial compression, the distribution and amount of vertical and horizontal reinforcement and the masonry strength on the wall behavior. The L-D curves obtained experimentally and analytically were similar. However, a large difference between wall stiffness obtained experimentally and analytically is experienced in some walls.

3- The correlation presented indicates that the 1/3-scale modeling technique can be used successfully to investigate the behavioral characteristics of partially reinforced masonry shear walls.

4- The spacing of horizontal reinforcement has a significant effect on the wall behavior (Increasing the spacing changes wall response from a ductile mode to a brittle mode).

5- For the same percentage of steel the load carrying capacity of wall panels tends to

increase with the decrease in the spacing of vertical and horizontal steel.

6- The amount of vertical steel influences more wall behavior and mode of failure than the amount of horizontal steel.

7- The higher the axial stress the more the tendency of the wall to fail in shear.

8- Increasing the aspect ratio of the wall panel increases the ductility of the wall and decreases the load carrying capacity.

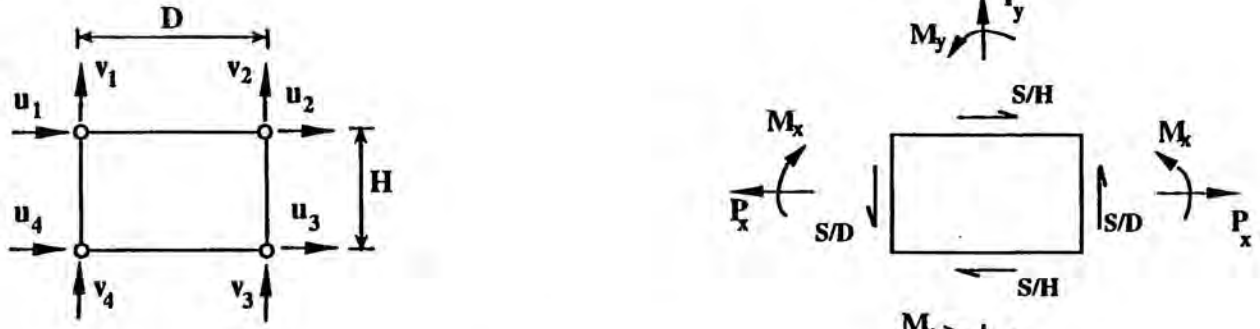

(a) Element Forces

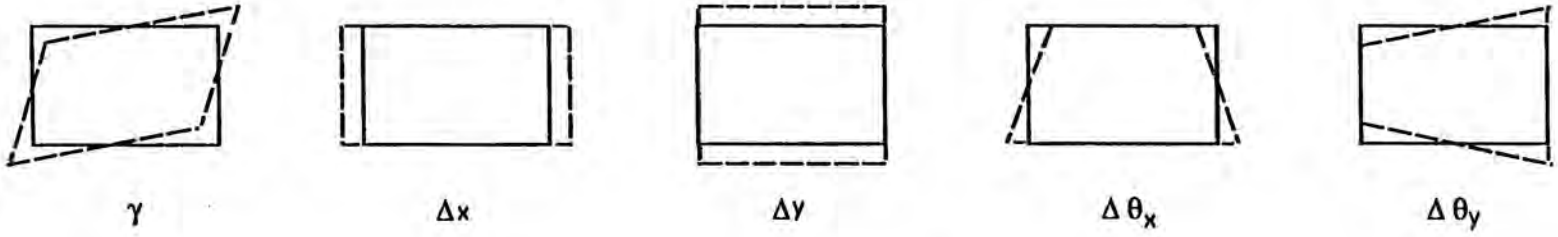

(b) Deformation Modes

Fig. 6.1 Element Forces and Deformation Modes of Finite Elements

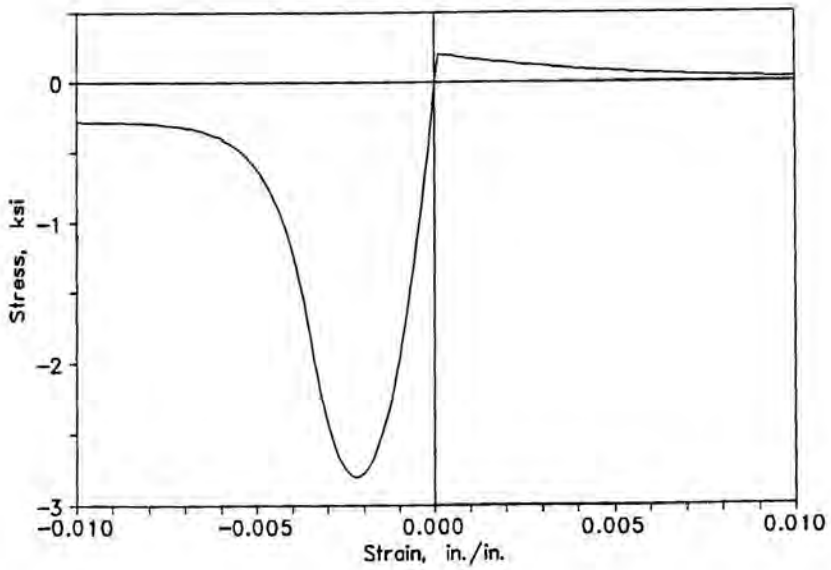

Fig. 6.2a Stress-Strain Curve for Masonry Model, Tension and Compression

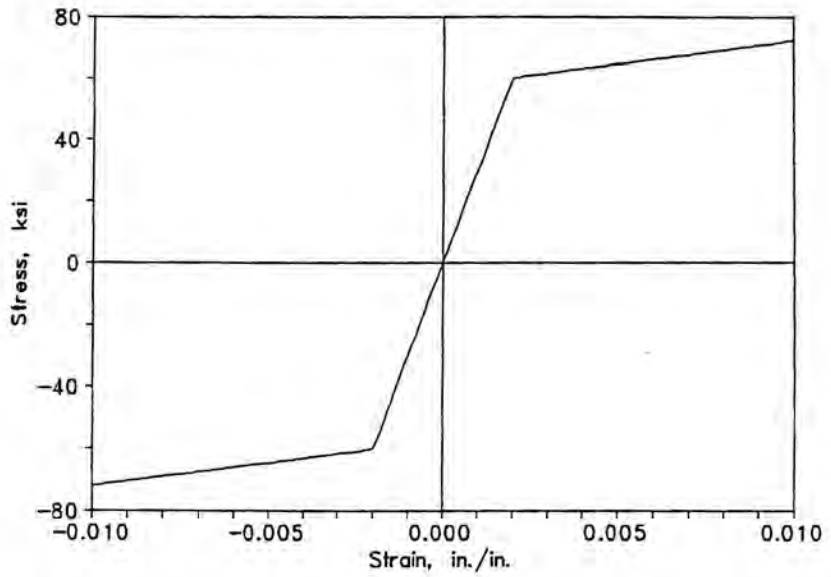

Fig. 6.2b Stress-Strain Curve for Reinforcement Model, Tension and Compression

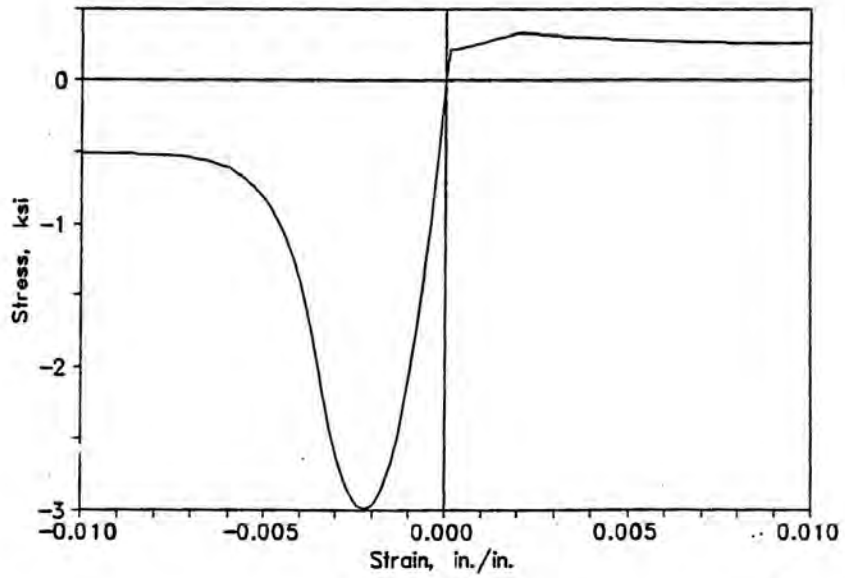

Fig. 6.3 Stress-Strain Curve for Reinforced Masonry Model, Tension and Compression

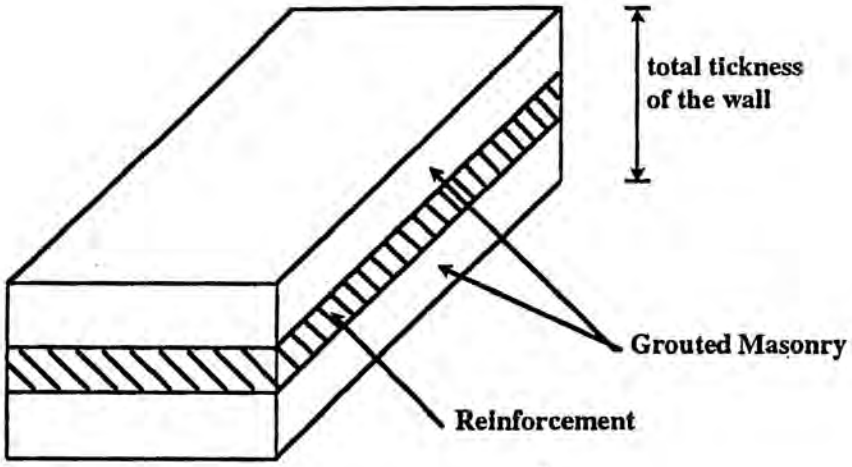

(a) Overlay Reinforced Masonry Element

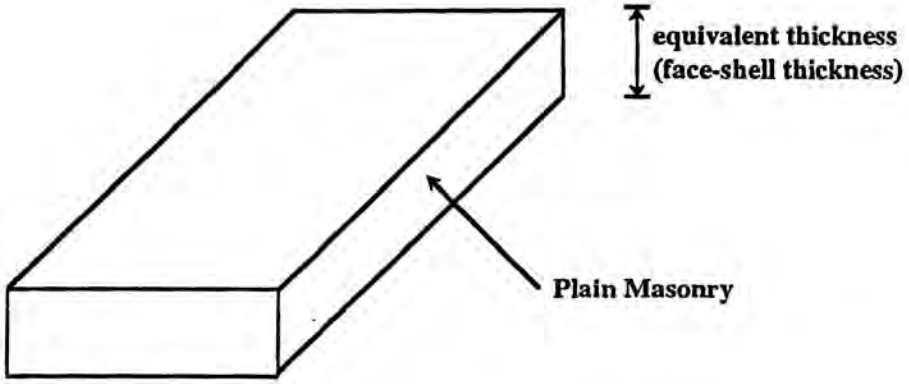

(b) Plain Masonry Element

Fig. 6.4 Overlay Element

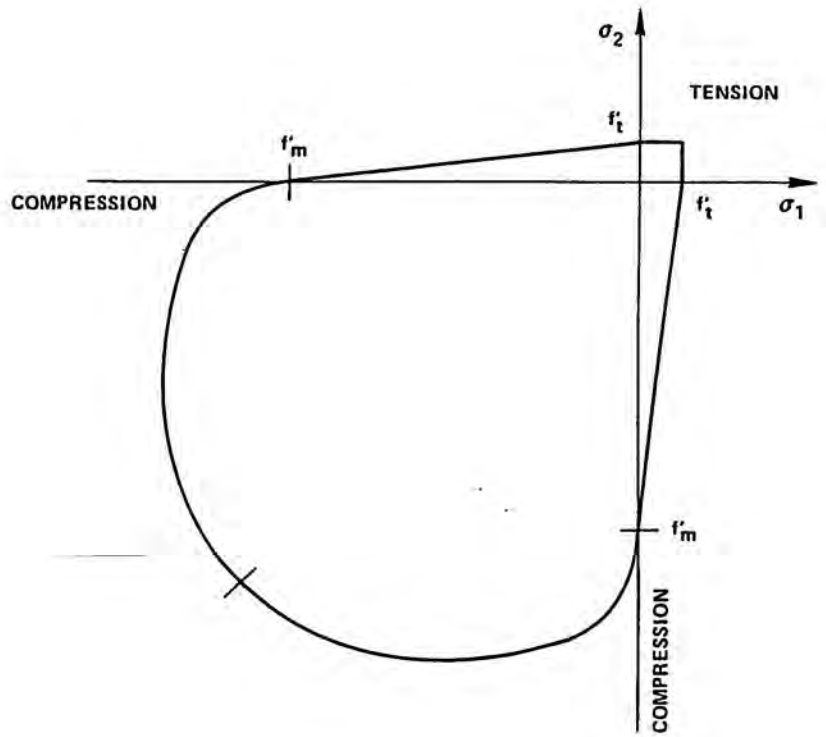

Fig. 6.5 Biaxial Strength Envelope for Masonry

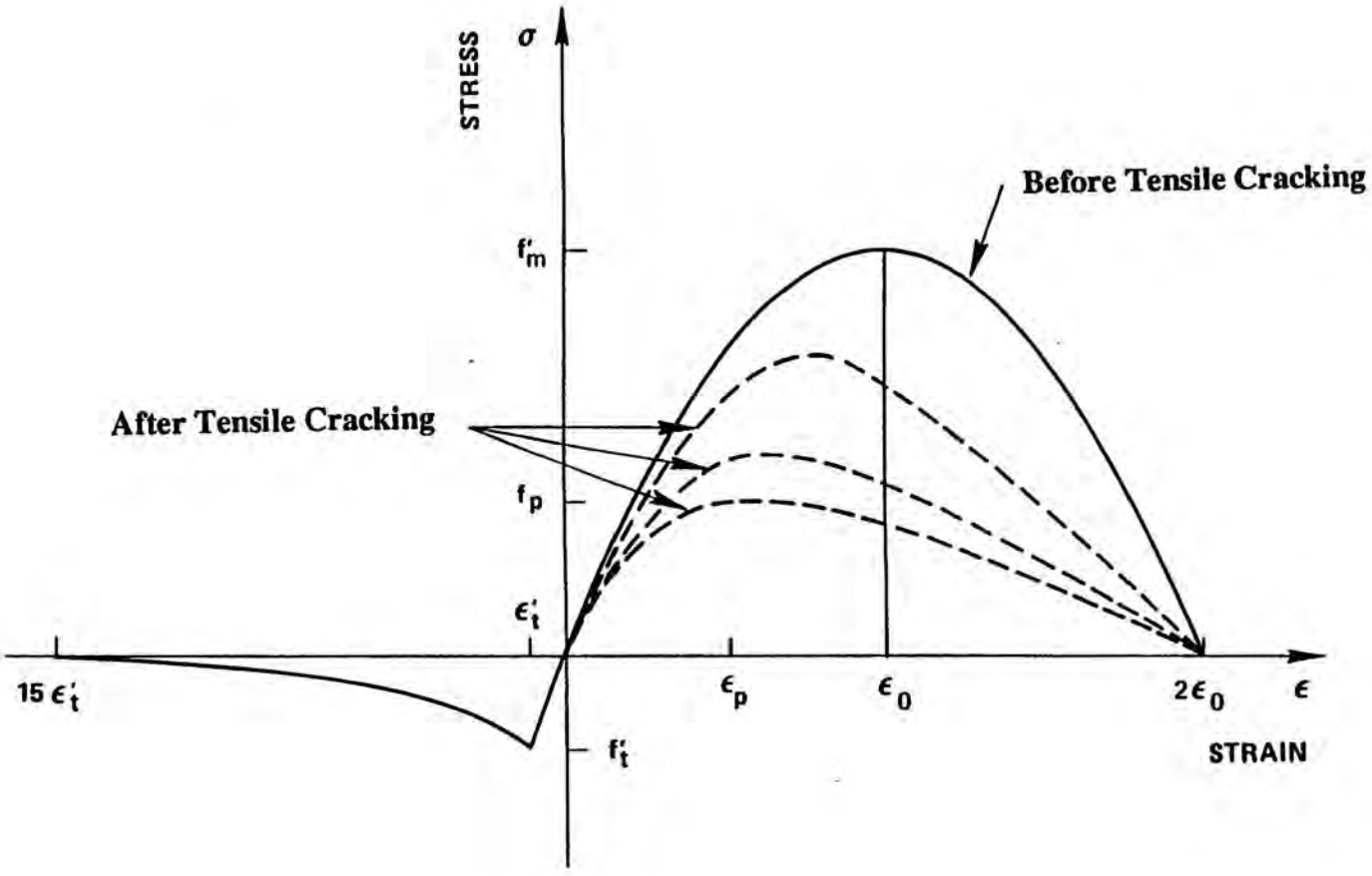

Fig. 6.6 Stress-Strain Relation for Masonry , Before and After Tensile Cracking

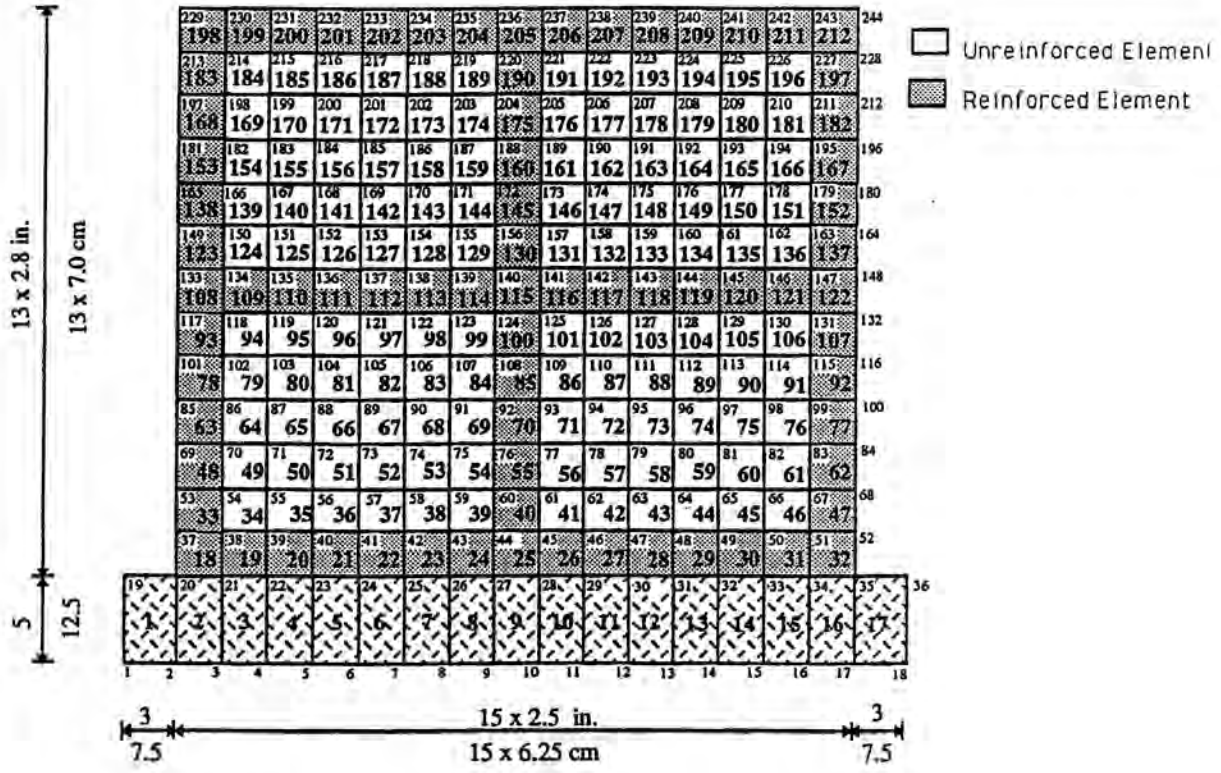

Fig. 6.7a Finite Element Mesh for Wall SWA

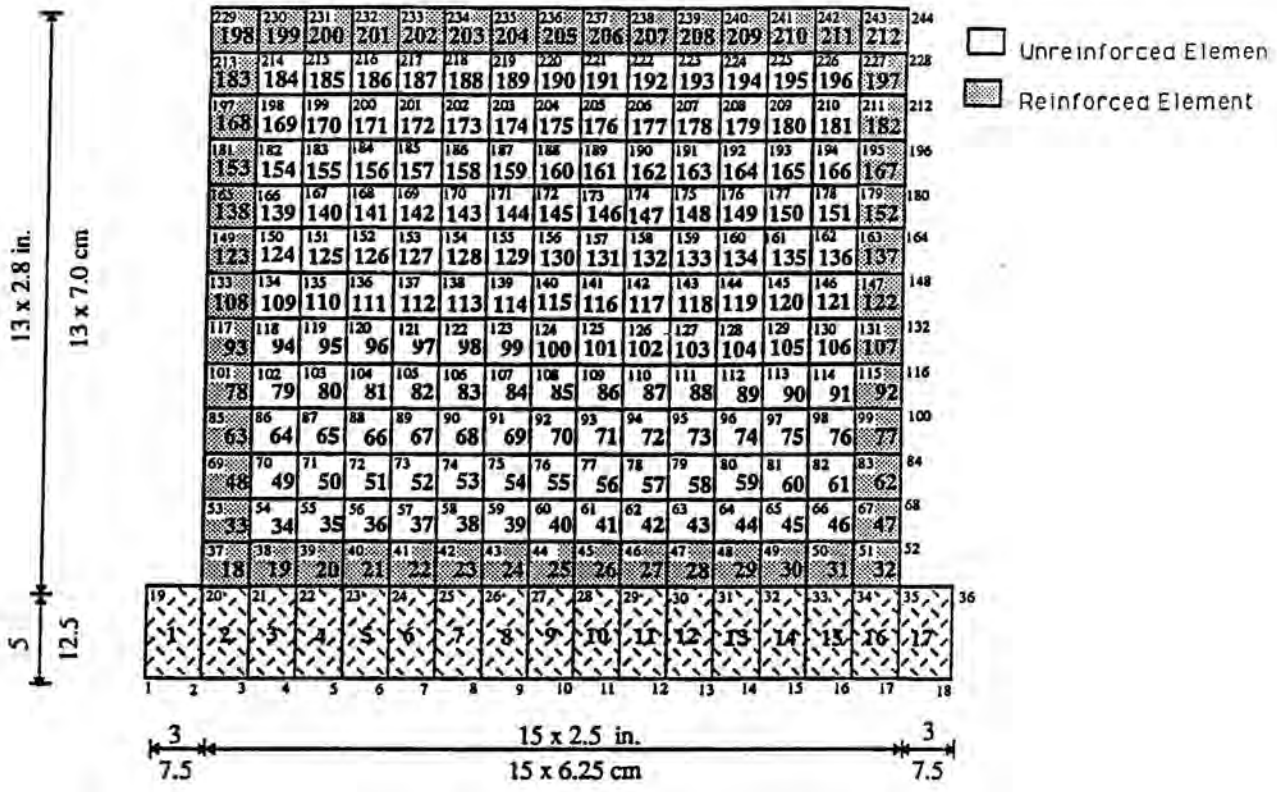

Fig. 6.7b Finite Element Mesh for Wall SWB

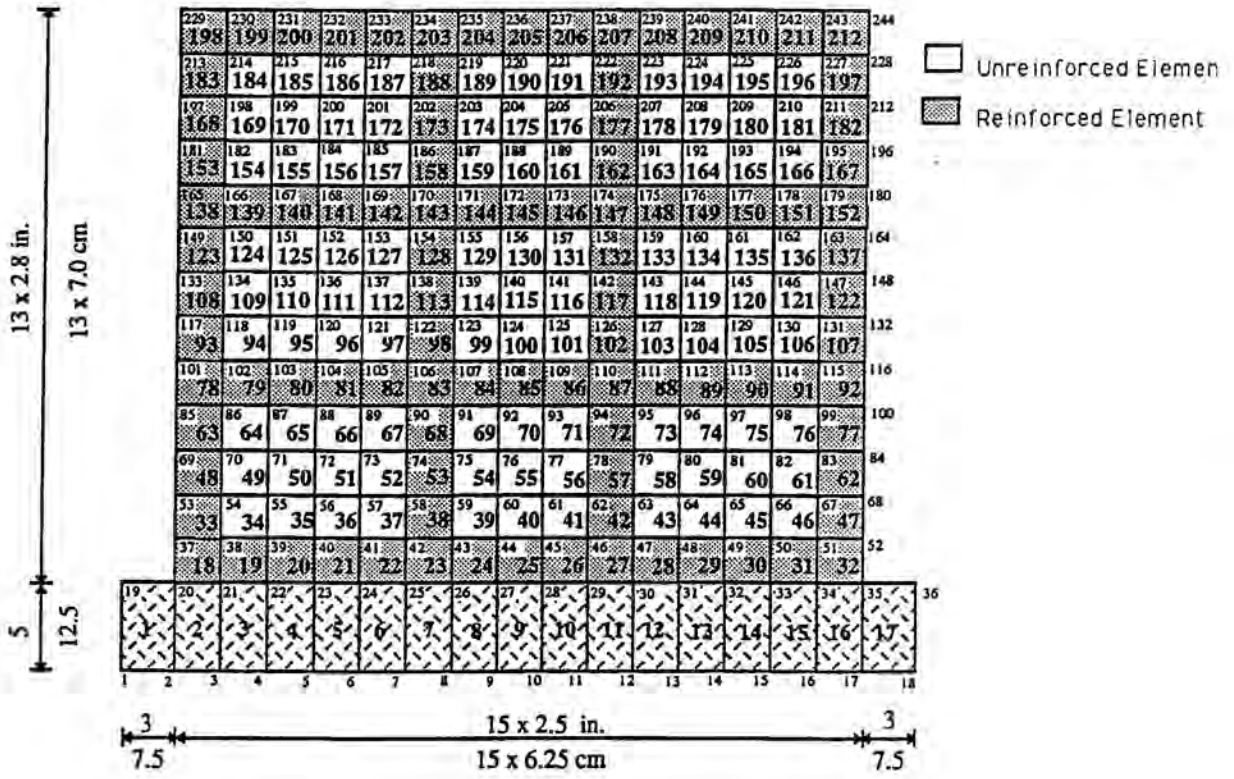

Fig. 6.7c Finite Element Mesh for Wall SWC

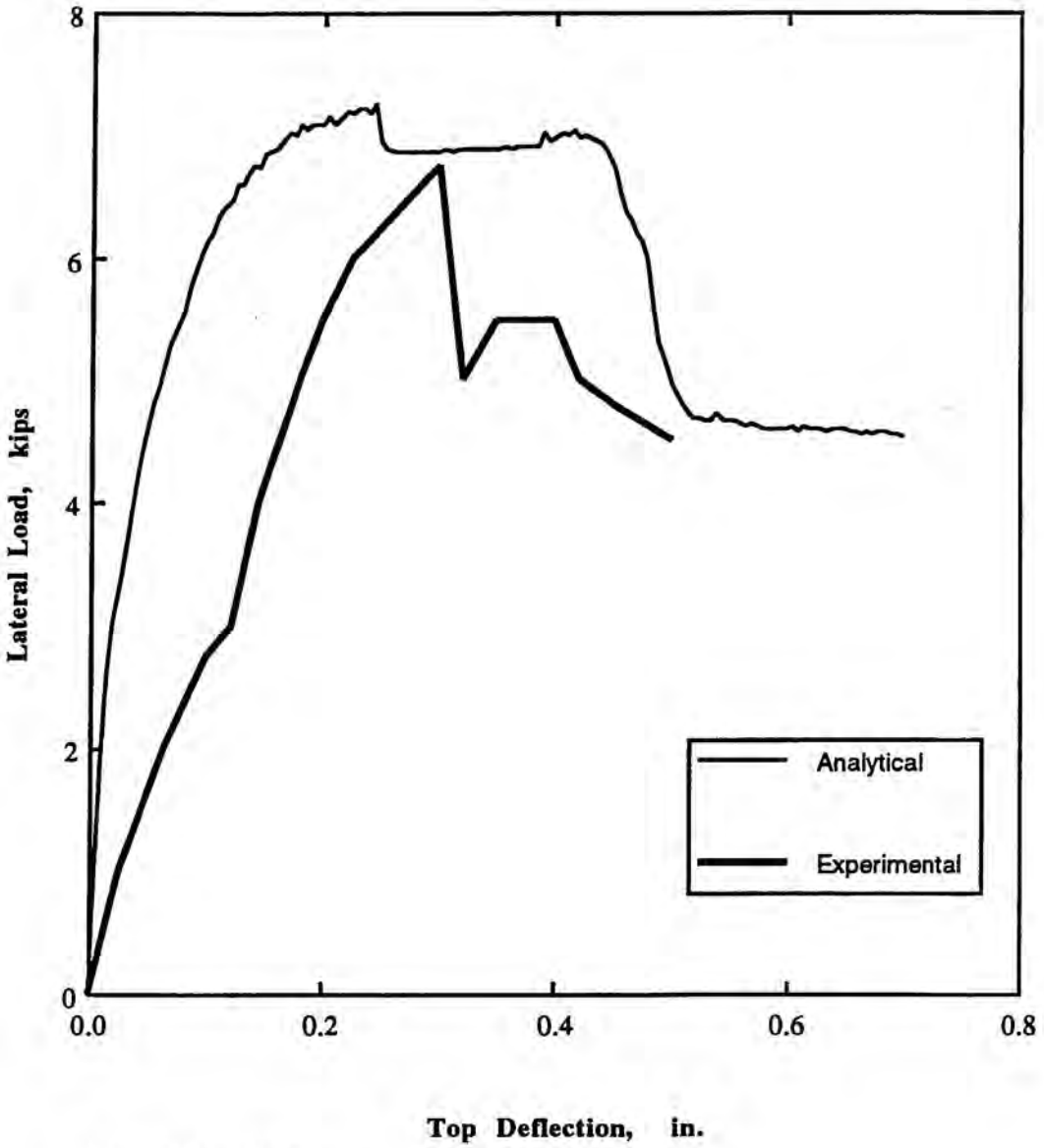

Note: 1 kip = 454 kg
1 in. = 2.54 cm

Fig.6.8 Comparison Between Experimental and Analytical L-D Curves of Wall SWA1

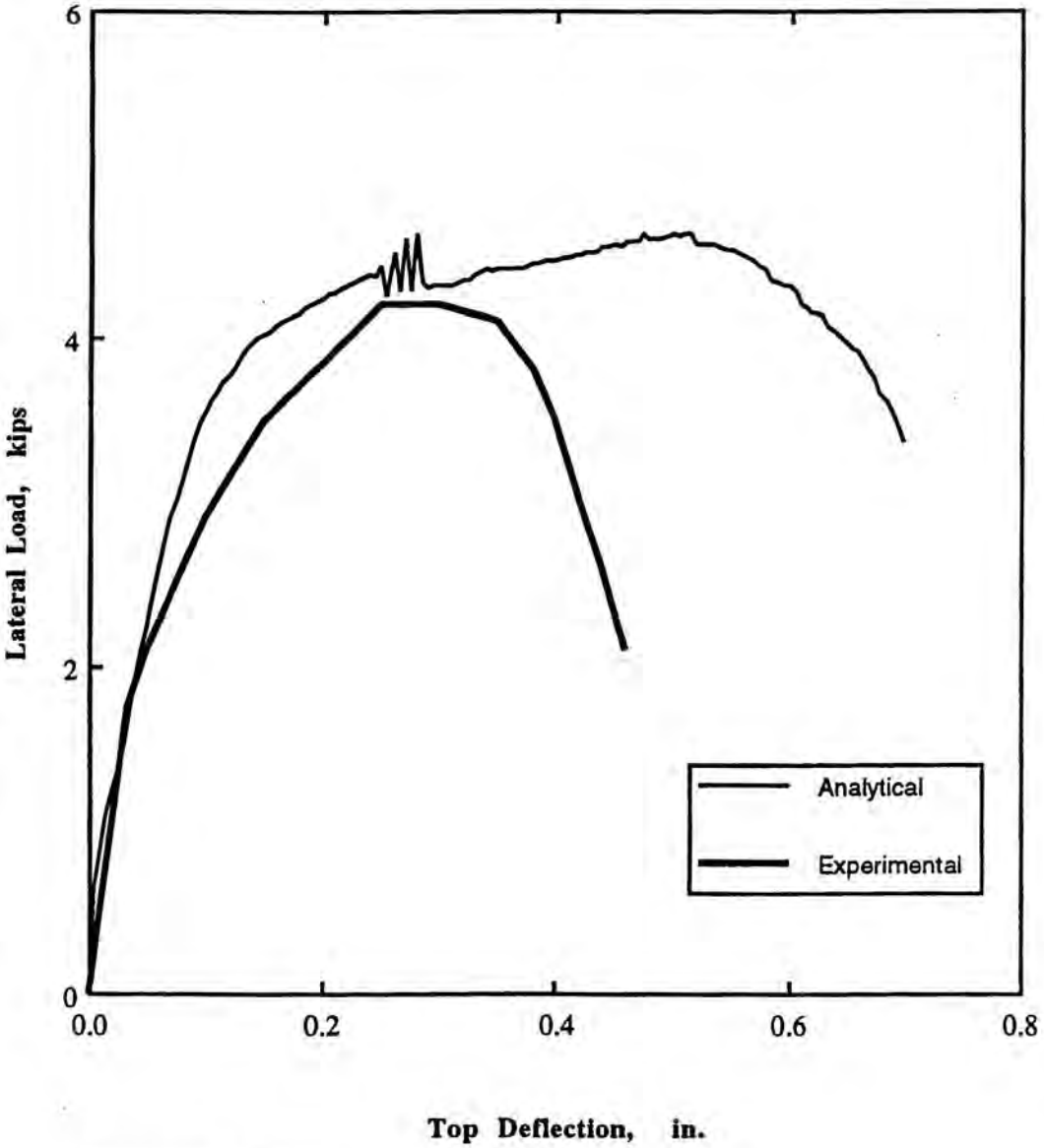

Note: 1 kip = 454 kg
1 in. = 2.54 cm

Fig.6.9 Comparison Between Experimental and Analytical L-D Curves of Wall SWA2

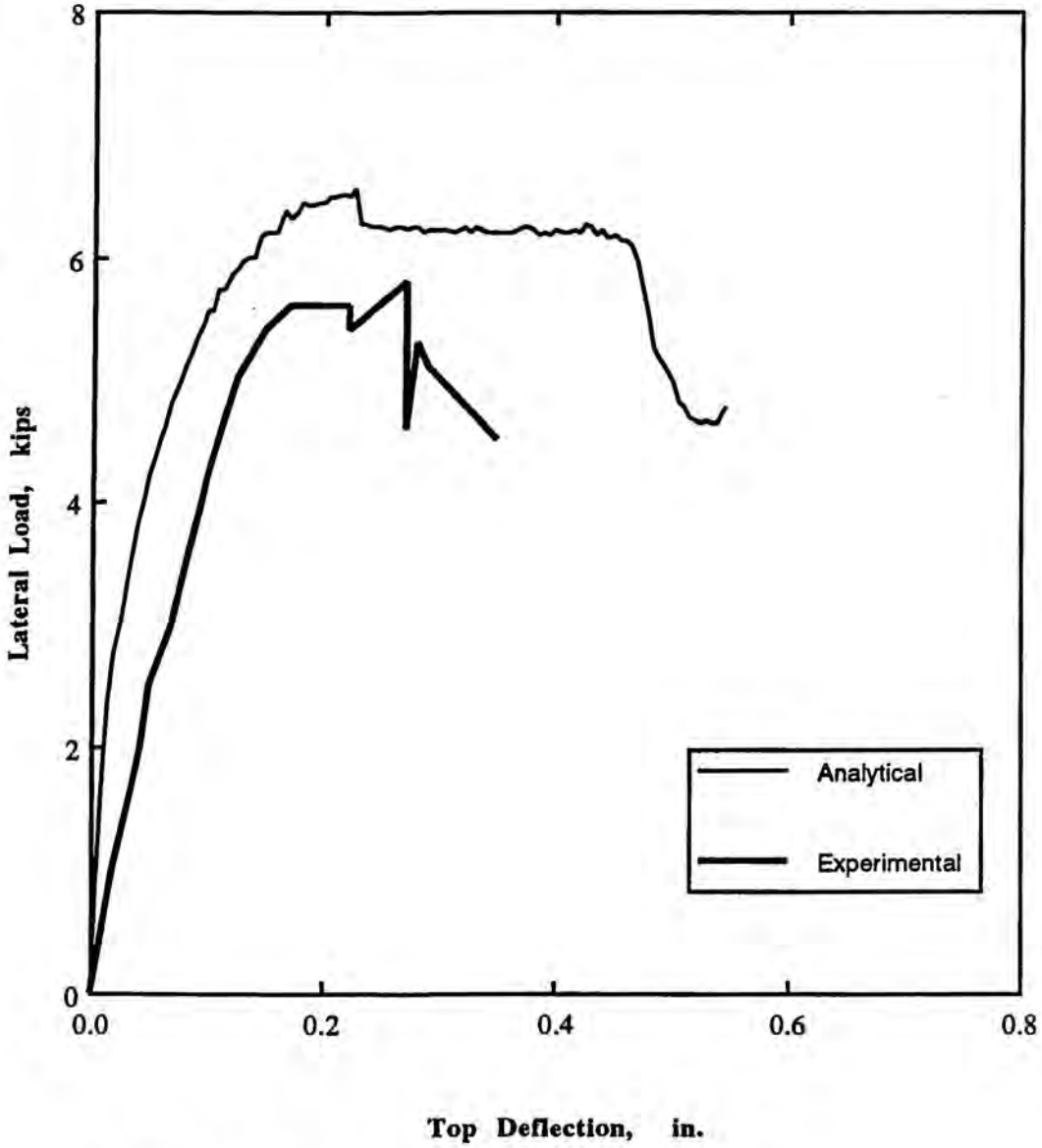

Note: 1 kip = 454 kg
1 in. = 2.54 cm

Fig.6.10 Comparison Between Experimental and Analytical L-D Curves of Wall SWA3

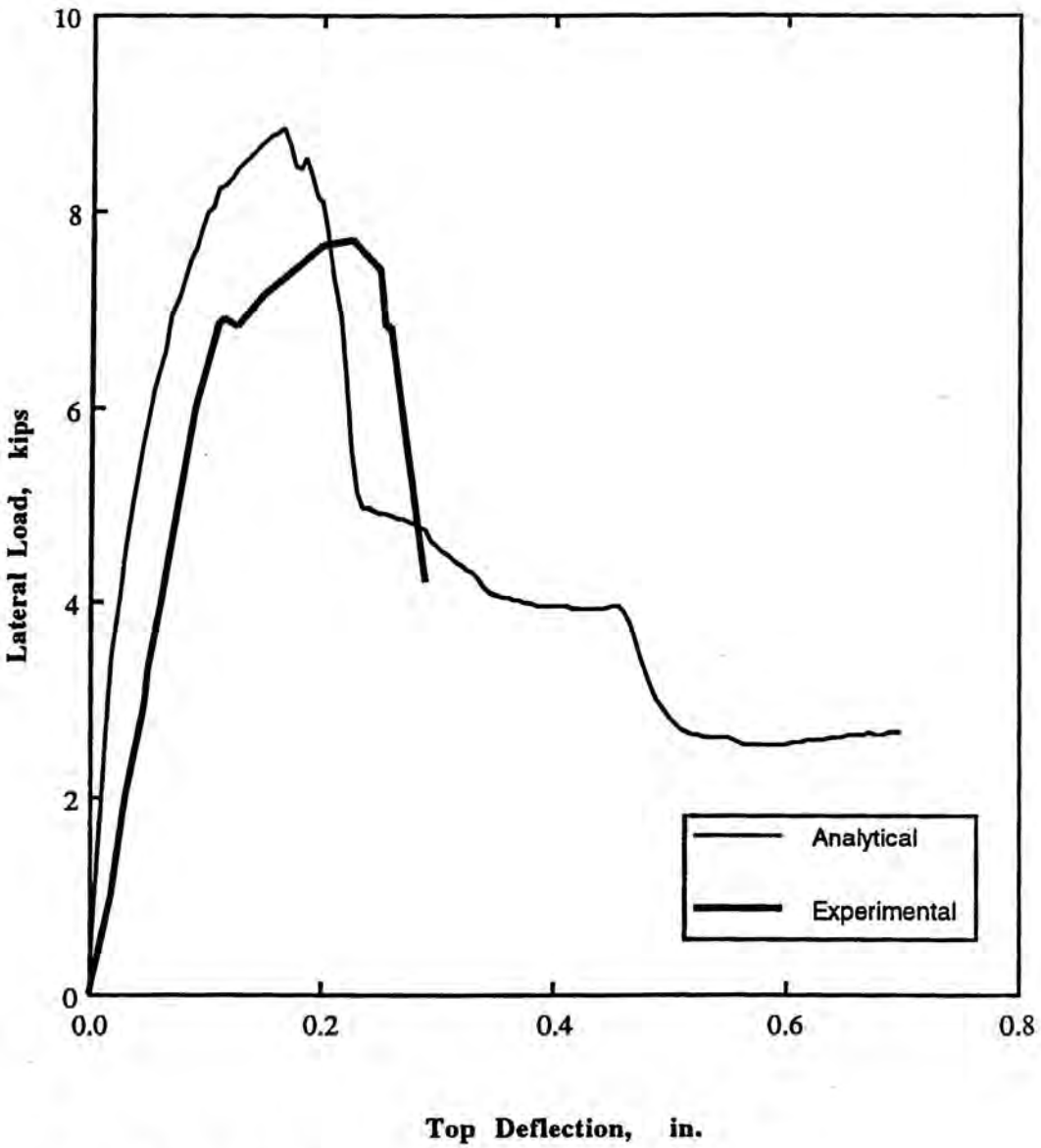

Note: 1 kip = 454 kg
1 in. = 2.54 cm

Fig.6.11 Comparison Between Experimental and Analytical L-D Curves of Wall SWA4

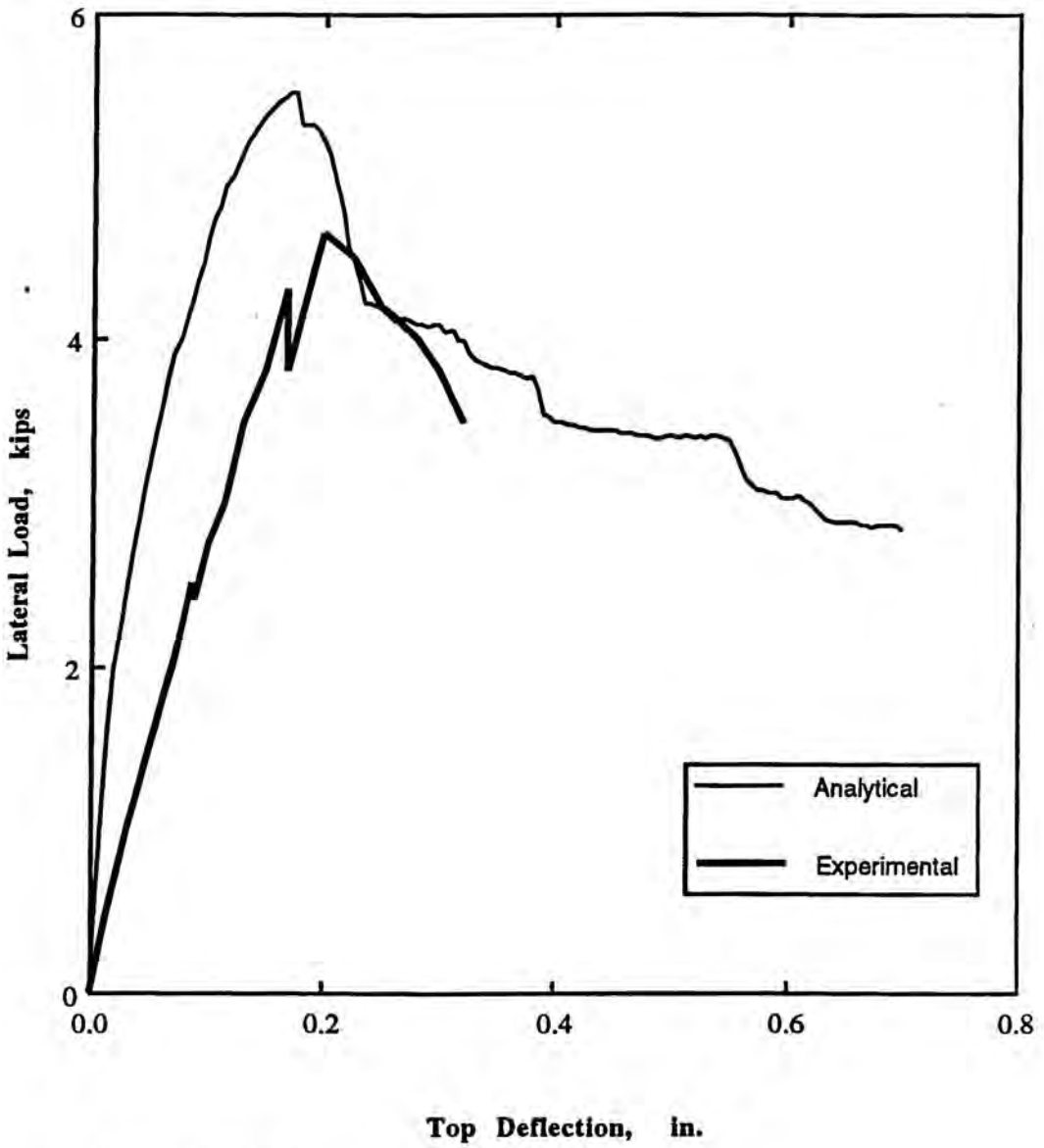

Note: 1 kip = 454 kg
1 in. = 2.54 cm

Fig.6.12 Comparison Between Experimental and Analytical L-D Curves of Wall SWA5

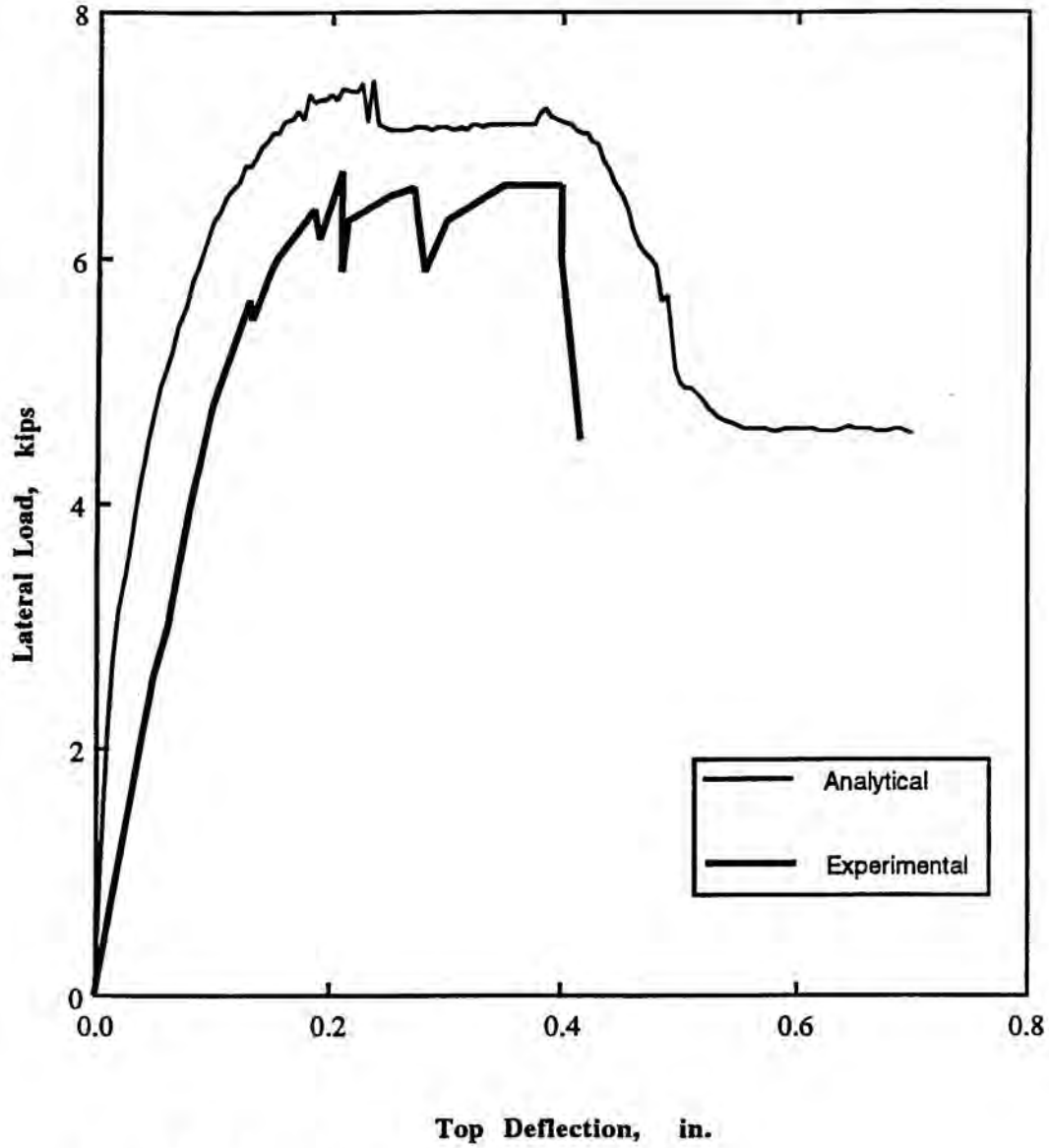

Note: 1 kip = 454 kg
1 in. = 2.54 cm

Fig.6.13 Comparison Between Experimental and Analytical L-D Curves of Wall SWA6

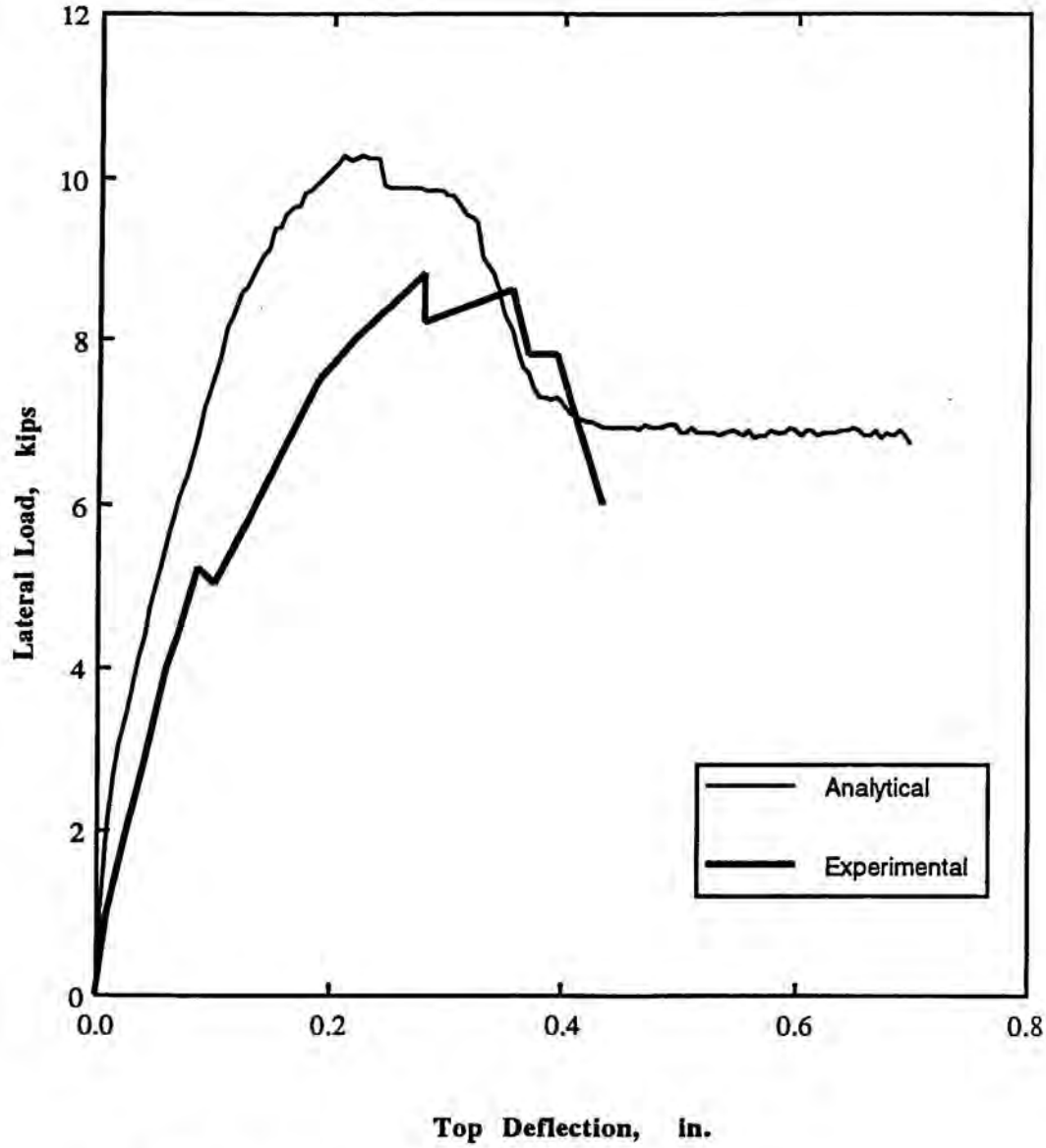

Note: 1 kip = 454 kg
1 in. = 2.54 cm

Fig.6.14 Comparison Between Experimental and Analytical L-D Curves of Wall SWA7

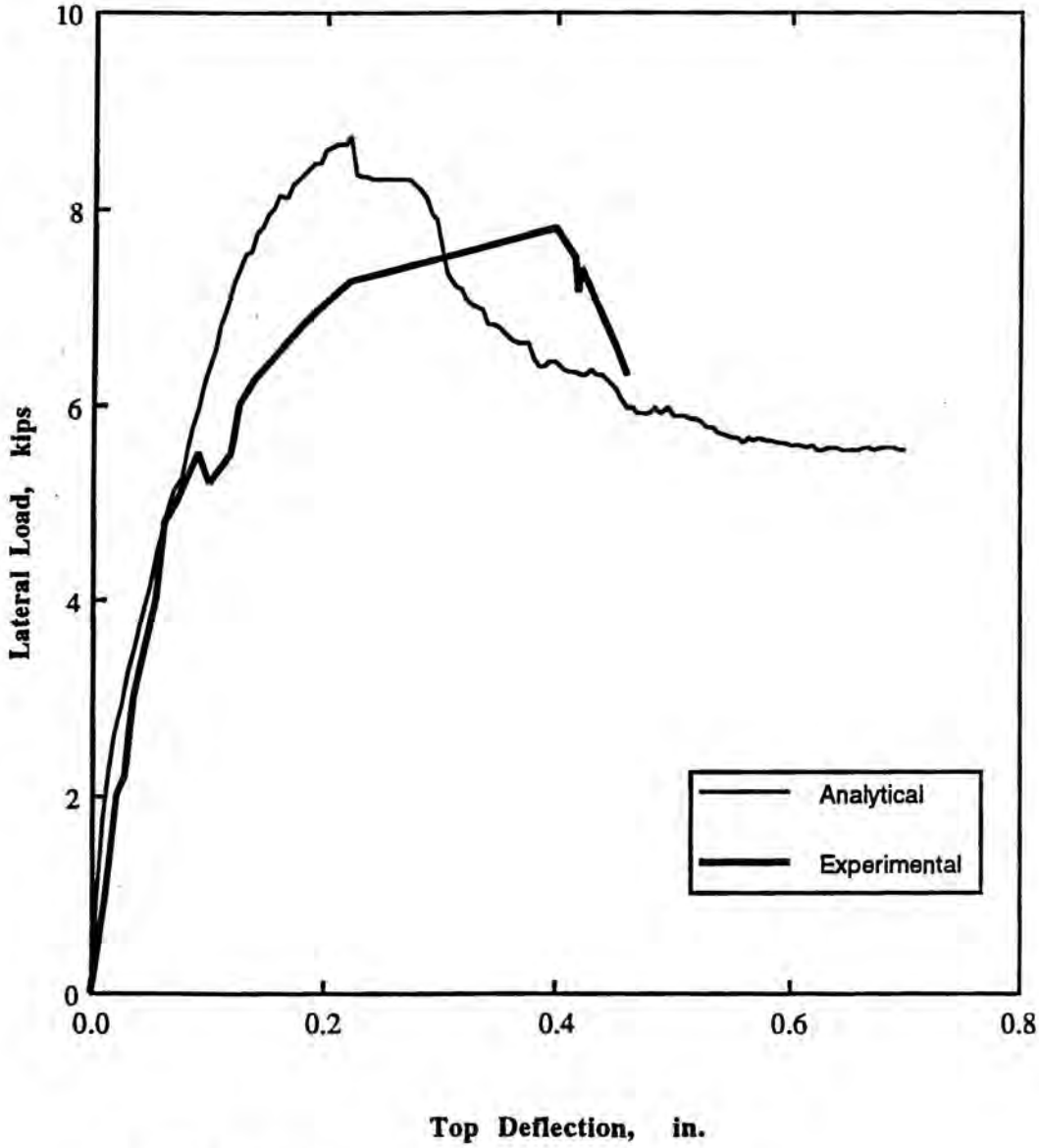

Note: 1 kip = 454 kg
1 in. = 2.54 cm

Fig.6.15 Comparison Between Experimental and Analytical L-D Curves of Wall SWA9

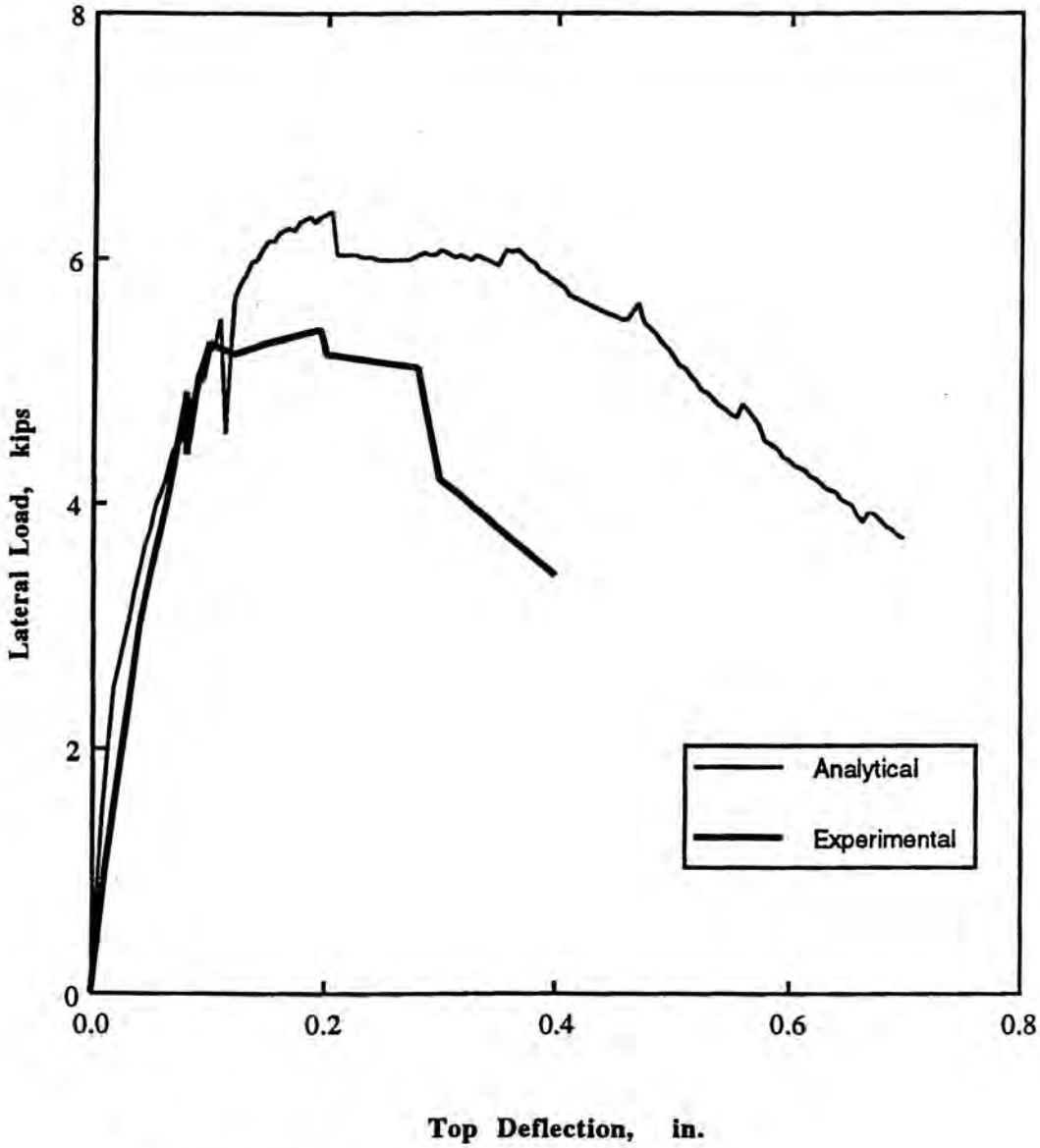

Note: 1 kip = 454 kg
1 in. = 2.54 cm

Fig.6.16 Comparison Between Experimental and Analytical L-D Curves of Wall SWB1

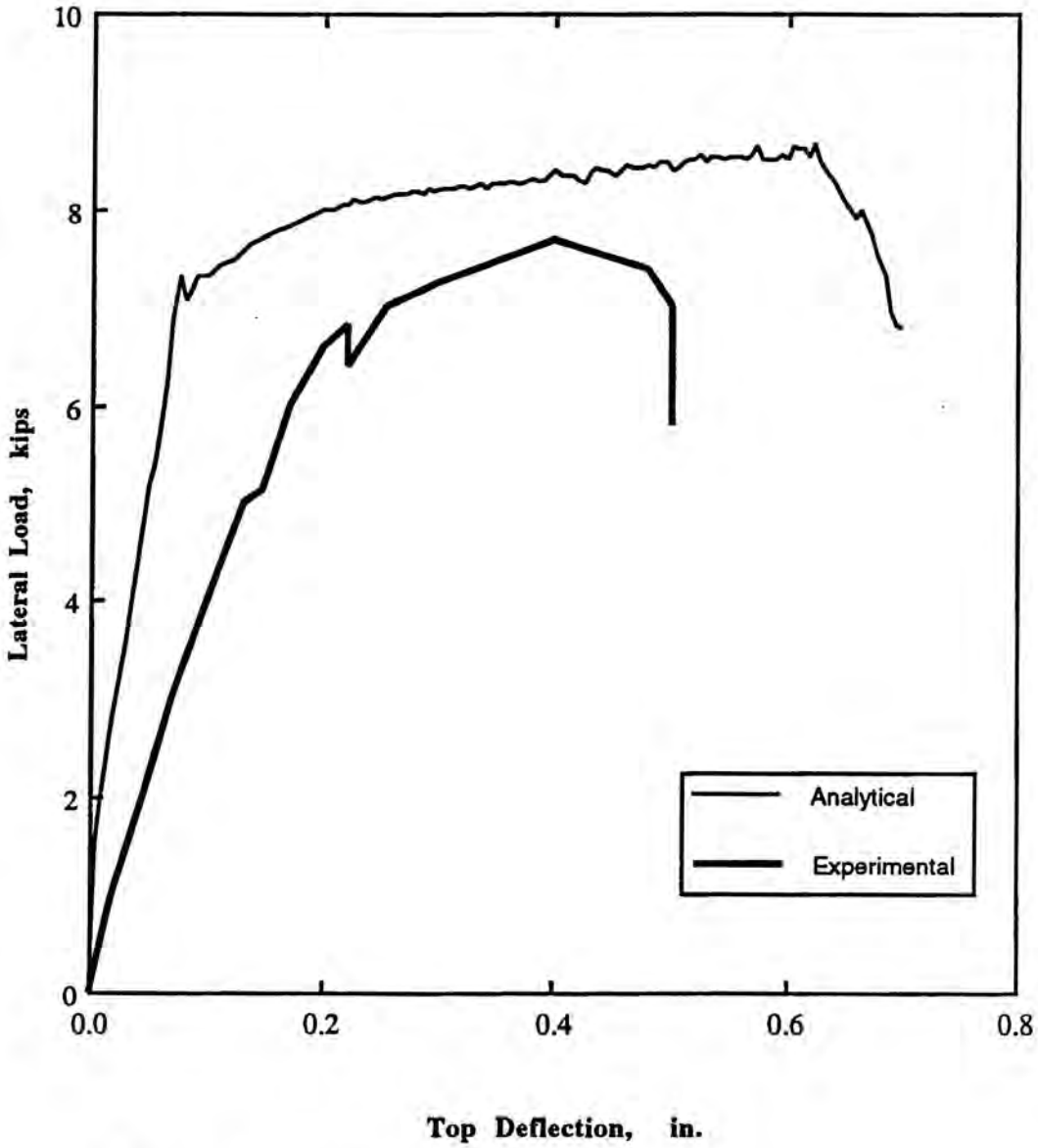

Note: 1 kip = 454 kg
1 in. = 2.54 cm

Fig.6.17 Comparison Between Experimental and Analytical L-D Curves of Wall SWC1

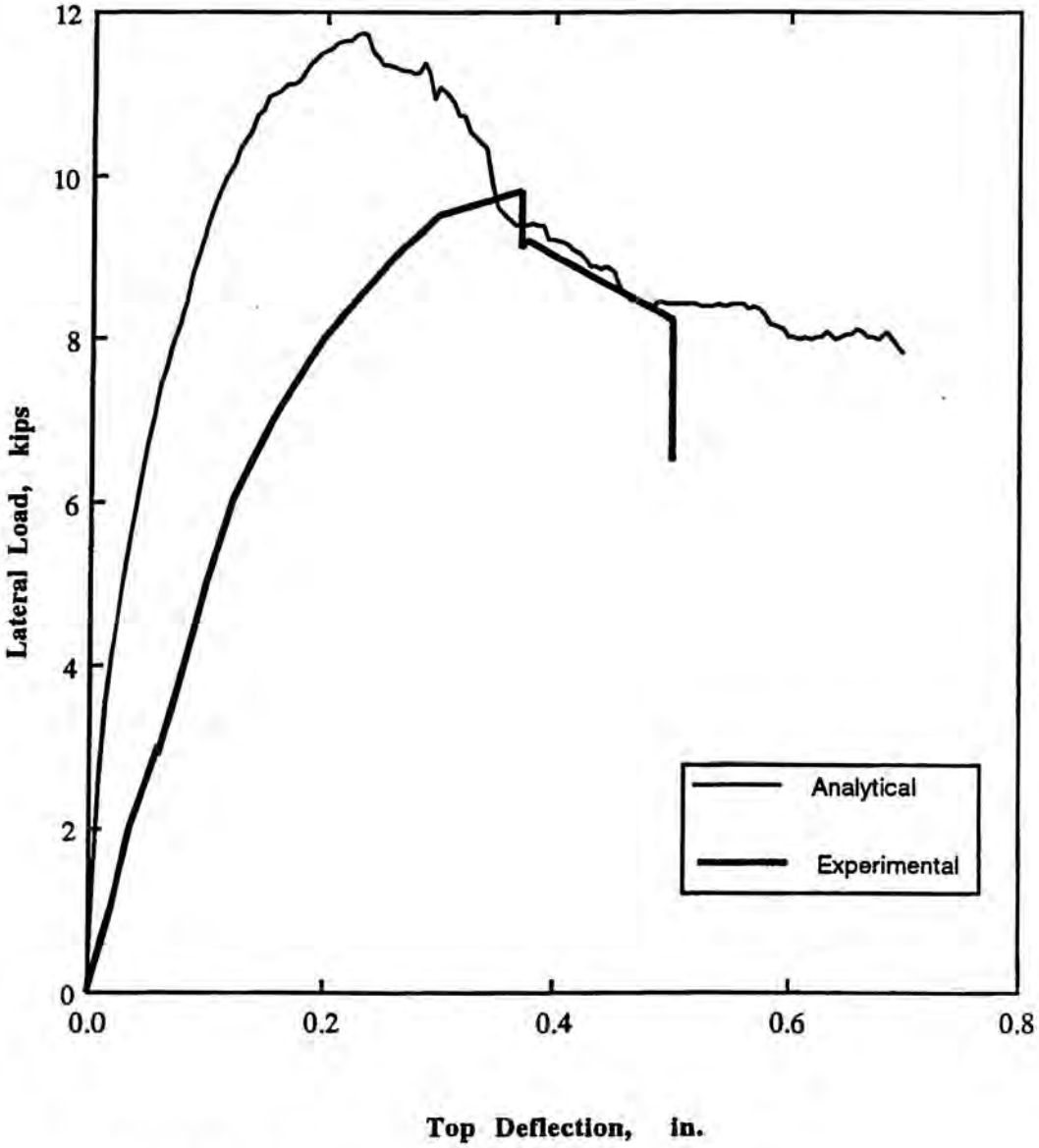

Note: 1 kip = 454 kg
1 in. = 2.54 cm

Fig.6.18 Comparison Between Experimental and Analytical L-D Curves of Wall SWC2

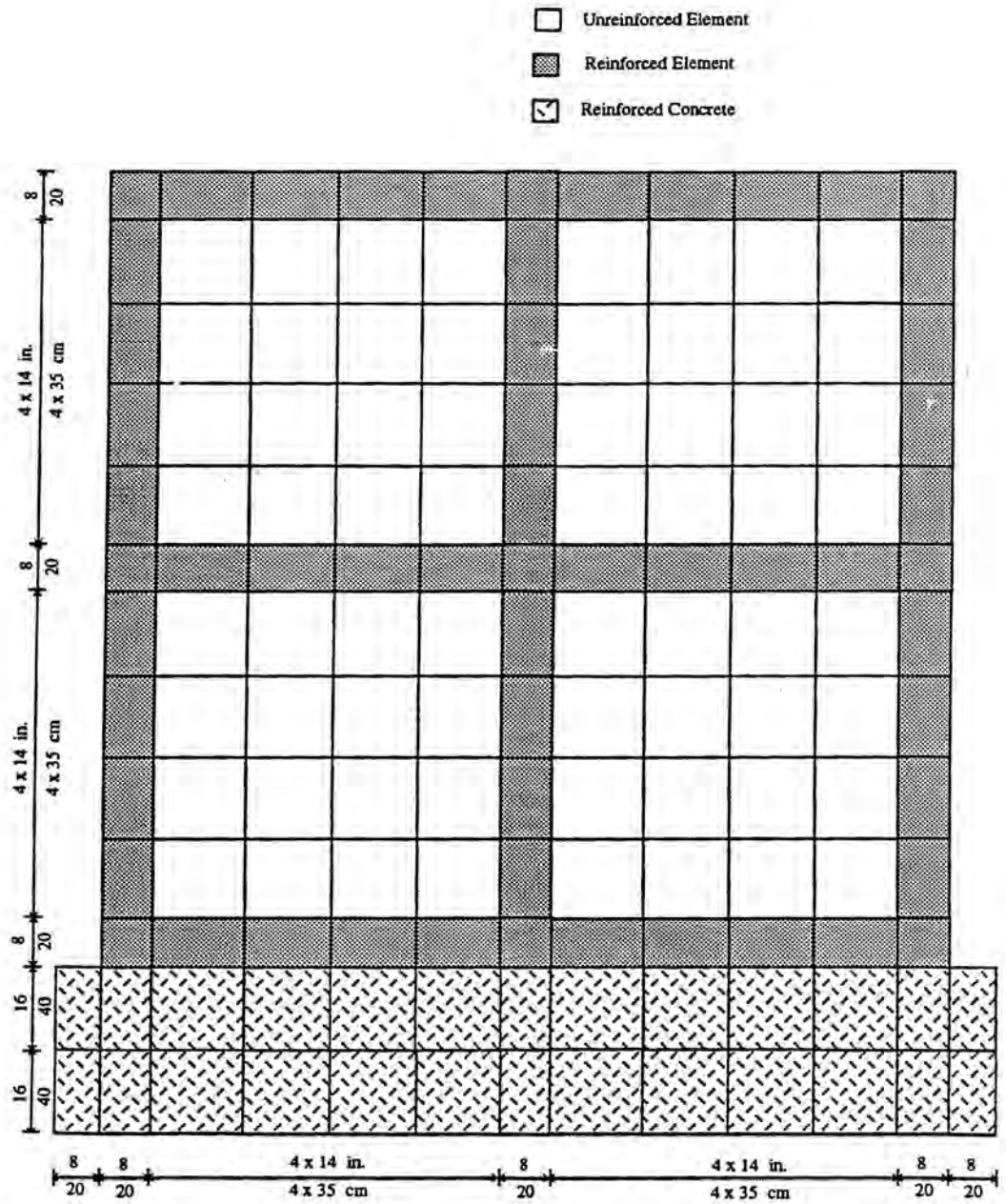

Fig. 6.19 Finite Element Mesh for Walls With Aspect Ratio of 1.0

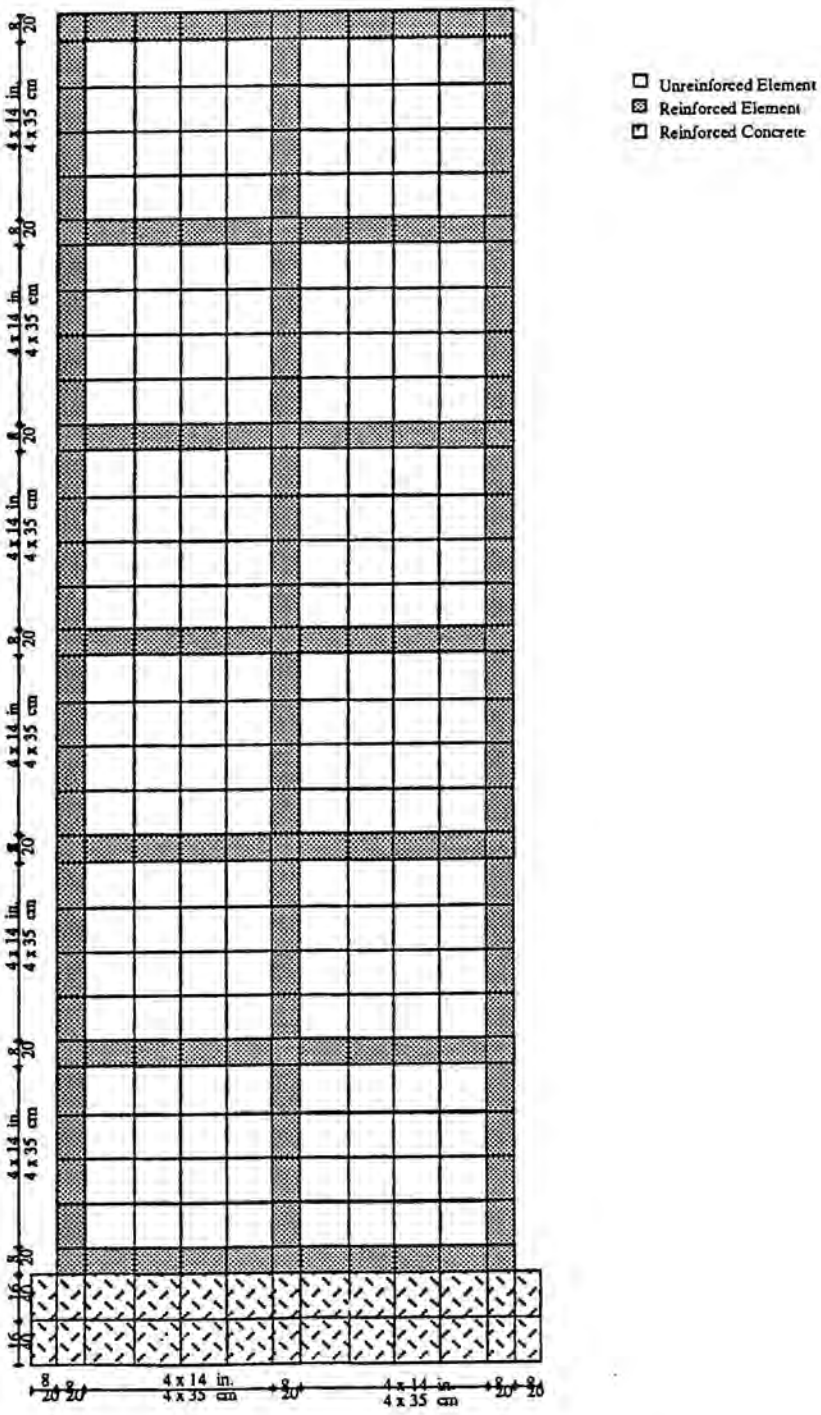

Fig. 6.20 Finite Element Mesh for Walls With Aspect Ratio of 3.0

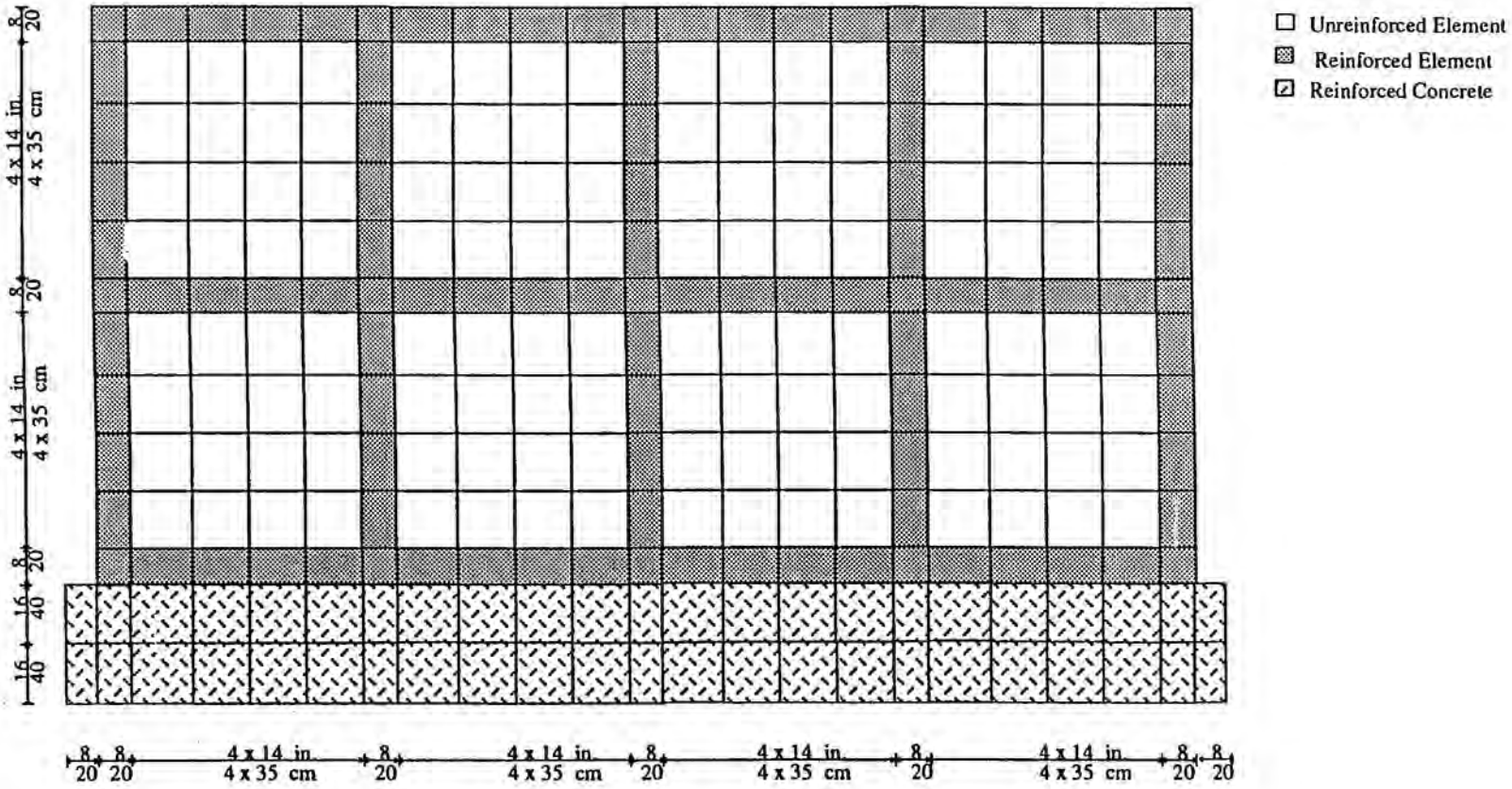

Fig. 6.21 Finite Element Mesh for Walls With Aspect Ratio of 0.5

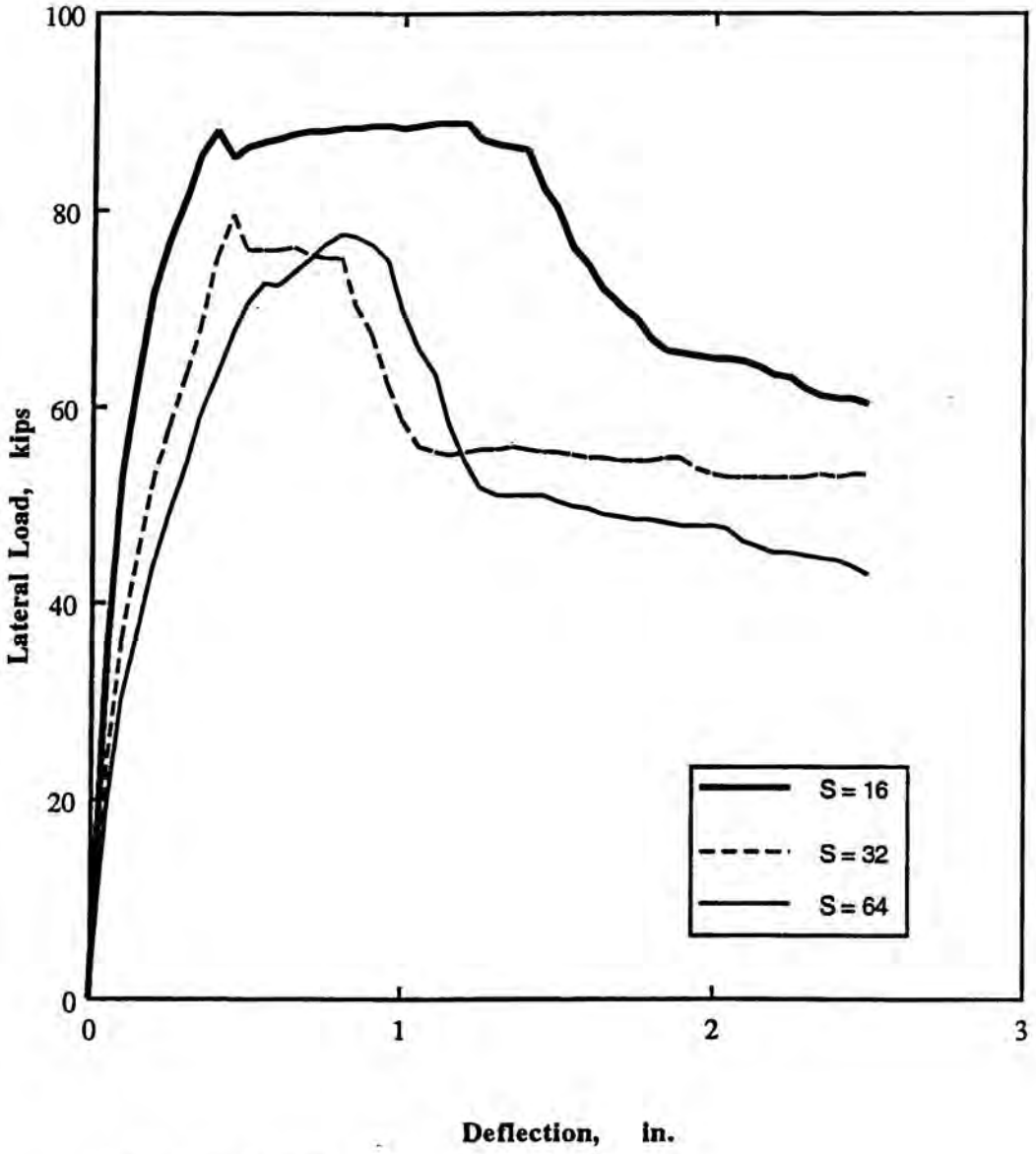

Note: 1 kip = 454 kg
1 in. = 2.54 cm

Fig. 6.22 Effect of Spacing of Vertical and Horizontal Steel on L-D Relationships

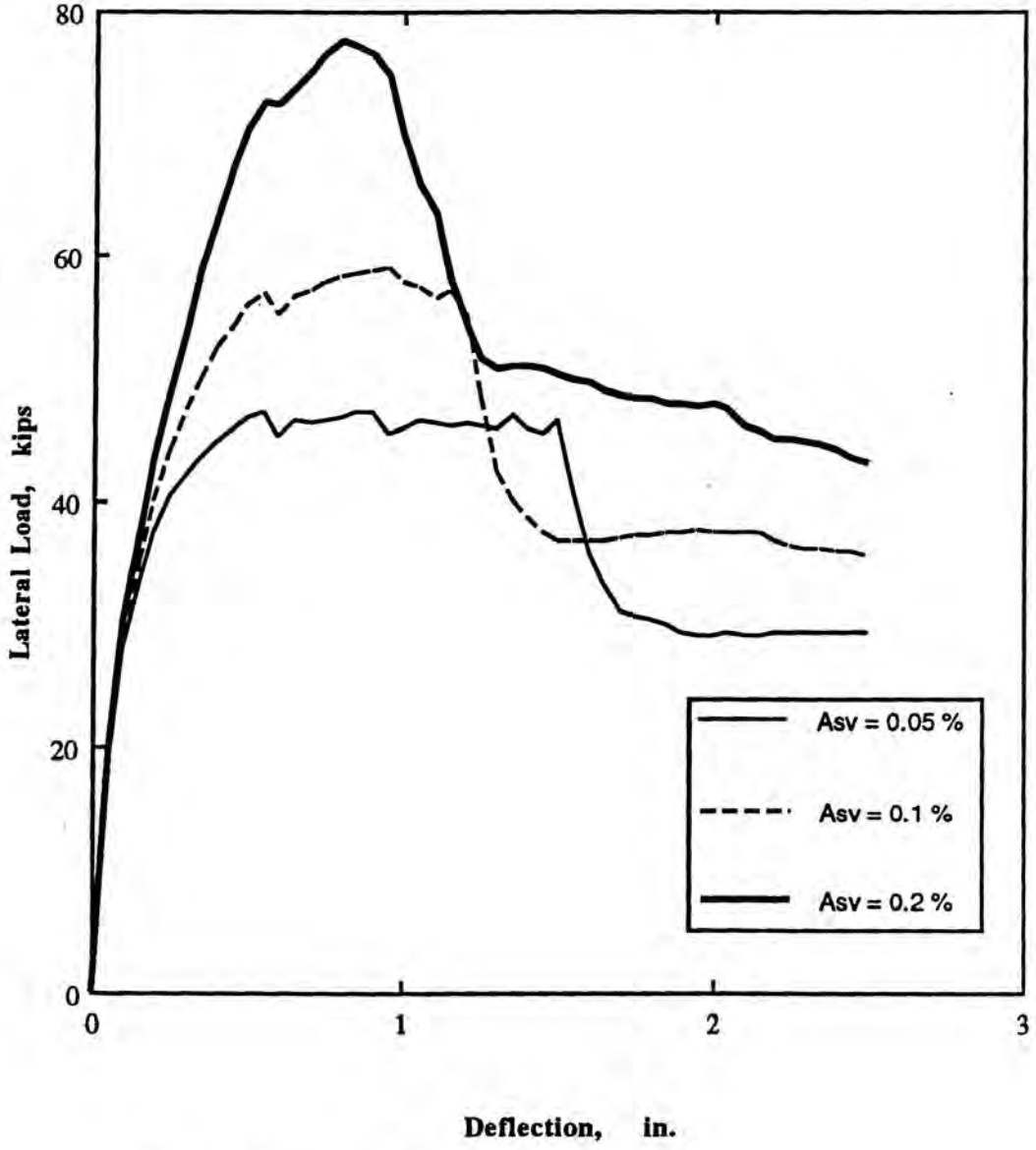

Note: 1 kip = 454 kg
1 in. = 2.54 cm

Fig. 6.23 Effect of Amount of Vertical Steel on L-D Relationships

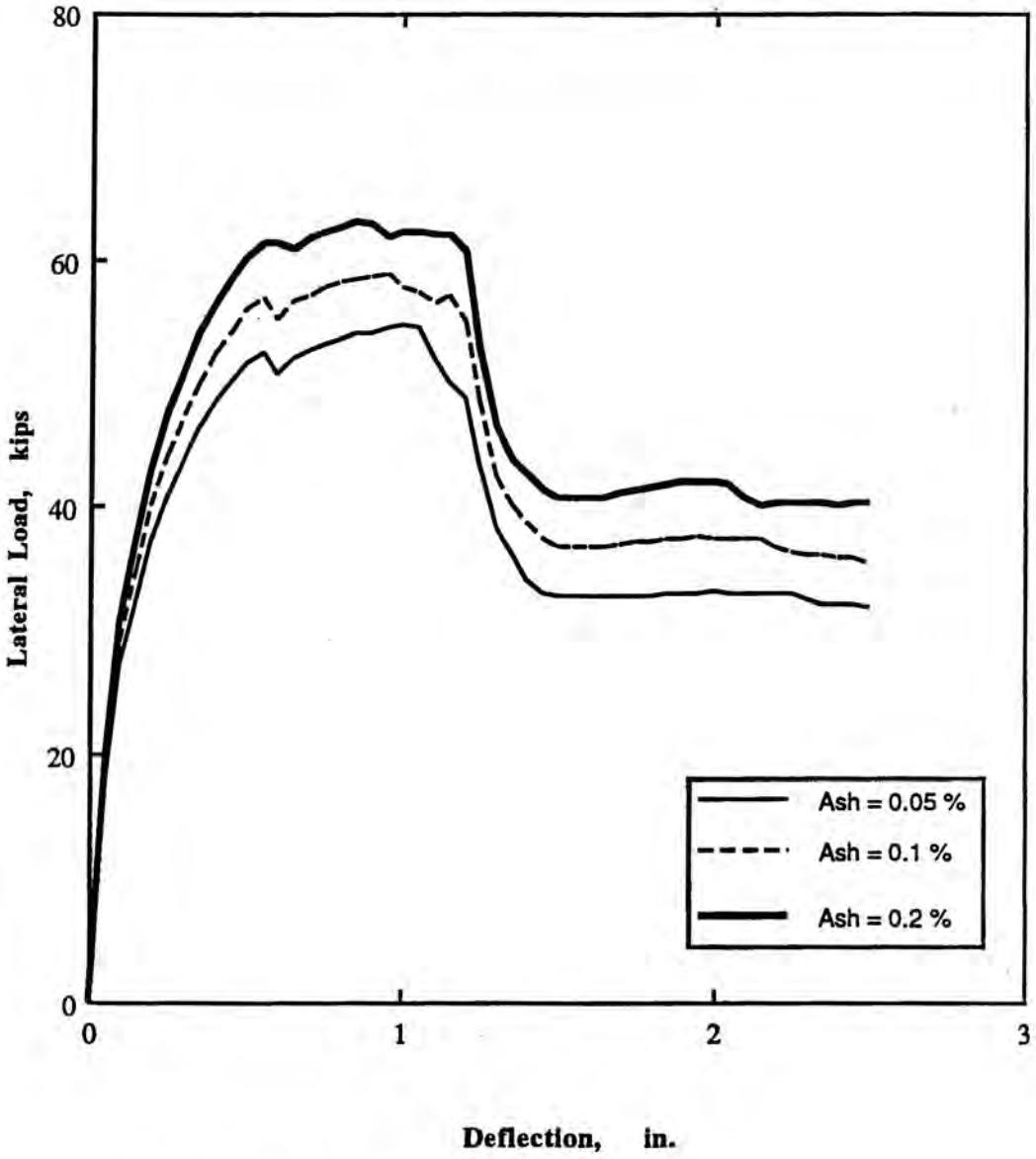

Note: 1 kip = 454 kg
1 in. = 2.54 cm

Fig. 6.24 Effect of Amount of Horizontal Steel on L-D Relationships

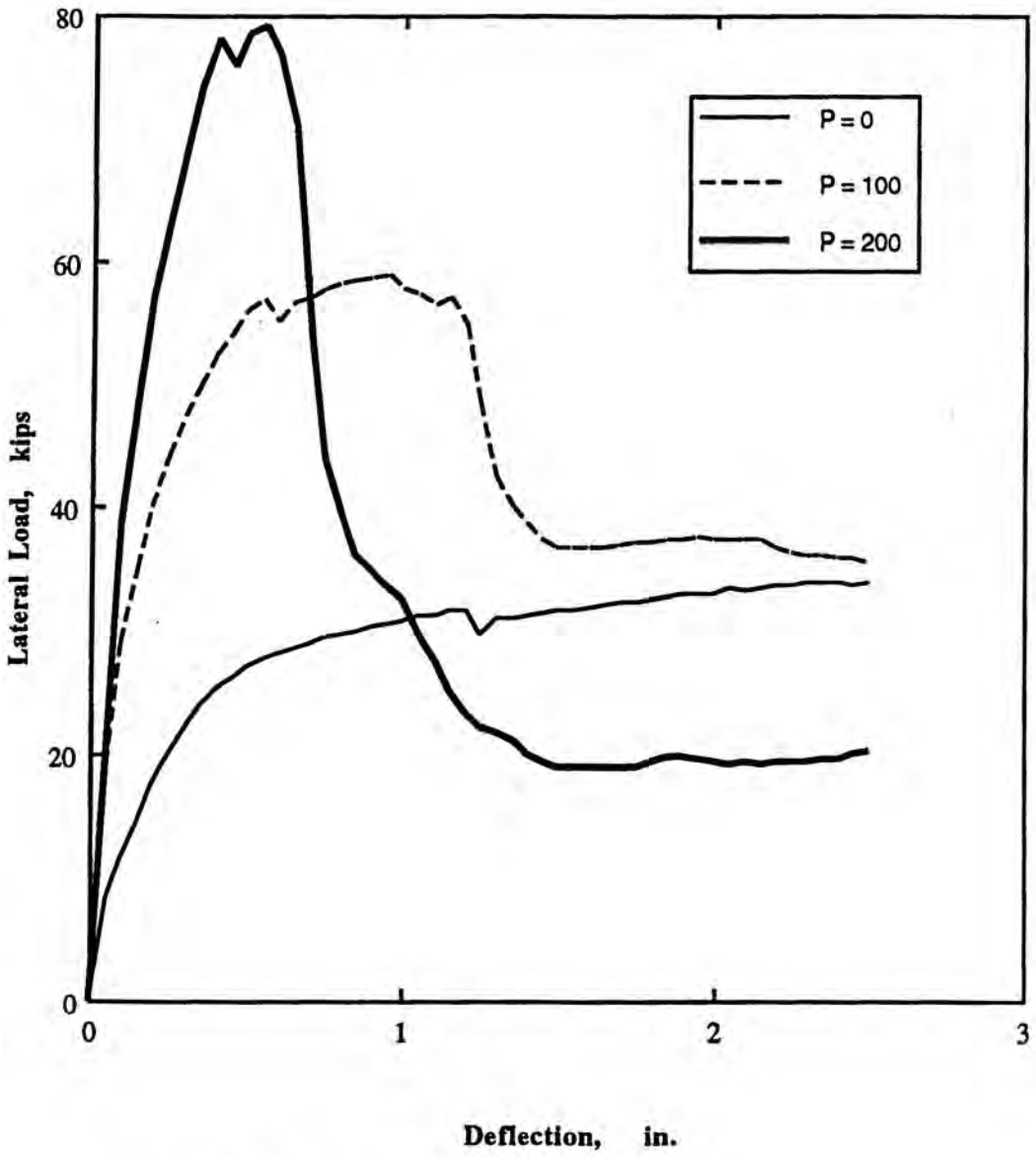

Note: 1 kip = 454 kg
1 in. = 2.54 cm

Fig. 6.25 Effect of Axial Compression on L-D Relationships

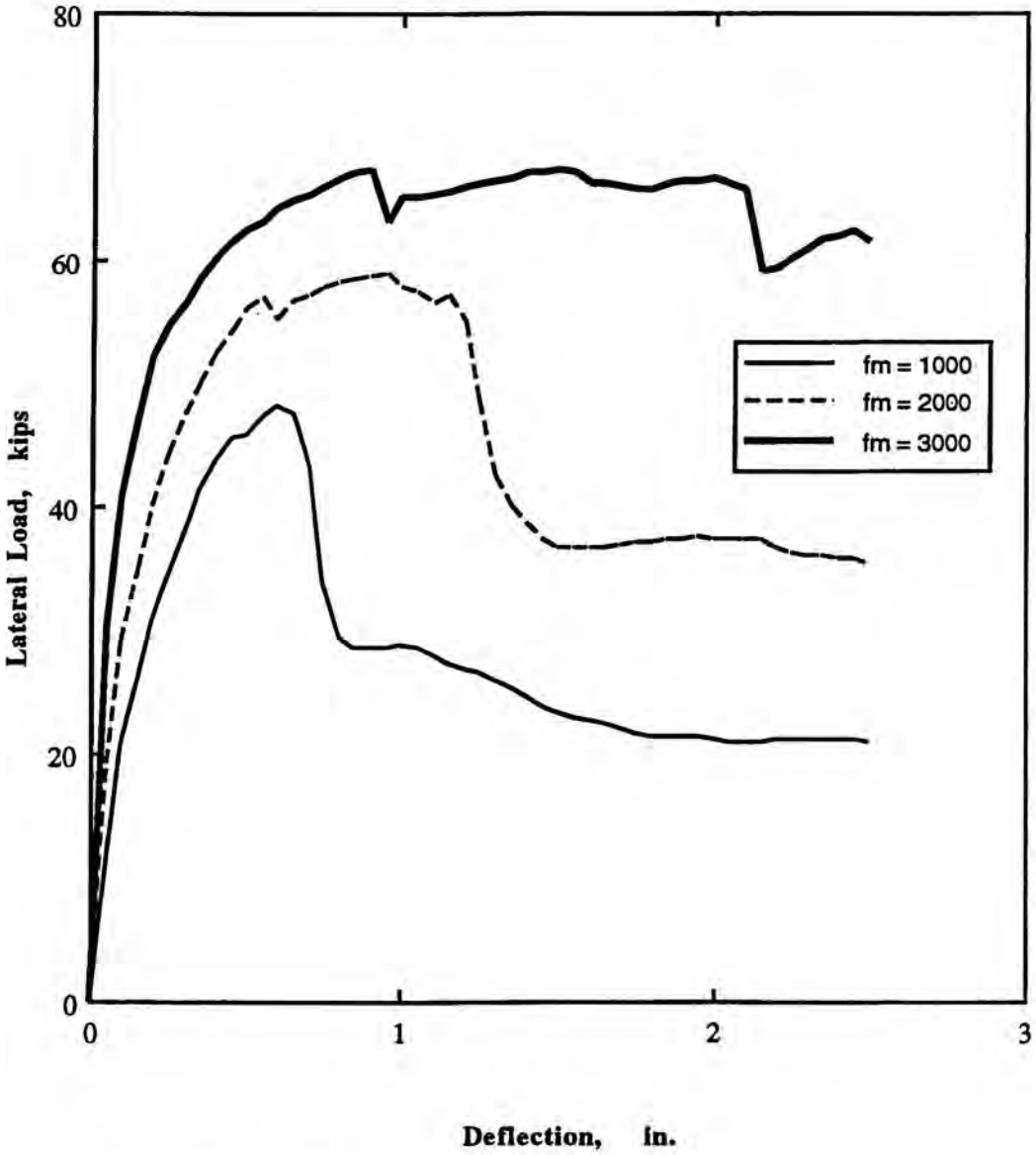

Note: 1 kip = 454 kg
1 in. = 2.54 cm

Fig. 6.26 Effect of Masonry Strength on L-D Relationships

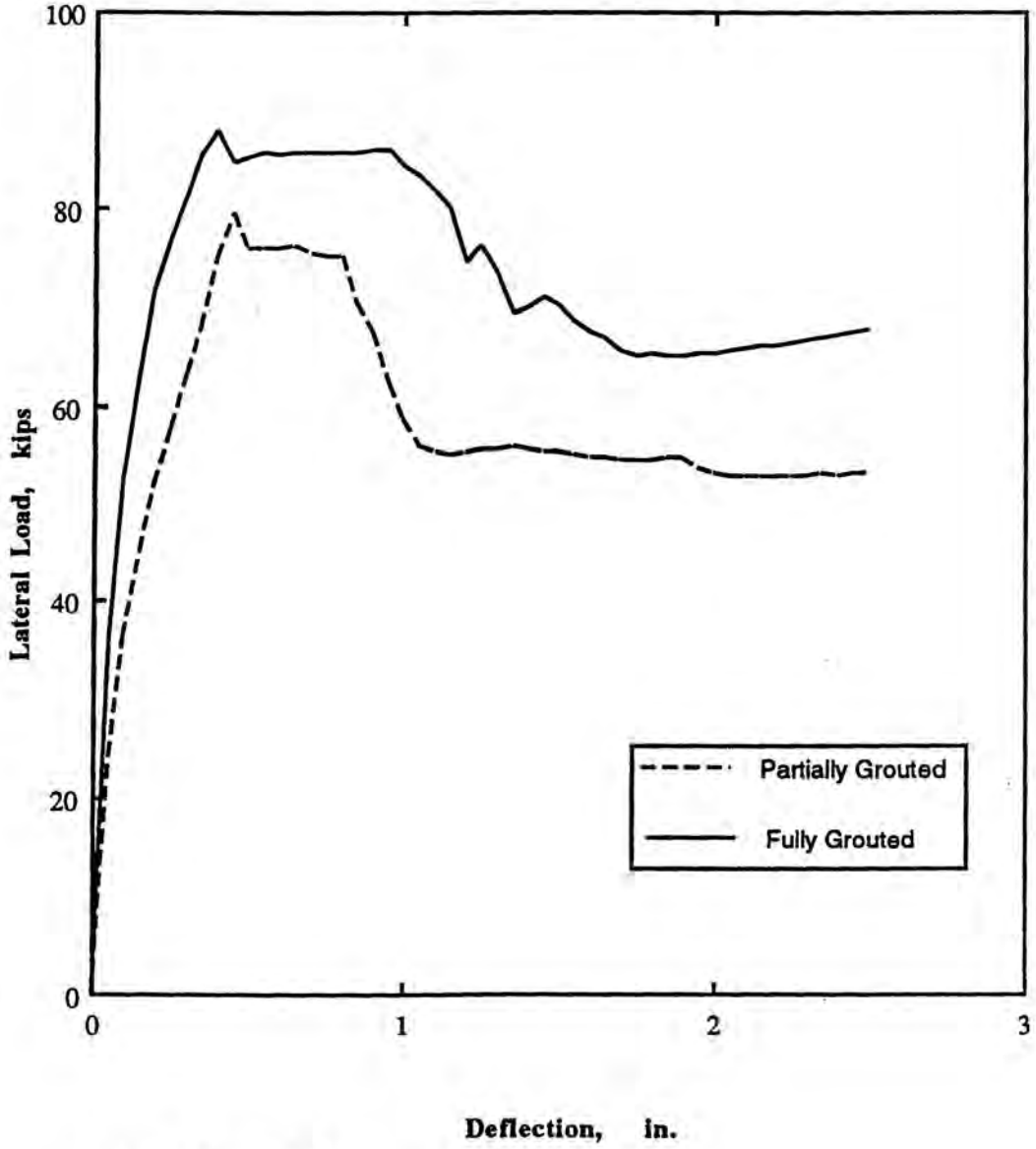

Note: 1 kip = 454 kg
1 in. = 2.54 cm

Fig. 6.27 Effect of Extent of Grouting on L-D Relationships for Wall with 32" (0.8 m) Spacing of Steel Bars

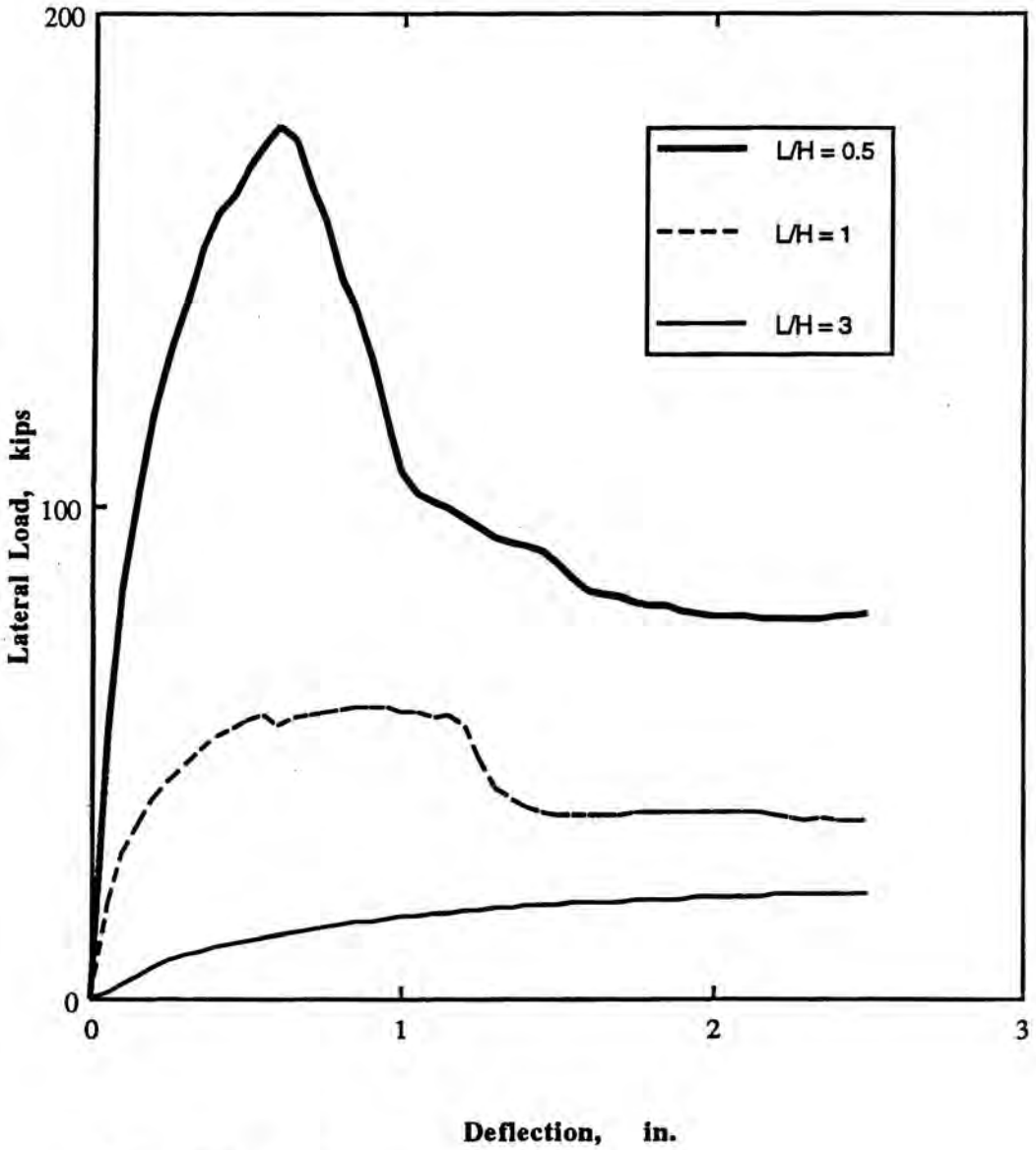

Note: 1 kip = 454 kg
1 in. = 2.54 cm

Fig. 6.28 Effect of Wall Aspect Ratio on L-D Relationships

CHAPTER 7
DESIGN METHODOLOGY

7.1 INTRODUCTION

Shear wall panels are usually subjected to simultaneous in-plane lateral and axial loads. Depending on load condition, level of axial load, and amount and distribution of vertical and horizontal reinforcement, two distinct load-deformation mechanisms can be identified. One is the flexural mechanism characterized by the tensile yielding of edge vertical reinforcement and/or compressive crushing of masonry at the toe of the wall panel. The other one is the shear mechanism characterized by diagonal tensile cracking. Current small-scale results, presented in this study, as well as full-scale experimental studies[127] have indicated that wall panels that fail in a predominantly shear mode exhibit a more brittle behavior than those dominated by flexural failure. However, due to the complexity of the shear cracking mechanism, no effective design criteria have yet been developed to prohibit brittle shear behavior. No theoretical formulation has been developed to give a design tool for partially reinforced masonry shear walls.

Lack of design information for partially reinforced concrete masonry shear walls is restricting structural designers from evolving new uses for this material. This can be overcame by further research on partially reinforced concrete masonry to develop design formulas and recommendations for structural elements[29].

To develop a rational design methodology for partially reinforced masonry shear walls, a better understanding of the behavior of these walls is needed. The shear capacity , the flexural capacity, and also the (physical) geometrical properties of these types of walls are necessary information for the development of a rational design methodology. Based on the experimental and analytical studies presented herein expressions for the geometric properties of partially reinforced walls, shear strength and flexural strength are proposed in the following sections .

7.2 EFFECTIVE AREA - ANALYTICAL FORMULATION

The cross-sectional area of partially reinforced masonry shear wall can be calculated from first principals. Fig. 7.1 shows the cross-section of partially grouted shear walls. From this Figure the area of ungrouted wall (area of face-shell bedding) is :

$$A_{ug} = A_{fs} = 2\, L_w\, t_s$$

Partially grouted area is the summation of ungrouted area and the area of grouted cells

$$A_{pg} = 2\, L_w\, t_s + 1/2\, n\, (l_b + t_w)\, (b - 2\, t_s) \qquad (7.1)$$

The ratio of the area of partially grouted walls can be expressed as:

$$A_{pg} / A_{ug} = 1 + [\, n\ (L_b + t_w)\, (b/\, t_s - 2) / (4\, L_w)\,] \qquad (7.2)$$

where

n = No. of grouted cells

L_b = Unit length

L_w = Wall length

t_s = Face-shell thickness

t_w = Web thickness

b = Wall thickness

A plot of the A_{pg} / A_{ug} ratio verses number of grouted cells n for different wall length L_w represented in Fig. 7.2. It can be noticed from this figure that as the number of grouted cells increases, the ratio increases up to n_{max} (fully grouted). A ratio close to 1.0 indicates very little increase in area due to grouted cells, i.e. large spacing of vertical steel.

The above formula is proposed to determine the area of partially grouted masonry shear walls, and has the following advantages:

a- In addition to shear walls this formula can be used for all types of walls like flexural walls where in this case $L_w = S$ and $n = 1$, where S is the spacing between grouted cells as shown in Fig. 7.1.b

$$A_{pg} / A_{ug} = 1+[(1/4\ S) (L_b + t_w) (b/t_s - 2)] \qquad \text{per spacing S}$$

b- This formula is valid for all cases starting from fully grouted walls to hollow walls (ungrouted) , where

For ungrouted walls $n = \text{zero}$

$$A_{pg} = A_{ug} = A_{fs} = 2\ L_w\ t_s \qquad \text{Area of face-shell bedding}$$

For fully grouted walls, using a strip of 16 in. = 40 cm. (full unit), $n = 2$

$$A_g = A_{ug} [1+\ n (L_b + t_w) (b/t_s - 2)\ / (4\ L_w)]$$
$$A_g = 2\ L_b\ t_s [1+ 2 (L_b + t_w) (b/t_s - 2)\ / (4\ L_b)]$$
$$A_g = 2\ L_b\ t_s + t_s (L_b + t_w)\ (b - 2\ t_s)$$
$$A_g = L_b [\ 2\ t_s + (b - 2\ t_s)]$$
$$A_g = L_b\ b \qquad \text{which is equal to the gross area of one unit}$$

This formula can be further simplified by considering the minimum requirement of face-shell and web thicknesses specified by ASTM C-140, where

$$b / t_s = 5.4 \qquad t_w = 0.06\ L_b$$

$$A_{pg} / A_{ug} = [1+ (0.9\ n\ L_b / L_w)] \qquad \text{for Shear Walls} \qquad (7.3)$$

$$A_{pg} / A_{ug} = [1+ (0.9\ n\ L_b / S)] \qquad \text{for Flexural Walls}$$

7.3 EFFECTIVE MOMENT OF INERTIA-ANALYTICAL FORMULATION

For the wide spacing of grouted cells in partially reinforced masonry walls it is unlikely that the full thickness of the wall will be effective in resisting lateral loads. For assessing the slenderness effect of the shear walls in the weak axis (out-of-plane direction) the effective moment of inertia of the cross-section of the wall should be calculated. The wall inertia is dependent upon the configuration of the units, mortar bedding area and the number of grouted cells. The moment of inertia of partially reinforced masonry walls could be calculated as follows:

$$I_{\text{partially grouted}} = I_{\text{face-shell}} + I_{\text{grouted cells}}$$

$$I_{pg} = 2\,[\,L_w t_s^3 / 12 + L_w t_s (b - t_s)^2 /4\,] + n\,[\,1/2(L_b + t_w)\,(b-2t_s)/12\,]$$

This formula can be simplified by considering the minimum specified face-shell and web thicknesses specified by ASTM C-140 where :

$$b = 5.4\,t_s \qquad t_w = 0.06\,L_b$$

$$I_{pg} = 2\,[\,L_w t_s^3 / 12 + L_w t_s (4.4\,t_s)^2 /4\,] + n\,[\,1/2(1.06\,L_b)\,(3.4\,t_s)/12\,]$$

$$I_{pg} = 9.85\,L_w t_s^3 + 1.75\,L_b t_s^3$$

$$I_{ug} = 9.85\,L_w t_s^3$$

$$I_{pg} / I_{ug} = 1 + 0.18\,n\,(L_b / L_w) \qquad (7.4)$$

As can be seen from this formula that the moment of inertia about the weak axis is mainly dependent upon the numbers of grouted cells for the same block type. The above formula is valid for ungrouted, partially grouted, as well as fully grouted walls. However, it has the disadvantage of neglecting the composite action of different materials (concrete blocks, mortar, grout and steel reinforcement). This would not result in an appreacable error because units, mortar and grout are more compatible for concrete masonry within

practical range of material properties. In addition, the steel percentage for partially reinforced masonry is very low so that the effect of steel on the moment of inertia can be ignored.

7.4 SHEAR STRENGTH

7.4.1 General

The ability of masonry structures to withstand lateral loads depends on the resistance of shear walls to the lateral loads. This resistance is dominated by the in-plane shear strength .

Similar to reinforced concrete, the shear strength of reinforced masonry walls depends upon several mechanisms such as the aggregate interlock forces, the dowel action of the vertical steel , the truss action of the flexural steel and shear reinforcement[107]. A physical model based on the analogy of combined truss and arch mechanisms has been proposed by Wakabayashi and Nakamura[144] for reinforced masonry shear walls. Nevertheless, the validity of this model for wall panels of effective aspect ratios greater than or equal to one is questionable because the arch mechanism is not likely to dominate once the major diagonal crack has developed.

7.4.2 Formulas for Reinforced Masonry Shear Walls

Empirical formula based on the normal concrete theory (potential shear crack inclined at 45° crosses the entire width of the wall) was proposed by Priestley[110] for calculating the shear force resisted by reinforced masonry shear walls in seismic regions. This formula depends mainly upon the shear reinforcement and aspect ratio of the wall. He assumed that, within the potential plastic hinge region wide flexure- shear cracks and the effects of load reversals are likely to reduce severely the efficiency of the components contributing to masonry shear strength, namely compression shear transfer, aggregate interlock, and dowel action. In such regions all shear consequently should be carried by shear reinforcement (masonry shear- resisting mechanisms are ignored) .

Akira Mastumura[89] proposed a formula based on experimental data, to predict the ultimate shear strength of reinforced masonry walls under different conditions such as various shear reinforcement ratios, shear-span ratios, axial stresses, strengths of materials

as well as two kinds of grouting, namely partially grouting and fully grouting. In this formula, the shear reinforcement is proportional to $(p_h f_y f'_m)^{1/2}$ which takes the combined action of the horizontal reinforcement and the strength of masonry for the part carried by shear reinforcement.

Based on the experimental data, a new formula was proposed by Shing[126] for calculating the shear strength of reinforced masonry shear walls similar to UBC-91[141], but taken into consideration the effect of the amount of vertical steel and the applied axial stress for the residual strength of masonry. This formula can be expressed as:

$$V_m = [0.0018 (p_v f_y + \sigma_c) + 2] A (f'_m)^{1/2} \quad (7.5)$$

$$V_s = [(L-2d) / s - 1] A_h f_y \quad (7.6)$$

where:

f_y = the yield strength of steel

A_h = the area of horizontal steel bars

σ_c = axial stress

A = the horizontal net cross-section area of the shear wall

s = the vertical spacing of the shear steel

f'_m = the nominal strength of masonry

L = the horizontal length of a wall

d = the distance of the extreme vertical steel from the edge of a wall

A comparison between UBC formula, Shing's formula, Mastumura's formula and Architectural Institute of Japan's formula were presented by Fattal and Todd[44] to study the accuracy of these formulas to predict the ultimate shear in masonry walls failing in shear. Their main conclusion was that for the range of studied parameters, both the UBC formula and the formula proposed by the Architectural Institute of Japan were found to be inadequate for the prediction of ultimate shear strength of masonry walls. The equation

proposed by Shing was found to predict the ultimate shear for only limited range of variables. The equation predicted by Mastumura was found to provide the best prediction of the four equations examined, but it lacks the consistency needed to be used for design.

It can be observed from Shing's formulae that, only the effect of the interior reinforcement is considered for the shear resistance and not all the horizontal reinforcement. Also the rate of increase of the normalized masonry strength with respect to the axial stress and the vertical steel has been taken based on an average slope of 0.0018 .

Similar to the ACI requirements (ACI 318-83) for reinforced concrete, a semi-empirical formula is adopted in the UBC-91 for calculating the shear strength of reinforced masonry shear walls. According to this formula, the nominal shear strength is [$V_n = V_m + V_s$] in which the residual shear strength of masonry after diagonal cracking is [$V_m = 1.2\ A\ (f'_m)^{1/2}$], where is the effective cross-section area of the shear wall, for walls with aspect ratio greater than or equal one and the resistance of horizontal reinforcement is [$V_s = A_{ph}\ f_y$]. It is specified in the code that the nominal shear strength of reinforced masonry shear walls Vn should not exceed $4\ A\ (f'_m)^{1/2}$. These specifications evidently are more conservative than the ACI requirements for reinforced concrete shear walls.

7.4.3 Proposed Formula for Partially reinforced masonry

As mentioned before, the nominal shear strength of partially reinforced masonry shear walls depends upon several mechanisms such as the aggregate interlock forces , the dowel action of the vertical steel and the truss action of the flexure and shear reinforcement. Following ACI 318 design for reinforced concrete and UBC-91 code for reinforced masonry, the nominal shear strength of partially reinforced masonry shear walls V_n can be expressed:

$$V_n = V_m + V_s \qquad (7.7)$$

In which

V_m is the residual strength of masonry after diagonal cracking

V_s is the shear strength of horizontal steel reinforcement

The ultimate shear loads, obtained experimentally for all the specimens dominated by shear failure, are divided by the effective horizontal area A_{pg} to get the ultimate shear strength τ_u and then normalized by dividing it by $(f'_m)^{1/2}$. The resulting normalized ultimate strength $\tau_u / (f'_m)^{1/2}$ is plotted in Fig. 7.3 against wall number to compare the experimental results with the maximum requirements specified by the UBC-91 code[141]. From this Figure it can be noticed that the $\tau_u / (f'_m)^{1/2}$ for the experimental results varies from 3 to 5 depending on the amount and distribution of steel reinforcement and the level of axial load. It is to noted that the UBC formula does not take into account the contribution of axial load and vertical steel in the calculation of residual strength. The formula considers all the horizontal steel, including top and bottom bars, to be equally effective in resisting shear .

The shear resistance of horizontal reinforcement should be estimated as based on the interior reinforcement only[126]. The interior reinforcement can be activated by a 45^o diagonal crack, while the top and bottom reinforcing bars do not have adequate development length to develop tensile resistance as shown in Fig. 7.4 (for shear walls having aspect ratio (h/d) equals one but for shear walls having (h/d) greater than one, only the top bars are taken into account and neglecting the bottom ones). Hence, it is reasonable in the case of partially reinforced masonry shear wall to propose the following formula for the shear resistance of the horizontal steel:

$$V_s = (m - 2) A_h f_y \qquad (7.8)$$

Where

m = the total numbers of bond beams in a shear wall

A_h = the cross-sectional area of the horizontal steel in bond beam

f_y = the yield stress of horizontal steel

It has been generally observed that the horizontal steel will not be activated until a diagonal cracking occurs. After diagonal cracking, the residual strength of masonry V_m is affected by several mechanisms namely, the shear resistance of masonry in compression toe Vc, the aggregate interlock forces V_a , and the dowel forces of the flexural reinforcement V_{di} as indicated in Fig. 7.4. The aggregate interlock forces depends on the applied axial stress and the amount of vertical steel, both of which resist crack opening and thereby enhance the aggregate-interlock forces.

Based on Equation. 7.8 the values of V_s were calculated for all the specimens dominated by shear failure and subtracted from the total shear strengths Vault obtained experimentally to get the measured values for V_m. The V_m obtained is then divided by the net horizontal area of wall panel A_{pg} as calculated from Equation. 7.1 and normalized by dividing it by $(f'_m)^{1/2}$. The resulting normalized masonry shear strength $\tau_m/(f'_m)^{1/2}$ is plotted in Fig. 7.5 against wall number for all shear specimens to compare the results with those obtained using the UBC Equations. As shown in the figure, the ratio $\tau_m/(f'_m)^{1/2}$ varies from about 3 to 4.2 for partially reinforced masonry and the code specification of 1.2 for reinforced masonry. This is because the code does not take into consideration the factors that affect on the residual strength of masonry. It can be noticed that UBC is apparently overconservative .

As mentioned before, the residual strength of masonry depends on the applied axial stress as well as the amount of vertical steel.

To examine the effect of axial stress, the $\tau_m/(f'_m)^{1/2}$ ratio is plotted against the axial stress σ_a. The rate of increase of the ratio $\tau_m/(f'_m)^{1/2}$ with respect to σ_a is 0.01 as indicated in Fig. 7.6.a, therefore

$$\tau_m/(f'_m)^{1/2} / \sigma_a = 0.01$$

$$\tau_m = 0.01\ \sigma_a\ (f'_m)^{1/2}$$

$$V_m = 0.01\ A_{pg}\ \sigma_a\ (f'_m)^{1/2}$$

Also to examine the effect of vertical steel, the $\tau_m/(f'_m)^{1/2}$ ratio is plotted against $p_v\ f_y$ and the rate of increase $\tau_m/(f'_m)^{1/2}$ with respect to $p_v\ f_y$ is 0.01 as shown in Fig. 7.6.b, therefore

$$\tau_m/(f'_m)^{1/2} / p_v\ f_y = 0.01$$

$$\tau_m = 0.01\ p_v\ f_y\ (f'_m)^{1/2}$$

$$V_m = 0.01\ A_{pg}\ p_v\ f_y\ (f'_m)^{1/2}$$

Based on the average slope of 0.01 of the rate of increase of the normalized masonry strength, the following formula for V_m is proposed:

$$V_m = [\ 1.2 + 0.01\ (p_v\ f_y + \sigma_a)\ ]\ A_{pg}\ (f'_m)^{1/2} \qquad (7.9)$$

where A_{pg} is the horizontal cross-sectional area of the partially reinforced masonry shear wall, and is calculated from Equation. 7.1

The proposed formula predicts the shear strength of partially reinforced masonry shear walls with reasonable accuracy. The coefficient 0.01 which exceeds the coefficient predicted by Shing (0.0018) for fully reinforced masonry indicates that both vertical steel and axial stress have a greater influence on partially reinforced masonry than on fully reinforced masonry. Also the coefficient 1.2, which is less than the coefficient 2.0 predicted by Shing indicates that the residual strength of masonry in partially reinforced masonry (almost plain masonry) is less than in case of fully reinforced masonry (fully grouted masonry). This is expected because in case of fully grouted walls, the grouted

cores provide continuity which helps to give masonry more resistance to tensile stress .

According to Equations. 7.7, 7.8, and 7.9 the nominal shear strength is evaluated for all the shear-dominated specimens and compared with the experimental results as presented in Fig.7.7. The comparison showed that the new formula consistently gives lower values than the experimental results and is sensitive to different design variables. Also it can be seen that the UBC formula grossly underestimates the nominal shear strength and is conservative compared to Shing's formula. This is because UBC formula does not reflect the effect of axial stress and vertical steel on the residual strength of reinforced masonry shear walls.

To further evaluate the proposed formula, the shear resistance of the horizontal reinforcement for all the shear-dominated specimens obtained from the new formula, UBC formula, Shing's formula and Priestley's formula are considered and plotted against wall number. The comparison of these formulas is indicated in Fig. 7.8. It can be noticed that the proposed formula and Shing's formula are almost the same whereas the UBC formula and Priestley's formula are close but overestimate the shear resistance. The reason is that both the UBC and Priestley's formulas take into account the area of the top and bottom reinforcing bars in the calculations, in addition to the internal bars in resisting the shear strength. The proposed formula and Shing's formula take only the intermediate horizontal steel.

The overall correlation of the proposed formula with the experimental results is excellent while the code formula substantially underestimates the residual strength of masonry but overestimates the shear resistance of the horizontal reinforcement. Recapitully UBC formula for reinforced masonry appears to be conservative.

Examination of Equation 7.7 for predicting the residual strength of partially grouted masonry indicates that the most significant parameter is the axial stress on the residual strength. The effect of different parameters on the residual strength of masonry is shown in Fig. 7.9. It can be observed that increasing the axial stress up to 15% of prism compressive strength (0.15 f'_m) results in an increase in the residual strength by about

180%. Moreover, as the compressive strength of masonry increases, the residual strength increases by the rate of square root of the gain in compressive strength. The yield strength of vertical steel shows a low increase rate in the residual strength. This rate increases as the percentage of vertical steel and the compressive strength of masonry increases. The plots presented in figure 7.9 could be considered as design charts where the residual strength of partially reinforced masonry shear walls could be obtained in forms of yield strength of vertical steel, compressive strength of masonry, and axial stress . Intermediate values of f_y, ρ_v and f'_m may be obtained by linear interpolation.

7.5 FLEXURAL STRENGTH

7.5.1 General

The flexural mechanism of shear wall panels subjected to axial and lateral loads is characterized by tensile yielding of the vertical reinforcement and/or compressive crushing of masonry at the toe of the wall panel. This type of failure results in a more ductile behavior compared to the shear mode of failure .

In general two types of approaches have been used to calculate the flexural strength of masonry shear walls. The first is based on the allowable stress (working stress) of the materials. In this approach the structural element is assumed to behave linearly elastic . The other method is based on the ultimate strength of the material, which is already widely used for reinforced concrete design, takes into account the behavior of the element beyond the elastic limit. The load and strength reduction factors that are determined from the probabilities of the failure must be applied.

The 1991 UBC code contains provisions for the calculation of nominal flexural strength of reinforced masonry shear walls. The effectiveness of the strength design approach greatly depends on the validity of these design provisions. It has been generally recognized that the simple flexure theory can be satisfactorily used to predict the flexural strength of slender reinforced concrete and masonry shear walls[113]. Design charts and tables for ultimate flexural strength of reinforced masonry shear walls with uniformly distributed steel over the length of the wall were developed by Priestley[113]. These charts and tables were based on ideal or nominal material strengths that is, strength reduction factors have not been directly incorporated. Comparison of flexural strength of walls with uniformly distributed steel with equivalent walls where the steel is concentrated at the wall ends with a maximum reasonable local steel ratio showed that there is a little loss resulting from uniformly distributed the steel. The slight reduction in flexural strength is more than compensated for improving the shear transfer when using uniform steel[113] .

7.5.2 Proposed Formula for Partially Reinforced Masonry

Using the simple flexural theory based on the assumption that plane sections remain plane after bending as stated in the 1991 UBC code, Shing[126] evaluated the nominal axial strength and moment capacity of a wall section with symmetrically distributed flexural reinforcement. The accuracy of this formula depends on the validity of the stress block as well as the kinematic assumptions. Klamerus[84] has observed from finite element analysis that the variation of flexural strain with respect to the distance from the neutral axis is far from being linear after the development of flexural cracks .

For these reasons, Shing has examined the sensitivity of the theoretical results to the values of the stress block parameters β & γ and the flexural strain variation. He concluded that, the influence of the section distortion and the value of β on the interaction diagram curve is negligible, and that the value of γ is significant only when a wall is in the tension-dominated part of interaction curve, so the simple formula would be valid.

Fortunately, as has been found for reinforced concrete shear walls, slenderness is usually not a major factor and this extra complexity can usually be avoided. Because of this, the ACI 530/ASCE approach for reinforced masonry which places limits on the magnitude of axial load to guard against significant effects of slenderness, is a simple and efficient method of design.

A number of investigators[107] have suggested the replacement of the actual shape of compressive stress block by an equivalent rectangular block as a mean of simplification. The equivalent rectangular block has been used for reinforced concrete members[107]. The rectangle block has a mean stress of $0.85\, f'_c$ and a depth of $\beta\, c$ where $\beta = 0.85$ for $f'_c \leq$ 4000 psi (280 kg/cm^2) ; β is reduced continuously by 0.05 for each 1000 psi (70 kg/cm^2) of strength in excess of 4000 psi. The reduction in β for high strength is not the case of masonry concrete block where f'_m usually less than 4000 psi. Therefore in this

analysis the value of β should be taken as o.85 without reduction

In this investigation, previous procedures are evaluated and utilized to determine the flexural strength of partially reinforced masonry shear walls. The basic assumptions made for the theoretical development of the flexural strength are as follows:

1- Plane section remains plane after deformation

2- The distribution of masonry compressive strength at ultimate moment is approximated by a rectangular stress block with stress level of 0.85 and a length of 0.85c, where c is the distance from the fiber of maximum strain to the neutral axis.

3- The maximum strain allowed by UBC at the extreme compression fiber is 0.003

4- The stress in the reinforcing bars f_s below the yield strength f_y is taken as the modulus of elasticity times the steel strain. When the steel achieves a strain ε_s greater than or equal to the strain at yield ε_y, the stress in the steel is considered independent of the strain and equal to the yield stress f_y

5- Masonry tensile strength is taken equal zero.

For cases where the axial load is relatively small and relatively light vertical reinforcement is used (case of partially reinforced concrete masonry) the small compression zone would result in a strain distribution that ensures yielding of virtually all the steel when the ultimate moment capacity is reached. The analysis of such walls is best carried out by assuming first that all the steel is yielded, then modifying the calculations later if it is found that some or all the steel is not reach the yield strength .

Figure 7.10 shows the strain and forces for partially reinforced masonry shear walls. From this figure:

$f_s = f'_s = f_y$ If all the steel is yielded, the internal forces are:

Compression in the masonry	$C_c = 1.445\ c\ t_s\ f`_m [1 + 4.6/c\ ]$
Compression in steel	$C_s = A`_s\ f_y$
Tension in steel	$T = A_s\ f_y$

Applying the static equilibrium of the internal forces

$$C_c + C_s = T + P_n$$

$$P_n = 2\gamma\beta c t_s f'_m [1 + 0.9 L_b n / c] - (A_s - A`_s) f_y \qquad (7.10)$$

To simplify this equation by substituting $\beta = 0.85$, $\gamma = 0.85$ & $n = 1$ for partially reinforced masonry shear walls where only one grouted cell is contained in the compression zone for most cases.

$$P_n = 1.445\, c\, t_s f'_m [1 + 0.9 L_b / c] - (A_s - A`_s) f_y$$

From this equation, it can be observed that the depth of the neutral axis from the extreme compression fibers c is given by

$$c = \frac{f_y (A_s - A_s^{'}) + P_n - 1.3 L_b t_s f_m^{'}}{1.445\, t_s f_m^{'}} \qquad (7.11)$$

By considering the strain gradient shown in Fig. 7.10, the above equation can be used to check whether the steel is yielding or not. The steel is at yield stress if its strain exceeds f_y/E_s . From similarity of the triangles of the strain diagram (Fig. 7.10)

Steel under tension

$$\varepsilon_s = \varepsilon_u (d-c) / c \qquad (7.12)$$

Steel under compression

$$\varepsilon`_s = \varepsilon_u (c-d) / c \qquad (7.13)$$

In case of Equations 7.12 and 7.13 result in the steel being not yielded, the depth of the neutral axis should be calculated again using the actual stress (f_s) in the steel instead of the yield stress (f_y) , where $f_s = \varepsilon_s E_s$

In this case an iterative procedure involving the satisfaction of the requirements of equilibrium of forces and compatibility of strains should be used to determine the position of the neutral axis to satisfy equilibrium .

The moment capacity of the wall panel is dependent upon the compressive strength of the masonry and the amount and distribution of vertical steel. Taking moments at point of application of axial load P_n (Fig. 7.10) yields:

$$M_n = C_c (L_w / 2 - \beta c / 2) + C_s (L_w / 2 - d_i) + T (L_w / 2 - d_i)$$

$$M_n = 0.723 c t_s f`_m [1 + 0.9 L_b / c] (L_w - 0.85 c) + \Sigma A_{si} f_{si} (L_w / 2 - d_i) \qquad (7.14)$$

The moment capacity M_n of the partially reinforced masonry shear walls can be calculated from Equation 7.14 where

A_{si} = the cross-section area of bar i

d_i = the distance of a bar i from compression edge

f_{si} = the stress in reinforcing bar i

c = the distance from neutral axis to compression fiber

L_w = the shear wall length

f'_m = the uniaxial compressive strength of a prism

L_b = the nominal block length

E_s = the elastic modulus of steel

Flexural Strength Reduction Factor

A flexural strength reduction factor is necessary as a factor of safety for design due to possible under-strength materials, dimensional tolerances, construction defects and inaccuracies in analysis. Values are recommended[110] for masonry shear walls varying from 0.65 to 0.85 based on the level of axial load. The ultimate flexural strength can be expressed as:

$$M_u = \phi M_n \tag{7.15}$$

where

$\phi = 0.85$ for zero axial stress

$\phi \geq 0.65$ for $0.1\, f'_m$ axial stress, an intermediate values for ϕ may be calculated by linear interpolation between $\phi = 0.85$ and $\phi = 0.65$ as the axial stress decreases from $0.1 f'_m$ to zero .

It is apparent from the experimental results that the flexural strength of partially reinforced masonry shear wall increases with the magnitude of the applied axial stress and the quantity of vertical reinforcement present. To assist the evaluation of test results, the ultimate moment capacity of the three flexural-dominated walls were calculated using Priestley's methods (the actual distribution of the steel and concentrated steel at the edges).

A comparison between the proposed formula, Priestley formulas, Shing formula and the experimental results is presented in Fig 7.11. It can be observed that the results obtained from the proposed formula are closed to that obtained from Shing's formula, since the two methods are based on the same ultimate strength design methodology. The results show that the proposed formula overestimated Priestley's formulas by about 19% & 15% for the distribution and concentrated steel reinforcement cases, respectively. This is expected since in Priestley's formula the total area of steel is replaced by an equivalent

lamina over the length of the wall for distributed steel. When an equivalent partial lamina is used for concentrated steel, the resultant of the tension force becomes closer to the neutral axis and therefore, the corresponding ultimate moment capacity decreases. The proposed formula considers the actual position of the steel reinforcement.

The comparison shown in Fig. 7.11 demonstrates that the proposed formula consistently underestimated the experimental results by about 16% for level of axial stress of 0.05 f'_m but at zero axial stress it overestimated the experimental results by about 6% This can be explained by the fact that, when no axial stress was applied, the bond slip and the partial pull-out of the tension reinforcement from the footing were very severe in the test, thereby the tension strain as well as the strain-hardening of the flexural reinforcement was reduced. In general, it can be concluded that the proposed formula is conservative for the range of parameters presented .

The moment capacity is normalized by $f'_m L^2_w t$, where t is the nominal thickness of wall and L_w is the length of the wall. The axial load is normalized by $f'_m L_w t$. The normalized capacity is plotted against the normalized axial load to get the interaction curves for flexure strength of partially reinforced masonry shear walls as shown in Fig. 7.12. The curves are plotted with four ratios of vertical steel and two values of yield strength: Grade 40 (2800 kg/cm^2) and Grade 60 (4200 kg/cm^2) for 32, 56 & 104 in (0.8, 1.44 & 2.64 m) spacing of vertical steel.

The interaction curves show that the distribution of vertical steel has a significant effect on the flexural strength of partially reinforced masonry shear walls. To clarify the comparison of the different vertical steel spacing, the ratios of the normalized moment of walls have spacing of 56 in. (1.44 m) Type A to walls have spacing 104 in. (2.64 m) Type B and the ratios of normalized moment of walls have spacing of 32 in. (0.8 m) Type C to walls have spacing 104 in. (2.64 m) Type B are plotted against the normalized axial load in Fig. 7.13. The trends are clear, it can be seen that the concentration of vertical steel results in a significant flexural strength enhancement. Type B gives 20% & 30% higher than Type A & C respectively. Elastic theory indicates that the concentrated steel at the wall ends

results in a moment about 33% higher than for the distributed reinforcement.

From the interaction curves presented in Fig. 7.12 the effect of spacing (concentrated bars versus distributed bars) of vertical steel can be studied as ia presented in Fig. 7.13. As can be observed the moment capacity of partially reinforced masonry shear walls with concentrated steel (spacing 104 in. = 2.64 m) is higher than for uniform bars distribution (spacing 32 in. = 0.81 m) particularly for higher level of axial load. On the other hand, for lower level or zero axial load, the normalized moments are almost the same. The flexural capacity is insensitive to the steel distribution at low axial stress. Increasing the normalized axial stress causes an increase in normalized moment up to 20% of normalized axial load. This observation is consistent with Priestley's conclusion for fully reinforced masonry walls .

It is also observed that a significant increase in moment capacity due to increasing the percentage of vertical steel is obtained. Values for intermediate values of $\rho\varpi$ may be found by linear interpolation between the two curves.

7.6 EVALUATION OF THE PROPOSED FORMULA

As reported earlier, a formula to predict the shear strength of partially reinforced masonry shear walls is proposed based on experimental data. To further evaluate this formula, the shear strengths for the walls with shear and shear/flexure predominant modes are calculated using the proposed formula and correlated with the analytical results. As shown on Fig. 7.14, the maximum difference between the shear strength calculated from the proposed formula and that obtained analytically is 14%. This illustrates that the proposed formula can accurately predict the shear strength of partially reinforced masonry shear walls.

Table 7.1 Comparison Between Analytical and Proposed Formula

Wall Number	Shear Strength Analytical kips (ton)	Proposed Formula kips (ton)	Difference %
SW2	59.0 (26.8)	63.1 (28.7)	7.0
SW3	77.5 (35.2)	76.4 (34.7)	1.5
SW4	54.8 (24.9)	58.5 (26.6)	7.0
SW7	79.3 (36.0)	83.1 (37.8)	5.0
SW8	48.1 (21.9)	47.8 (21.7)	0.5
SW10	75.3 (34.2)	86.0 (39.0)	14.0

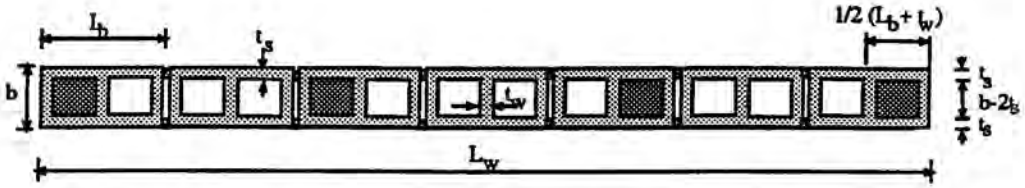

Fig. 7.1.a Typical Cross-Section of Partially Grouted Shear Walls

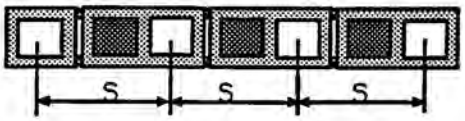

Fig. 7.1.b Spacing of Grouted Cells for Flexural Walls

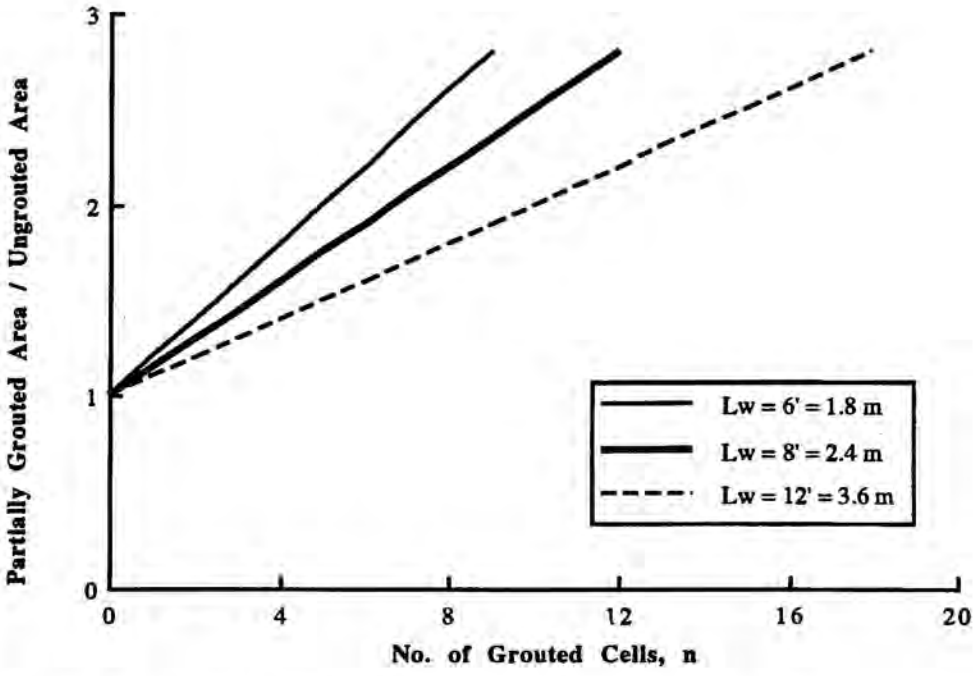

Fig. 7.2 Relationship Between Ratio of Partially Grouted to Ungrouted Area and No. of Grouted Cells

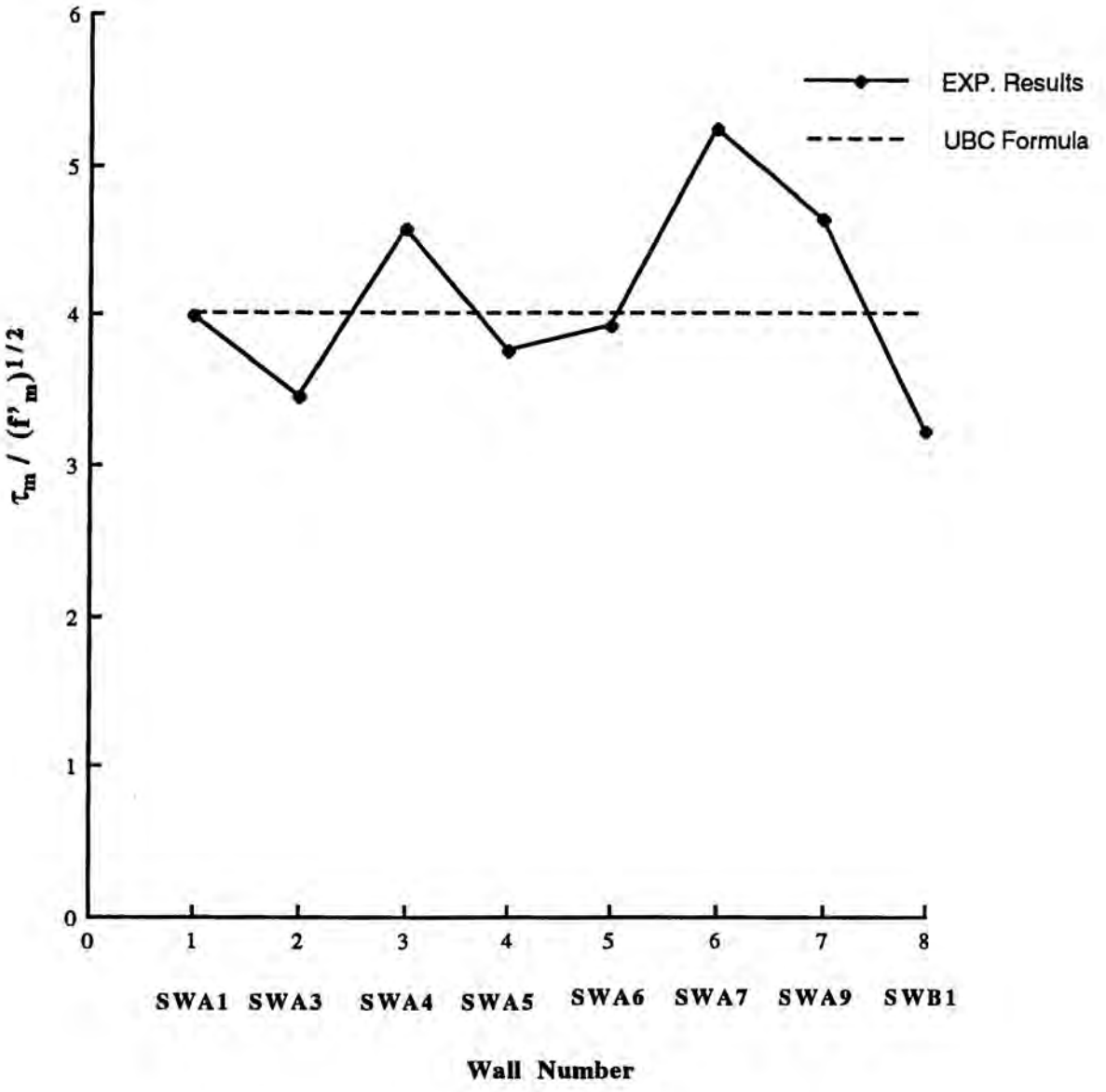

Fig. 7.3 Normalized Shear Strength of Masonry

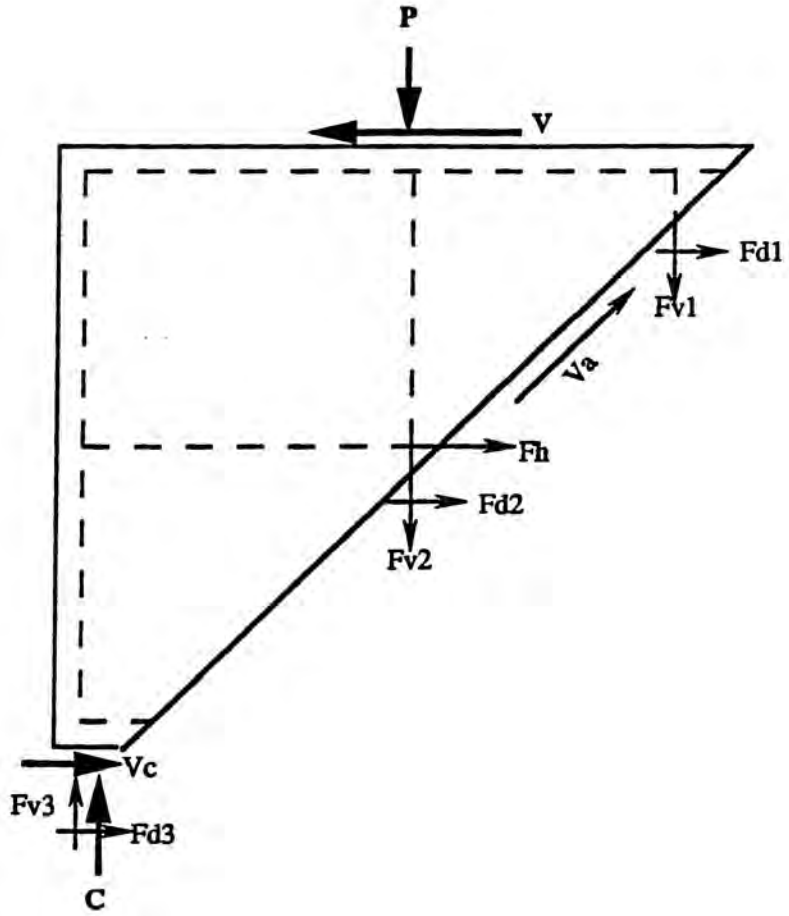

Fig. 7.4 Shear Resistance Mechanism of Partially Reinforced Masonry Shear Walls

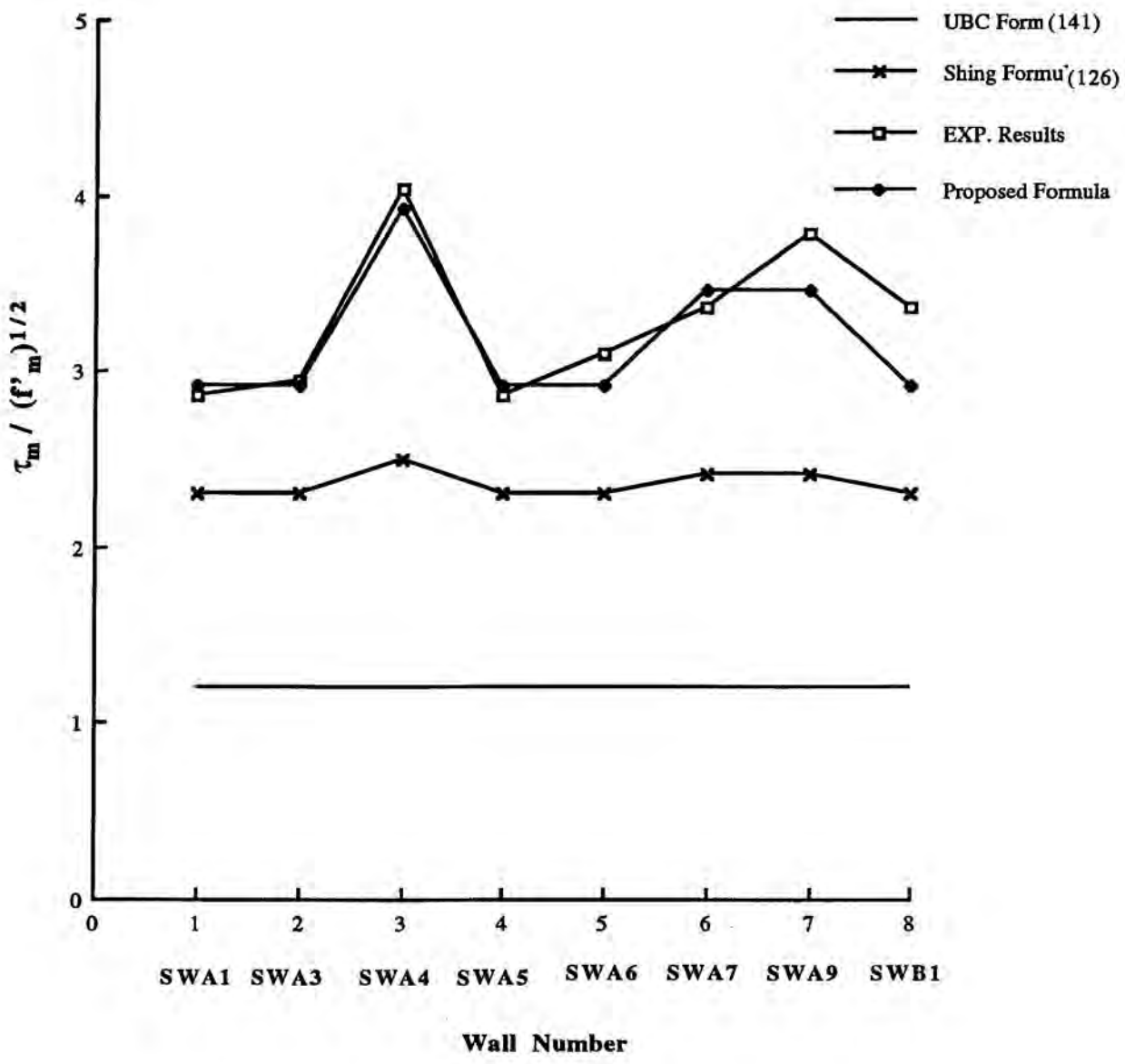

Fig. 7.5 Normalized Residual Strength of Masonry

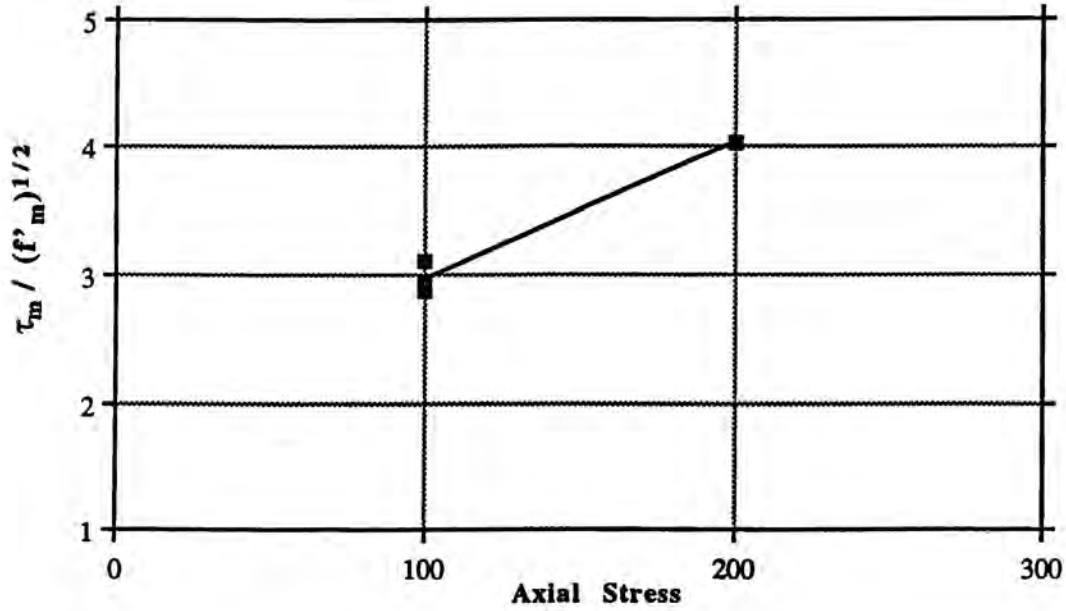

Fig. 7.6.a Effect of Axial Stress on the Residual Strength of Masonry

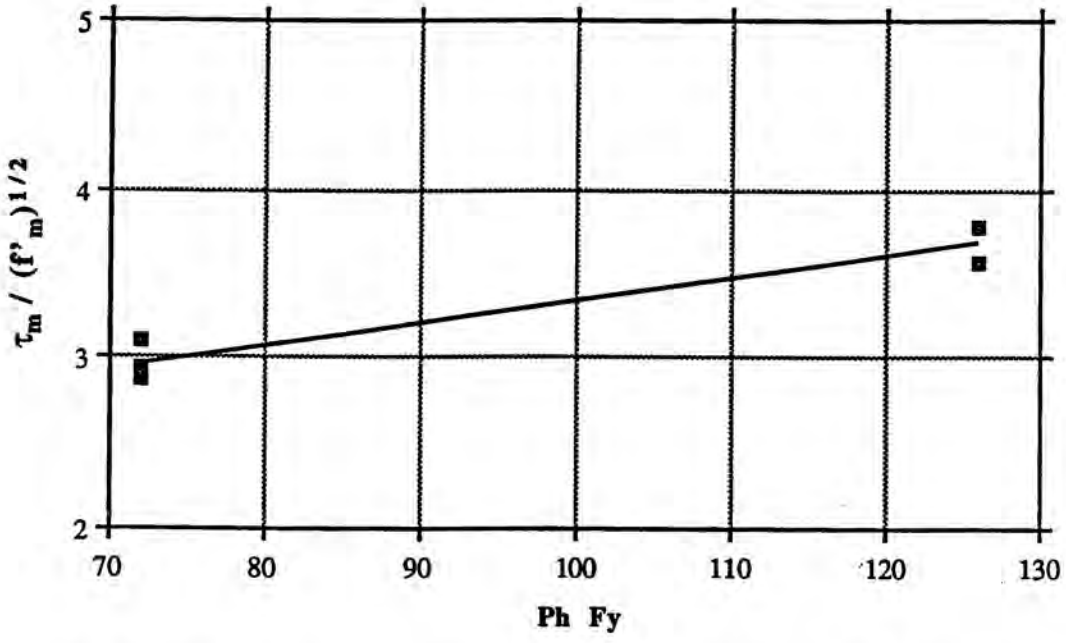

Fig. 7.6.b Effect of Vertical Steel on the Residual Strength of Masonry

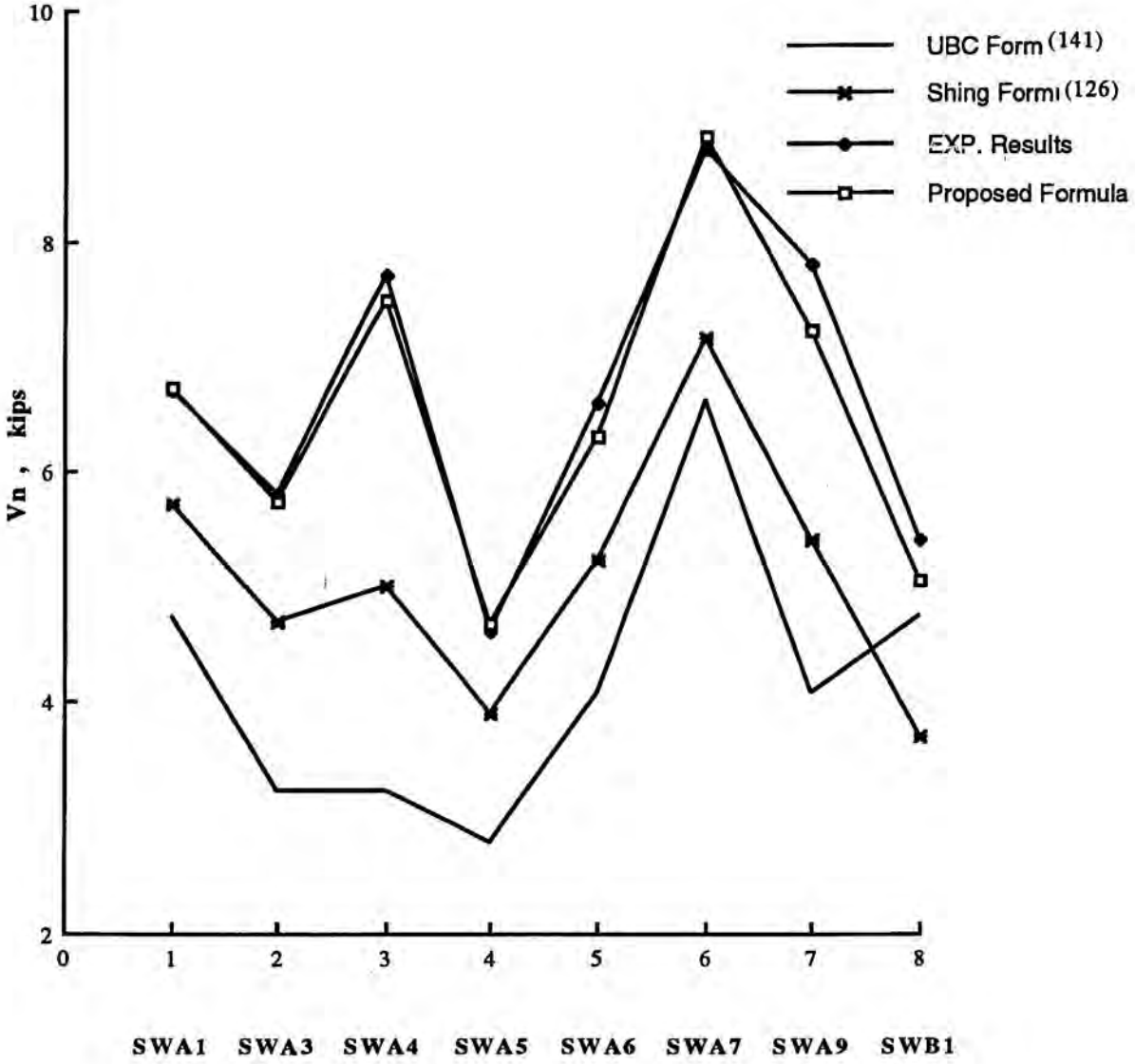

Note: 1 kip = 454 kg

Fig. 7.7 Nominal Shear Strength of Masonry Shear Walls

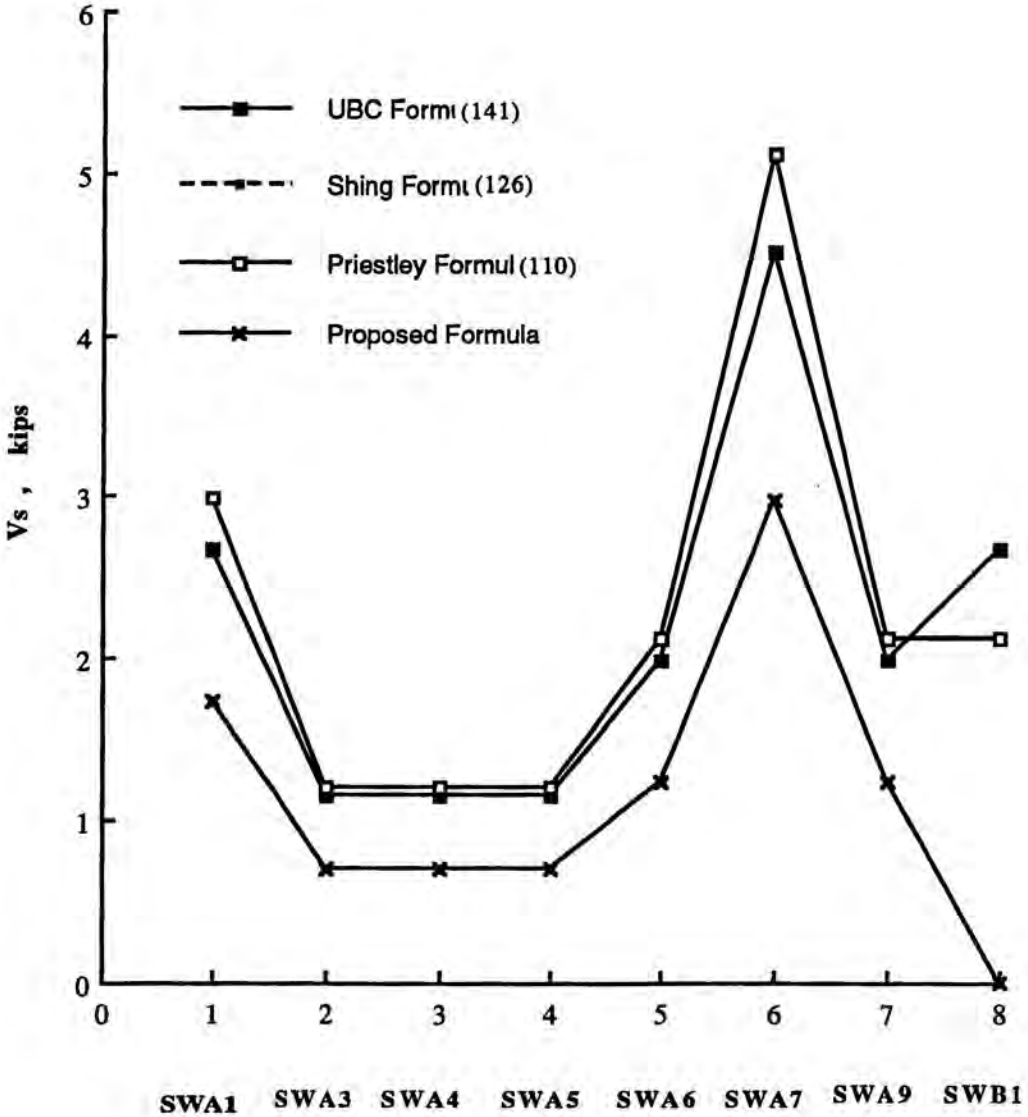

Note: 1 kip = 454 kg

Fig. 7.8 Shear Resistance of Horizontal Reinforcement

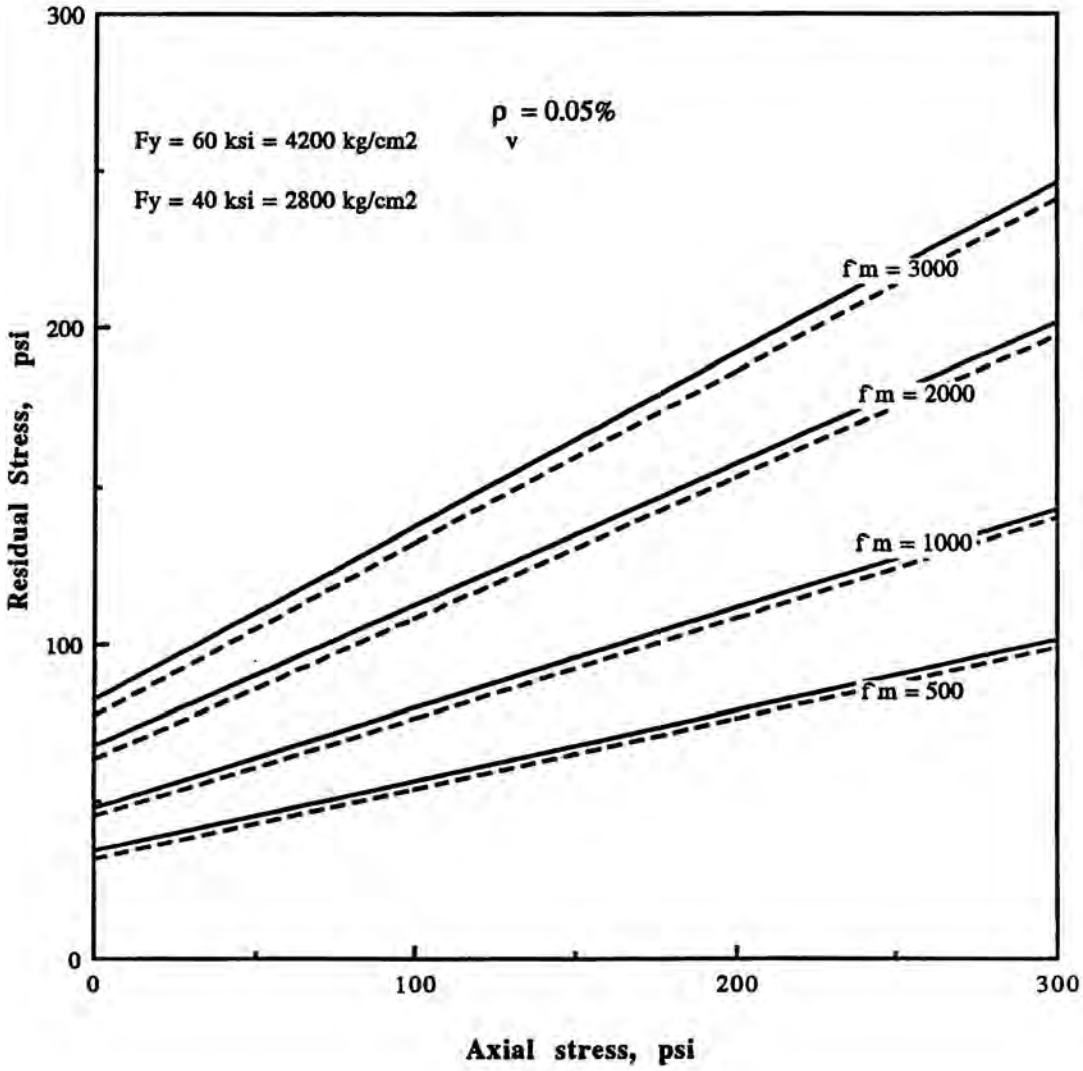

Fig. 7.9a Masonry Residual Stress of Partially Reinforced Masonry Shear Walls (Design Charts)

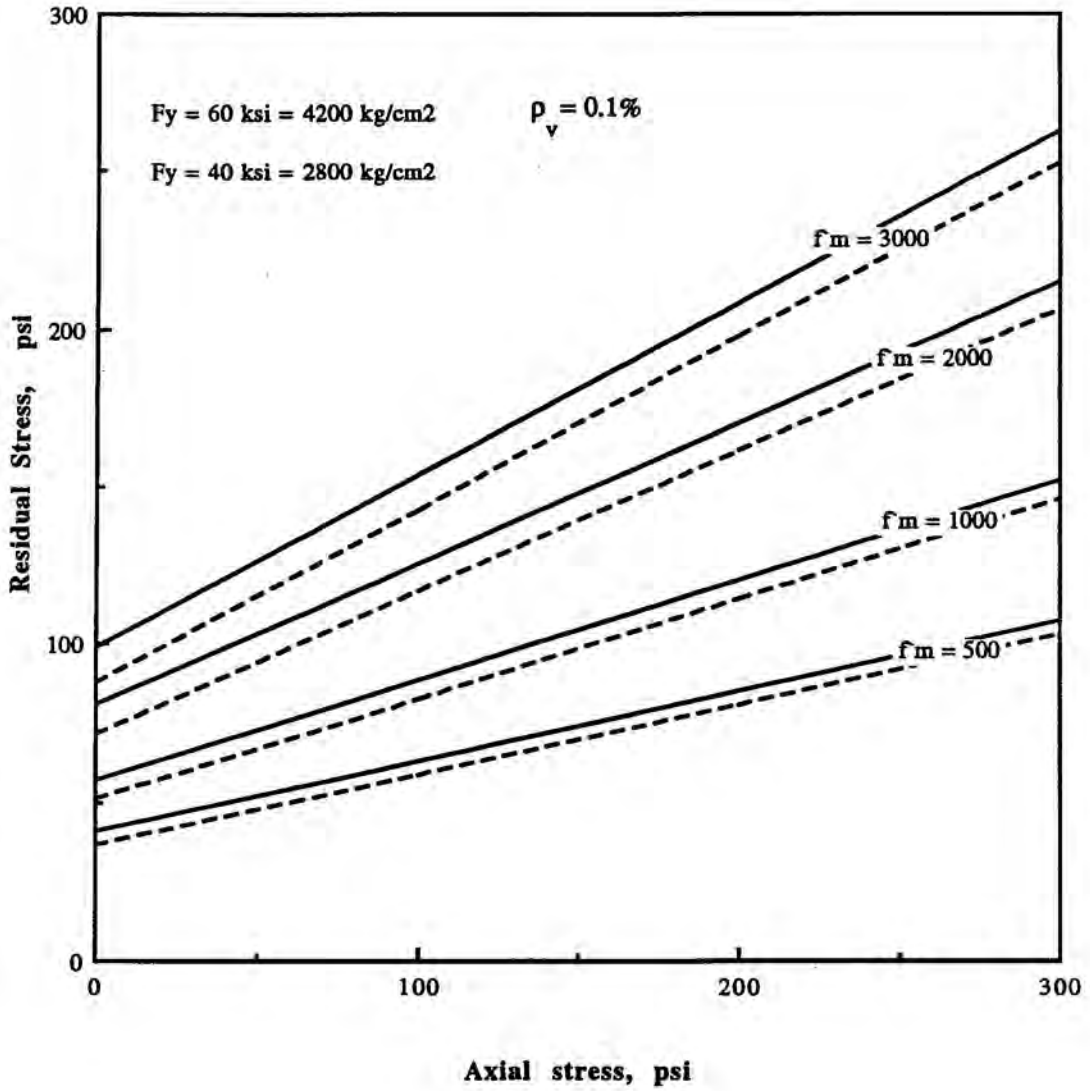

Fig. 7.9b Masonry Residual Stress of Partially Reinforced Masonry Shear Walls (Design Charts)

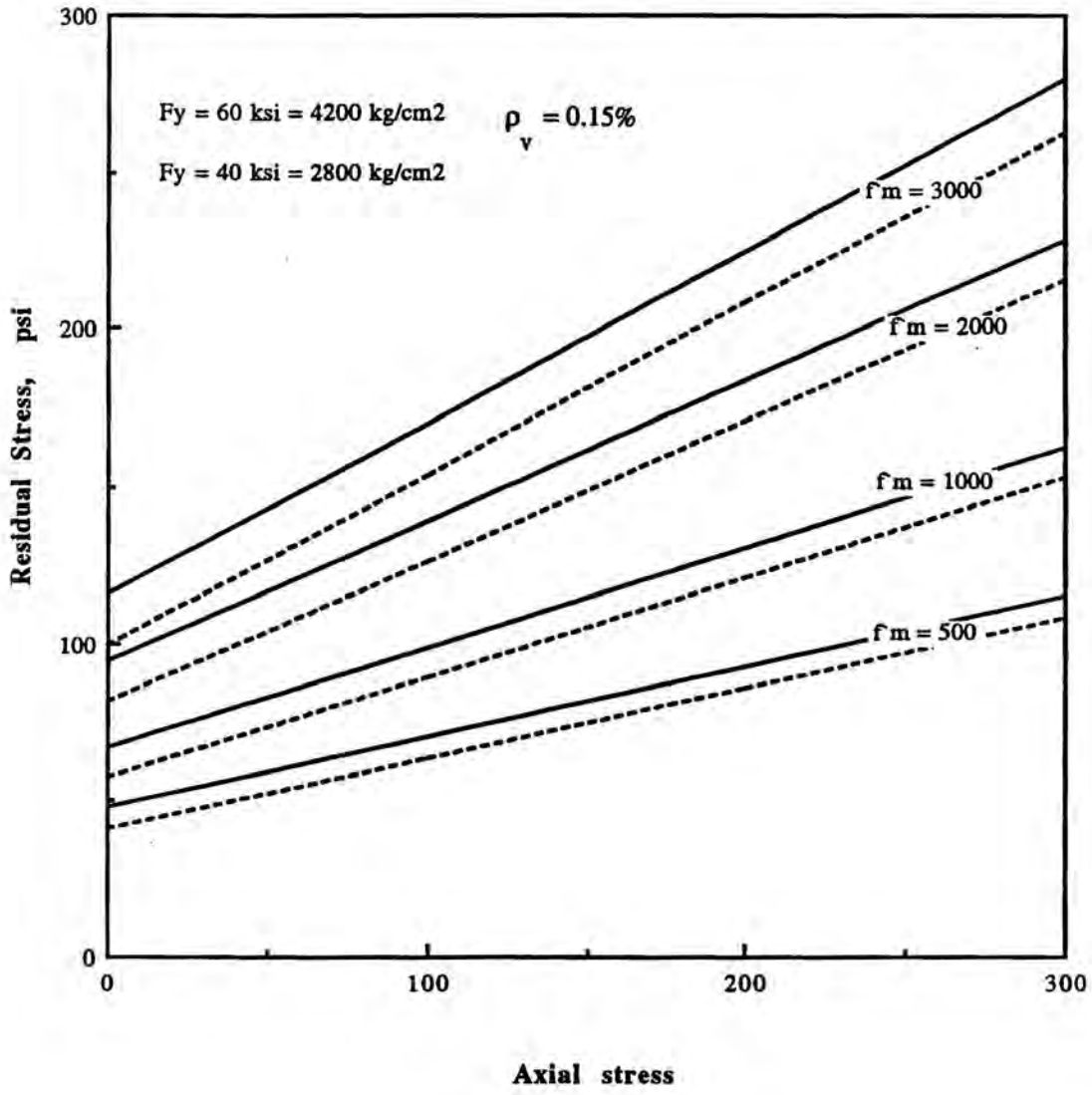

Fig. 7.9c Masonry Residual Stress of Partially Reinforced Masonry Shear Walls (Design Charts)

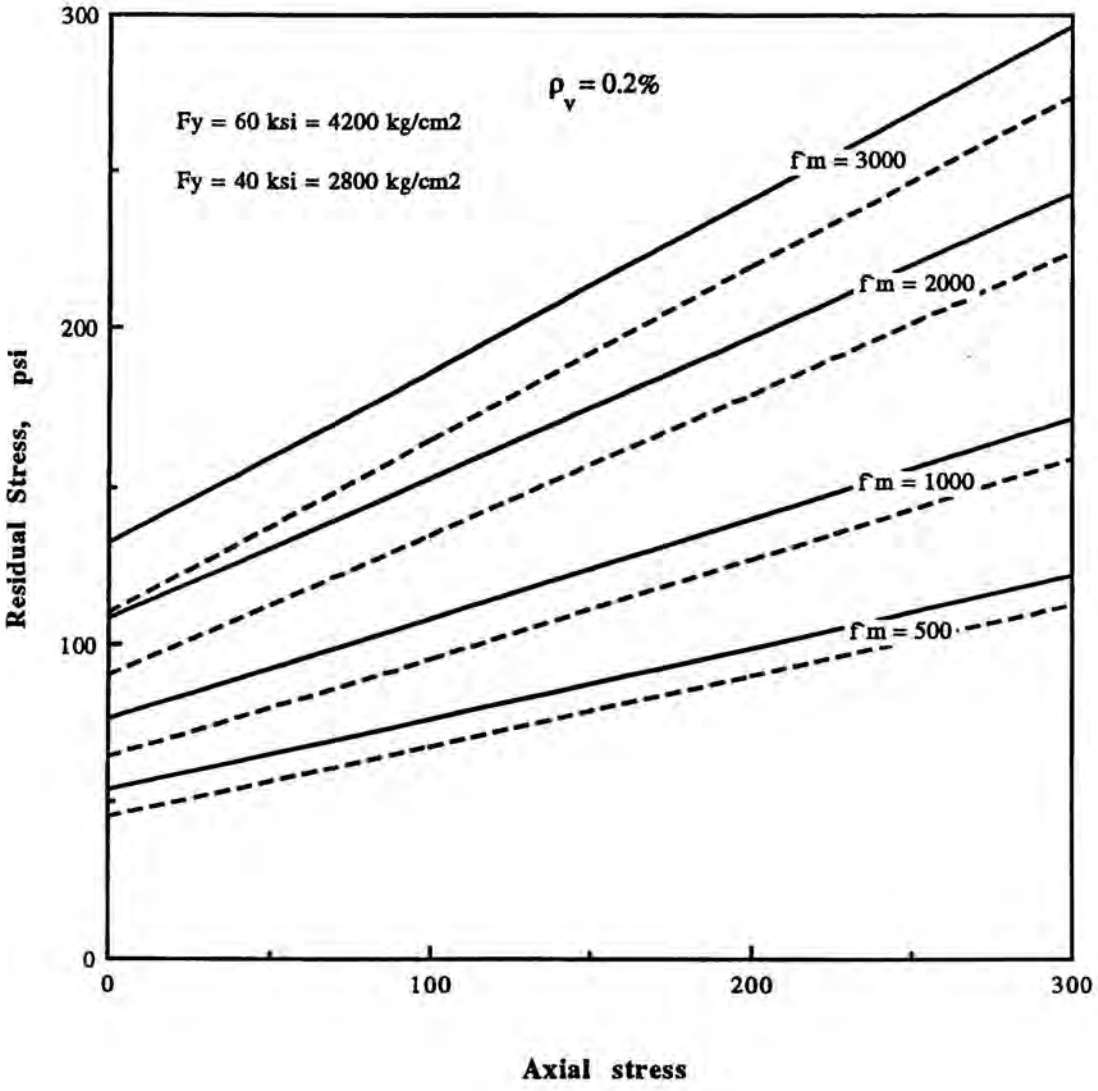

Fig. 7.9d Masonry Residual Stress of Partially Reinforced Masonry Shear Walls (Design Charts)

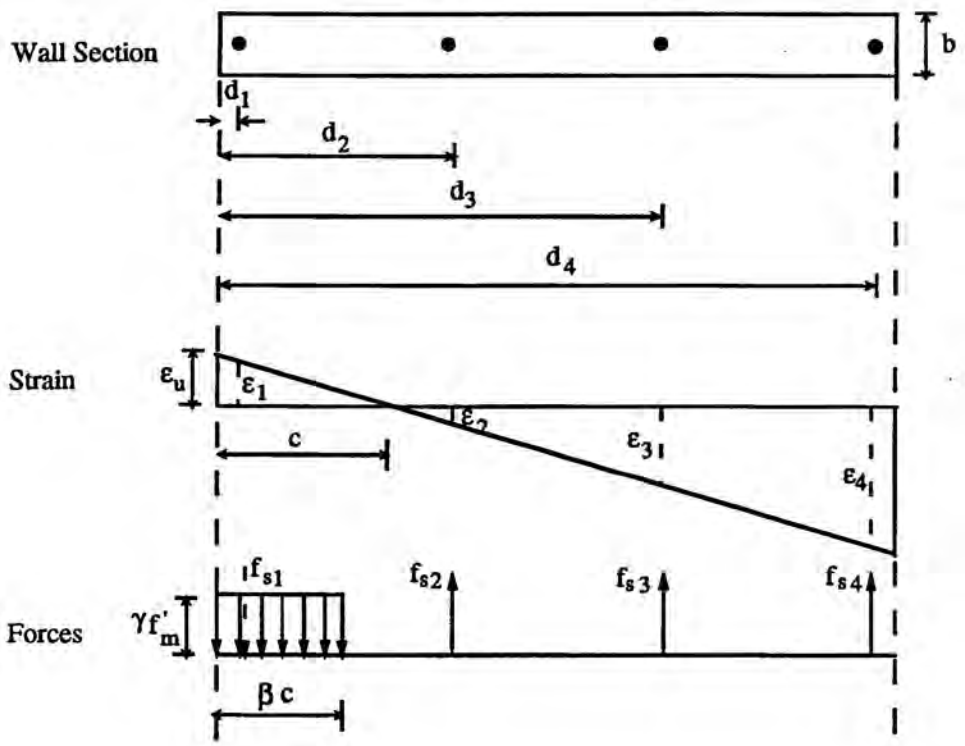

Fig. 7.10 Flexural Strain and Stress of Partially Reinforced Masonry Shear Wall

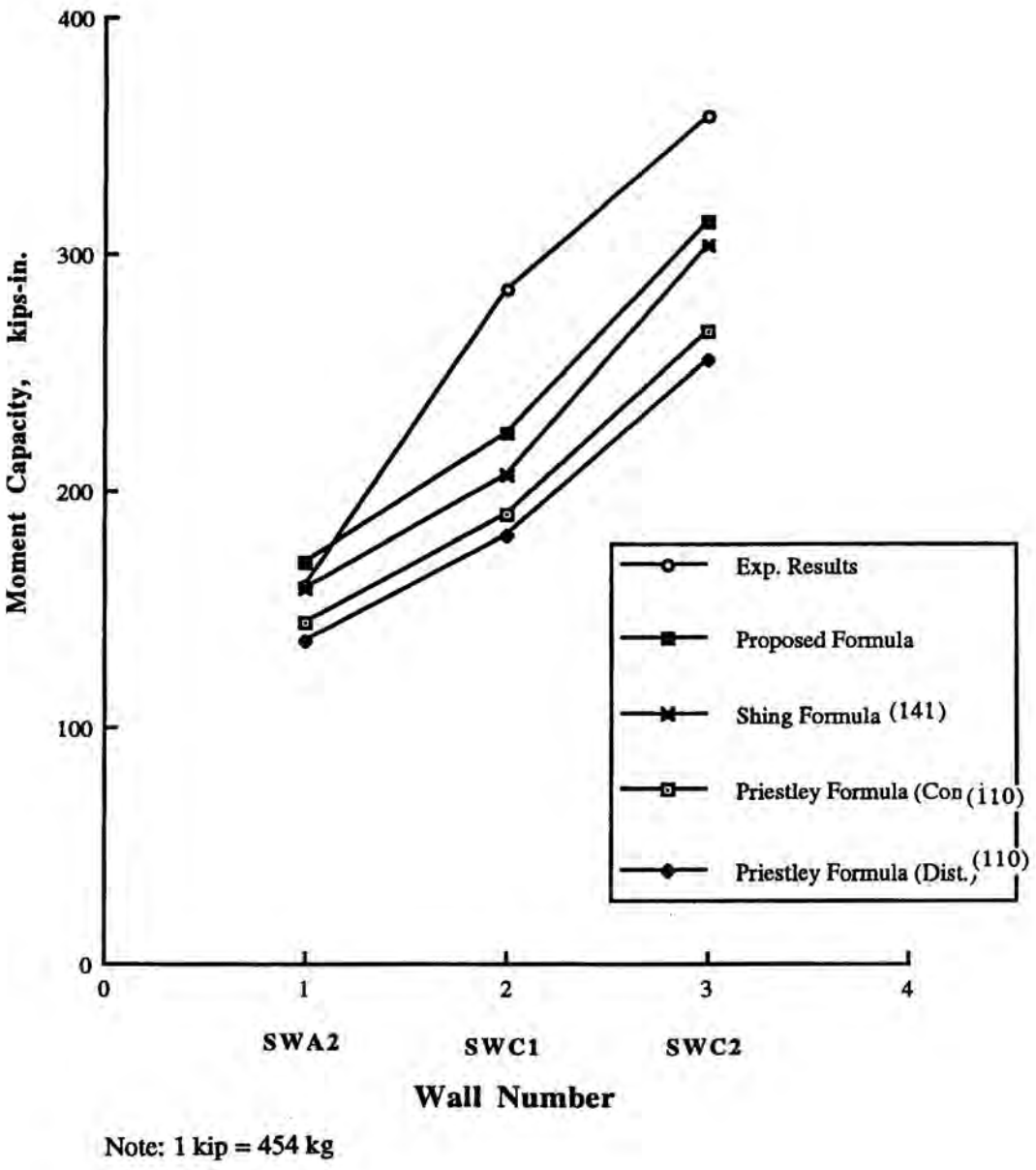

Note: 1 kip = 454 kg

Fig. 7.11 Flexural Capacity of Partially Reinforced Masonry Shear Walls

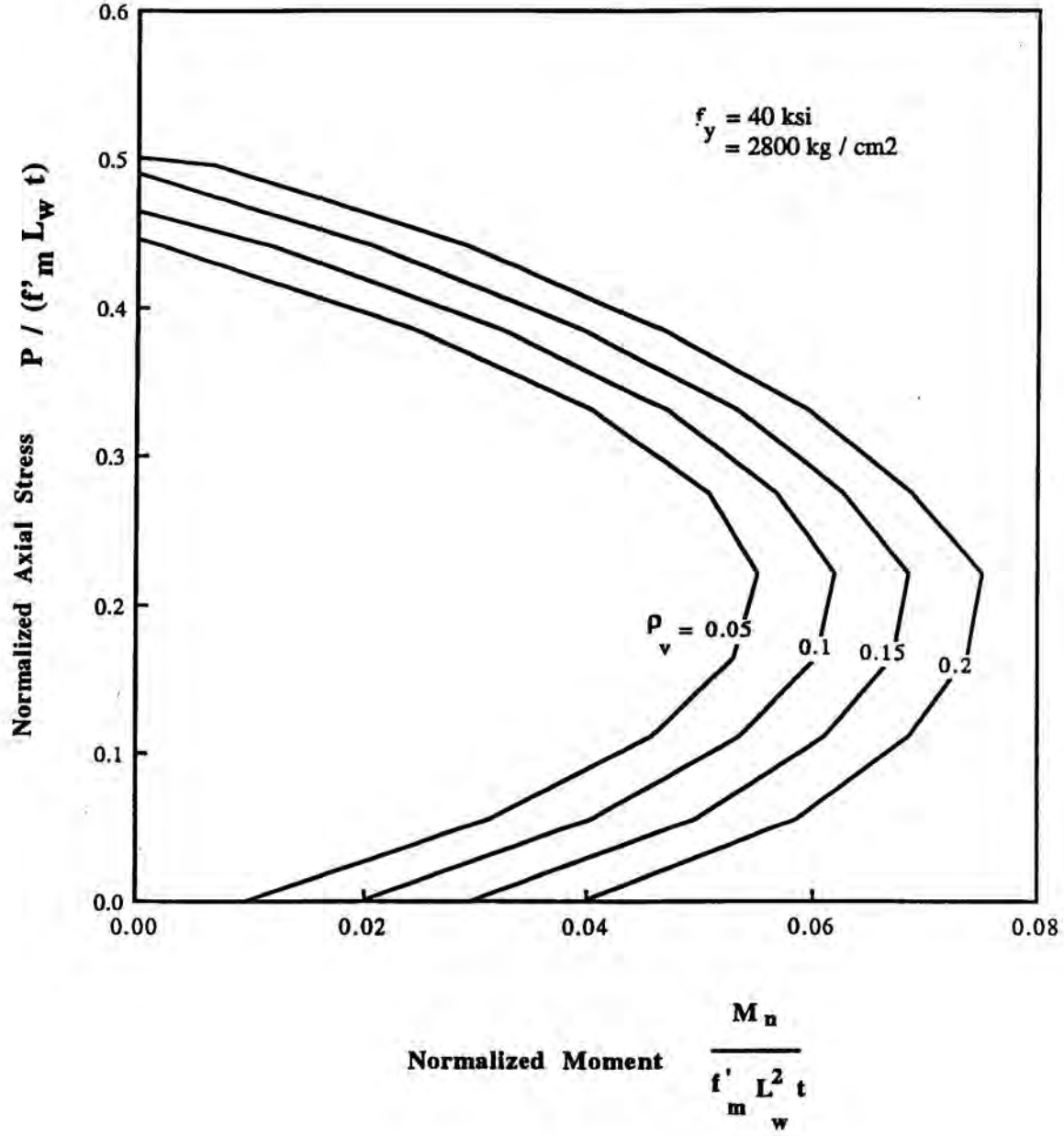

Fig. 7.12a Dimensionless Interaction Curves for Flexure Strength of Partially Reinforced Masonry Shear Walls with Spacing 56 in. (1.42 m.)

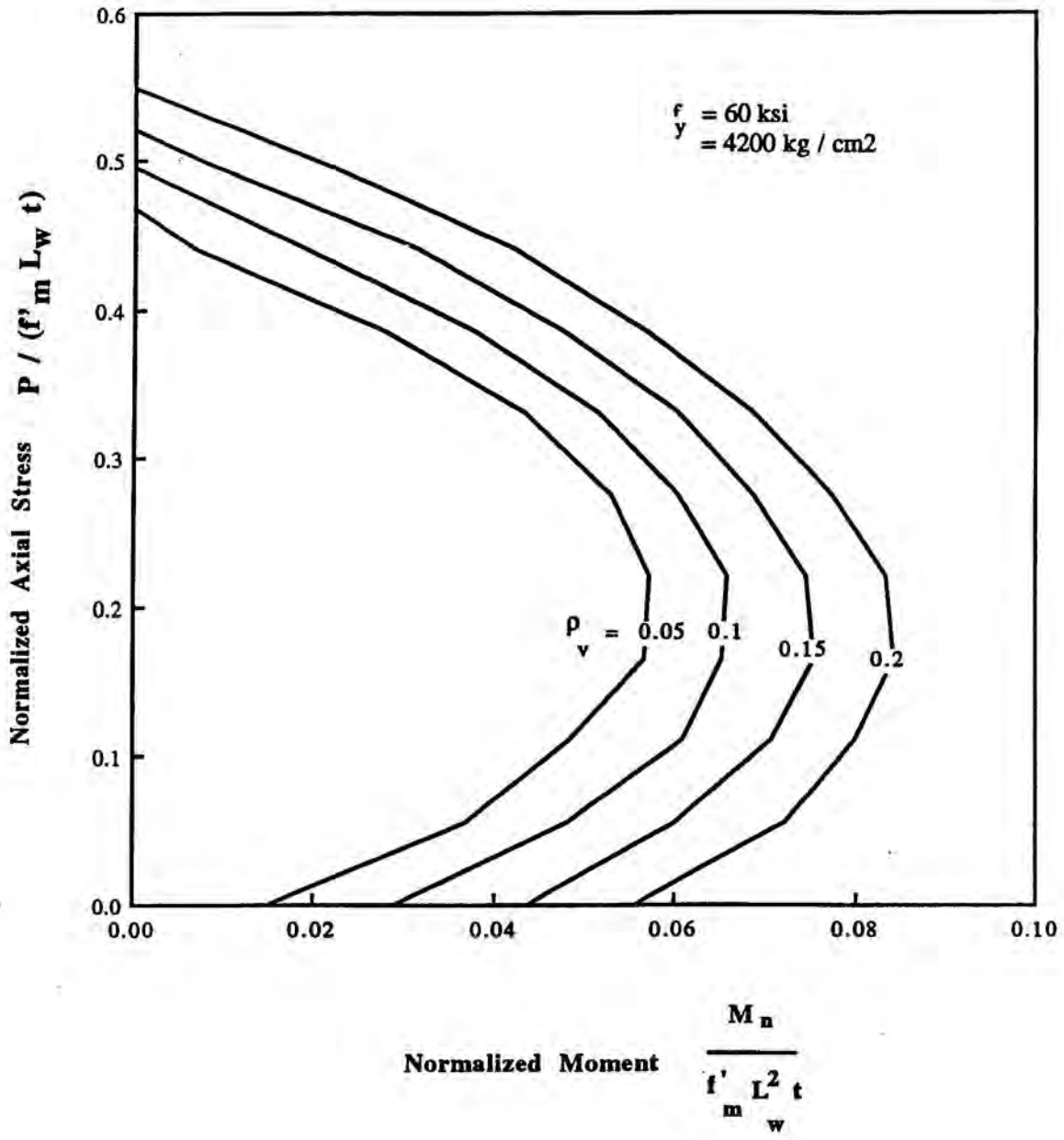

Fig. 7.12b Dimensionless Interaction Curves for Flexure Strength of Partially Reinforced Masonry Shear Walls with Spacing 56 in. (1.42 m.)

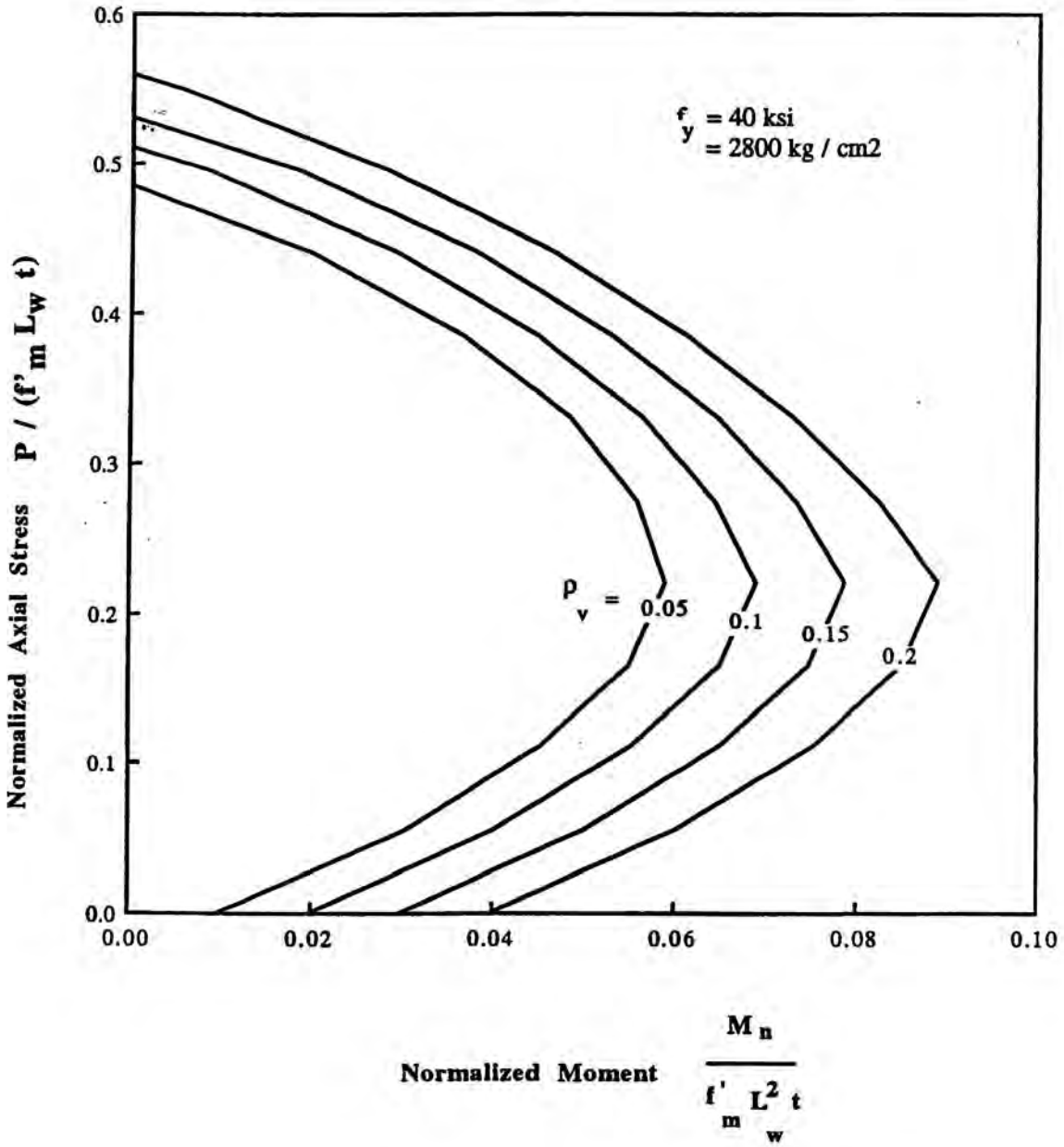

Fig. 7.12c Dimensionless Interaction Curves for Flexure Strength of Partially Reinforced Masonry Shear Walls with Spacing 104 in. (2.64 m.)

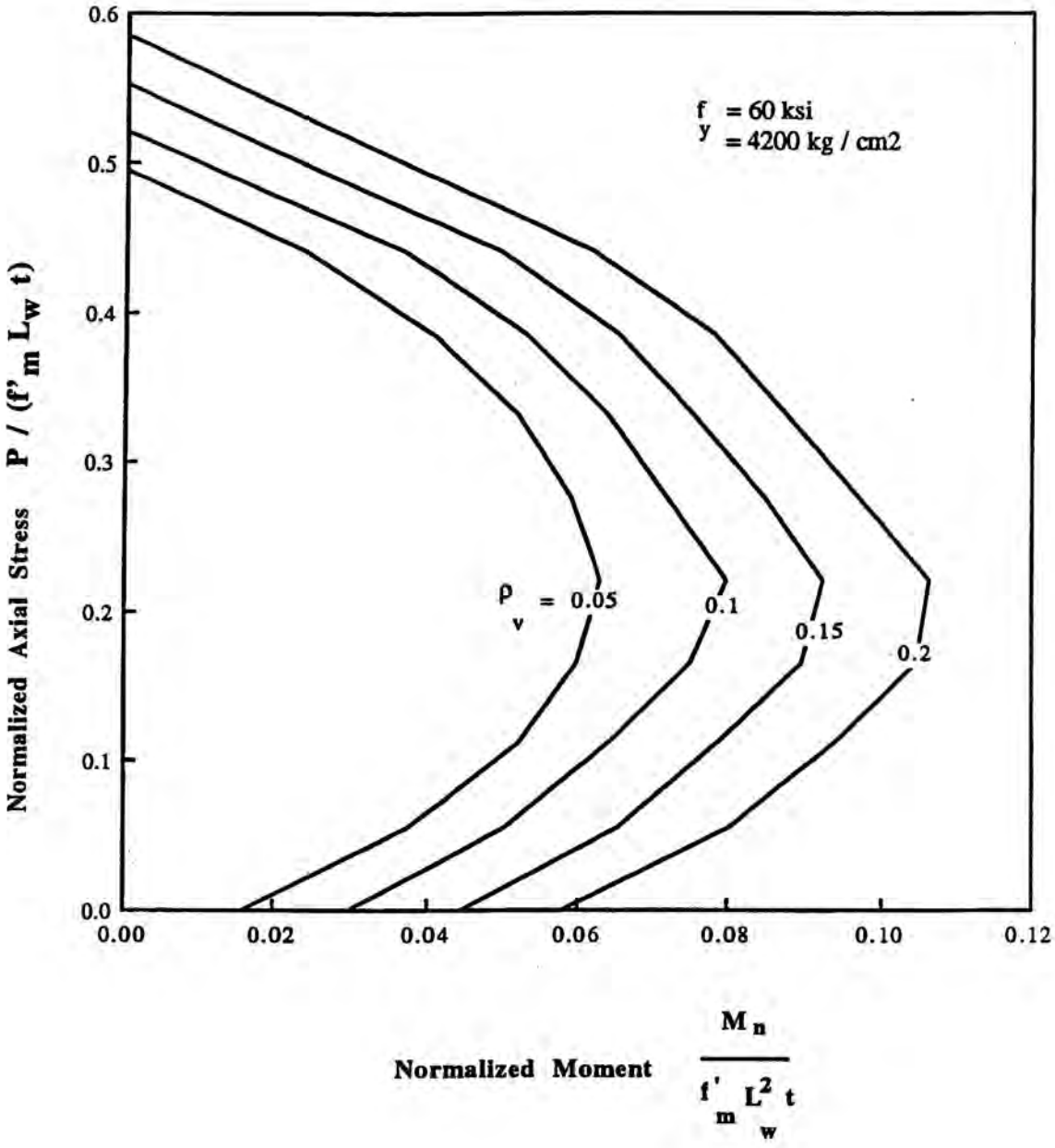

Fig. 7.12d Dimensionless Interaction Curves for Flexure Strength of Partially Reinforced Masonry Shear Walls with Spacing 104 in. (2.64 m.)

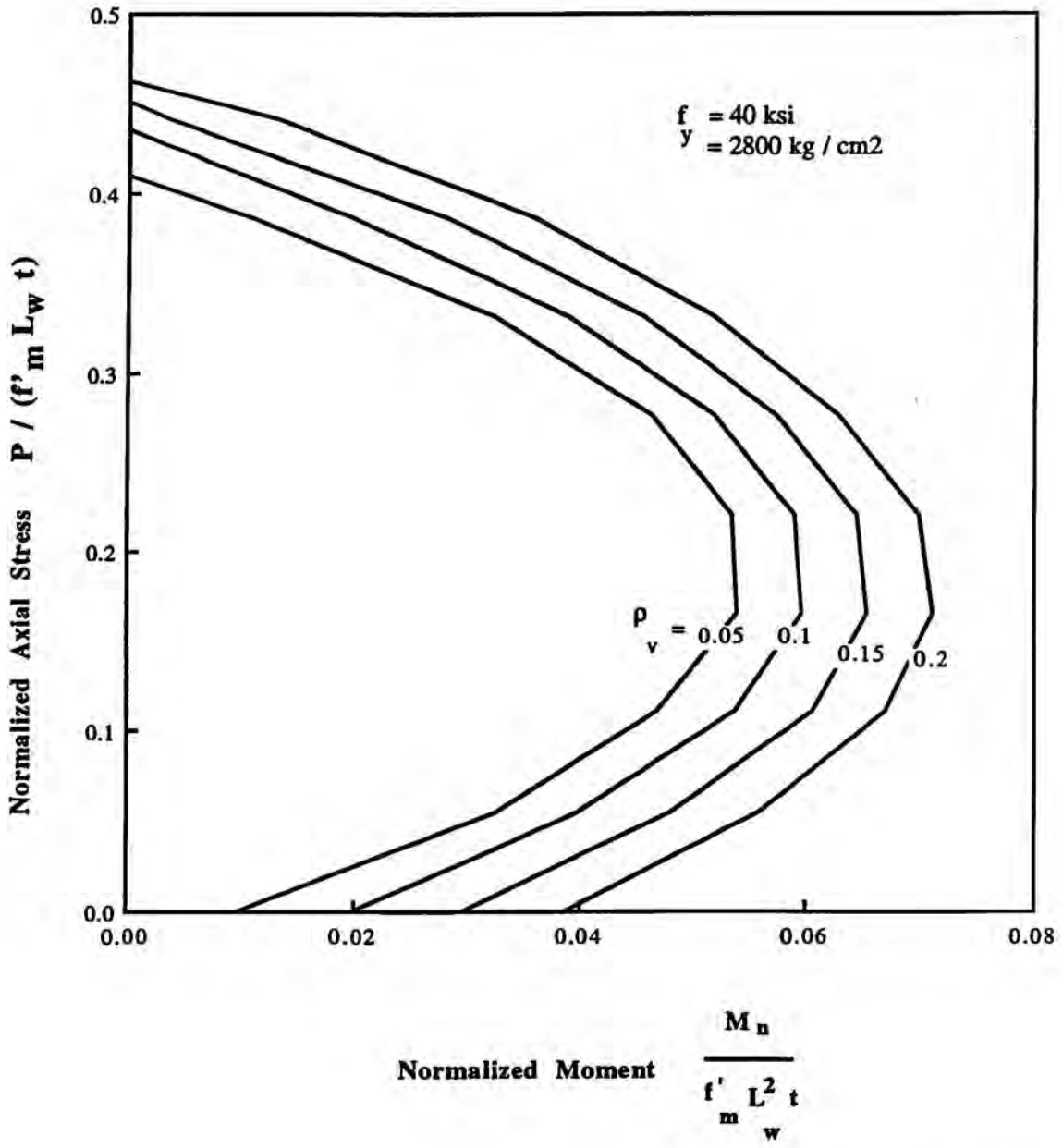

Fig. 7.12e Dimensionless Interaction Curves for Flexure Strength of Partially Reinforced Masonry Shear Walls with Spacing 32 in. (0.81 m.)

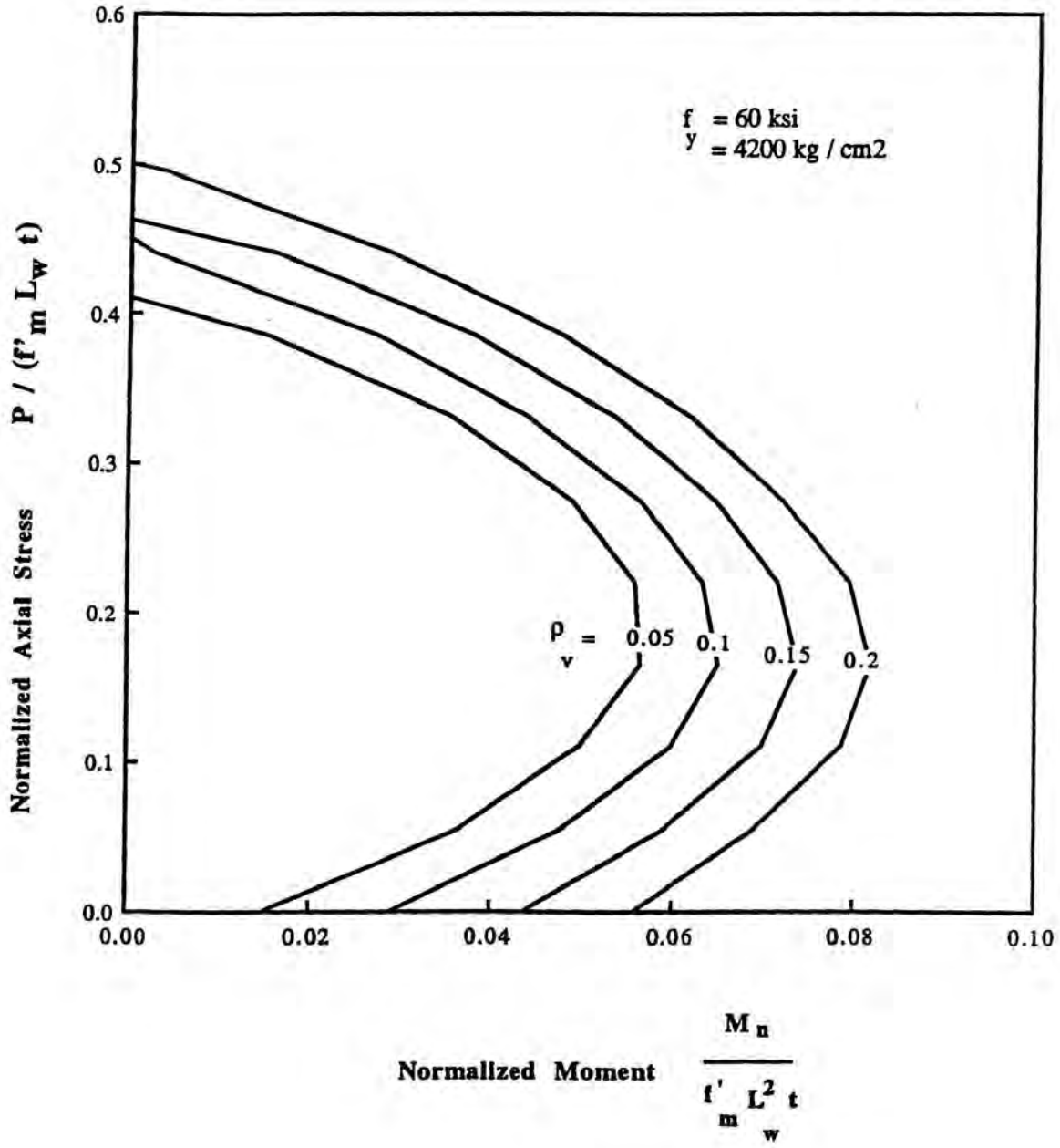

Fig. 7.12f Dimensionless Interaction Curves for Flexure Strength of Partially Reinforced Masonry Shear Walls with Spacing 32 in. (0.81 m.)

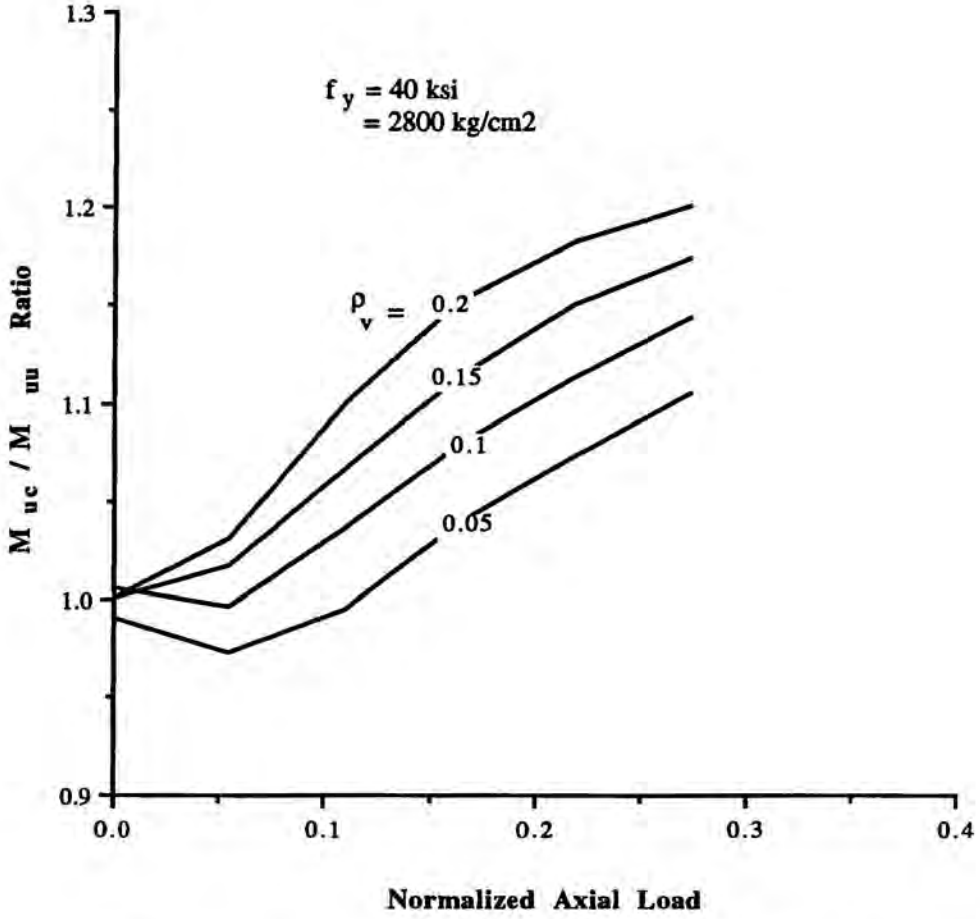

Fig. 7.13 Ratio of Flexural Strength of Walls having Steel Spacing of 104 in. To Walls having Steel Spacing of 32 in.

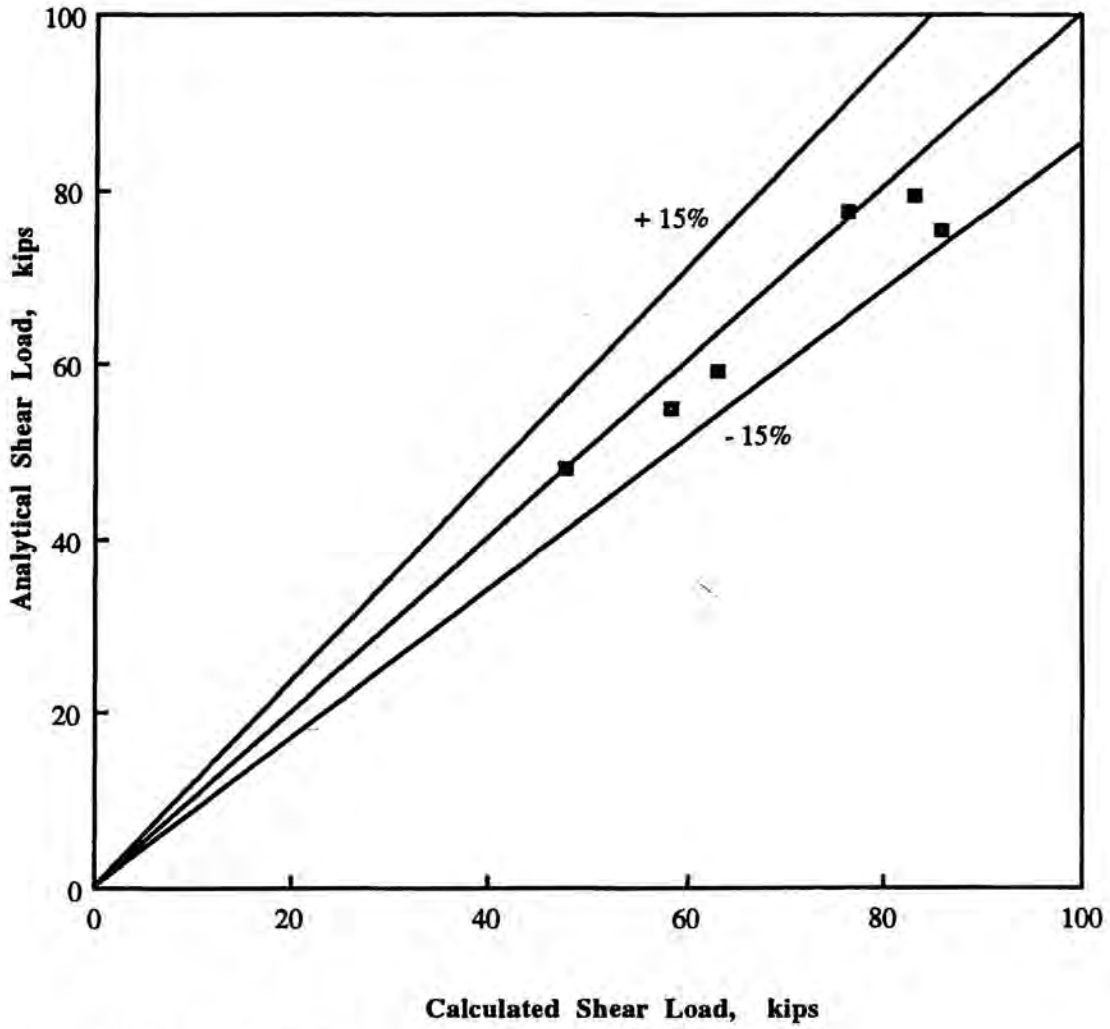

Note: 1 kip = 454 kg

Fig. 7.14 Accuracy of the Proposed Formula for Shear Strength

CHAPTER 8
SUMMARY AND CONCLUSIONS

8.1 SUMMARY

The methodology and techniques of using small-scale direct models of masonry component materials at 1/3-scale have been presented and correlated to available prototype component materials. The physical properties and mechanical characteristics of each model masonry component material used in the study have also been presented. Moreover, the effects of both the method of vibration during manufacture of the blocks and the grain size of block aggregates on the physical and mechanical properties were investigated. Correlation of the model units and prototype results have ranged from excellent to good.

The methodology of using small-scale direct models of concrete masonry and techniques of fabrication and testing of small masonry assemblages at 1/3-scale have been presented. Basic strength evaluation tests on model grouted and ungrouted masonry assemblages along with their corresponding control specimens were carried out to determine their compressive strength, shear capacity along the bed joints, and splitting tension at different orientations with the bed joints. Behavior characteristics of these model assemblages were investigated and discussed. The effects of a number of parameters on the behavior of model masonry assemblages were investigated along with direct correlation to prototype results. These include grouting, type of mortar bedding, and block strength .

In order to investigate experimentally the behavioral characteristics of partially reinforced masonry shear walls a modeling techniques was employed. A total of thirteen 1/3-scale models of partially reinforced concrete masonry shear walls were constructed and tested at the Structural Testing Laboratory of Drexel University under in-plane lateral loads, with and without axial precompression. Eleven shear walls were tested under monotonic loading, and two shear walls were tested under fully reversed cyclical loading. In addition, one infilled frame was chosen to be tested under monotonic loading. The following five

parameters were investigated: axial precompression, block strength, lateral load, amount and distribution of vertical and horizontal steel. The experimental results provided detailed information on the strength, shear stiffness, ductility and deformational characteristics of partially reinforced masonry shear walls. These results were compared with finite element analysis performed within the scope of this research. Based on the experimental results, an empirical formula was developed to determine the shear strength of partially reinforced masonry shear walls and an analytical approach was presented to calculate the geometrical properties (i.e., effective area and effective moment of inertia) of partially reinforced masonry. An analytical formula to calculate the flexure strength of partially reinforced masonry shear walls is developed as well. Finally the UBC-91 design methodology is evaluated with regard to both shear and flexure strength .

8.2 CONCLUSIONS

Conclusions concerning the technique and methodology of testing 1/3-scale component materials and small assemblages were presented at the end of Chapters 2 and 3, respectively while the behavior characteristics of 1/3-scale partially reinforced masonry shear walls were presented in Chapter 5. The overall conclusions of the research test program with regard to partially reinforced shear walls are presented below:

1- Excellent correlation between model and prototype results in predicting the mechanical properties of masonry concrete blocks in terms of overall behavior was achieved. Modeling techniques at 1/3-scale are capable of predicting the mechanical and physical properties of prototype masonry assemblies.

2- The load carrying capacity of the wall panels tends to increase with the decrease in spacing of vertical and horizontal steel for the same amount of reinforcement.

3- The behavior of partially reinforced masonry shear walls is highly sensitive to the distribution of horizontal and vertical steel reinforcement. The distribution of the reinforcement controls the mode of failure. The less spacing of vertical and horizontal steel

changes the behavior from a brittle shear mode (where behavior is governed by diagonal tensile cracking) to a flexural mode (where behavior is governed by yielding of the vertical reinforcement and crushing of the masonry at the toe) due to increased the shear resistance provided by bond beams and the dowel action of the vertical steel, thereby increasing wall ductility .

4- The distribution of horizontal and vertical reinforcement increases the shear strength of the wall and decreases the flexural strength. Concentration of vertical steel at the ends increases the flexural strength of the wall with little increase in shear strength. This leads to the conclusion that the flexural strength of a partially reinforced masonry wall panel depends on the distribution of vertical reinforcement while the shear strength is mainly dependent on the distribution of horizontal reinforcement.

5- Increasing the amount of vertical reinforcement favors the shear failure, and therefore decreases the wall ductility. The amount of vertical reinforcement has the ability to change the wall behavior from a brittle shear failure to a ductile flexural failure as the vertical reinforcement ratio decreases rather than the amount of horizontal reinforcement. The flexural strength of partially reinforced masonry wall increases with the quantity of vertical reinforcement present, while the shear strength increases with the quantity of horizontal reinforcement.

6- The diagonal cracking load is observed to be nearly constant for all walls exhibiting the same axial stress and block strength. It is dependent on the diagonal tensile strength of the masonry as well as the level of axial stresses, regardless of the amount and distribution of vertical and horizontal steel.

7- The first crack occurred at load ranging from 40-60 percent of the ultimate load for walls that have failed in flexure. However, for walls that have failed in shear, the range was 60-80 percent. This indicates that walls behaving in a flexure mode accommodate more load post cracking than walls that fail in shear.

8- The infilled frame showed a 25% reduction in cracking load compared to the

partially reinforced masonry wall having the same amount and location of steel. This indicates a different serviceability condition under service load for the two systems.

9- The ductility of the walls under cyclic loading were almost half the ductility of the wall under monotonic loading due to the repetitive opening and closing of the cracks under reversed loading. This indicates that the ability of partially reinforced masonry shear walls to develop a large deformation capacity under cyclic load is limited. Therefore, its application is not recommended in moderate or high seismic areas .

10- Increasing the axial stress up to 15% of the prism compressive strength (0.15 f'_m) causes an increase in the residual strength by approximately 180%. Moreover, as the compressive strength of masonry increases, the residual strength increases by the rate of square root of the gain in compressive strength. The yield strength of vertical steel shows a low rate increase in the residual strength; this rate increases as the percentage of vertical steel increases, and also as the compressive strength of masonry increases .

11- The axial stress has a significant impact on the shear stiffness measured at lateral loads greater than or equal to 50% of the ultimate load .

12- The vertical steel and axial stress have a more pronounced effect on the residual strength of partially reinforced masonry than on fully reinforced masonry shear walls.

13- The approach of the UBC-91 to evaluate the shear strength of reinforced masonry ignores the effect of vertical steel and axial stresses on the residual strength of masonry. Further, this approach takes into account the effect of top and bottom horizontal bars in addition to the internal bars in resisting the shear strength. This resulted in overestimating the shear reinforcement and underestimating the residual strength and, significantly, underestimating the nominal shear strength obtained experimentally in this research.

14- Grouting the unreinforced parts of wall panels for 32 in. (0.8 m) spacing, has no effect on the wall behavior, but has higher load carrying capacity by about 12%.

15- Wall aspect ratio has a very significant effect on behavior and shear resistance of the wall. Increasing the aspect ratio of the wall panel increases the ductility of the wall but

decreases the shear resistance of the wall. The shear resistance for wall having h/d = 0.5 is higher than walls having h/d = 1.0 & 3.0 by about 45% & 300% respectively.

16- The design concept of reinforced masonry for in-plane flexure can be used to a great extent to predict the in-plane flexure strength of partially reinforced masonry shear walls. However, minor modifications, regarding the effective width of the wall, have to be made to accounte for the grouted cells.

17- The proposed formula for predicting the shear strength consistently gives lower values than the experimental results and higher values than formula proposed by UBC-91 for fully reinforced masonry. It is sensitive to different design variables.

18- The application of the proposed formula to full-scale shear walls analyzed analytically, illustrates the satisfactory accuracy of that formula for predicting the shear strength of partially reinforced masonry shear walls.

8.3 RECOMMENDATIONS FOR FUTURE STUDIES

The in-plane behavior of partially reinforced masonry shear walls have not yet been fully addressed. Research presented in this study is only a beginning. Additional research is required to achieve the full potential of partially reinforced masonry shear shear walls.

It is evident that the shear strength is very much influenced by the effect of aspect ratio of the wall panel. The current study has focussed on a single aspect ratio. In this respect, further experimental studies of the aspect ratio and wall geometry on the shear behavior is necessary. Additional research is required to evaluate the effect of size and location of openings on the behavior of partially reinforced masonry shear walls. Research areas warranting particular scrutiny include walls under axial load, eccentric load and out-of-plane load and, walls with returns.

Further, experimental studies are necessary to develop a formula for predicting the shear stiffness of partially reinforced masonry under service loading.

REFERENCES

1 Abboud, B.E.,"The Use of Small Scale Direct Models for Concrete Block Masonry Assemblages and Slender Reinforced Walls Under Out-of-Plane Loads" Ph. D. Thesis Drexel University, Philadelphia, PA, 1987.

2 ACI 530-88 / ASCE 5-88 "Building Code Requirement for Masonry Structures" American Concrete Institute, Detroit 1988.

3 Ahmed, M.H.,"Behavior of Reinforced Brick-To-Brick Walls" International Symposium on Reinforced Prestressed Masonry, Edinburgh, August, 1984.

4 Ali, A. "Behavior of Reinforced Concrete Block Masonry Walls Under Concentrated Loads" M.Sc. Thesis, Ain Shams University 1989.

5 Agbabian Associates, "Rock Mechanics and Mining Engineering Computer Model and Code Reviews and Analysis, Vol. II: Code Implementation Topical Report", (R-8414-5650). EL Segundo, CA: September 1984.

6 American Concrete Institute, "Models for Concrete Structures", ACI Publication SP-24, Detroit, Michigan, 1971.

7 American Society for Testing and Materials ASTM C-1006, "Standard Test Method for Splitting Tensile Strength of Masonry Units" Annual Book of Standard, Volume 4.05, Philadelphia, PA, 1985.

8 American Society for Testing and Materials, ASTM C-150 "Standard Specification for Portland Cements", Annual Book of Standards , Vol. 4.02, Philadelphia, PA, 1985.

9 American Society for Testing and Materials, ASTM C-140 "Standard Methods of Sampling and Testing Concrete Masonry Units", Annual Book of Standards, Vol. 4.05, Philadelphia, PA, 1985.

10 American Society for Testing and Materials, ASTM C-615, "StandardSpecification for Deformed and Plain Billet Steel Bars for Concrete Reinforcement", Annual Book of Standards, Vol. 1.04, Philadelphia, PA, 1985.

11 American Society for Testing and Materials, ASTM C-67, "Standard Methods of Sampling and Testing Brickand Structural Clay Tile", Annual Book ofStandards, Vol. 4.05, Philadelphia, PA, 1987.

12 American Society for Testing and Materials, ASTM C-144, "Standard Specification for Aggregates for Masonry Mortar", Annual Book of Standards, Vol. 4.02, Philadelphia,PA, 1987.

13 American Society for Testing and Materials, ASTM C-270, "Standard Specification for Mortar Unit Masonry", Annual Book of Standards, Vol.4.05,Philadelphia,PA,

1987.

14 American Society for Testing and Materials, ASTM C-476, "Standard Specification for Grout for Masonry ", Annual Book of Standards, Vol.4.05, Philadelphia,PA, 1987.

15 American Society for Testing and Materials, ASTM C-1019, "Standard Test Method of Sampling and Testing Grout", Annual Book of Standards, Vol.4.05, Philadelphia, PA,1987.

16 American Society for Testing and Materials, ASTM C-447, "Standard Test Methods for Compressive Strength of Masonry Prisms", Annual Book ofStandards, Vol. 4.07, Philadelphia, PA, 1985.

17 American Society for Testing and Materials ASTM C-331, "Standard Specification for Lightweight Aggregates for Concrete Masonry Units" Annual Book of Standards, Vol. 4.05, 1980.

18 Amrhein, J.E., "The Future of Masonry", Proceedings of the 4th North American Masonry Conference, Los Angeles, California, August, 1987.

19 Baker, L.R., "Manufacture and Testing of Model Brick Wind Panels", Proceedings of Structural Models Conference, Sydney, Australia, Sponsored by the School of Architectural Science, University of Sydney, 1972.

20 Balachandran, K., "An Investigation of the Strength of Concrete Masonry Shear Wall Structures", Ph.D. Thesis, The University of Florida, 1974.

21 Becica, I.J. and Harris, G. H. "Ultimate Strength Behavior of Hollow Concrete Masonry Prisms Under Axial and Bending" Proceedings of the Second North American Masonry Conference, University of Maryland, College Park, Maryland, August 1982.

22 Benjamin, J.R. and Williams, H. A., "The Behavior of One Story Brick Shear Walls", Proc. ASCE, Journal of Structural Division, Vol. 84, No ST4, 1958.

23 Blume, J.G., "Analysis of Brick Walls Subjected to Axial Compression and In-Plane Shear", Proceedings of the 2nd International Brick Masonry Conference, stoke-on-Trent, April,1977.

24 Boult, B. F., "Concrete Masonry Prisms Testing", Journal of the American Concrete Institute, Vol. 76,April 1979, No 76-32, pp. 707-721.

25 Brochelt, J. G. and Brown, R. H., "An indirect Tensile Test for Masonry Units", ASTM Journal of Testing and Evaluation, Vol. 4, No 4, 1978.

26 Brochelt, J. G. and Brown, R. H., "An Indirect Tensile test for Masonry Units", ASTM Journal of Testing and Evaluation, Vol. 6, March 1978.

27 Canadian Standard Association " Masonry Design and Construction for Buildings"

S304-M78, Rexdale, Ontario, Canada.

28 Cervenca, V. "Constitutive Model for Cracked Reinforced Concrete", ACI Journal No. 6, Nov-Dec 1985, PP 877-882.

29 Chandrakeerthy, S. and Hamid, A.A., "Partially Reinforced Concrete Masonry as an Alternative Building Material in Developing Countries", Proc. the 3rd International Masonry Seminar for Developing Countries (Mauritiues, July 1990).

30 Cheema, T. S., "Anchorage Behavior and Prism Strength of Grouted Concrete Masonry", Ph. D. Thesis, University of Texas at Austin, May 1981.

31 Cheema, T.S. and Klingner, R.E., "Compressive Strength of Concrete Masonry Prisms", ACI Journal, Jan.-Feb. 1986.

32 Chia, C., Hamid, A. A., and Harris, H. G., "Monotonic and Cyclic Behavior of Joint Reinforced Block Masonry Walls Under Out-of-Plane Lateral Loading", Report No Stl-01/88, Drexel University, Philadelphia, PA, January 1988.

33 Clark, L. A., "Flexural Crack Similitude in Slabs Spanning One Way",London, Cement and Concrete Association, Technical Report 42-496, October 1974.

34 Cook, R.D. "Concepts and Applications of Finite Element Analysis" New York, N.Y. John Wiley and Sons, 1981.

35 Davies, S.R. and Ahmed A.E. "An Approximate method for Analysis Composite Wall-Beams", Proceedings Br. Ceram. Soc. Vol. 27, 1978.

36 De Vekey, R.C., "The Shear Resistance of damp-proof-cource (DPC) Materials",Building Research Establishment, April 1983.

37 Drysdale, R. G. and Hamid, A. A., "In-Plane Tensile Strength of Concrete Masonry", National Research Council Canada Journal of Civil Engineering, Vol. 9 No. 3, 1982, pp. 413-421.

38 Drysdale, R. G., Hamid, A. A., and Heiderbrecht, A. C., "Tensile Strength of Concrete Masonry", Journal of Structural Division. Proceedings ASCE, Vol. 105, No St7, July 1979.

39 Drysdale, R. G. and Hamid, A. A., "Behavior of Concrete Block Masonry Under Axial Compression", ACI Journal Vol. 76, No 6, June 1979.

40 Elmo, C.H., George, B.W. andElwood, L.O., "Effect of Maximum Size Aggregate on Compressive Strength of Mass Concrete" ACI, Publication No SP-6, 1963.

41 Elnawawy, O.A. and Hamid, A.A., "Flexural Strength of Partially Grouted Concrete Block Masonry Using Small-Scale Model Wall Elements", Report No STL-02/89, Department of Civil and Architectural Engineering, Drexel University, Phila, PA 19104.

42 Essawy, A.S. "Strength of Hollow Concrete Block Masonry Walls Subjected to Lateral Out-Of-Plane Loading", Ph.D. Thesis, McMaster University 1986.

43 Ewing, R.D., El-Mustapha, A.M. and Kariotis, J.C. "A Finite Element Computer Program for the Nonlinear Static Analysis of Reinforced Masonry Building Components", Report No. 2.2-1, EKEH, California 90274.

44 Fattal, S.G. and Todd, D.R. "Ultimate Strength of Masonry Shear Walls: Prediction vs Test Results", U.S. Dept. of Commerce, NIST, MD 20899, October 1991.

45 Fiorato, A.E., Sozen, M.A., and Gamble, W.L., "An Investigation of the Interaction of Reinforced Concrete Frames with Masonry Filler Walls", University of Illinois, Civil Engineering Studies, Structural Research Series No 370, Urbana, IL., November 1970.

46 Fishburn and Cyrus, C., "Effect of Mortar Properties on Strength of Masonry", NBS Monograph 36, National Bureau of Standards, Washington, DC, Nov. 1961.

47 Foster, P.K. "Prism Tests for Design and Control of Brick Masonry" New Zealand Pottery and Ceramics Research Association Technical Report, No. 22.

48 Fouad, H.A. "Behavior of Partially Grouted Concrete Block Masonry Walls Under Concentrated Loads" M.Sc. Thesis, Ain Shams University 1990.

49 Ghanem, G.M., Essawy, A.S. and Hamid, A.A. "Effect of Steel Distribution on the Behavior of Partially Reinforced Masonry Shear Walls", 6th Canadian Masonry Symposium, Sasktoon, Canada, June 1992.

50 Giuffre, A. and Modena, C. "Reinforced Masonry in Seismic Areas Studies for the New Italian Code", Proceedings of the 7th international Brick Masonry Conference, Melbourne, Australia, 17-20 Feb. 1985.

51 Haller, P., "Load Capacity of Brick Masonry", Designing Engineering and Constructing with Masonry Products, F.B. Johnson, Ed., Gulf Publishing Co., Houston, Texas, May 1967.

52 Hamid, A. A., "Behavior Characteristics of Concrete Masonry", Ph. D., Thesis, McMaster University, Hamliton, Canada, 1978.

53 Hamid, A. A., Drysdale, R. G., and Heidebrecht, A. C., "Shear Strength of Concrete Masonry Joints", Journal of the Structural Division, Proceedings ASCE, Vol. 105, No ST7, Proc. Paper 14670, July 1979, pp. 1227-1240.

54 Hamid, A.A. and Draysdale, R.G., "Flexural Tensile Strength of Concrete Block Masonry", Journal of Structural Engineering, Vol. 114, No 1, January 1988.

55 Hamid, A.A., Abboud, B.E., Farah, M.W., Hatem, M.K. and Harris, H.G., "Response of Reinforced Block Masonry Walls to Out-of-Plane Static Loads", Report No 3.2(a), US-Japan Coordinated Program for Masonry Building Research, Department of Civil and Architectural Engineering, Drexel University, Phila, PA

19104, 1984.

56 Hamid, A.A., Assis, G.F. and Harris, H.G., "Material Models for Grouted Block Masonry", Report No 1.2(a)-1, US-Japan Coordinated Program for Masonry Building Research, Department of Civil and Architectural Engineering, Drexel University, Phila, PA 19104, 1988.

57 Hamid, A.A., Elnawawy, O.A. and Farah, M.W., "Strengthening of Existing Hollow Block Masonry Walls", Proceedings of the 8th International Brick/Block Masonry Conference, Dublin, Ireland, 1988.

58 Hamid, A.A. and Chandrakeerthy, S.R., "Compressive Strength of Partially Grouted Concrete Block Masonry Using Small-Scale Model Wall Elements", paper in progress.

59 Hamid, A.A. and Ghanem, G.M. "Behavior of Partially Reinforced Masonry Walls", Proc. 9th International Brick/Block Masonry Conference (Burlin, Germany, October 1991).

60 Hamid, A.A. and Abboud, B.E., "Direct Modeling of Concrete Block Masonry Under In-Plane Loading" , Report No MS83-1, Dept. of Civil Engineering, Drexel University, Philadelphia, PA, 1983.

61 Hamid, A.A., Abboud, B.E., and Harris, H.G., "Direct Modeling of Concrete Block Masonry Under Axial Compression" , Masonry: Research, Application and Problems, ASTM STP 871, American Society for Testingand Materials, Philadelphia, PA, 1985.

62 Hamid, A.A. and Drysdale, R.G. "Suggested Failure Criteria for Grouted Concrete Masonry Under Axial Compression", ACI Journal Vol. 76, No. 10, October 1979.

63 Hamid, A.A. and Drysdale, R.G. "Tension Failure Criteria for Plane Concrete Masonry", Journal of Structural Engineering ASCE Structural Div. Vol. 76, No. 10, October 1979.

64 Hamid, A.A. and Abboud, B.E., "Direct Modeling of Concrete Block Masonry Under Shear and In-Plane Tension" , Journal of Testing and Evaluation, JTEVA, Vol. 14, No 2, March 1986.

65 Harris, H.G., Sabnis, G.M., and White,R. N., "Reinforcement for Small Scale Direct Models of Concrete Structures",Paper No SP-24-6,Models for Concrete structures, ACI SP-24, American Concrete Institute, Detroite, MI, PP. 141-158.

66 Harris, H.G. and Becica, I.J., "Direct Small Scale Modeling of ConcreteMasonry", Proceedings, Symposium on Advances in Civil Engineering Mechanics, EMD-ASCE, 23-25 May 1977.

67 Harris, H.G. and Becica, I.J., "Behavior of Concrete Masonry Structures and Joint Details Using Small Scale Direct Models", Proceedings of the North American

Masonry Conference, Boulder, Colorado, August 1978.

68 Harris, H. G., Sabnis, G. M., and White, R. N., "Small Scale Direct Models of Reinforced and Prestressed Concrete Structures", Report No. 326, Dept. of Structural Engineering, Cornell University, Ithaca, NY, September 1966.

69 Hatzinikolas, M., "Shear Behavior of Masonry Walls Subdivided by Floor Slabs", Proc. First Canadian Masonry Symp. E.L. Jessop and N.A. Ward, Eds., Calgary, Canada, June 1976, pp. 304-323.

70 Hegmeir, G., Krishnamoorthy, G., Nunn, R., and Moorthy, T. "Prism Tests forthe Compressive Strength of Concrete Masonry" Proceedings of the North American Masonry Conference, Boulder Colorado, August 1978.

71 Hegemier, G.A. and Arya, S.K. "Finite Element Method for Interface Problems", Journal of Structural Div. ASCE, Vol. 108, No. ST2, Feb 1982, PP. 327-342.

72 Hegemier, G. A., Arya, S. K., Krishnamoorthy, G. and Furgerson,R. "On the Behavior of Joints in Concrete Masonry" Proc. North American Masonry Conference, University of Colorado, Boulder, Co, August 1978, pp. 4.1-4.22.

73 Hendry, A.W. and Bradshaw, R.E., "Crushing Tests on Story Height Walls 4.5 in. Thick." Proc. of the Brit. Cer. Society No 41 July 1965.

74 Hendry, A.W. and Murthy, C.K., "Compressive Tests on One-Third and One-sixth Scale Model Brickwork Piers and Walls", British Ceramic Society Proceedings, No 4, July 1965.

75 Hidalgo, P.A., Mayes, R.L., McNiven, H.D. and Clough, R.W., "Cyclic Loading Test of Masonry Single Piers", Vol. 1 No UCB/EERC-78/27, Earthquake Engineering Research Center, Univ. of California, Berkeley, CA, Nov. 1978.

76 Hidalgo, P.A., Mayes, R.L., McNiven, H.D. and Clough, R.W., "Cyclic Loading Test of Masonry Single Piers", Vol. 3 No UCB/EERC-79/12, Earthquake Engineering Research Center, Univ. of California, Berkeley, CA, Nov. 1979.

77 Hilsdorf, H.K., "Investigation into the Failure Mechanism of Brick Masonry Loaded in Axial Compression"Proceedings of International Conference on Masonry Structural Systems, Texas, Nov. 1967.

78 Hirashi, H., "Flexural Behavior of Reinforced Masonry Walls",First Meeting of the US-Japan Joint Technical Coordinating Committee on Masonry Research, Tokyo, Japan, August, 1985.

79 Huizer, A., "Effect of mortar properties on compression prism, shear bond,and bending bond control tests for clay brick masonry", Research Report CE 75-6, Department of Civil Engineering, University of Calgary, Canada, Dec.1975.

80 Imai, H. and Miyamoto, M., "Seismic Behavior of Reinforced Masonry Walls with

Small openings", Fourth Meeting of the US-Japan Joint Technical Coordinating Committee on Masonry Research, San Diago, CA, October,1988.

81 James Colville and Amde, M., "Compressive Strength of Hollow Concrete Masonry" Fifth North American Masonry Conference University of Illinois at Urbana-Champaign June, 1990.

82 Johanson,F.B. and Thompson,J.N., "Development of Diametral Testing Procedures to Provide a Measure of Strength Characteristics of Masonry Assemblages", Designing, Engineering and Construction with Masonry Product, F . B . Johanson, ed., Gulf Publishing Co., Houston, Texas, May 1969.

83 Jolly, R., "Shear Strength; A Predictive Technique for Masonry Walls", Ph.D.Thesis, Brigham Young University, Provo, Utah, 1976.

84 Klamerus, E.W. 1988 "Experimental and Analytical Evaluation of the Inelastic Behavior of Reinforced Masonry Shear Walls" Thesis Presented to the University of Colorado, at Boulder, Colo., in Partial Fulfillment of the requirements for the degree of Master of Science.

85 Kingsley, R.G. and Atkinson, R.H., "A Comparison of the Behavior of Clay and Concrete Masonry in Compression", Technical Report by Atkinson-Noland and Associates, Inc., Boulder, Colorado, Sept. 1985.

86 Labrouki, B., "Material Characterization of 1/3-Scale Direct Models of Block Masonry Components", M. SC. Thesis Drexel University, Philadelphia, PA, 1989.

87 Larbi, A., "Behavior of Block Masonry Shear Walls Under In-Plane Monotonic and Reversed Cyclic Loads Using 1/3-Scale Direct Models", M. SC. Thesis, Drexel University , Philadelphia, PA, 1989.

88 Mann, W., "Statische Auswertung Von Druckversuchen an Mauerwerkskorpern in Geschlossener Darstellurgmit Hilf Von Potenzfunktionen"Proc. 6th Int. Brick Masonry Conference, Rome 1982, pp. 86-98.

89 Matsumura, A., "Shear Strength of Reinforced Hollow Unit Masonry Walls", Proceedings, 4th North American Masonry Conference, Paper No 50, Los Angeles, CA, 1987.

90 Maurenbrecher, A.H., "Compressive Strength of Hollow Concrete Blockwork", Proc. Fourth Canadian Masonry Cymp., University of New Brunswich, 1986, Vol. 2 pp. 997-1009.

91 Mayes, R.L., Omote, Y., and Clough, R.W., "Cyclic Shear Tests of Masonry Piers, Vol. 1 Test Results", Report No. UCB/EERC-76/8, Earthquake Engineering Research Center, Univ. of California, Berkeley, CA, May, 1976.

92 Mayes, R.L., Omote, Y., and Clough, R.W., "Cyclic Shear Tests of Masonry Piers", Vol. 2 No UCB/EERC-76/16, Earthquake Engineering Research Center,

Univ. of California, Berkeley, CA, June, 1976.

93 Mayes, R. L. and Clough, R. W., " A Literature Survey : Compressive Tensile, Bond and Shear Strength of Masonry" Report NO. ELPC 75-15, College of Engineering, University of California, Berkeley, CA, June 1975.

94 Meli, R., "Behavior of Masonry Walls Under Reversed Lateral Loads", Proceedings of the 5th World Conference on Earthquake Engineering, Rome, 1972.

95 Meli, R., Zeevaert, A.W. and Esteva, L.M., "Behavior of Masonry Walls Under Reversed Lateral Loads", Engineering Institute of Maxico, Report No 156, July 1968.

96 Meli, R., Zeevart, W. and Esteva, L., "Mechanical Properties of Masonry", Institute of Ingenieria, UNAM, Infome, No 288, July 1971.

97 Mohr, G.A., "Slender Load Bearing Brickwork Walls With Returns", M.Sc.Thesis, University of Melbourne, Civil Engineering Dept., 1970.

98 Morsy, E.H. and Fatma, E., "Towards Appropriate Testing and Evaluation Methods for Masonry Materials" General Organization for Housing, Building and Planning Research, Egypt.

99 Morsy, E.H., "An Investigation of Mortar Properties Influencing Brick work Strength", Ph.D. Thesis, Edinburgh University, 1968.

100 Moustafa,S.,"Ultimate Load test of a segmentally constructed prestressed concrete I beam", Journal of Prestressed Concrete Institute, Vol. 19 no. 4, 1974, pp. 54-75.

101 Murthy, C.K. and Hendry, A.W., "Model Experiments in Load Bearing Brickwork", in Building Science, Vol. 1, Pergamon Press, London, 1966.

102 Owen, D.R.J. and Hinton, E. "Finite Elements in Plasticity: Theory and Practice", Swansea, UK: Pineridge Press Limited, 1980.

103 Page, A.W. "Finite Element Model for Masonry", Journal of Structural Div. ASCE, Vol. 104, No. ST8 Aug. 1978.

104 Page, A.W. "A Biaxial Failure Criterion for Brick Masonry in the Tension-Tension Range", International journal of Masonry Const. Vol. 1, No. 1 March 1980.

105 Page, A.W. and Ali, S. "Cracking Analysis of Solid Concrete Masonry Subjected to Concentrated Loads", ACI Journal Vol. 86, No. 4, 1989.

106 Page, A.W., Kleeman and Dhanasekar "An In-Plane Finite Element Model for Brick Masonry", ASCE, Strucural Congress 85 Chicago, Illinois, Sept. 1985.

107 Park, R. and Paulay, T. 1975 "Reinforced Concrete Structures", John Wiley and Sons, Inc., New York, N.Y.

108 Pieper, K. and Trautsch, W., "Shear Tests on Walls", Proceedings of Second International Brick Masonry Conference Stoke-on-Trent, Apr. 1970.

109 Pook, L. L., Stylianou, M. A. and Dawe, J. L., "Experimental Investigation of the Influence of Compression on the shear Strength of Masonry Joints", Proceedings Fourth Canadian Masonry Symposium, University of New Brunswick, 1986.

110 Preistley, M. J. N., "Seismic Design of Concrete Masonry Shear Walls", Journal of the American Concrete Institute, Proceedings Vol. 83, No 1, Jan.-Feb. 1986, pp. 58-68.

111 Priestley, M.J.N. and Limin, H. "Seismic Behavior of Flanged Masonry Shear Walls", Report No, 4.1-1, Joint Technical Coordinating Committee on Masonry Research, May 1988.

112 Priestley, M. J. N. ,"Seismic Resistance of Concrete Masonry Shear Wall", Bullettin of the New Zealand National Society for Earthquake Engineering,Vol. 10 No 1, 1977.

113 Priestley, M.J.N. "Flexural Strength of Rectangular Uniform Masonry Shear Walls with Distributed Reinforcement", The Masonry Society, Vol. 5, No. 2 Dec. 1986.

114 Priestley, M.J.N. and Bridgeman, D.O., "Seismic Resistance of Brick Masonry Walls", Bulletin of the New Zealand National Society for Earthquake Engineering, Vol. 7, No 4, Dec. 1974.

115 Richardson, I.R. and Hasquil, G., "Model Brick Walls", Final Year Research Project, University of Melbourne, Civil Engineering Dept., 1968.

116 RILEM-Committee 76-LUM "Load Bearing Unit Masonry", Paper LUM 86-1, Draft for General Recommendations for Methods of Testing Load Bearing Masonry, 1986.

117 Robert R. Schneider and Walter L Dickey "Reinforced Masonry Design", TEXTBOOK, Prentice-Hall, Inc., Inglewood Cliffs, New Jersey 07632.

118 Rostampour, M., "Aspects of the design of multistory buildings in light weight concrete blockwork", ph.D. Thesis, University of Edinburgh, Scotland, July 1973.

119 Sabnis, G.M., Harris, H.G., White, R. H., and Mirza, S., "Structural Modeling and Experimental Techniques", Prentice Hall, Englewood Cliffs, NJ, 1981.

120 Saw, C.B. "Linear Finite Element Analysis of Walls on Beams", Bldg-Sci, Vol. 9, 1974.

121 Schneider, R.R., "Lateral Load Tests on Reinforced Grouted Masonry Shear Walls", University of Southern California Engineering Center, Report No 70-101, 1959.

122 Schubert, P. and Glitza, H., "Festigkeits und Verformungs werte Von Mauermortel

und Wandbausteinen", Institute fur Bauforschung der RWTH Aachen, Bericht F 37, Januar 1978.

123 Scrivener, J.C., "Static Racking Tests on Masonry Walls", Designing, Engineering and Constructing with Masonry Products, Edited by F.B. Johnson, Gulf Publishing Company, Houston, Texas, May 1969.

124 Scrivener, J.C., "Concrete Masonry Wall Panel Tests Static Racking Tests with Predominant Flexural Effect", New Zealan Concrete Construction, Vol. 10, No 7, Wellington, July 1966.

125 Self, M. W., "Structural Properties of Loadbearing Concrete Masonry", Masonry: Past and Present, ASTM STP 589 American Society for Testing and Materials, 1975.

126 Shing, P.B., Noland, J.L., Spaeh, H., and Klamerus, E., "Response of Reinforced Masonry Story Height Walls to Fully Reversed In-Plane Loads", Department of Civil Engineering, University of Colorado, Boulder, September, 1986.

127 Shing, P.B., Schuller, M. and Hoskere, V.S. "In-plane Resistance of Masonry Shear Walls", Journal of Structural Engineering ASCE, Vol.116, No.3,March 1990.

128 Shing, P. B., Noland, J. L., Spaeh, H., and Klamerus, E., "Inelastic Behavior of Masonry Wall Panels Under In-Plane Cyclic Loads", The 4th North American Masonry Conference, Los Angeles, August 1987.

129 Shing, P. B., Noland, J. L., Spaeh, H., and Klamerus, E., "Behavior of single Story Reinforced Masonry Shear Walls Under In-Plane Cyclic Lateral Loads", Report of the Fourth Meeting of the US-Japan Joint Technical Committee on Masonry Research, San Diego, CA, USA, October 17-19, 1988.

130 Sinha, P.B. and Hendry, A.W., "Racking Tests on Story Height Shear Wall Structures With Openings Subjected to Precompression", Designing, Engineering, and Constructing with Masonry Products, Edited by F.B. Johnson, Gulf Publishing Company, Houston, Texas, May 1969.

131 Sinha, P.B. and Hendry, A.W., "Further Tests on Model Brick Walls and Piers", Proceedings of the British Ceramic Society, No17, 1970.

132 Sinha, B.P., "Model Studies Related to Load Bearing Brickwork", Ph.D. Thesis, University of Edinburgh, Scotland, 1967.

133 Sinha, B.P., Maurenbrecher, A.H.P., and Hendry, A.W., "Model and Full Scale Tests on a Five-Story Cross-Wall Structure Under Lateral Loading", Proceedings of Second International Brick Masonry Conference, Stoke-on-Trent, April 1970.

134 Smith, S.T., "Model Brick Wall Study", Final Year Research Project, University of Melbourne, Civil Engineering Dept., 1961.

135 Stafford Smith, B. and Carter, C.,"Hypothesis of shear failure of brickwork", Journal of the Structural Division, Proc. of ASCE, ST4, Vol. 97, April 1971, pp. 1055-1062.

136 Standard Association of New Zealand "Code of Practice for Masonry Design", (N 25 4203 P), Weillington 1985, 130 pp.

137 Stockl, S. and Hofmann, P., "FE-Calculations for Various Test Set-Ups todetermine the Shear bond Properties of Mortar Joints in Masonry", Report Submitted to the RILEM Committee LUM 76, June 1988.

138 Stockl, S. and Hofmann, P., "Tests on the Shear Bond Behavior in the Bed Joints of Masonry", Masonry International, No 9 December 1986.

139 Sveinsson, B.I., McNiven, H.D. and Sucu0glu, H., "Cyclic Loading Tests of Masonry Single Piers, Vol. 4 Additional Tests with Height to Width Ratio of 1", Report No UCB/EERC-85/15, Earthquake Engineering Research Center, Univ. of California, Berkeley, CA, December, 1985.

140 Taylor, D.I. and Spurgeon, S., "Model Brick Walls", Final Year Research Project, University of Melbourne, Civil Engineering Dept., 1968.

141 Uniform Building Code, 1988 Edition, International Conference of Building Officials, "Masonry Codes and Specifications", CA, May 1988.

142 Vecchio, F.J. and Collins, M.P. "The Response of Reinforced Concrete To In-Plane Shear and Normal Stresses", (Publication No. 82-03). Toronto, Canada, University of Toronto, March 1982.

143 Voigt, H., "Consideration and Investigations on the Basic Principle of Model Tests in Brickwork and Masonry Structures", Library Communication, No 932, Building Research Station, Garston, Watford, England, 1956.

144 Wakabayashi, M. and Nakamura, T., "Reinforcing Principle and Seismic Resistance of Brick Masonry Walls", Proceedings Eight World Conference on Earthquake Engineering, Vol. V, 1984, San Francisco.

145 Williams, D., "Seismic Behavior of Reinforced Masonry Shear Walls ", Ph.D. Thesis, University of Canterbury, Christchurch, New Zealan, 1971.

146 Yancey, C.W., Fattal, S.C. and Dikkers, R.D., "Review of Research Literature on Masonry Shear Walls" USA, Dept. of Commerce, NISTIR , 4512, Feb. 1991.